

APPENDIX C

**PHOTOCHEMICAL MODELING FOR THE DFW
ATTAINMENT DEMONSTRATION SIP REVISION FOR THE
2008 EIGHT-HOUR OZONE STANDARD**

2015-014-SIP-NR

Proposal
December 9, 2015

**APPENDIX C: PHOTOCHEMICAL MODELING FOR THE
DFW ATTAINMENT DEMONSTRATION SIP REVISION FOR
THE 2008 EIGHT-HOUR OZONE STANDARD**

APPENDIX C: PHOTOCHEMICAL MODELING FOR THE DFW ATTAINMENT DEMONSTRATION SIP REVISION FOR THE 2008 EIGHT-HOUR OZONE STANDARD 1

1. OVERVIEW 2

2. PHOTOCHEMICAL MODEL CONFIGURATION: THE NEW 2014 MODELING PLATFORM 3

3. BASE CASE MODELING..... 8

4. CAMX MODEL PERFORMANCE EVALUATION 12

4.1. OPERATIONAL EVALUATIONS13

4.1.1. *Statistical Measures*13

4.1.2. *Graphical Measures*.....14

4.2. DIAGNOSTIC EVALUATIONS15

4.2.1. *Sensitivity Analyses*.....15

4.2.2. *Diagnostic Analyses*.....15

4.3. EPISODIC MODEL PERFORMANCE ASSESSMENT FOR OZONE16

4.3.1. *Assessments Based on all Hourly Modeled-Observed Pairs*16

4.3.2. *Assessments Based on Daily Peak Modeled-Observed Pairs at Monitor Sites*17

4.3.3. *Assessments Based on Daily Peak Modeled-Observed Concentrations Unpaired in Space and Time*
17

4.3.4. *Episodic Model Performance Assessment*18

4.4. STATISTICAL PERFORMANCE MEASURES21

4.5. GRAPHICAL PERFORMANCE MEASURES28

4.5.1. *Time Series and Scatter Plots for Selected Monitors*28

4.5.2. *Peak Ozone Tile Plots*.....46

4.5.3. *Summary*64

4.6. BACKGROUND MODEL PERFORMANCE EVALUATION64

4.6.1. *Summary and Conclusions*.....70

4.7. AIRCRAFT MODEL PERFORMANCE EVALUATION70

5. DIAGNOSTIC EVALUATIONS..... 75

5.1. SENSITIVITY ANALYSES.....75

5.1.1. *Alternative Chemistry Mechanisms: CB05 vs. CB6r2d3*.....75

5.1.2. *MEGAN vs. GloBEIS biogenic emissions*.....81

5.1.3. *Highly-Reactive VOC Sensitivity*.....86

5.2. DIAGNOSTIC ANALYSES89

5.2.1. *Retrospective Modeling – 2012*.....89

5.2.2. *Observational Modeling – Weekday/Weekend*.....93

5.2.3. *Process Analysis*.....96

5.2.4. *Source Apportionment Analysis-Anthropogenic Precursor Culpability Assessment (APCA)/Ozone Source Apportionment Technology (OSAT)*.....97

6. BASELINE (2006) AND FUTURE CASE (2018) MODELING 111

6.1.	BASILINE MODELING.....	111
6.2.	FUTURE BASILINE MODELING	113
6.2.1.	<i>Alternative Future Design Value Calculations</i>	116
6.2.2.	<i>Unmonitored Area Analysis</i>	123
6.2.3.	<i>Ozone Metrics</i>	125
7.	MODELING ARCHIVE AND REFERENCES.....	126
7.1.	MODELING ARCHIVE.....	126
7.2.	MODELING REFERENCES.....	126

1. OVERVIEW

Photochemical modeling involves two major phases, the base case modeling and the future year modeling. The purpose of the base case modeling phase is to evaluate the model’s ability to adequately replicate measured ozone and ozone precursor concentrations during recent periods with high observed ozone concentrations (the base case episode). The purpose of the future year modeling phase is to predict attainment year ozone design values, as well as to evaluate the effectiveness of controls in reaching attainment. The Texas Commission on Environmental Quality (TCEQ) developed a Modeling/Analysis protocol describing the process to be followed to model base case and future year ozone formation in the Dallas-Fort Worth (DFW) area, and submitted the plan to the Environmental Protection Agency (EPA) for review and approval.

The performance evaluation of the base case modeling provides a measure of the adequacy of the model in correctly replicating the relationship between ozone and the emissions of ozone precursors (e.g., oxides of nitrogen (NO_x) and volatile organic compounds (VOC)). The performance evaluations of the base case modeling are composed of two types, operational (e.g., statistical and graphical evaluations) and diagnostic (e.g., sensitivity and probing tools evaluations). As recommended in the EPA guidance (EPA-454/B-07-002, April 2007), these evaluations are considered as a whole in a “weight-of-evidence” approach, rather than individually, in deciding the adequacy of the model in replicating the relationship between ozone and the emissions of ozone precursors and thereby establishing the level of confidence that can be placed in the response of ozone in the model to various control measures.

Future year modeling involves several steps. The first is creating a modeling baseline, which is similar to the base case except that it removes non-systematic emissions variability (e.g. emission events). The future year emissions are developed by applying growth and control factors to the baseline year emissions. Future year ozone design values (attainment test) are then determined using the ratio of the future year to the baseline year modeled ozone concentrations. This ratio is called the relative response factor (RRF).

Both the baseline and future years are modeled using the base case episode meteorological data as inputs. The same meteorological data are used for modeling both the baseline and future years, and thus, the ratio of future year modeled ozone concentrations to the baseline year concentrations provides a measure of the response of ozone to the change in emissions.

The future year ozone design value is calculated by multiplying the RRF by a baseline year ozone design value (DV_B). The DV_B is the average of the regulatory design values for the three consecutive years containing the baseline year (see Figure 1-1: *Baseline Design Value Calculation Illustration*). When the calculated future year ozone design value is equal to or less than 0.075 ppm (75 ppb), this signifies modeled attainment. When the calculated future year ozone design value is greater than 75 ppb, the model can be used to test the effectiveness of various control measures that may be needed.

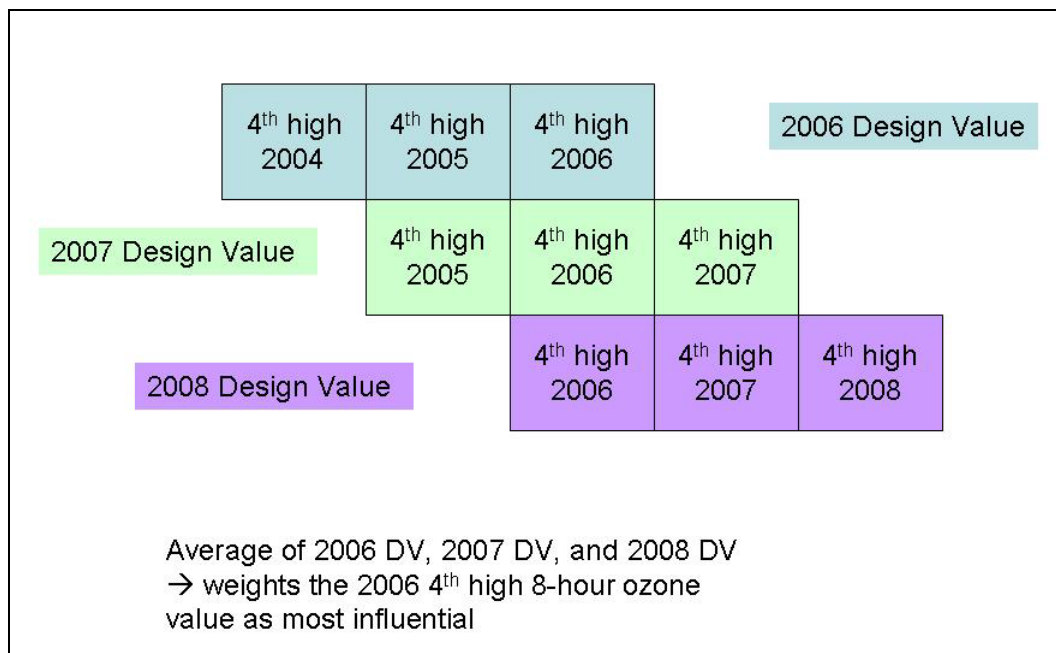


Figure 1-1: Baseline Design Value Calculation Illustration

2. PHOTOCHEMICAL MODEL CONFIGURATION: THE NEW 2014 MODELING PLATFORM

The modeling described in this document uses a revised modeling platform that offers several advantages and technical advances over previous attainment demonstration modeling conducted in Texas. Table 2-1: *Major Enhancements Between the 2011 and 2014 Modeling* illustrates the major enhancements between the previous round of DFW Attainment Demonstration (AD) SIP revision modeling and the current round.

Table 2-1: Major Enhancements Between the 2011 and 2014 Modeling Platforms

Category	2011 Modeling Platform	2014 Modeling Platform
Episodes	May 31 through July 2, 2006	May 31 through July 2, 2006; August 13 through September 15, 2006
Projection Year	2012	2018
Model Domain	36×36 km Eastern U.S. with 12×12 km and 4×4 km nested grids (Figure 2.1 - a)	36×36 km Continental U.S. with 12×12 km and 4×4 km nested grids (Figure 2.1 - b)
Meteorological Model	MM5 v3.7.3	WRF v3.2
Photochemical Model	CAMx 5.5	CAMx 6.10 patch 1

Category	2011 Modeling Platform	2014 Modeling Platform
Chemical Mechanism	CB05	CB6 r2
Boundary Conditions	CAMx 2006 and 2018 runs for Continental U.S. using MOZART BCs. 2012 BCs average of 2006 and 2018.	GEOS-Chem 2006, 2018
Biogenic Emissions	Global Biogenic Emissions System (GloBEIS)	Model of Emissions of Aerosols and Gases from Nature (MEGAN) v2.10
On-Road Mobile Source Emissions	MOVES 2010a	MOVES 2010b
Area/Non Road Mobile Source Emissions		Improvements to commercial marine, aircraft, rail, oil & gas production and exploration emissions.

The TCEQ used the Comprehensive Air quality Model with extensions (CAMx) version 6.10 (with patch 1) (Environ, 2014). The model is based on well-established treatments of advection, diffusion, deposition, and chemistry. Another important feature is that NO_x emissions from large point sources can be treated with the plume-in-grid (PiG) sub-model, which helps avoid the artificial diffusion that occurs when point source emissions are introduced into a grid volume. In addition, the TCEQ has many years of experience with CAMx. CAMx was used for the modeling conducted in the Houston-Galveston-Brazoria (HGB) and Beaumont-Port Arthur (BPA) nonattainment areas, as well as for modeling being conducted in other areas of Texas (e.g., San Antonio), and by EPA to support the Cross-State Air Pollution Rule (CSAPR). The [model software and the CAMx user's guide](http://www.camx.com) are publicly available at <http://www.camx.com>.

CAMx version 6.10 includes a number of upgrades and features from previous versions, the most notable being support for the new CB6 Carbon Bond chemistry module, which was used in the modeling for this SIP revision. The CB6 represents a more complete characterization of atmospheric chemical processes than did its predecessor CB05. The CB6 mechanism increases the number of emitted species from 16 to 21 and gas-phase species from 51 to 77. Photolysis reactions are increased from 23 to 28, and gas-phase reactions from 156 to 218. Significant improvements were made to reactions involving toluene, xylenes, benzene, isoprene, and di-nitrogen pentoxide (N₂O₅). This modeling used CB6r2, which includes further modifications to isoprene chemistry and more detailed treatment of organic nitrates, which tend to reduce regional ozone concentrations and improve model performance compared with base CB6.

In addition to the CAMx inputs developed from the meteorological and emissions modeling, inputs are needed for initial and boundary conditions, spatially resolved surface characteristic parameters, spatially resolved albedo/haze/ozone (i.e., opacity) and photolysis rates, and a chemistry parameters file.

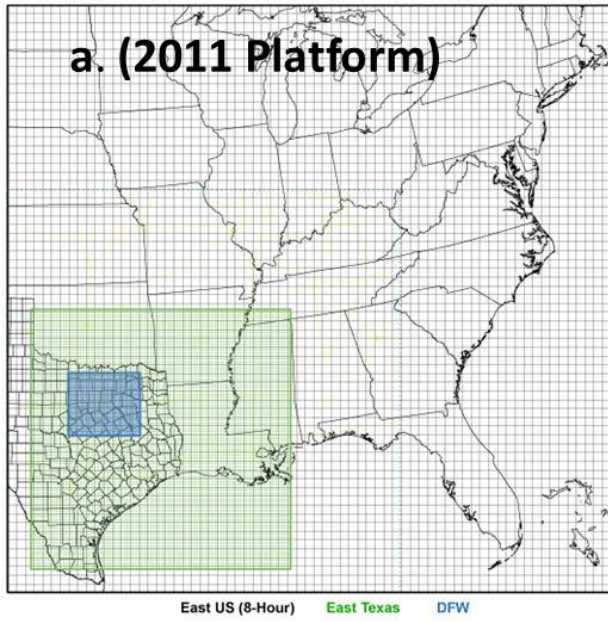
The TCEQ contracted with Environ (Environ, 2013) to derive episode-specific boundary conditions from the Goddard Earth Observing Station global atmospheric model with Chemistry (GEOS-Chem) model runs for 2006, 2012, and 2018. Boundary conditions were developed for each grid cell along all four edges of the outer modeling domain at each vertical layer for each episode hour. This work also produced initial conditions for each of the episodes. The TCEQ used these episode-specific initial and lateral boundary conditions for this modeling study.

Surface characteristic parameters, including topographic elevation, leaf area index, vegetative distribution, and water/land boundaries are input to CAMx via a land-use file. The land-use file provides the fractional contribution (0 to 1) of twenty-six land-use categories, as defined by Zhang et al (2003). For the 36 km domain, the TCEQ developed the land-use file using version 3 of the Biogenic Emissions Landuse Database (BELD3) for areas outside the U.S. and the 2006 National Land Cover Dataset (NLCD) for the U.S. For the 4 km and 12 km domains the TCEQ used updated land-use files developed by Texas A&M University (Popescu et al., 2012), which were derived from more highly resolved data collected by the Texas Parks and Wildlife Department, Landscape Fire and Resource Management Planning Tools Project (LANDFIRE), LandSat, National Institute of Statistics and Geography (INEGI), and the NLCD. Monthly averaged Leaf Area Index (LAI) was created from the eight-day 1 km resolution MODIS MCD15A2 product.

Spatially-resolved opacity and photolysis rates are input to CAMx via a photolysis rates file and an opacity file. These rates, which are specific to the chemistry parameters file for the CB6 mechanism, are also input to CAMx. The TCEQ used episode-specific satellite data from the Total Ozone Mapping Spectrometer (TOMS) to prepare the clear-sky photolysis rates and opacity files. Photolysis rates are internally adjusted by CAMx according to cloud and aerosol properties using the inline Tropospheric Ultraviolet and Visible (TUV) radiation model.

depicts the modeling domains used in CAMx in both (a) the 2011 DFW AD SIP Revision and (b) the current (2014) SIP revision along with the defining parameters of the map projections used (c). Both domains use a Lambert Conformal Conic (LCC) projection, but the new platform uses different projection parameters to be consistent with that used by EPA and several regional and state modeling applications. The outer (36 km × 36 km) grid for the new projection is referred to as the Regional Planning Organization (RPO) grid since it used by those groups, but it is also often referred to as the Continental U.S. (CONUS) grid. The larger outer grid allows for boundary conditions estimated from the GEOS-Chem model to be directly applied to the new 2014 modeling platform, obviating the need for an intermediate model run to develop boundary conditions for the smaller grid system used previously.

Like the earlier modeling platform, the 2014 version includes both 12 km × 12 km and 4 km × 4 km nested grids, but both of these have been expanded significantly. The 12 × 12 km grid depicted in blue in Figure 2-1 (b) covers all or nearly all of Texas, Louisiana, Oklahoma, and New Mexico, and includes much of northern Mexico and the northwestern Gulf, while the 4 km × 4 km East Texas grid covers the eastern two-thirds of Texas and includes all of the state's nonattainment and near-nonattainment areas. Although some graphics presented for the DFW area only depict part of the 4 km × 4 km grid, the entire innermost grid is modeled at 4 km × 4 km resolution. The domain specifications for the 2014 modeling platform are detailed in Table 2-2: *CAMx Modeling Domain Dimensions*. The vertical layer structure, shown in Table 2-3: *CAMx Vertical Layer* shows the vertical dimensions for the three-dimensional CAMx grid system (unchanged from the 2011 modeling). The accompanying graphic illustrates how the vertical dimensions increase with altitude.



C. Lambert Conformal Projection parameters for 2011 and 2014 modeling platforms

Parameter	2011 Platform	2014 Platform
First true latitude (α)	30°N	33°N
Second true latitude (β)	60°N	45°N
Central longitude (γ)	100°W	97°W
Origin	(100°W, 40°N)	(97°W, 40°N)
Spheroid	Perfect sphere, radius=6370 km	

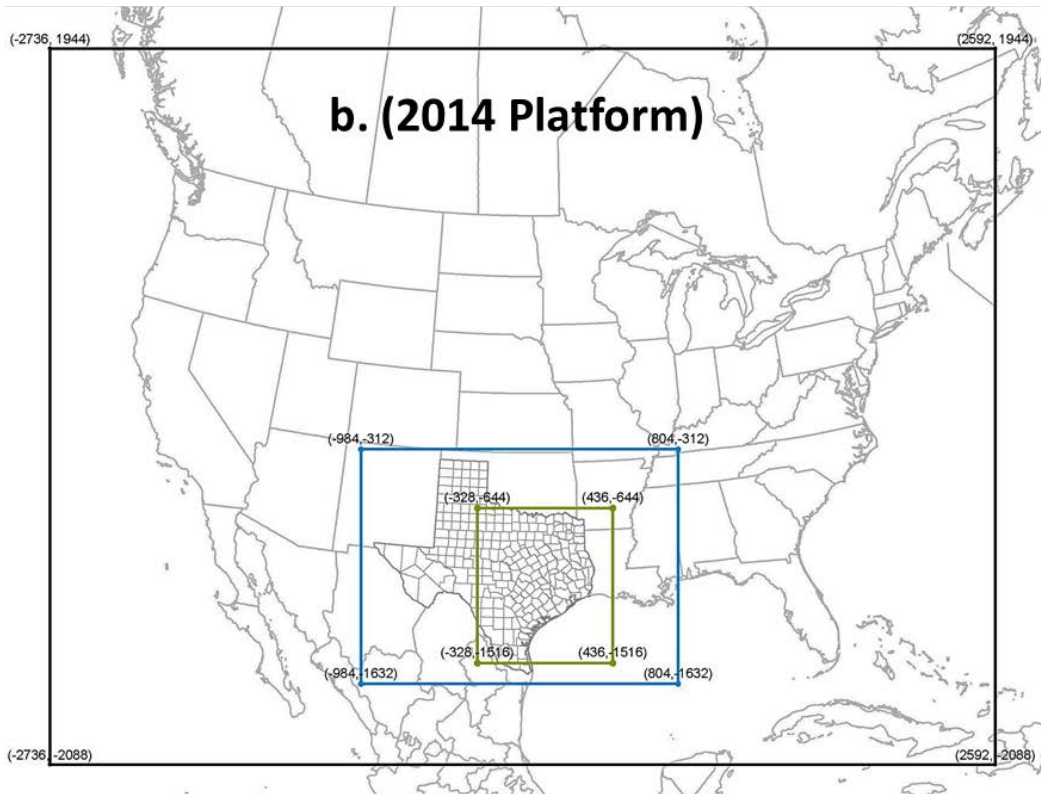


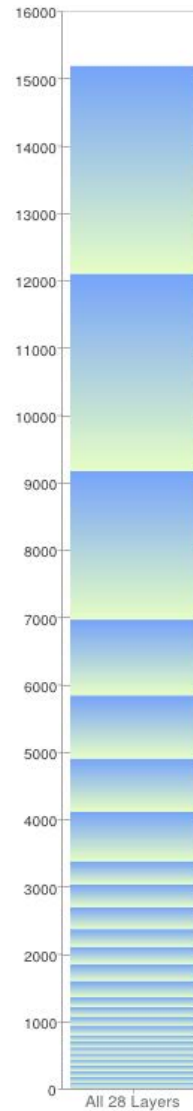
Figure 2-1: DFW Photochemical Modeling Domains
(a) 2011 modeling platform on the Eastern U.S. Grid; (b) 2014 modeling platform on the RPO (CONUS) Grid; (c) Map projection parameters for 2011 and 2014 platforms.

Table 2-2: CAMx Modeling Domain Dimensions

Domain	Easting Range (km)	Northing Range (km)	East/West Grid Points	North/South Grid Points
36 km	(-2736, 2592)	(-2088, 1944)	148	112
12 km	(-984, 804)	(-1632, -312)	149	110
4 km	(-328, 436)	(-1516, -644)	191	218

Table 2-3: CAMx Vertical Layer Structure

CAMx Layer	MM5 Layer	Top (m AGL)	Center (m AGL)	Thickness (m)
28	38	15179.1	13637.9	3082.5
27	36	12096.6	10631.6	2930.0
26	32	9166.6	8063.8	2205.7
25	29	6960.9	6398.4	1125.0
24	27	5835.9	5367.0	937.0
23	25	4898.0	4502.2	791.6
22	23	4106.4	3739.9	733.0
21	21	3373.5	3199.9	347.2
20	20	3026.3	2858.3	335.9
19	19	2690.4	2528.3	324.3
18	18	2366.1	2234.7	262.8
17	17	2103.3	1975.2	256.2
16	16	1847.2	1722.2	256.3
15	15	1597.3	1475.3	249.9
14	14	1353.4	1281.6	243.9
13	13	1209.8	1139.0	143.6
12	12	1068.2	998.3	141.6
11	11	928.5	859.5	137.8
10	10	790.6	745.2	90.9
9	9	699.7	654.7	90.1
8	8	609.5	564.9	89.3
7	7	520.2	476.0	88.5
6	6	431.7	387.8	87.8
5	5	343.9	300.4	87.0
4	4	256.9	213.7	86.3
3	3	170.5	127.7	85.6
2	2	84.9	59.4	51.0
1	1	33.9	16.9	33.9



Note: AGL - Above ground level.

3. BASE CASE MODELING

This CAMx model configuration was applied to the June 2006 and August-September 2006 episodes using episode-specific meteorological parameters and emissions. The two episode periods encompass the twin peaks of the bimodal distribution of ozone exceedances characteristic of eastern Texas, and specifically the DFW area, as illustrated in *Figure 3-1: MDA8 exceedance days in DFW and other areas of Texas*. During the 33-day June ozone episode, 17 days had one or more maximum daily eight-hour average (MDA8) ozone concentrations that exceeded the 2008 ozone National Ambient Air Quality Standard (NAAQS) threshold of 75 parts per billion (ppb). The 34-day August-September episode had 12 exceedance days. The exceedance days in these episodes exemplify the meteorological conditions conducive to ozone formation in the area (see the Conceptual Model for Ozone Formation in Chapter 5).

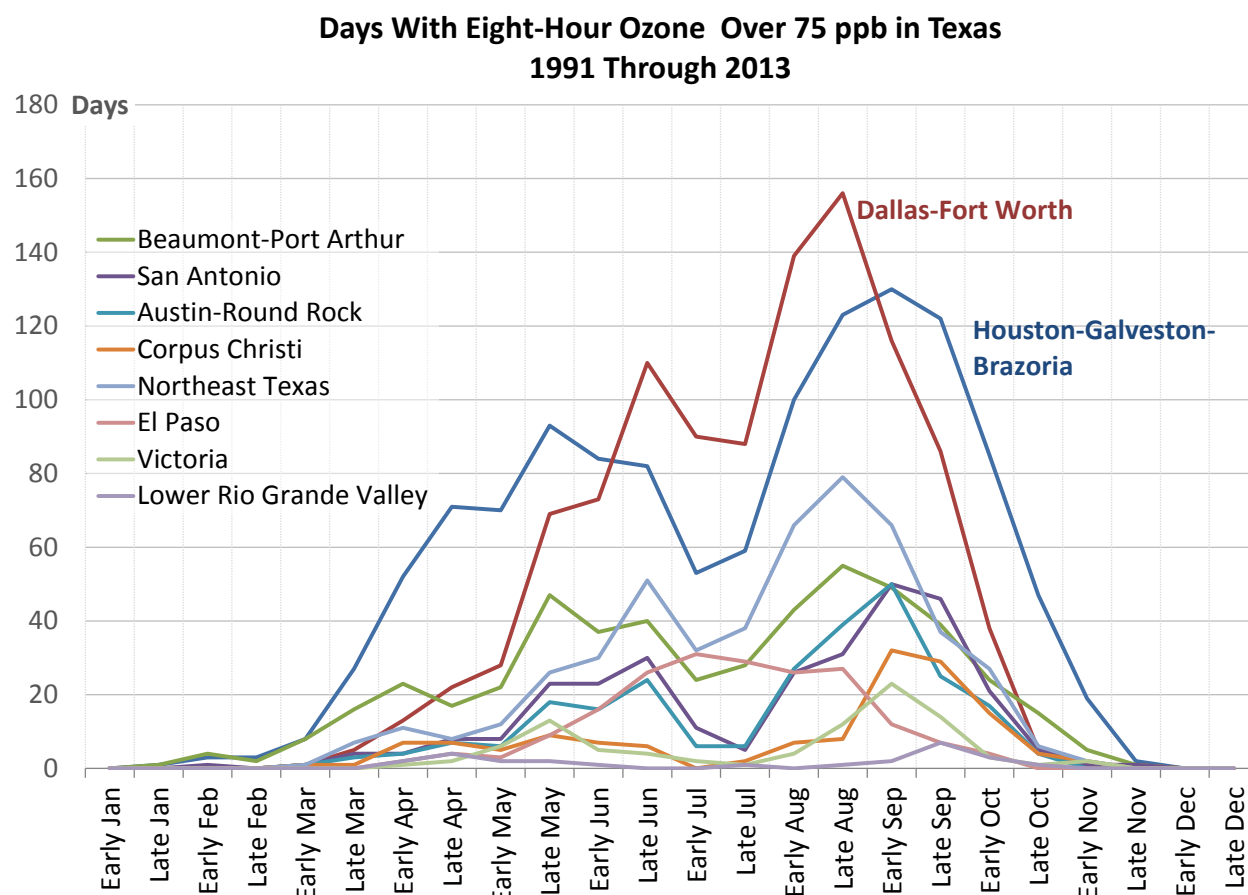


Figure 3-1: MDA8 exceedance days in DFW and other areas of Texas

Figure 3-2: *DFW MDA8 Ozone by Monitor* - Top: June 2006, Bottom: August-September 2006 shows the MDA8 ozone concentrations observed over the June episode (top) and over the August-September episode (bottom). Many days in both episodes experienced MDA8 ozone concentrations above 90 ppb, which were similar in magnitude to the monitor-specific baseline design values. Also of note are the periods with lower ozone values that occurred after frontal passages and times of strong southerly flow, particularly in the latter episode.

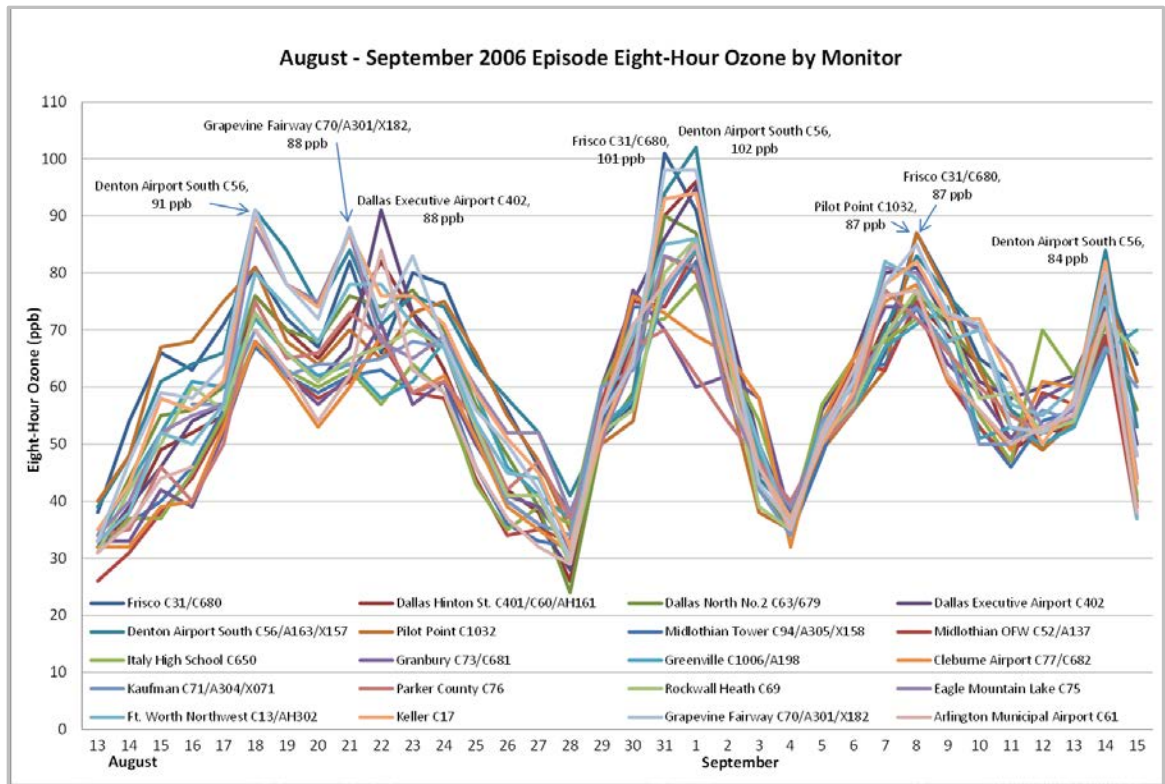
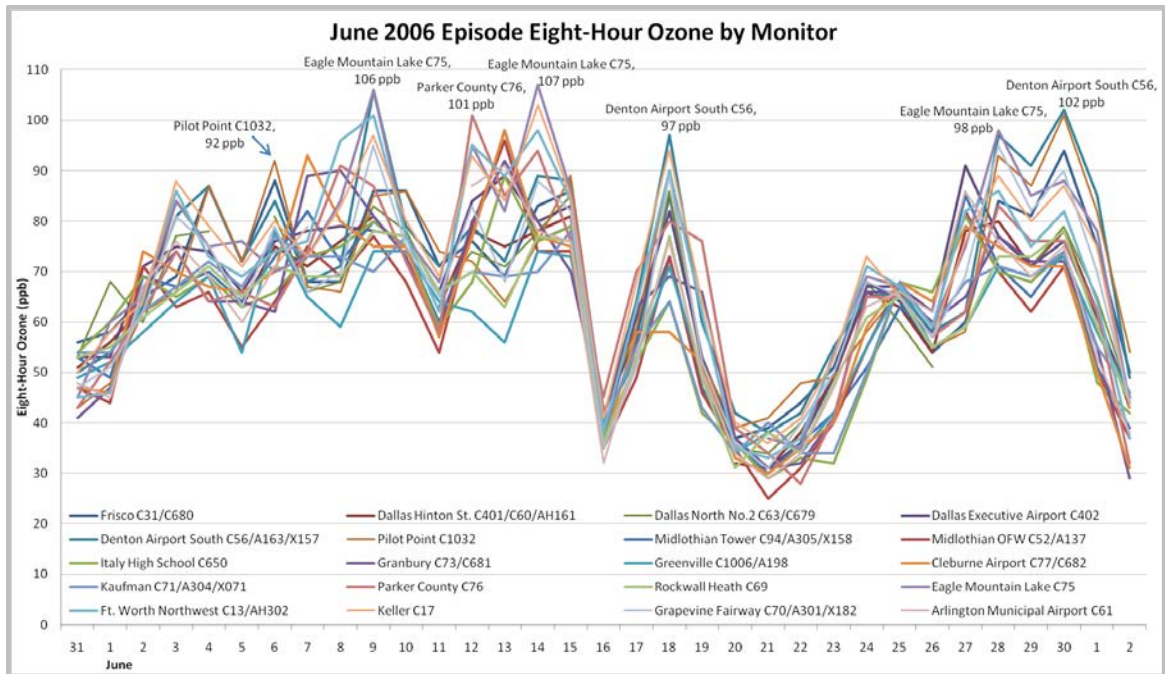


Figure 3-2: DFW MDA8 Ozone by Monitor - Top: June 2006, Bottom: August-September 2006

Figure 3-3: DFW area monitors exhibits the locations of the monitors in and around the DFW nonattainment area.

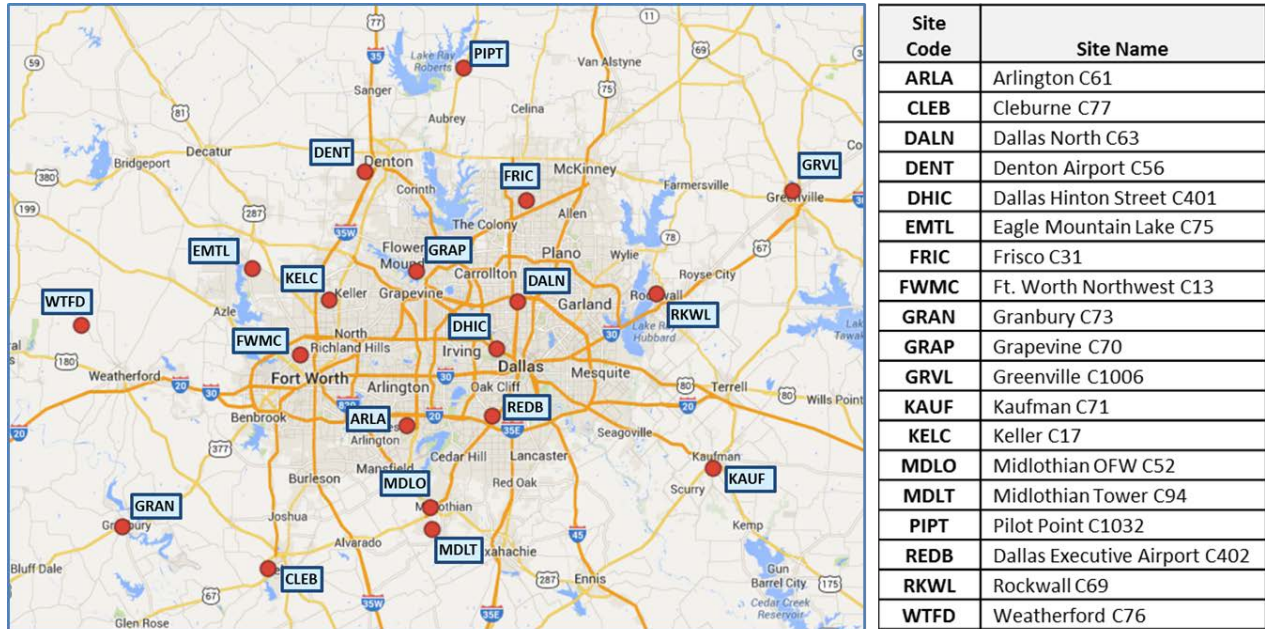


Figure 3-3: DFW area monitors

Table 3-1: *DFW Monitor-Specific MDA8 Ozone Data during the June 2006* summarizes the observed concentrations at the DFW monitors during the June 2006 episode. The monitors that recorded the highest design values since 2005 (Eagle Mountain Lake C75, Denton Airport South C56, Keller C17, and Fort Worth Northwest C13), also observed the most exceedance days (16) of the 2008 ozone standard, and also showed the highest peak eight-hour concentrations. Table 3-2: *DFW Monitor-Specific MDA8 Ozone Data during the August-September 2006 Episode* shows that during the latter episode most sites experienced fewer exceedance days and the highest MDA8 ozone concentrations tended to be lower than during the June episode. This trend is somewhat contradictory to Figure 3-1, which shows that typically more exceedances occur in August than in June. While the June episode offers abundant days with MDA8 ozone concentrations > 65 ppb for every monitor, the August episode offers somewhat fewer but still a minimum of six days at each monitor. Since calculation of the relative response factors used to predict future design values should ideally be based on at least 10 days with modeled MDA8 ozone concentrations within 10 ppb of the 2008 ozone NAAQS, it seems likely that each listed monitor will have ample support for its RRF calculations from the combination of the two episodes.

Table 3-1: DFW Monitor-Specific MDA8 Ozone Data during the June 2006 Episode

Monitor	Max MDA8 Ozone (ppb)	Days ≥ 85 ppb	Days ≥ 75 ppb	Days ≥ 65 ppb	Site-specific Baseline Design Value (ppb)
Eagle Mountain Lake C75	107	8	16	23	93.3
Denton Airport South C56	106	9	13	20	93.3

Monitor	Max MDA8 Ozone (ppb)	Days ≥ 85 ppb	Days ≥ 75 ppb	Days ≥ 65 ppb	Site-specific Baseline Design Value (ppb)
Keller C17	103	8	16	22	91.0
Grapevine Fairway C70	95	5	12	20	90.7
Fort Worth Northwest C13	101	8	14	20	89.3
Parker County C76	101	5	11	18	87.7
Frisco C31	94	7	12	20	87.7
Cleburne Airport C77	98	2	10	18	85.0
Dallas Executive Airport C402	91	2	14	21	85.0
Dallas North No.2 C63	86	2	9	19	85.0
Arlington Municipal Airport C61	91	3	10	16	83.3
Granbury C73	92	3	7	18	83.0
Dallas Hinton St. C401	84	0	12	15	81.7
Rockwall Heath C69	78	0	6	17	77.7
Greenville C1006	78	0	1	12	75.0
Kaufman C71	78	0	3	18	74.7
Pilot Point C1032*	101	9	11	18	81.0*
Midlothian Tower C94*	98	2	8	17	80.5*
Midlothian OFW C52*	96	1	5	15	77.7*

* PIPT, MDLT, and MDLO did not measure enough data from 2004 through 2008 to calculate a complete baseline design value (DV_B). The DV_B shown uses all available data.

Table 3-2: DFW Monitor-Specific MDA8 Ozone Data during the August-September 2006 Episode

Monitor	Max MDA8 Ozone (ppb)	Days ≥ 85 ppb	Days ≥ 75 ppb	Days ≥ 65 ppb	Site-specific Baseline Design Value (ppb)
Eagle Mountain Lake C75	88	2	9	14	93.3
Denton Airport South C56	102	3	9	15	93.3
Keller C17	94	4	10	16	91.0
Grapevine Fairway C70	98	5	9	15	90.7
Fort Worth Northwest C13	86	2	8	16	89.3
Parker County C76	77	0	2	11	87.7
Frisco C31	101	3	9	18	87.7
Cleburne Airport C77	78	0	3	10	85.0
Dallas Executive Airport C402	95	3	6	15	85.0
Dallas North No.2 C63	90	2	6	13	85.0
Arlington Municipal Airport C61	85	1	5	8	83.3
Granbury C73	77	0	1	7	83.0
Dallas Hinton St. C401	96	2	5	14	81.7
Rockwall Heath C69	86	1	3	14	77.7
Greenville C1006	84	0	2	11	75.0
Kaufman C71	86	1	2	11	74.7
Pilot Point C1032*	87	1	8	15	81.0*
Midlothian Tower C94*	82	0	1	6	80.5*
Midlothian OFW C52*	84	0	3	7	77.7*

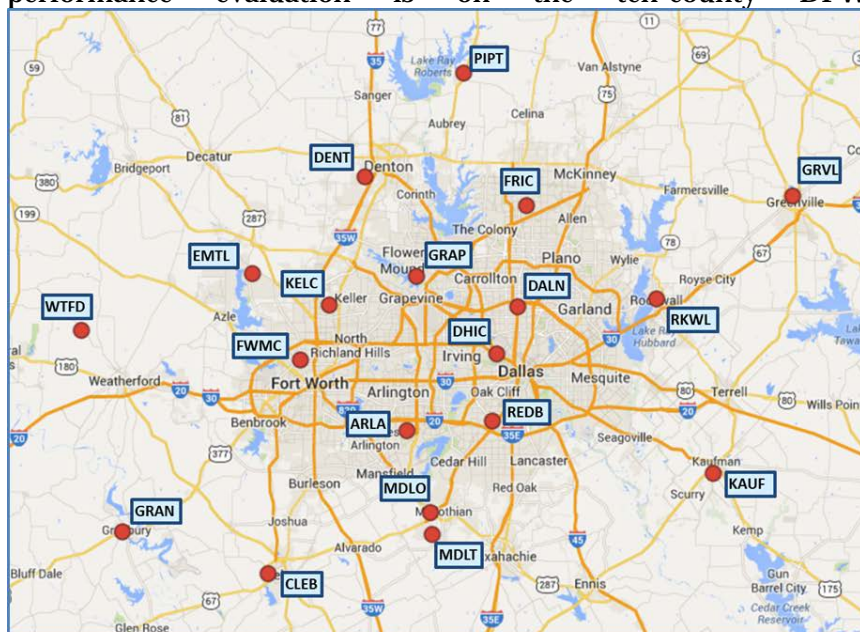
* PIPT, MDLT, and MDLO did not measure enough data from 2004 through 2008 to calculate a complete baseline design value (DV_B). The DV_B shown uses all available data.

4. CAMx MODEL PERFORMANCE EVALUATION

The CAMx modeling results were compared to the measured ozone and ozone precursor concentrations at all regulatory monitoring sites, which resulted in a number of modeling iterations to implement improvements to the meteorological and emissions modeling and subsequent CAMx modeling.

The performance evaluation of the base case modeling demonstrates the adequacy of the model to correctly replicate the relationship between levels of ozone and the emissions of NO_x and VOC. The model's ability to suitably replicate this relationship is necessary to have confidence in the model's prediction of the response of ozone to various control measures. As recommended in the EPA modeling guidance (EPA, 2007), the TCEQ has incorporated the recommended eight-hour performance measures into its evaluations but focuses largely on one-hour performance analyses, especially in the DFW area. The localized small-scale (i.e., high resolution) meteorological and emissions features characteristic of the DFW area require model evaluations to be performed at the highest resolution possible to determine whether or not the model is getting the right answer for the right reasons. Although the primary focus of the model

performance evaluation is on the ten-county DFW nonattainment area (



Site Code	Site Name
ARLA	Arlington C61
CLEB	Cleburne C77
DALN	Dallas North C63
DENT	Denton Airport C56
DHIC	Dallas Hinton Street C401
EMTL	Eagle Mountain Lake C75
FRIC	Frisco C31
FWMC	Ft. Worth Northwest C13
GRAN	Granbury C73
GRAP	Grapevine C70
GRVL	Greenville C1006
KAUF	Kaufman C71
KELC	Keller C17
MDLO	Midlothian OFW C52
MDLT	Midlothian Tower C94
PIPT	Pilot Point C1032
REDB	Dallas Executive Airport C402
RKWL	Rockwall C69
WTFD	Weatherford C76

Figure 3-3: DFW area monitors

), the TCEQ evaluated the model performance at some of the more rural monitors within Texas to assess how well the model replicates background ozone for DFW.

Also in accordance with the EPA modeling guidance, the TCEQ conducted two types of performance evaluations, operational and diagnostic. Operational evaluations include statistical and graphical measures, which compare the modeled ozone and ozone precursors to measured concentrations. Diagnostic evaluations compare the response of the model to changes in the inputs (sensitivity analyses), such as emissions, and the predictive capability of the model (diagnostic analyses), such as retrospective modeling.

4.1. Operational Evaluations

4.1.1. Statistical Measures

Statistical measures provide a quantitative evaluation of model performance. The TCEQ used EPA recommended statistics (EPA, 2007) in evaluating performance of the base case modeling, including the Unpaired Peak Accuracy (UPA), the Mean Normalized Bias (MNB) and the Mean Normalized Gross Error (MNGE). For each of these statistical measures, which use measured and modeled pairs in their calculation, the TCEQ used a modeled value based on a bi-linear interpolation of the ozone concentrations in the four grid cells around and including the monitor.

The UPA statistic compares the difference between the maximum modeled ozone concentration and the highest monitored ozone concentration found over all hours and over all monitoring stations for each day simulated. This comparison was made for both one- and eight-hour peak ozone concentrations. EPA has recommended a range of $\pm 15\text{-}20\%$ for one-hour ozone UPA comparisons, however, no range has been recommended for the eight-hour UPA comparisons. This statistic is more suited to assessing model under-prediction than over-prediction, because the model simulates ozone concentrations across the entire domain, whereas only a relatively few locations are actually monitored. Even if the model predicted the observations perfectly, its

maximum predicted concentration would exceed the maximum observed concentration unless the modeled maximum happened to occur at precisely the location of a monitor.

The MNB statistic compares the relative difference between modeled and monitored ozone concentrations, paired in time and space, averaged over all hours and over all monitoring stations. The MNB was calculated for individual episode days (i.e., averaged over all monitoring stations) and individual sites (averaged over all days). The MNB provides a measure of the model's tendency to over- or under-predict monitored ozone concentrations. A positive bias indicates that the model's ozone concentrations are higher than measured, and a negative bias indicates the converse. A bias near zero is desirable, although this does not necessarily mean the model is replicating ozone concentrations well, since combining large positive and negative relative differences can result in a near zero MNB. Since the MNB is a relative measure, it involves dividing the difference between modeled and observed concentrations by the observed concentration. For this reason, a cutoff value is used to prevent division by zero or by very small numbers.

For one-hour ozone, EPA has recommended a range of \pm 5-15% for the MNB, for monitored ozone concentration of 60 ppb or greater. For eight-hour ozone, EPA also recommends limiting the calculation of the MNB to monitored ozone concentrations over a minimum threshold of 40 ppb or 60 ppb, but no range is given for consideration of suitable performance. The TCEQ computes the MNB for both the one- and eight-hour ozone concentrations using a minimum threshold of 60 ppb for the one-hour and 40 ppb for the eight-hour. The MNB can be either positive or negative, the former indicating the model is predominantly over-predicting ozone concentrations, the latter indicating a predominant under-prediction (an MNB of zero would mean the model equally over- and under-predicted).

The MNGE statistic is similar to the MNB, except that the absolute value of the relative differences between modeled and monitored ozone concentrations, paired in time and space, averaged over all hours and over all monitoring stations is used. The MNGE was calculated for individual episode days (i.e., averaged over all monitoring stations) and individual sites (averaged over all days). This statistic is representative of the overall deviation between the modeled and monitored concentrations and is always greater than or equal to zero.

Also similar to the MNB, EPA recommends only calculating the MNGE for measured and modeled pairs where the monitored ozone concentration is greater than a minimum threshold. The TCEQ computes the MNGE for both the one- and eight-hour ozone concentrations using a minimum threshold of 60 ppb for the one-hour and 40 ppb for the eight-hour. For one-hour, the EPA-recommended range for MNGE is \leq 30-35%, but for eight-hour no range is specified.

4.1.2. Graphical Measures

Graphical measures provide a qualitative evaluation of model performance. The TCEQ used time series plots, scatter plots and peak ozone tile plots as recommended in the EPA guidance.

Time series plots are used to compare the hourly modeled concentrations with those measured at a monitor for each hour of an episode. This comparison is used to assess how well the model predicts diurnal and/or daily variation in the ozone and ozone precursor concentrations at specific locations. Comparing the time series of modeled versus measured concentrations of ozone and ozone precursors can indicate whether the model is correctly replicating the physico-chemical processes by which ozone was actually generated. Because of the large number of monitors used in the model performance evaluation and number of pollutants provided by CAMx (over 30, including some combined species like NO_x and reactive oxides of nitrogen

(NO_y)), it is not feasible to provide a comprehensive set of time series graphics for every pollutant and monitor in this document. Time series of hourly ozone and key precursors are provided for specific monitors selected because of their measured ozone concentrations or to show performance for specific precursors.

Scatter plots of hourly measured and modeled ozone and precursor concentrations show overall patterns of under- and/or over-prediction for the episode. In addition, on the scatter plots are the measured versus modeled quantile-quantile (QQ) plots, which plot the same measured and modeled concentrations as shown in the normal scatter plot, but the respective values are independently sorted from smallest to largest. The QQ plots indicate the comparability of the distributions of the measured versus modeled concentrations. If the QQ plot lies near the 1-1 line (also depicted on the plots), then it indicates that the model produces about the same number of low, medium, and high values as the monitor.

Tile plots of MDA8 ozone (overlaid with monitored maximum values) were developed to provide a visual means of assessing where the model predicts daily maximum eight-hour ozone concentrations compared to observations.

4.2. Diagnostic Evaluations

4.2.1. Sensitivity Analyses

Sensitivity analyses were conducted to check the response of the modeled ozone to changes in model inputs including meteorological parameters and precursor emissions. The results of these analyses were also used in quality assuring the input. The TCEQ conducted several sensitivity analyses, including alternative chemical mechanisms (CB05 vs. CB6r2), alternative biogenic emissions (GloBEIS vs. MEGAN), and reduced emissions of highly reactive VOCs (HRVOC) from biogenic and mobile sources.

4.2.2. Diagnostic Analyses

Diagnostic analyses were conducted to focus on the model's change in predicted ozone to changes in the ozone precursor emissions. The TCEQ conducted several diagnostic analyses, including retrospective modeling, observational modeling and source apportionment analysis.

In past SIP revisions a retrospective modeling analysis was conducted using a year prior to the SIP base case. The year prior to the SIP base case was used to allow the use of a modeling inventory that was readily available from previous SIP revision. Since a prior year was used the retrospective analysis was conducted with the model in backcast mode to obtain ozone design values for the prior year. Model response to emission changes over time could then be evaluated by comparing the predicted design values with the previously observed design values. A somewhat different approach was followed for this SIP revision since the last DFW AD SIP revision was based on a 2012 attainment year. So it was now possible to conduct a retrospective modeling analysis but in a forecast mode (from the 2006 base case to 2012 using a 2012 inventory based on that developed for the previous DFW AD SIP revision) and compare modeled predicted design values with those observed in 2012.

The observational modeling was conducted for weekdays and weekends. Weekend emissions in urban areas tend to be lower than weekday emissions primarily due to lower traffic volumes (i.e., fewer miles driven). The effect is most pronounced on weekend mornings, especially Sundays, since commuting is much lower than weekdays.

The source apportionment analysis was conducted on the future (2018) year modeling. This analysis provides an estimate of the contribution to the 2018 modeled ozone concentration from the various emission source categories in selected regions.

4.3. Episodic Model Performance Assessment for Ozone

This section presents a set of episode-wide performance assessments for one-hour and MDA8 ozone for the base case episodes. These episodic assessments are similar to the usual statistical and graphical performance measures, but are calculated across all days in the episode to provide overall model performance assessments. It would be inappropriate to rely on these summary metrics instead of performing a detailed day-by-day performance assessment; nevertheless, episode-wide statistics can provide a first-order basis for assessing model performance and for comparing performance of the current modeling platform with the one used previously. For these assessments, days with eight-hour observed ozone below 60 ppb were excluded.

4.3.1. Assessments Based on all Hourly Modeled-Observed Pairs

The first assessment (Episode Mean Relative Bias) is an extension of the usual mean normalized bias (MNB) statistic, but instead of being calculated across monitors and hours within each day, Assessment 1 is calculated across all monitors and all hours of all days in the episode. Therefore, Assessment 1 quantifies the model's tendency to over-predict or under-predict measured (observed) ozone concentrations for the overall episode. Assessment 1 is calculated as:

$$Assessment\ 1 = (IJK)^{-1} * \sum_i \sum_j \sum_k \frac{(M_{ijk} - O_{ijk})}{O_{ijk}} * 100 \quad (1)$$

where i represents one of I episode days, j represents one of J monitors, and k represents one of K hours included in the calculation ($K \leq 24$). O_{ijk} is observed ozone concentration on day i at monitor j for hour k . M_{ijk} similarly represents the modeled value at monitor j for the indicated day and hour. Model values at the monitor locations are calculated through bilinear interpolation from the four grid cell centers nearest the monitor. As is the case with the usual MNB statistic, data points with observed one-hour ozone concentrations less than 60 ppb are not included in this case, and consequently the days with monitored ozone concentrations less than 60 ppb were excluded from the calculations. Note that this performance metric, along with the three that follow, is not calculated for eight-hour ozone concentrations. Because the eight-hour concentration for an hour only differs from that of the previous hour by a single hourly concentration, both the observed and modeled values in Assessment 1 are highly inter-correlated and interpretation of the result would be very difficult.

A related statistic (Episode Mean Bias) uses the non-normalized differences to calculate the model bias in the original units of measurement (ppb) instead of percent like Assessment 1. It is shown below:

$$Assessment\ 1_A = (IJK)^{-1} * \sum_i \sum_j \sum_k (M_{ijk} - O_{ijk}) \quad (1_A)$$

The third assessment (Episode Mean Relative Error) presented is similar to Assessment 1, but the $(M - O)$ differences are replaced by their absolute values as shown below:

$$Assessment\ 2 = (IJK)^{-1} * \sum_i \sum_j \sum_k \frac{|M_{ijk} - O_{ijk}|}{O_{ijk}} * 100 \quad (2)$$

This statistic measures the overall difference between modeled and observed values, and as such includes both the bias and the spread of the differences. The lower bound for this statistic is the absolute value of the bias calculated in Equation 1, but can be considerably larger in cases where the model under-predicts on some days and over-predicts on others.

The fourth assessment (Episode Mean Error) is similar to Assessment 1_A, but uses the absolute differences instead of the relative differences as shown:

$$\text{Assessment } 2_A = (IJK)^{-1} * \sum_i \sum_j \sum_k |M_{ijk} - O_{ijk}| \quad (2_A)$$

Again, this metric is represented in the original units of measurement (ppb) instead of percent.

4.3.2. Assessments Based on Daily Peak Modeled-Observed Pairs at Monitor Sites

Assessments 3-4_A are based on the daily peaks observed and modeled at each monitor location. While these assessments are particularly suited to eight-hour ozone concentrations, it is still informative to calculate these assessments for one-hour peaks. In this (and the following) section, modeled and observed daily peak concentrations represent either one-hour or MDA8 values.

Assessment 3 (Episode Mean Site Peak Relative Bias) is akin to Assessment 1, except the sum is taken over only two indices (site and day):

$$\text{Assessment } 3 = (IJK)^{-1} * \sum_i \sum_j \frac{(M_{ij} - O_{ij})}{O_{ij}} * 100 \quad (3)$$

Assessment 3_A (Episode Mean Site Peak Bias) uses non-normalized Modeled - Observed values, and is in units of ppb (the formula is omitted for brevity).

Assessment 4 (Episode Mean Site Peak Error) is similar to Assessment 3, but with the parentheses replaced by absolute value symbols (see Equations 1 and 2). Assessment 4_A (Episode Mean Site Peak Error) is similar to Assessment 2_A, but with one fewer summation indices. These two formulae are also omitted.

4.3.3. Assessments Based on Daily Peak Modeled-Observed Concentrations Unpaired in Space and Time

This assessment compares two values per day, domain-wide peak modeled ozone concentration and the domain-wide observed concentration. This assessment is primarily useful for ensuring that the model is simulating peak concentrations that are reasonably close to the highest observed values. Because the model simulates ozone concentrations across the domain while the observed concentrations are limited to the monitor locations, it is reasonable to expect the modeled peak to exceed the observed peak.

Assessment 5 (Episode Relative Mean Domain-Wide Peak-Peak Comparison) is similar to Assessment 3, but this time the sum is taken only over days:

$$\text{Assessment } 5 = I^{-1} * \sum_i \frac{(M_i - O_i)}{O_i} * 100 \quad (4)$$

Similarly, Assessment 5_A (Episode Mean Domain Wide Peak-Peak Comparison) provides the mean modeled-observed non-normalized difference (equation not shown).

4.3.4. Episodic Model Performance Assessment

Using these ten model performance assessments, model performance is summarized for the current base case (Reg2h) for both the June and August/September, 2006 episodes. For comparison purposes, the Reg2_MVS base case used in the 2011 AD SIP revision is also shown.

Figure 4-1: *Normalized episode mean DFW one-hour ozone performance statistics* compares the one-hour relative assessments across model platforms and Figure 4-2: compares the one-hour assessments (non-normalized) across episodes and platforms. Note that for metrics comparing hourly observed-modeled data pairs (mean bias and error and relative mean bias and error) data points are excluded in cases where the observed concentration is < 60 ppb. For metrics comparing peak one-hour modeled and observed concentrations (both paired and unpaired), days with observed peak ozone concentrations < 60 ppb were excluded: June 16, 20, 21, and 22; July 2; August 13 and 28; and September 4, 2006.

Two facets of Figure 4-1 are immediately evident: First, the Reg2h base case corrects the under-prediction bias seen previously with Reg2_MVS in the June period (first set of bars, Episode Mean Relative Bias) and only slightly over-predicts the station peaks (third set of bars, Episode Mean Site Peak Relative Bias), whereas Reg2_MVS under-predicted those values. The unpaired peak comparison (fifth set of bars, Episode Mean Domain-wide Peak-Peak Comparison) shows some larger difference with Reg2h, but it is not unreasonable to expect some disparity since the modeled peak can occur at locations some distance from the nearest monitor. The second observation is that the bias for the August/September episode (first set of bars, Episode Mean Relative Bias) is considerably greater than for the June episode, despite similar model configurations.

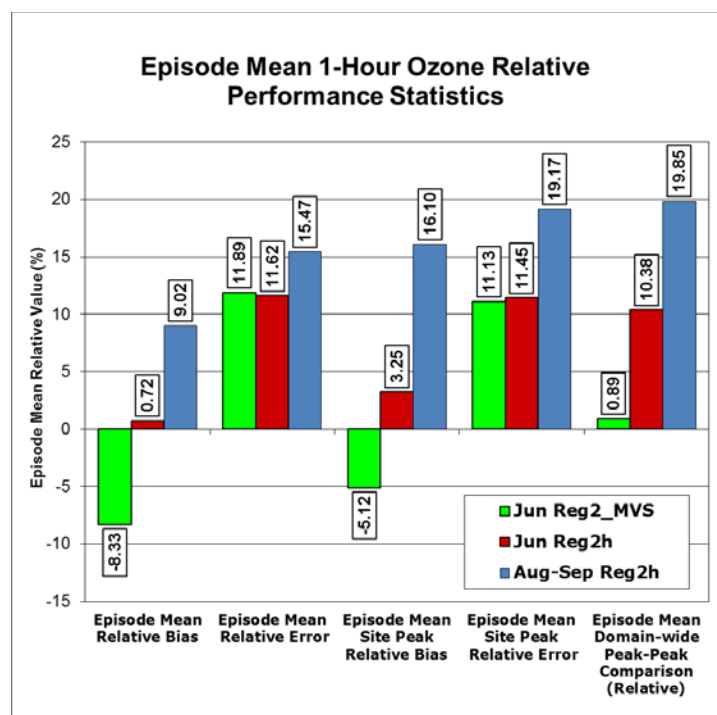


Figure 4-1: Normalized episode mean DFW one-hour ozone performance statistics

Figure 4-2: Episode mean DFW one-hour ozone performance statistics allows us to consider the bias in terms of ppb, rather than percent, and it shows that for the August-September episode, on average Reg2h over-predicts monitored ozone concentrations > 60 ppb by over 6 ppb (first set of bars) and over-predicts monitor peaks by nearly 10 ppb (third set of bars), compared with only about 2 ppb in the June episode.

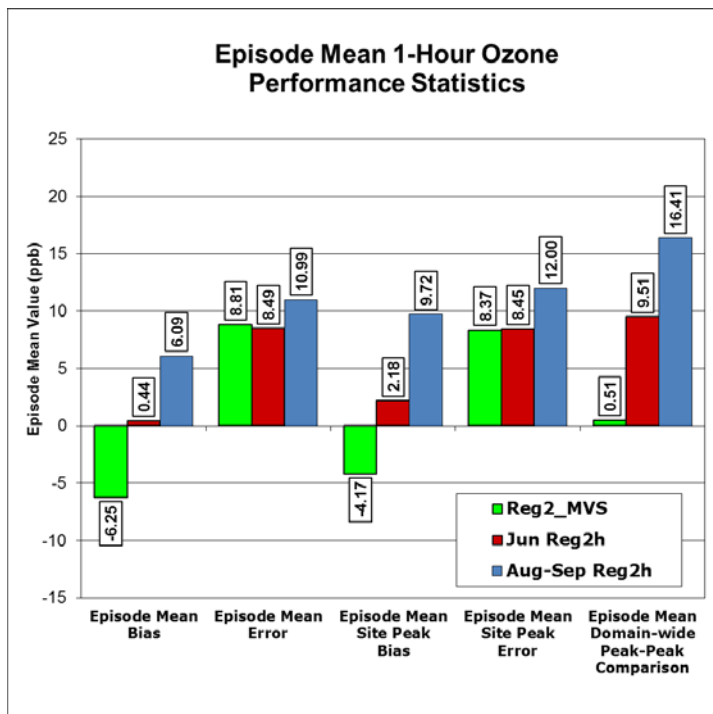


Figure 4-2: Episode mean DFW one-hour ozone performance statistics

Figure 4-3: and Figure 4-4: Episode mean DFW MDA8 ozone performance statistics Figure 4-4: compare the maximum daily eight-hour average ozone statistics among model configurations. These comparisons are based only on MDA8 ozone concentrations (Assessments 3-5_A), since comparisons between rolling eight-hour averages are not particularly meaningful. The same days excluded for the one-hour comparisons discussed above are excluded here as well. For the June episode, model performance for both reg2h and reg2_MVS is comparable, except the under-predictive bias seen in reg2_MVS is replaced with an over-prediction of similar magnitude in ppb as seen in Figure 4-4, first set of bars. As shown in Figure 4-3, the relative bias and error are somewhat higher for reg2h because over-prediction is more common at low ozone concentrations; hence the divisors are smaller in Assessments 3, 4, and 5 above). For the August/September episode, the average over-prediction of observed MDA8 ozone values is over 10 ppb (Figure 4-4, first set of bars), which is sufficient to cause concern. The TCEQ is investigating the causes of this bias and will take appropriate steps to ameliorate it, if possible, in the near future.

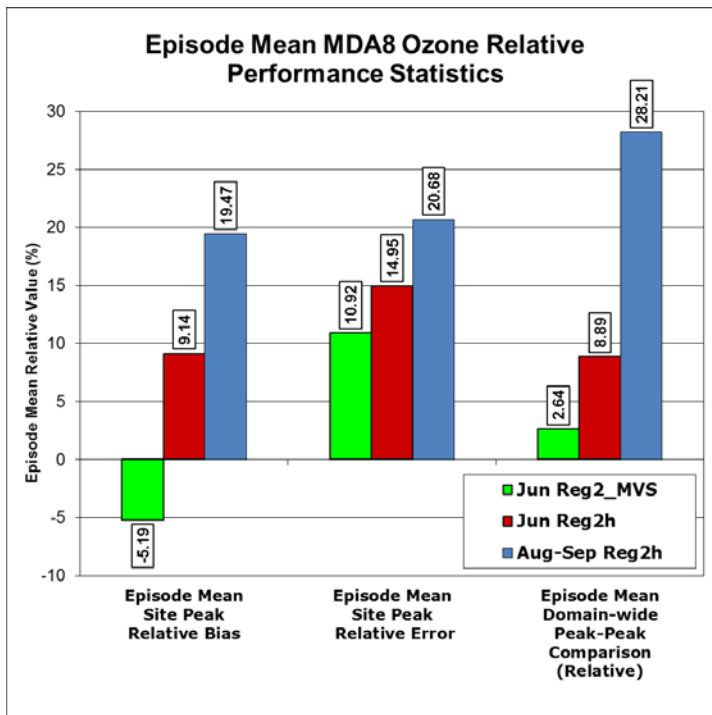


Figure 4-3: Normalized episode mean DFW MDA8 ozone performance statistics

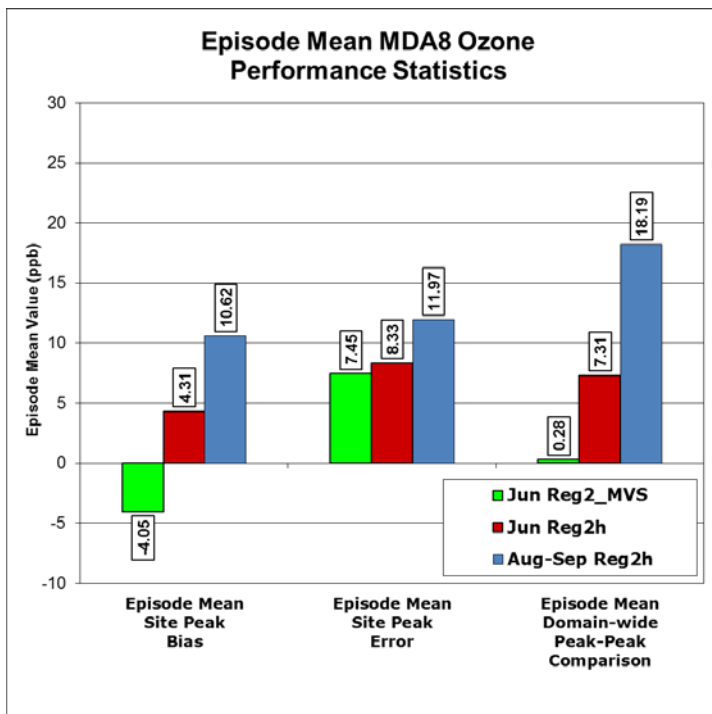


Figure 4-4: Episode mean DFW MDA8 ozone performance statistics

4.4. Statistical Performance Measures

The statistical measures UPA, MNB and MNGE were calculated comparing measured and bi-linearly interpolated modeled ozone concentrations for all episode days and regulatory monitors. *Figure 4-5: Modeled and observed one-hour and MDA8 ozone concentrations for the June 2006 episode* shows comparisons of peak area-wide one-hour and MDA8 ozone concentrations with observations for the June episode. While the actual UPA statistic is not displayed directly, it is shown implicitly by the dashed lines above and below the line representing the observations. These dashed lines show the nominal $\pm 15\%$ error bound often used as a rule-of-thumb measure of model peak predictive accuracy. If a modeled value lies outside the $\pm 15\%$ bounds then it may indicate some performance issues on that day, especially if the modeled peak lies below the lower band indicating insufficient ozone produced on that day. The model generally produces peaks higher than observed, since the model peak can occur anywhere in the area while the monitored peak can be located at only a few discrete locations. Modeled peaks far and/or consistently above the upper band, however, may indicate that the model is producing peak concentrations that are too high. Along with the current base case (reg2h) values, the figure shows the reg2_MVS values from the 2011 DFW ozone attainment demonstration.

The top panel in Figure 4-5 shows that the reg2h base case and the reg2_MVS base case both track fairly well the rise and fall of the observed ozone concentrations. The reg2h modeling shows a small tendency for under-prediction, with only June 17 and June 18 falling outside the lower 15% range, while the reg2_MVS modeling tended to produce lower ozone peaks overall. Both base cases generally stayed within the upper 15% range, although Reg2h did stray far outside the line on June 3, and to a lesser extent on June 7, 8, 12, and 29, and also for the low-ozone days on June 16 and 20 through 23. In general, though, both the current reg2h and past reg2_MVS base cases predicted the domain-wide one hour peaks well.

A similar picture is seen in the lower panel of Figure 4-5 for MDA8 ozone. Again, both reg2h and reg2_MVS follow the rise and fall of eight-hour ozone through the June episode, with higher ozone peaks in the former. The modeled peak concentration for reg2h only fell below the lower 15% bound on one day (June 17), and stayed within the upper 15% range on all but four days with peak MDA8 ozone > 70 ppb (June 3, 8, 12 and 29).

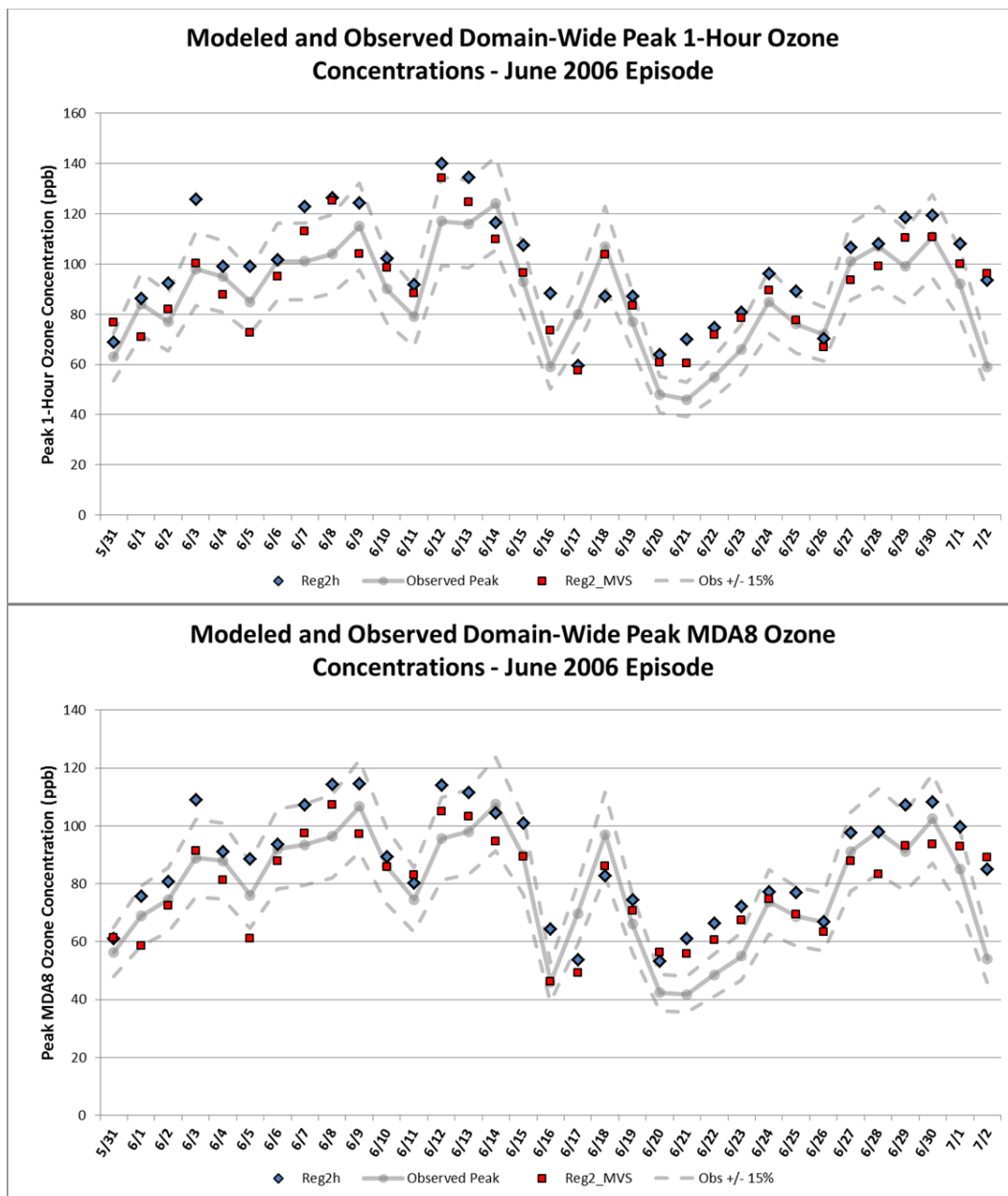


Figure 4-5: Modeled and observed one-hour and MDA8 ozone concentrations for the June 2006 episode

Observed ozone peaks are shown in gray, with $\pm 15\%$ bands. The reg2h base case is depicted in blue, while the reg2_MVS base case values are depicted in red.

Figure 4-6: Modeled and observed one-hour and MDA8 ozone concentrations for the August/September 2006 episode, on the other hand, shows that the reg2h base case concentrations of both one-hour and MDA8 ozone are significantly higher than the observed peaks on most days. The magnitude and frequency of over-prediction indicates that the model in general predicts ozone peaks too high to simply result from the disparity in spatial coverage between the model and the monitoring network. However, the model did track quite well a four-day ozone event beginning on August 30 and running through September 2.

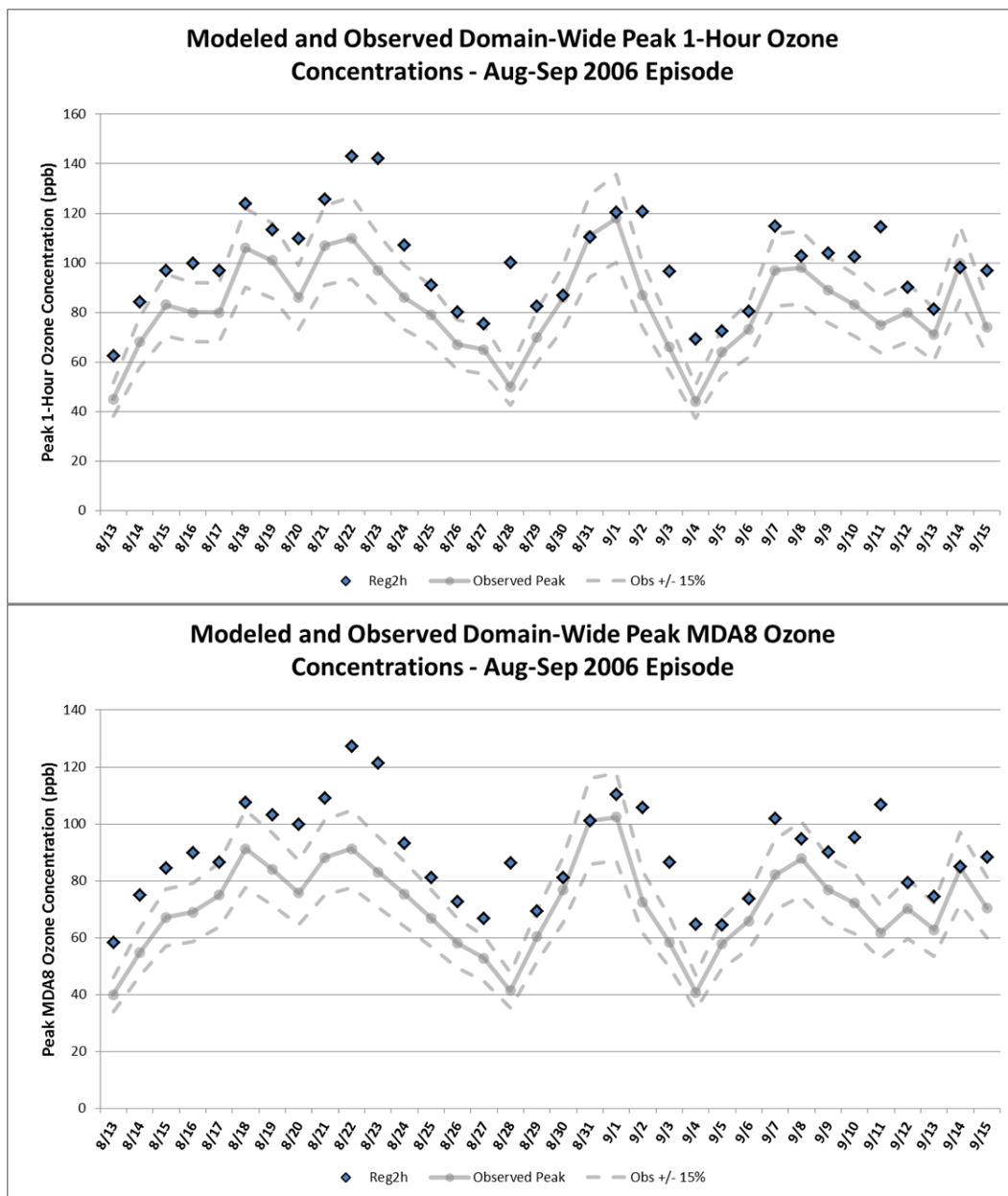


Figure 4-6: Modeled and observed one-hour and MDA8 ozone concentrations for the August/September 2006 episode

Observed ozone peaks are shown in gray, with +/- 15% bands. The reg2h base case is depicted in blue.

Figure 4-7: Model mean relative bias and error for days in the June 2006 episode shows the daily model, error, and peak ozone predictions for the reg2h and previously-used reg2_MVS base cases for both one-hour and MDA8 ozone concentrations. The plots (known colloquially as “soccer goal” plots because of the resemblance to a bird’s eye view of one end of a soccer field), indicate the originally recommended error tolerances of 15% and 30% for relative bias and error for one-hour ozone (top). Although EPA has not established similar tolerances for eight-hour ozone, the goal box is shown on the eight-hour plots (bottom) for reference. Most days modeled lie within the goal, indicated by the red dashed lines, for both One-hour and MDA8 ozone concentrations and show a slight shift to the right for reg2h, reflective of the modest increase in

ozone concentrations in the newer base case, but overall statistical performance based on relative bias and error is very similar between the 2011 and 2014 platforms.

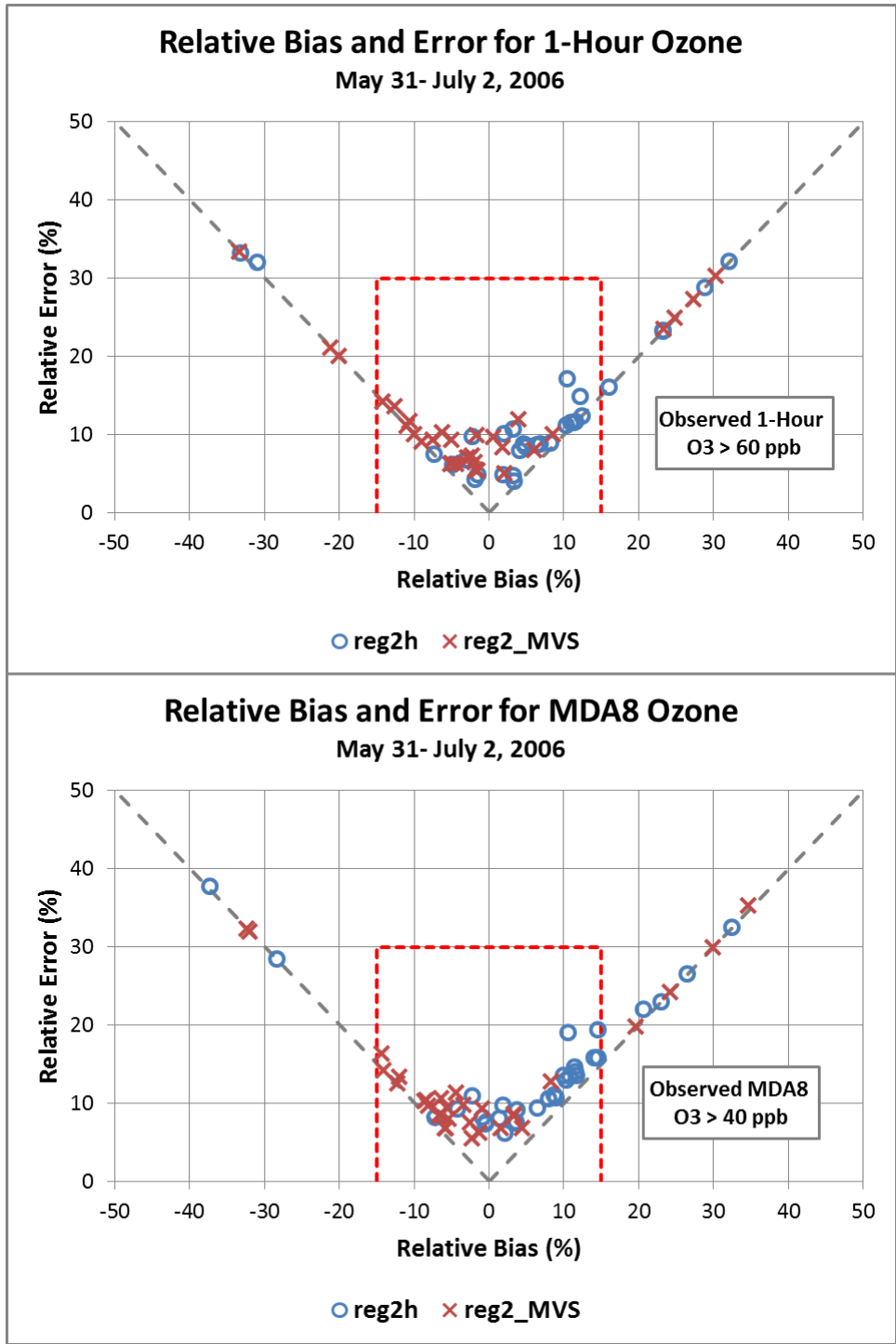


Figure 4-7: Model mean relative bias and error for days in the June 2006 episode

Figure 4-8: Model mean relative bias and error for days in the August/September 2006 episode is similar to the previous figure, except it plots the August-September performance statistics for the reg2h base case only. In this case, over half of the modeled days lie outside the box to the right, reflecting the pervasive over-prediction seen throughout the episode.

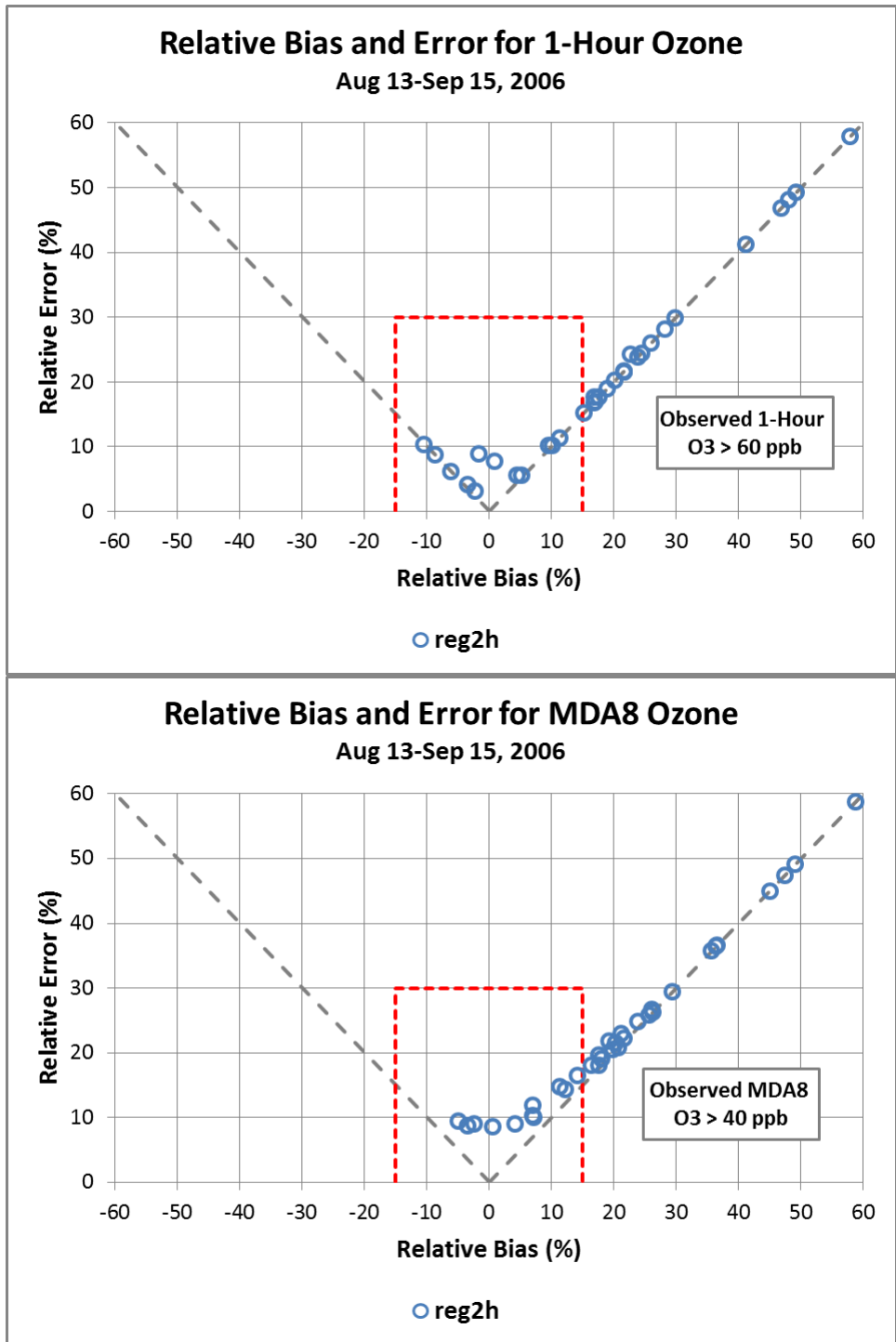


Figure 4-8: Model mean relative bias and error for days in the August/September 2006 episode

Table 4-1: Model mean relative bias and error for one-hour and MDA8 ozone concentrations by site, June 2006 episode shows important performance metrics calculated across days at each site for the June episode. These metrics show how model performance varies spatially and how well the model predicts ozone concentrations at monitors with the highest design values. The four metrics displayed are mean relative bias and mean error for one-hour concentrations with observed concentrations above 60 ppb and mean relative bias and error for MDA8 ozone with observed concentrations above 40 ppb. The table is color coded to highlight the best- and worst-performing sites: light blue indicates bias within $\pm 5\%$ and error $\leq 10\%$, while light yellow indicates bias between 5 and 10% (+ or -) or error between 10% and 15%. Orange shading indicates bias $\geq 10\%$ or error $\geq 15\%$. Note that all sites attain the nominal performance goals of 15% bias and 30% error for both one-hour and MDA8 ozone.

For one-hour ozone, all but two sites, Eagle Mountain Lake and Grapevine, show relative bias within the -5 to 5% range, and only two sites have relative error > 15%, showing good model performance at nearly all area monitoring locations. For MDA8 ozone, all sites show some positive bias except Eagle Mountain Lake, but only Greenville and Grapevine show bias > 10%. These latter two sites are joined by Midlothian OFW as the only sites with > 15% error. The best performing sites overall were three sites on the outskirts of the DFW area: Cleburne, Granbury, and Kaufman, while Grapevine exhibited the overall worst performance (although still within the nominal EPA error bounds).

Table 4-1: Model mean relative bias and error for one-hour and MDA8 ozone concentrations by site, June 2006 episode

Site	Peak 1-hour Ozone Mean Relative Bias	Peak 1-hour Ozone Mean Relative Error	MDA8 Ozone Mean Relative Bias	MDA8 Ozone Mean Relative Error
Arlington C61	3.89	13.51	7.17	13.51
Cleburne C77	0.64	9.47	4.38	9.37
Dallas North C63	-2.01	16.79	7.19	14.97
Denton Airport C56	0.04	11.08	4.51	10.95
Dallas Hinton Street C401	1.36	13.13	9.03	13.72
Eagle Mountain Lake C75	-5.52	12.22	0.07	9.96
Frisco C31	-1.55	12.38	5.25	11.85
Fort Worth Northwest C13	-1.54	12.21	1.51	10.08
Granbury C73	1.41	9.2	4.58	8.96
Grapevine C70	5.81	15.22	12.85	16.8
Greenville C1006	2.26	12.18	11.19	17.33
Kaufman C71	2.06	9.92	8.62	14.6
Keller C17	-1.44	11.12	3.81	11.12
Midlothian OFW C52	4.32	13.63	8.66	15.3
Midlothian Tower C94	1.64	11.09	5.64	12.25
Pilot Point C1032	1.23	10.76	7.89	12.62
Dallas Exec. Airport C402	-2.14	11.99	3.5	12.71
Rockwall C69	1.73	10.73	6.77	13.84

Site	Peak 1-hour Ozone Mean Relative Bias	Peak 1-hour Ozone Mean Relative Error	MDA8 Ozone Mean Relative Bias	MDA8 Ozone Mean Relative Error
Weatherford C76	-0.13	9.34	2.33	7.76

Table 4-2: Model mean relative bias and error for one-hour and MDA8 ozone concentrations by site, August/September 2006 episode is similar to Table 4-1 but for the August/September episode. Two additional colors, light red (pink) and medium-red were added to indicate sites with bias between 15% and 20% or error between 20 and 25%, and bias > 20% or error > 25%, respectively.

The best performing sites are Weatherford, Midlothian Tower, and Grapevine with one-hour relative bias < 5% and error < 15%, though the MDA8 bias and error are higher. Most sites exhibit a MDA8 bias > 15%.

Table 4-2: Model mean relative bias and error for one-hour and MDA8 ozone concentrations by site, August/September 2006 episode

Site	Peak 1-hour Ozone Mean Relative Bias	Peak 1-hour Ozone Mean Relative Error	MDA8 Ozone Mean Relative Bias	MDA8 Ozone Mean Relative Error
Arlington C61	12.85	16.95	25.35	26.38
Cleburne C77	8.79	13.34	20.04	20.96
Dallas North C63	11.07	19.64	19.67	20.85
Denton Airport C56	9.09	15.58	17.16	19.16
Dallas Hinton Street C401	4.4	18.46	17.76	19.76
Eagle Mountain Lake C75	6.51	16.82	14.59	17.39
Frisco C31	11.82	17.54	17.96	19.4
Fort Worth Northwest C13	9.49	17.68	16.55	19.47
Granbury C73	10.39	19.8	19.91	22.11
Grapevine C70	4.7	11.75	13.19	17.25
Greenville C1006	8.93	17.01	18.28	20.07
Kaufman C71	10.76	13.91	21.17	22.41
Keller C17	10.9	13.53	24.18	24.95
Midlothian OFW C52	15.77	17.83	18.49	18.95
Midlothian Tower C94	4.27	13.15	16.67	20.72
Pilot Point C1032	12.89	16.51	21.12	22.59
Dallas Executive Airport C402	5.78	14.75	18.5	19.94
Rockwall C69	10.49	12.95	15.43	16.43
Weatherford C76	4.27	9.72	9.66	12.18

4.5. Graphical Performance Measures

The statistical measures presented above provide a high-level assessment of the model's ability to predict high ozone concentrations, and to some extent can be used in a pass-fail approach to judging model performance on individual days and at specific monitoring locations, but offer few clues to how the model performs across space and time, nor to the processes leading to the model's predictions. Time series plots offer the opportunity to follow ozone formation through the course of a day, and scatter plots provide a visual means to see how the model performs across the range of observed ozone and precursor concentrations and (via QQ plots) to see how well the distribution of modeled concentrations matches those observed. Peak ozone contour plots show how high ozone is distributed spatially on each day and how the modeled spatial distribution matched that observed across the monitoring network, and animated contour plots provide insights into the diurnal life cycle of ozone and its precursors including emissions, photochemical production, advection, dispersion, and removal.

Time series and scatterplots are ideal for examining model performance at specific monitoring locations. The next section will focus on five representative locations: Kaufman (KAUF), a site typically upwind of the densely-populated DFW urban core which often measures background air entering the DFW area, Hinton Street (DHIC) and Fort Worth Northwest (FWMC), two urban sites with speciated hourly hydrocarbon measurements, and Eagle Mountain Lake (EMTL) and Denton (DENT), two sites downwind of the DFW area that typically measure the highest ozone concentrations. Note that ozone concentrations are always plotted on the same scale (0–140 ppb) to allow cross-comparability among sites, but for other pollutants the scale varies from site to site. On the scatter plots ozone is plotted linearly, but other pollutants, which often exhibit a wide range of concentrations, are plotted on a log-log scale.

4.5.1. Time Series and Scatter Plots for Selected Monitors

4.5.1.1. Kaufman

As seen in Figure 3-3 above, Kaufman C71 (KAUF) is southeast of the DFW area and on most days measures concentrations of ozone and NO_x characteristic of background air entering the urban areas. Time series and scatter plots of modeled and measured ozone and NO_x for the June 2006 episode are shown in *Figure 4-9: Time series showing observed ozone (top) and NO_x (center) at Kaufman C71 for the June 2006 episode*. The diurnal ozone pattern is simulated fairly well at Kaufman C71 (top panel) but the model generally over-predicts ozone concentrations. This is especially evident in the scatter plot at lower left in the figure. The model simulates observed ozone concentrations in the 70 ppb range well as exhibited by the QQ plot in purple, showing only about a 5 ppb bias in this range. At around 40 ppb, the bias is higher though. Modeled NO_x concentrations are generally quite good, except for a few very high observations at night or in the early morning.

Figure 4-10: Time series showing observed ozone (top) and NO_x (center) at Kaufman C71 for the August-September 2006 episode shows the same data for the August-September 2006 episode. Again the model shows a tendency to over-predict ozone, especially at lower concentrations and especially at night, but the model does do slightly better in this episode for the highest observed concentrations. NO_x, on the other hand, tends to be generally under-predicted in this episode at all concentrations.

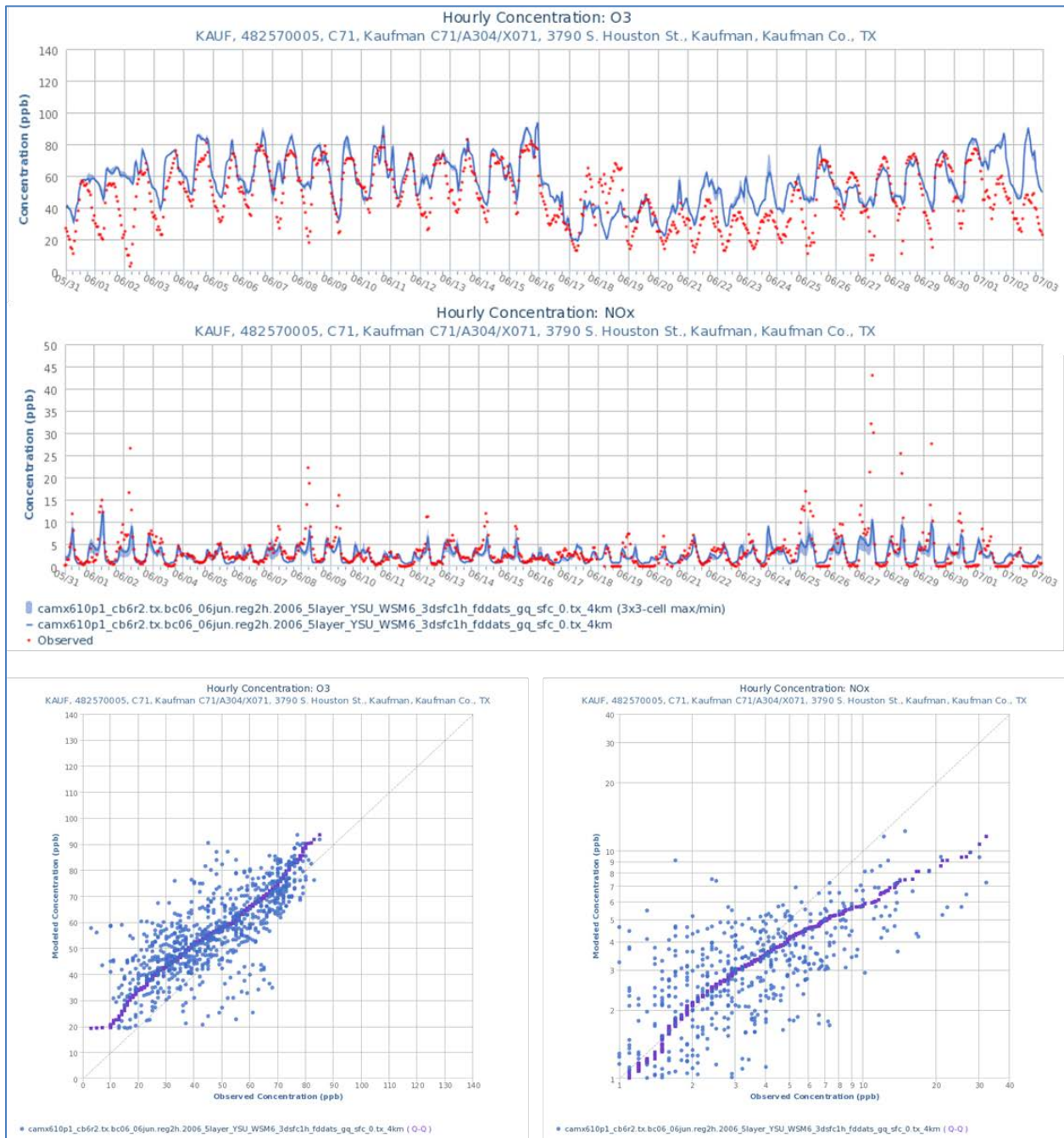


Figure 4-9: Time series showing observed ozone (top) and NO_x (center) at Kaufman C71 for the June 2006 episode

Shaded bands indicate the minimum and maximum concentrations within the 3×3 array of grid cells centered on the monitor. Also shown are scatter plots of the same data (bottom), overlaid with QQ plots.

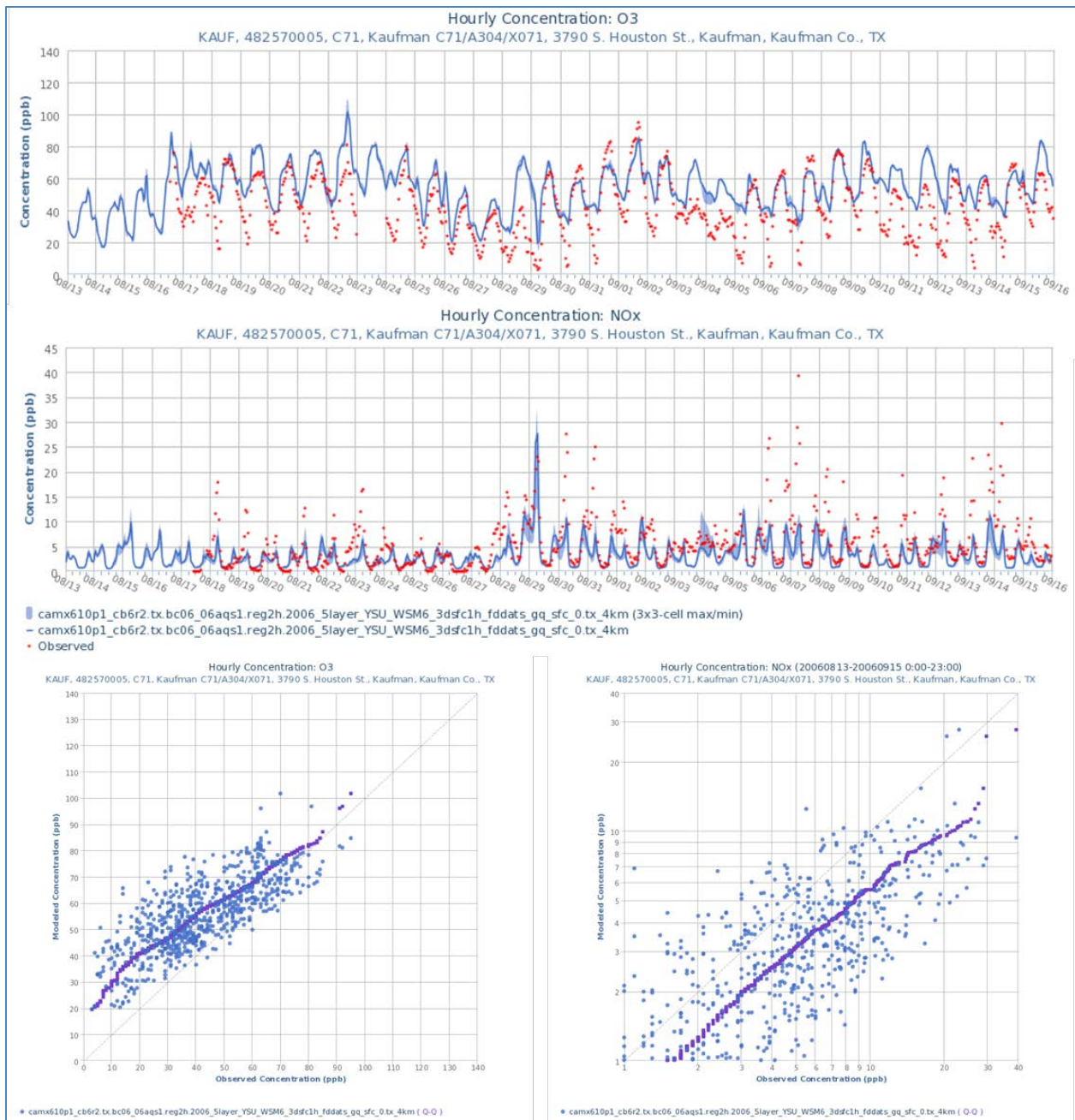


Figure 4-10: Time series showing observed ozone (top) and NO_x (center) at Kaufman C71 for the August-September 2006 episode

Shaded bands indicate the minimum and maximum concentrations within the 3x3 array of grid cells centered on the monitor. Also shown are scatter plots of the same data (bottom), overlaid with Q-Q plots.

4.5.1.2. Hinton Street

The Hinton Street C401 (DHIC) monitor site is located in a light-industrial area approximately eight km northwest of downtown Dallas. Because of its urban location it typically does not record the highest ozone concentrations in the area (these are usually farther downwind of the urbanized areas), but occasionally sees high ozone. Figure 4-11 shows time series and scatter plots of modeled and measured ozone and NO_x for the June 2006 episode. Ozone performance

for this site is quite good in June, with the diurnal ozone pattern replicated well. The scatter plot at bottom left shows almost no bias across the entire range of observed concentrations.

NO_x, on the other hand, tends to be over-predicted by up to 50%. It is worth noting that the modeled and observed concentrations, especially of primary pollutants such as NO_x, are somewhat incommensurate particularly in urban or industrial areas. The modeled concentrations are representative of the average concentration over a 4 km × 4 km area, while monitored concentrations can be heavily influenced by nearby sources such as highways or stationary emission sources. Thus, even a systematic bias in pollutant concentrations does not necessarily indicate a problem with model performance¹, although such a pattern widely repeated across the modeling domain would be cause for concern and bears investigation. The Hinton Street site itself is within one km of the Interstate 35 freeway, less than one-half km of a major arterial, and less than 100 meters (m) from a large publisher, so influences from these nearby sources should be taken into account when interpreting observations at this location.

Figure 4-12: *Time series showing observed ozone (top) and NOX (center) at Hinton Street C401 for the August-September 2006 episode.* Shaded bands indicate the minimum and maximum concentrations within the 3×3 array of grid cells centered on the monitor. Also shown are scatter plots of the same data (bottom), overlaid with QQ plots. shows the same information as Figure 4-11 but for the August/September episode. Overall model performance for this episode is fair, with much of the bias seen in the ozone scatter plot (bottom left in the figure) due to over-predictions on a few low-ozone days and on a couple of high-ozone days, August 23. NO_x concentrations show the same modest positive bias seen in the June episode.

Because Hinton Street C401 also has an automatic Gas Chromatograph (auto-GC) speciated hydrocarbon monitor, it provides an opportunity to examine performance of several ozone precursors (keeping in mind the above caveats about commensurability). *Figure 4-13: Time series showing observed and modeled concentrations of four CB6 species (top to bottom): PAR, ETH, OLE, and ISOP at Hinton Street C401 for the June 2006 episode.* Shaded bands indicate the minimum and maximum concentrations within the 3×3 array of grid cells centered on the monitor. shows time series of four CB6 hydrocarbon species: PAR, ethene (ETH), terminal olefins (OLE), and isoprene (ISOP) for the June episode. PAR (top series in Figure 4-13) does not represent a distinct chemical species but rather a class of bonds between carbon atoms in hydrocarbon compounds. As such, it is composed of pieces of a very wide variety of organic molecules, but despite its high concentrations it has very low reactivity in ozone photochemistry. It is interesting, nonetheless, because it can represent the large mass of overall hydrocarbons emitted into the atmosphere from myriad sources. PAR is not measured directly; the “observed” PAR values are derived from the auto-GC measurements by applying the same speciation to the specific hydrocarbons measured as that used to transform the emissions inventory into the chemical classes used in the CB6 chemical mechanism. Since the auto-GC only reports concentrations of 46 species, it is somewhat limited in scope compared with the inventory, which included thousands of individual compounds. But the compounds measured constitute the bulk of inventoried hydrocarbons, so useful comparisons can still be made. The CB6 species OLE is another hybrid species, but is primarily propene plus some additional bits of other olefinic compounds. ETH and ISOP are treated individually in CB6.

¹ Ozone, on the other hand, is a secondary pollutant formed in the atmosphere and is less prone to vary dramatically across a scale of a few kilometers. As such, its modeled and measured concentrations are rather more commensurate than those of primary pollutants. Even ozone can exhibit relatively sharp concentration gradients due to titration by large NO_x sources or in conjunction with tight plumes of highly reactive VOCs, but rarely to the extent seen with some other pollutants.

Figure 4-13 shows that the model over-predicts PAR, as well as ETH and OLE by a significant margin throughout the June episode. The model had previously over-predicted PAR, ETH, and OLE in the 2011 SIP revision, but the magnitude of over-prediction was smaller in each case. On the other hand, isoprene is modeled very well (it was under-predicted in 2011) with the exception of a few late-afternoon peaks probably caused by suppressed vertical mixing by the WRF meteorological model late in the day. *Figure 4-14: Time series showing observed and modeled concentrations of four CB6 species (top to bottom): PAR, ETH, OLE, and ISOP at Hinton Street C401 for the August-September 2006 episode. Shaded bands indicate the minimum and maximum concentrations within the 3×3 array of grid cells centered on the monitor.* shows the same pollutants for the August/September episode, and again the PAR, ETH, and OLE are over-predicted significantly. Isoprene is predicted reasonably well for this episode, although the late-afternoon spikes are more prevalent and intense.

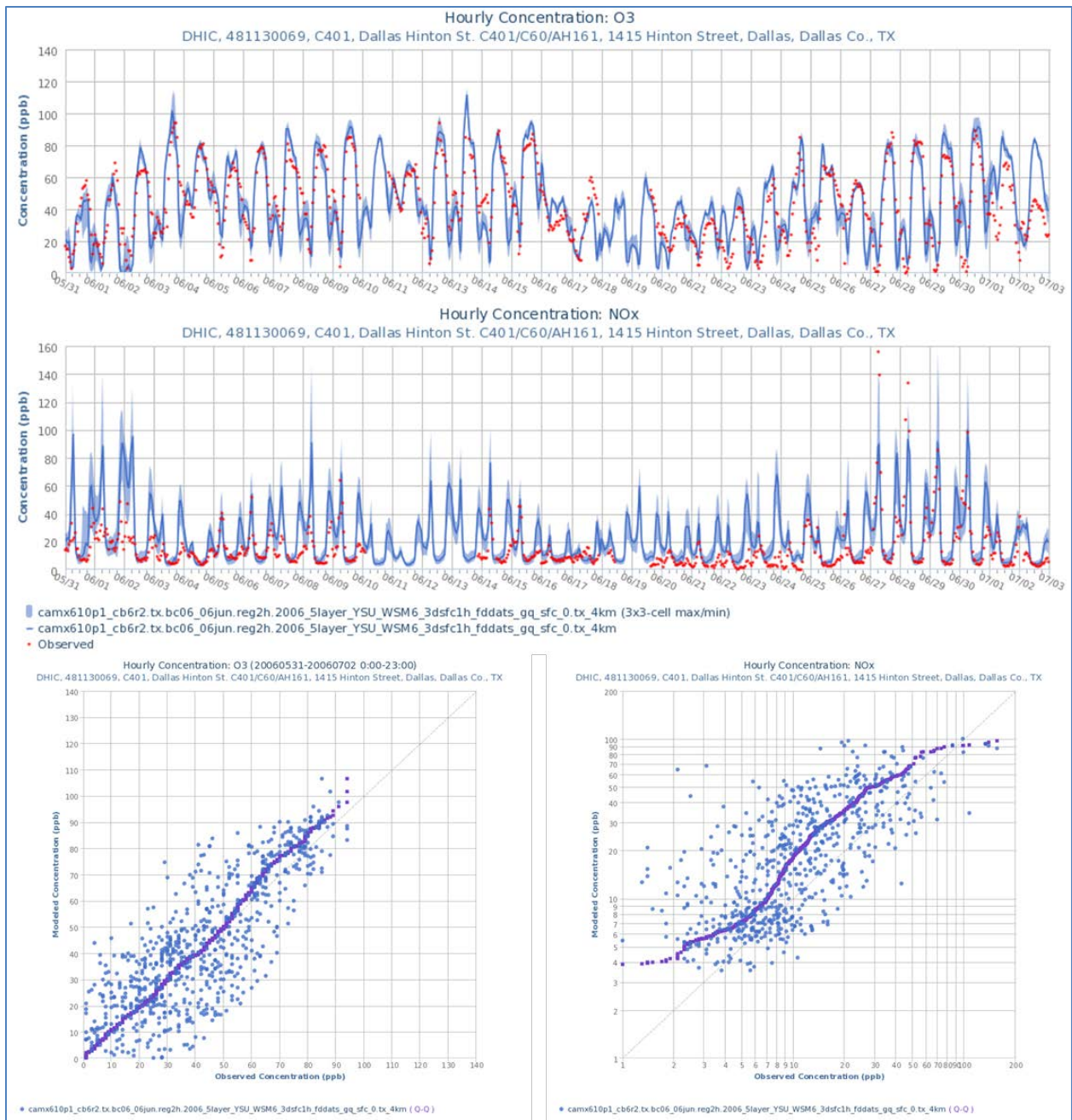


Figure 4-11: Time series showing observed ozone (top) and NO_x (center) at Hinton Street C401 for the June 2006 episode. Shaded bands indicate the minimum and maximum concentrations within the 3×3 array of grid cells centered on the monitor. Also shown are scatter plots of the same data (bottom), overlaid with Q-Q plots.

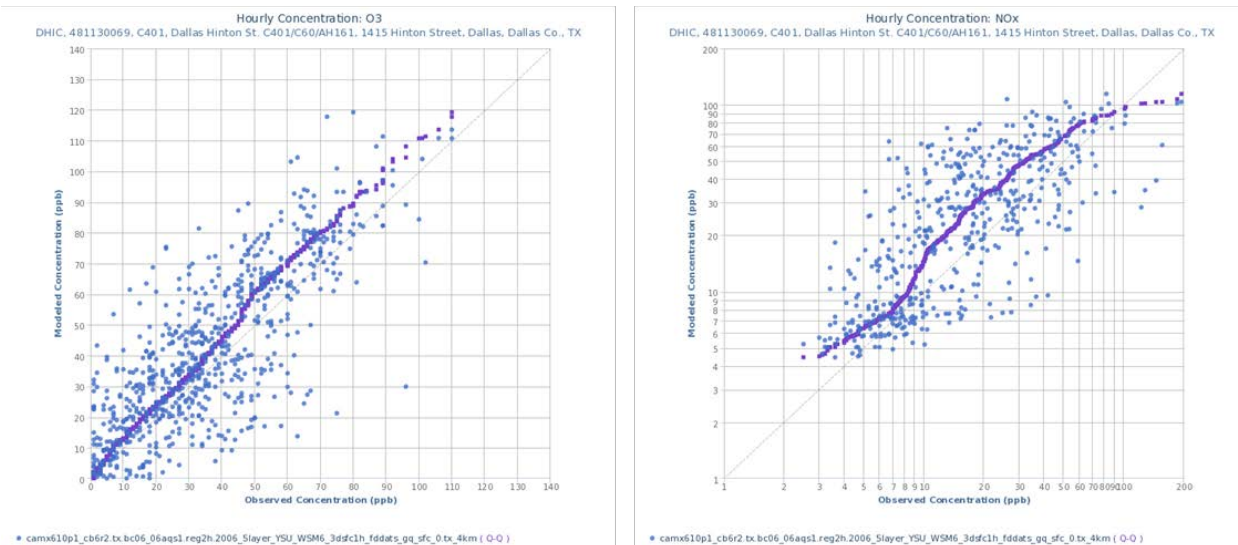
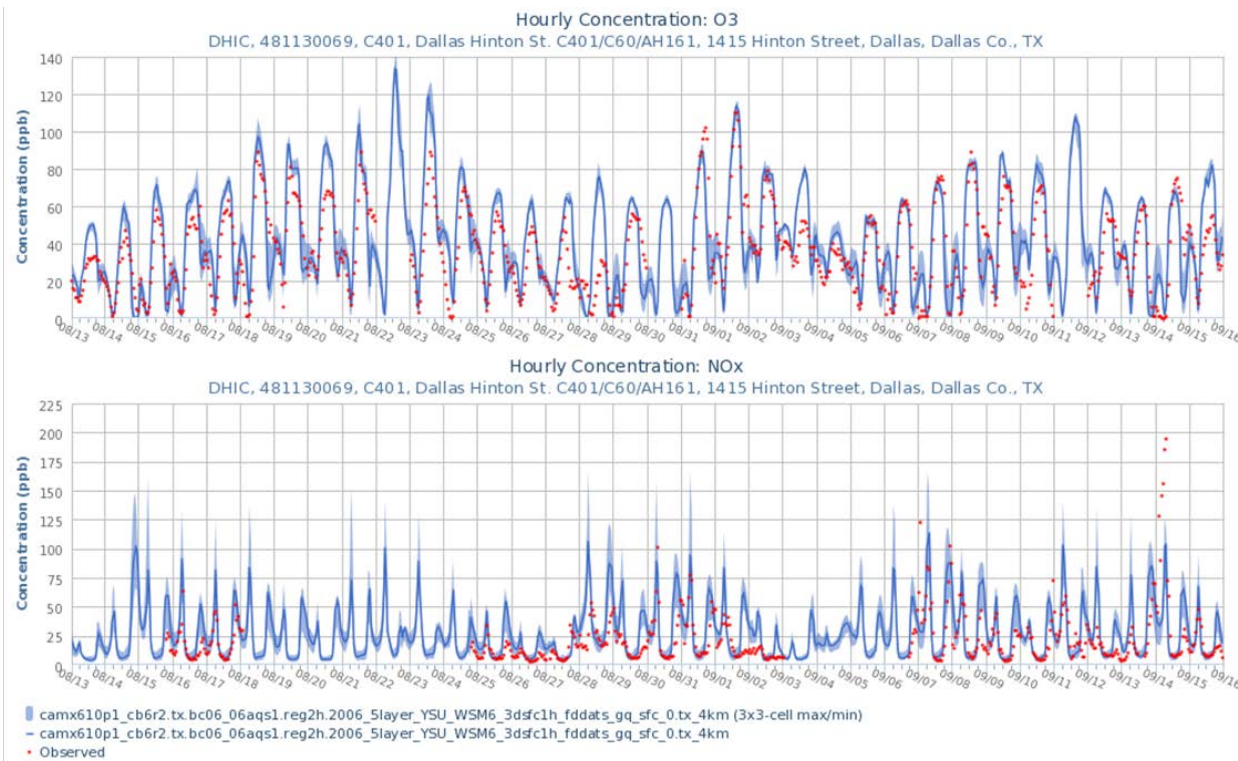


Figure 4-12: Time series showing observed ozone (top) and NO_x (center) at Hinton Street C401 for the August-September 2006 episode. Shaded bands indicate the minimum and maximum concentrations within the 3×3 array of grid cells centered on the monitor. Also shown are scatter plots of the same data (bottom), overlaid with QQ plots.

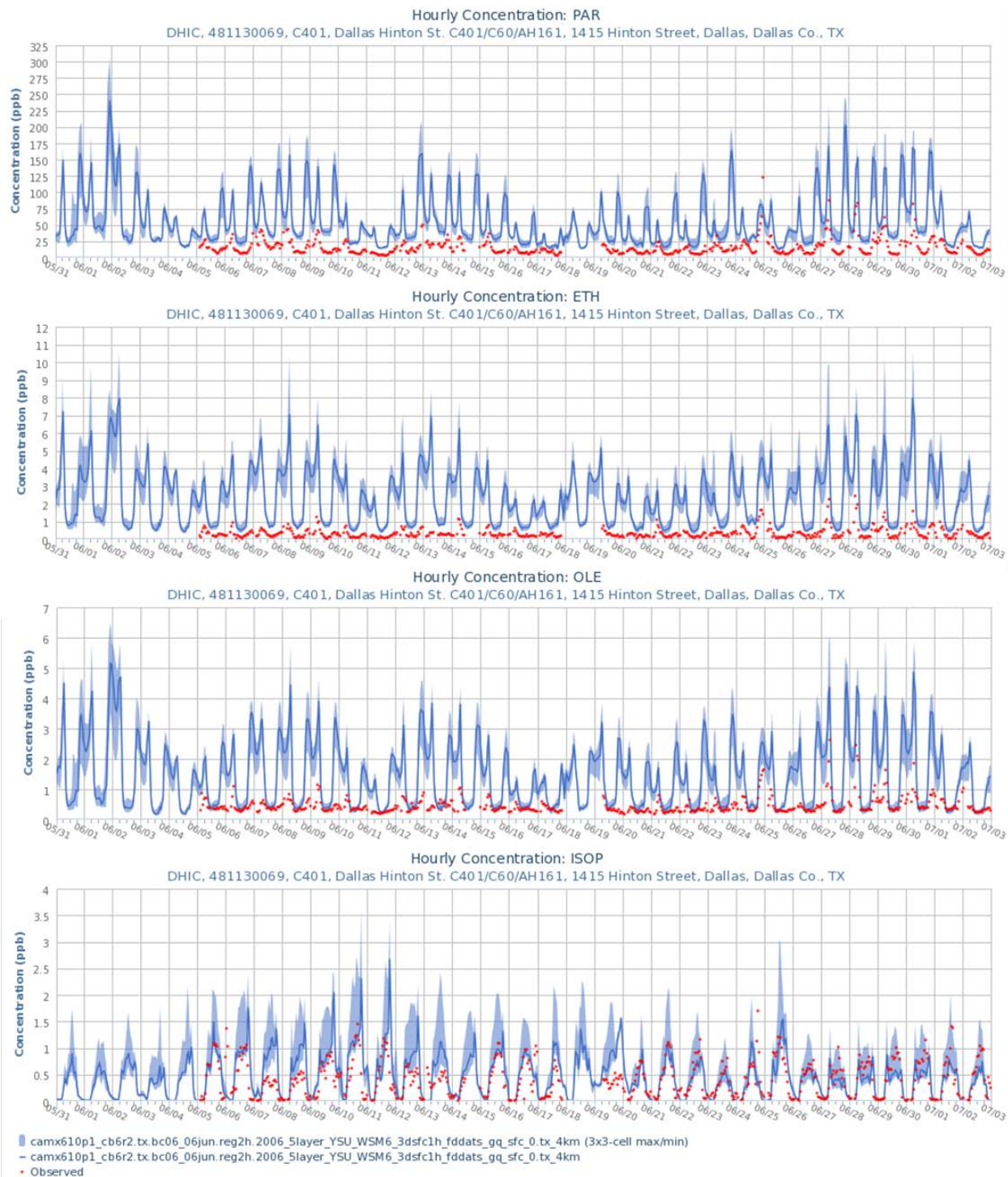


Figure 4-13: Time series showing observed and modeled concentrations of four CB6 species (top to bottom): PAR, ETH, OLE, and ISOP at Hinton Street C401 for the June 2006 episode. Shaded bands indicate the minimum and maximum concentrations within the 3×3 array of grid cells centered on the monitor.

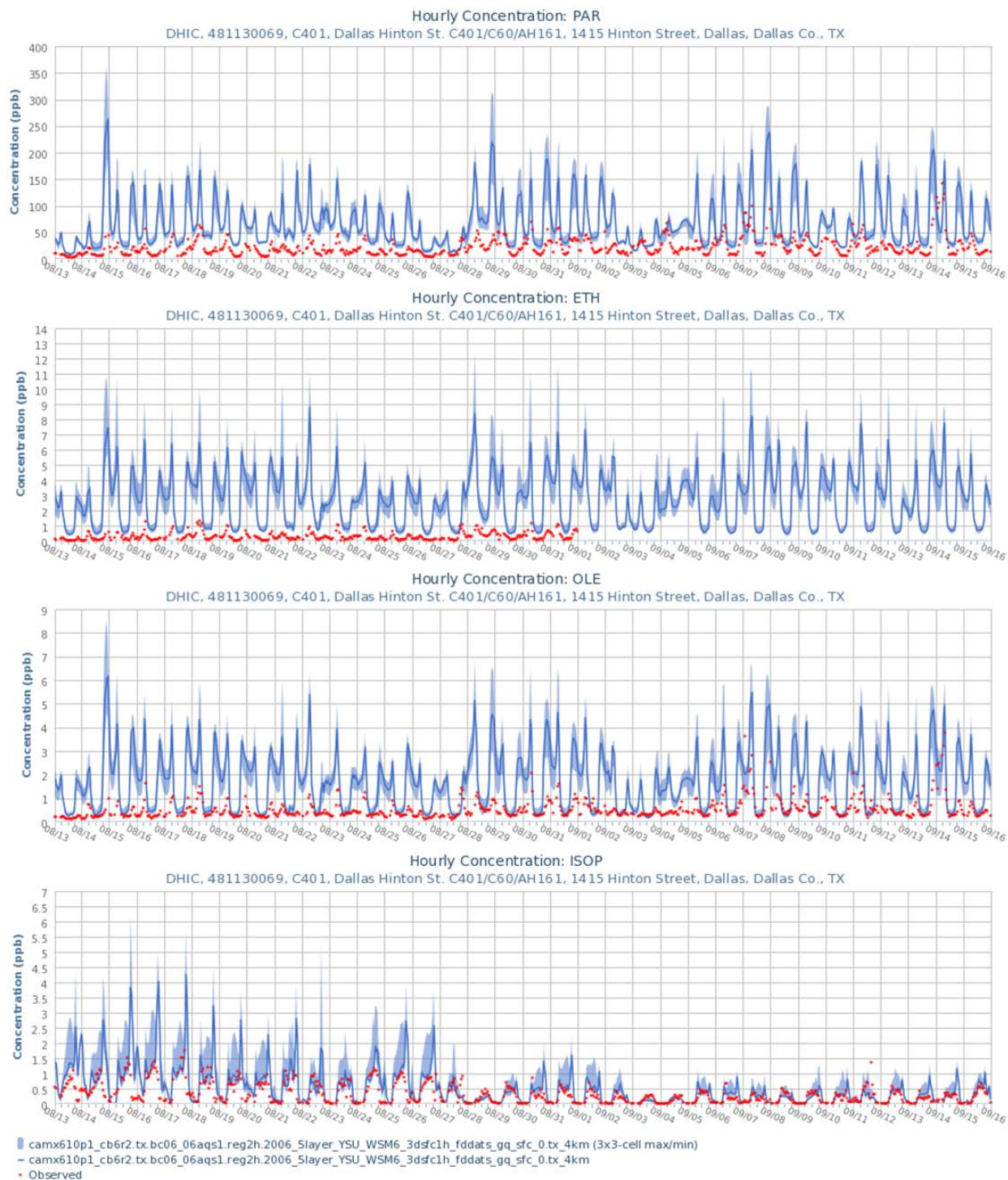


Figure 4-14: Time series showing observed and modeled concentrations of four CB6 species (top to bottom): PAR, ETH, OLE, and ISOP at Hinton Street C401 for the August-September 2006 episode. Shaded bands indicate the minimum and maximum concentrations within the 3x3 array of grid cells centered on the monitor.

4.5.1.3. Fort Worth Northwest

The Fort Worth Northwest C13 (FWMC) site is located near the south end of the main runway of the Meacham Airport in north-central Fort Worth. The airport is used by private, charter, and commuter aircraft and does not serve large jetliners. The monitor sees some arterial traffic but is over two miles from the nearest freeway so is not as heavily influenced by on-road mobile sources as is Hinton Street.

Figure 4-15: Time series showing observed ozone (top) and NO_x (center) at Fort Worth Northwest C13 for the June 2006 episode. Shaded bands indicate the minimum and maximum concentrations within the 3×3 array of grid cells centered on the monitor. Also shown are scatter plots of the same data (bottom), overlaid with Q-Q plots. shows time series and scatter plots of ozone and NO_x for the June episode at Fort Worth Northwest. The model shows good agreement with observed ozone in June except for over-predicting high peaks on June 9 and 12. NO_x is also simulated fairly well during this period, although the model shows a tendency to over-predict midrange NO_x concentrations. *Figure 4-16: Time series showing observed ozone (top) and NO_x (center) at Fort Worth Northwest C13 for the August-September 2006 episode. Shaded bands indicate the minimum and maximum concentrations within the 3×3 array of grid cells centered on the monitor. Also shown are scatter plots of the same data (bottom), overlaid with Q-Q plots.* is similar to Figure 4-15 but is for the August-September episode. In this case, the model over-predicts the peaks on most days, and over-predicts ozone in general as evidenced by the scatter plot at the lower left of the figure. NO_x concentrations are again simulated reasonably well with midrange over-prediction similar to that observed in the June episode.

Figure 4-17: Time series showing observed and modeled concentrations of four CB6 species (top to bottom): PAR, ETH, OLE, and ISOP at Fort Worth Northwest C13 for the June 2006 episode. Shaded bands indicate the minimum and maximum concentrations within the 3×3 array of grid cells centered on the monitor. shows time series of observed and modeled PAR, ETH, OLE, and ISOP at Fort Worth Northwest for the June episode, and while PAR, ETH, and OLE are somewhat over-predicted by the model, the magnitude of over-prediction is much smaller than was seen at Hinton Street. Isoprene, on the other hand, is over-predicted significantly at this location. This discrepancy may be due at least in part to the monitor location in an open space (an airfield) with little nearby vegetation, while the modeled concentrations are averages for 4 km × 4 km grid cells which contain significant amounts of urban forest. *Figure 4-18: Time series showing observed and modeled concentrations of four CB6 species (top to bottom): PAR, ETH, OLE, and ISOP at Fort Worth Northwest C13 for the August-September 2006 episode. Shaded bands indicate the minimum and maximum concentrations within the 3×3 array of grid cells centered on the monitor.* shows the same time series for the August-September episode, and the evaluation of modeled concentrations is the same as for June. It is interesting to note that the modeled isoprene concentrations are quite low (though not as low as measured) after September 2.

Some discussion of the high modeled concentrations of ETH and OLE seen in this modeling platform is warranted, since these alkenes are both considered to be HRVOC and can lead to significantly enhanced and rapid ozone production in certain cases as seen downwind of the Houston Ship Channel. In the 2011 DFW AD SIP revision, the modeled concentrations of these pollutants were reasonably close to the observed values, so the question arises as to what changed between 2011 and 2014. Two contributors to the increased HRVOC concentrations have been identified: MEGAN produces biogenic emissions estimates much richer in ETH and OLE than did the GloBEIS biogenic emission model, and the updated speciation used for on-road mobile sources contains higher fractions of these HRVOCs than the older speciation used in the 2011 modeling demonstration. To assess the impact of increased ETH and OLE on ozone

concentrations, a sensitivity analysis was conducted wherein the emissions of these species were greatly reduced. The sensitivity results showed a rather minor effect on modeled ozone concentrations (see Section 5.1.3 for results of the sensitivity analysis). The TCEQ plans to continue investigating these and other discrepancies between the modeled and observed concentrations and update the modeling platform as needed.

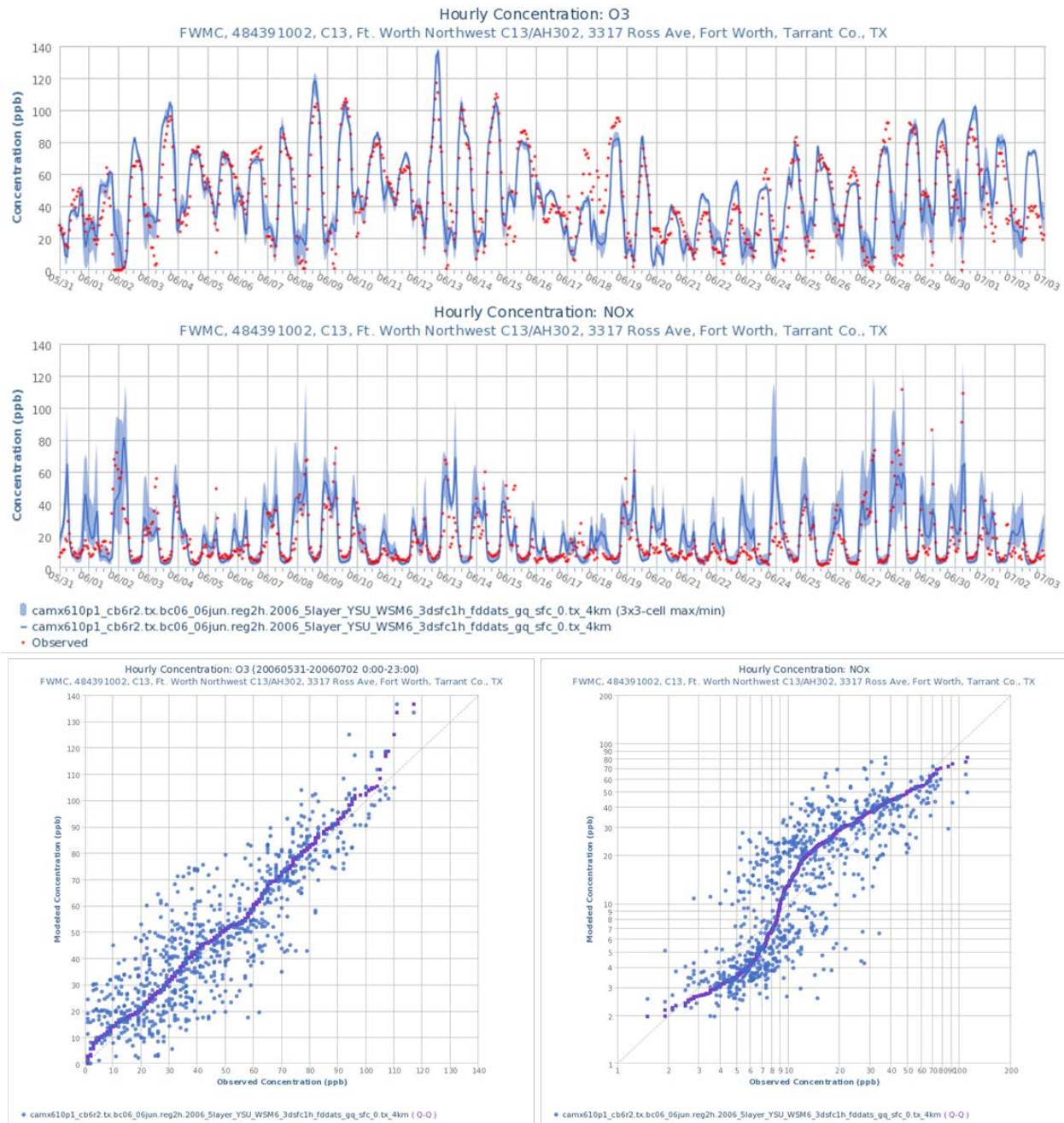


Figure 4-15: Time series showing observed ozone (top) and NO_x (center) at Fort Worth Northwest C13 for the June 2006 episode. Shaded bands indicate the minimum and maximum

concentrations within the 3×3 array of grid cells centered on the monitor. Also shown are scatter plots of the same data (bottom), overlaid with Q-Q plots.

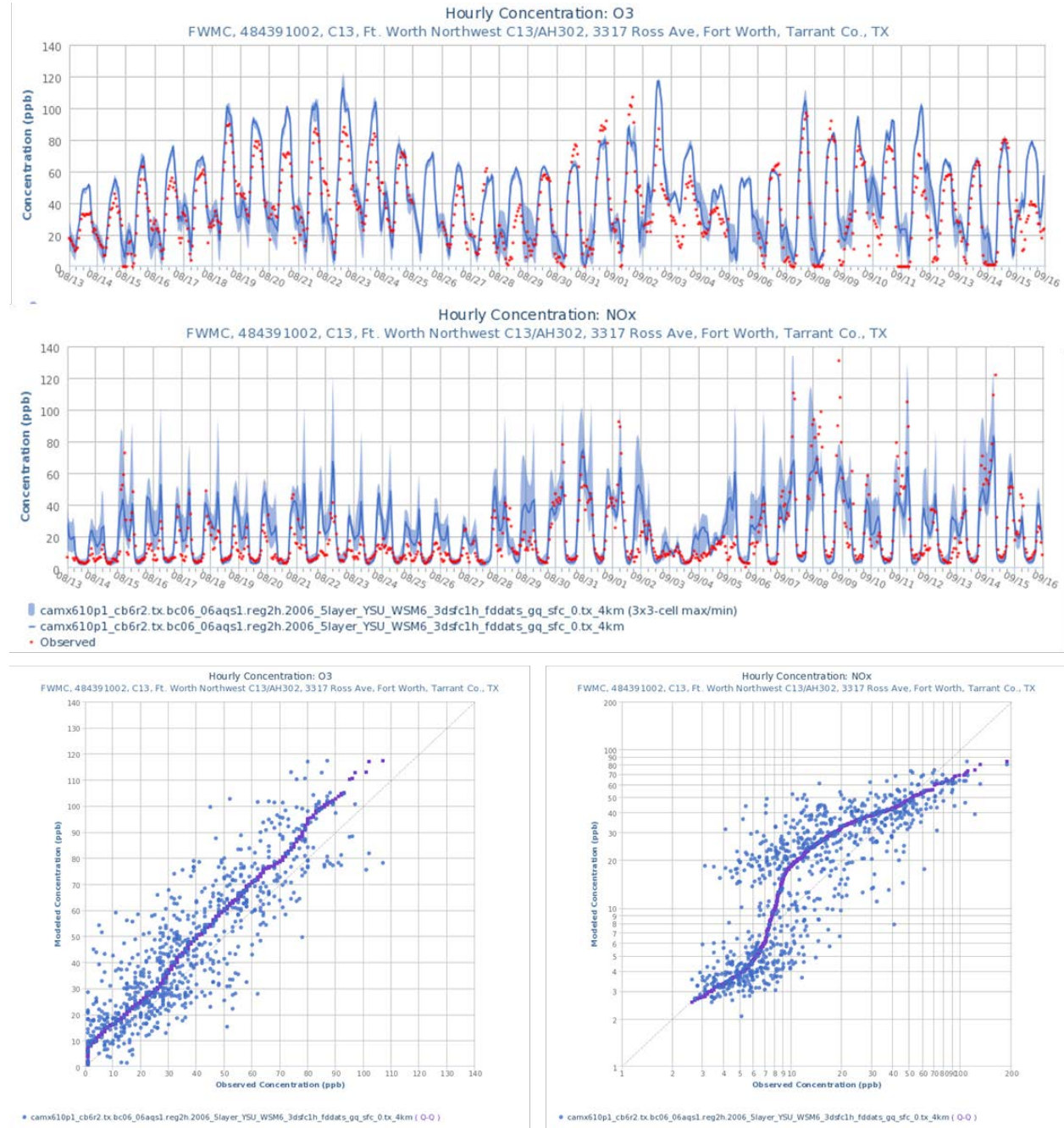


Figure 4-16: Time series showing observed ozone (top) and NO_x (center) at Fort Worth Northwest C13 for the August-September 2006 episode. Shaded bands indicate the minimum and maximum concentrations within the 3×3 array of grid cells centered on the monitor. Also shown are scatter plots of the same data (bottom), overlaid with Q-Q plots.

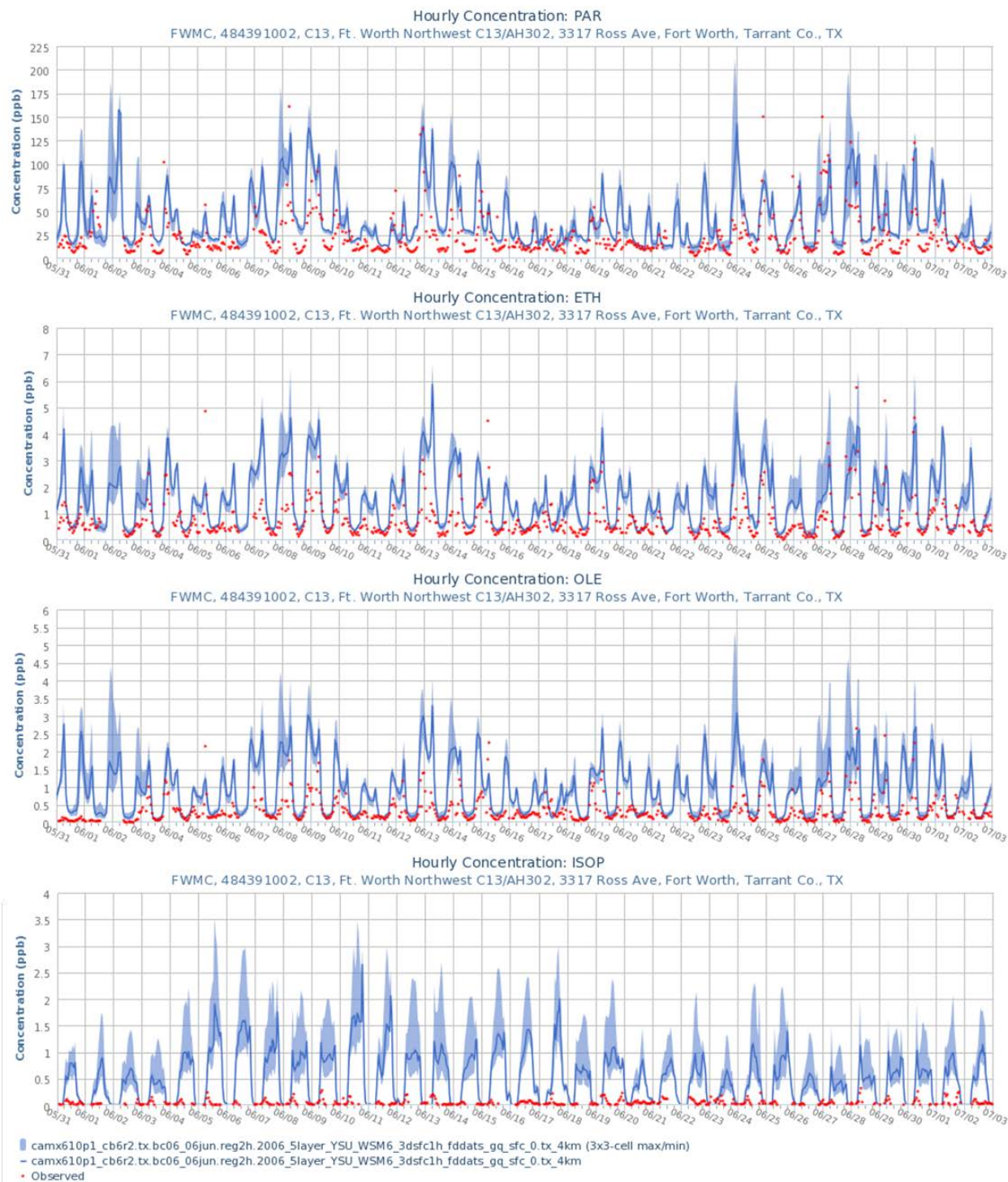


Figure 4-17: Time series showing observed and modeled concentrations of four CB6 species (top to bottom): PAR, ETH, OLE, and ISOP at Fort Worth Northwest C13 for the June 2006 episode. Shaded bands indicate the minimum and maximum concentrations within the 3x3 array of grid cells centered on the monitor.

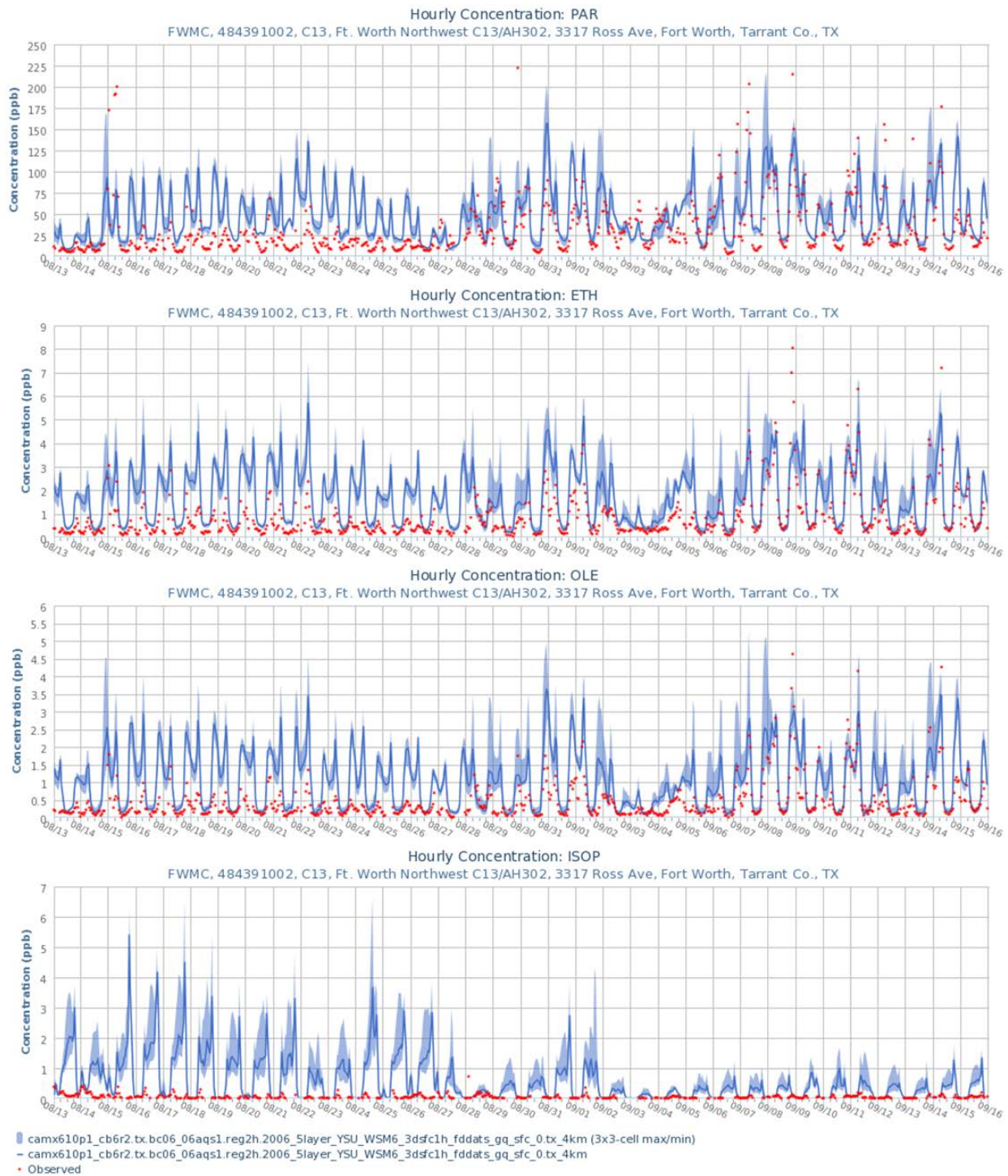


Figure 4-18: Time series showing observed and modeled concentrations of four CB6 species (top to bottom): PAR, ETH, OLE, and ISOP at Fort Worth Northwest C13 for the August-September 2006 episode. Shaded bands indicate the minimum and maximum concentrations within the 3×3 array of grid cells centered on the monitor.

4.5.1.4. Denton Airport

The Denton Airport (DENT) site is located near the south end of the runway of the Denton County Airport a couple of miles southwest of the City of Denton. The site is about 1.3 miles northwest of Interstate 35 West and is east of a large industrial park, which includes a truck assembly plant. With the exception of I-35W, most of these sources infrequently influence the observations at the site since the prevailing ozone-season winds are southerly to southeasterly. The site instead generally observes air masses from the highly urbanized areas of Dallas and Tarrant counties.

Figure 4-19: Time series showing observed ozone (top) and NO_x (center) at Denton Airport C56 for the June 2006 episode. Shaded bands indicate the minimum and maximum concentrations within the 3×3 array of grid cells centered on the monitor. Also shown are scatter plots of the same data (bottom), overlaid with Q-Q plots. shows time series and scatter plots of ozone and NO_x at the Denton Airport site for the June 2006 episode. For the most part, ozone is simulated quite well, although the model failed to capture a fairly significant ozone peak observed on June 18. Otherwise, outside of some overnight over-prediction, the model faithfully reproduced observed ozone concentrations. NO_x is also reproduced fairly well, though the model shows a modest tendency for over-prediction.

Figure 4-20: Time series showing observed ozone (top) and NO_x (center) at Denton Airport C56 for the August-September 2006 episode. Shaded bands indicate the minimum and maximum concentrations within the 3×3 array of grid cells centered on the monitor. Also shown are scatter plots of the same data (bottom), overlaid with Q-Q plots. shows the same figures for the August-September 2006 episode, and in this case the model also predicted the observed ozone peaks fairly well, although the model significantly over-predicted lower and intermediate ozone concentrations. This tendency contributes to the over-prediction of MDA8 ozone concentrations for this episode seen in Table 4-2. NO_x is over-predicted in a similar magnitude to the June episode, particularly in the mid-ranges.

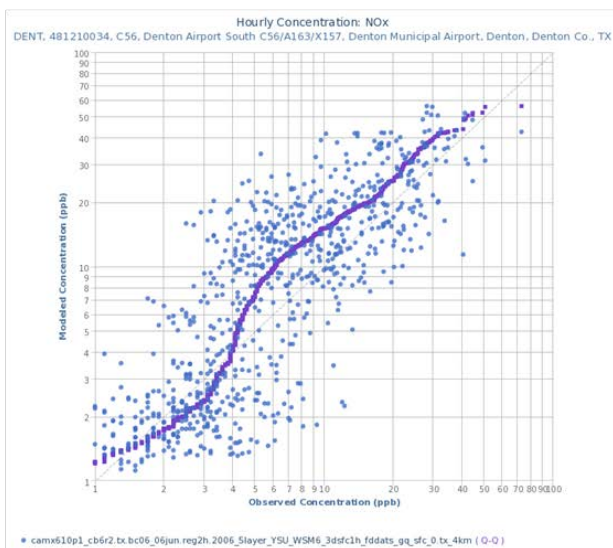
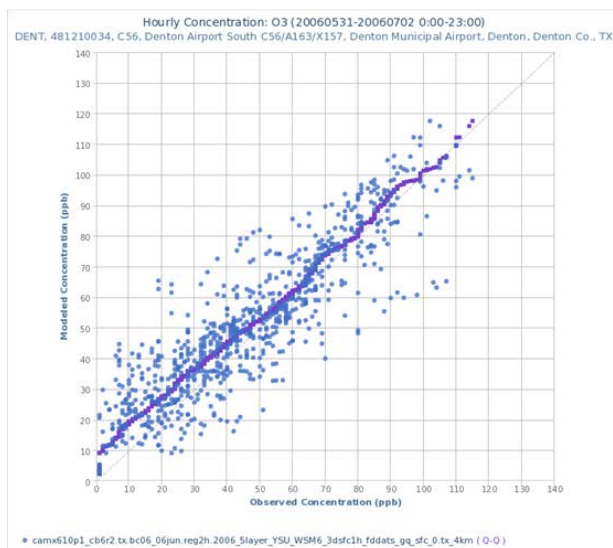
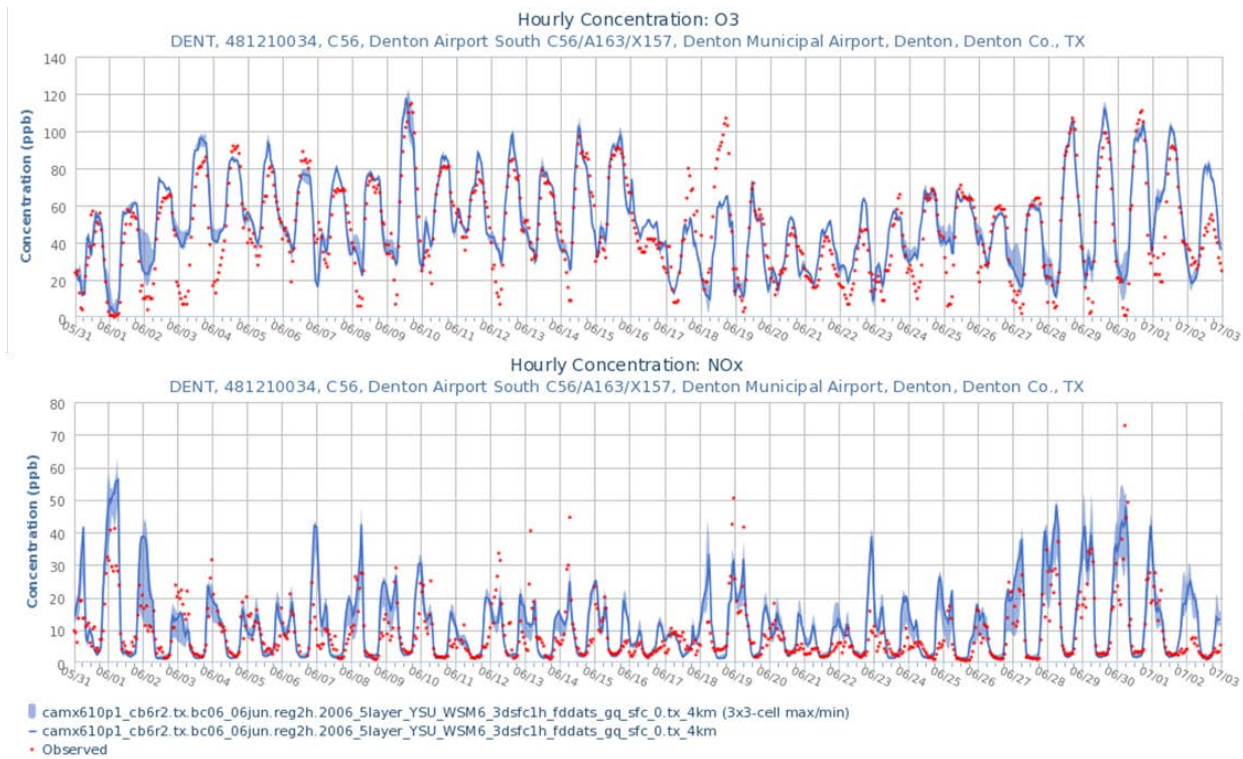


Figure 4-19: Time series showing observed ozone (top) and NO_x (center) at Denton Airport C56 for the June 2006 episode. Shaded bands indicate the minimum and maximum concentrations within the 3×3 array of grid cells centered on the monitor. Also shown are scatter plots of the same data (bottom), overlaid with Q-Q plots.

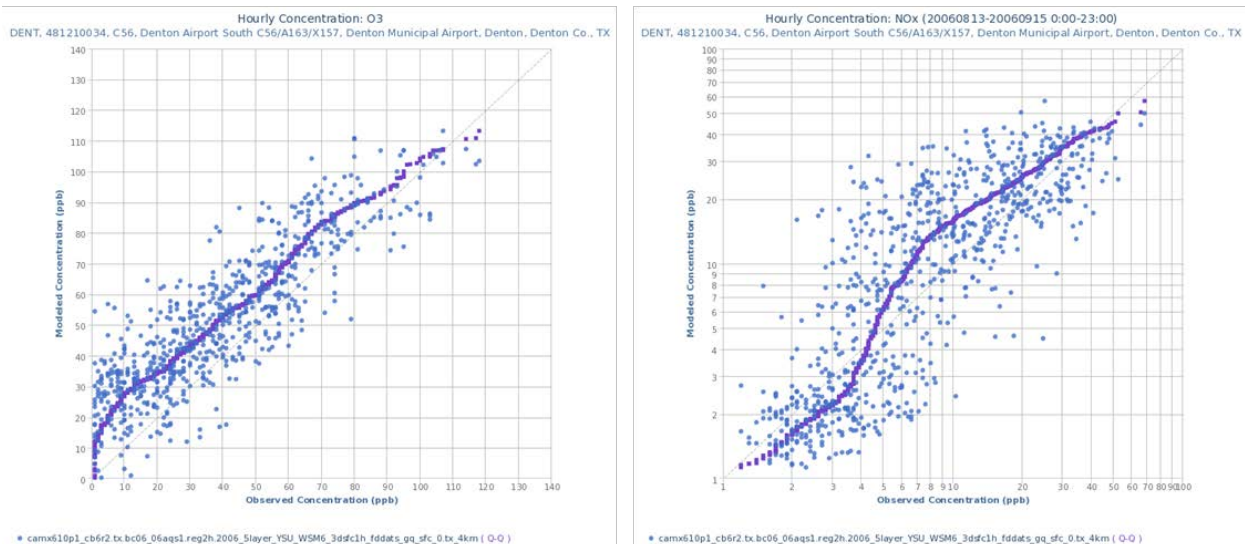
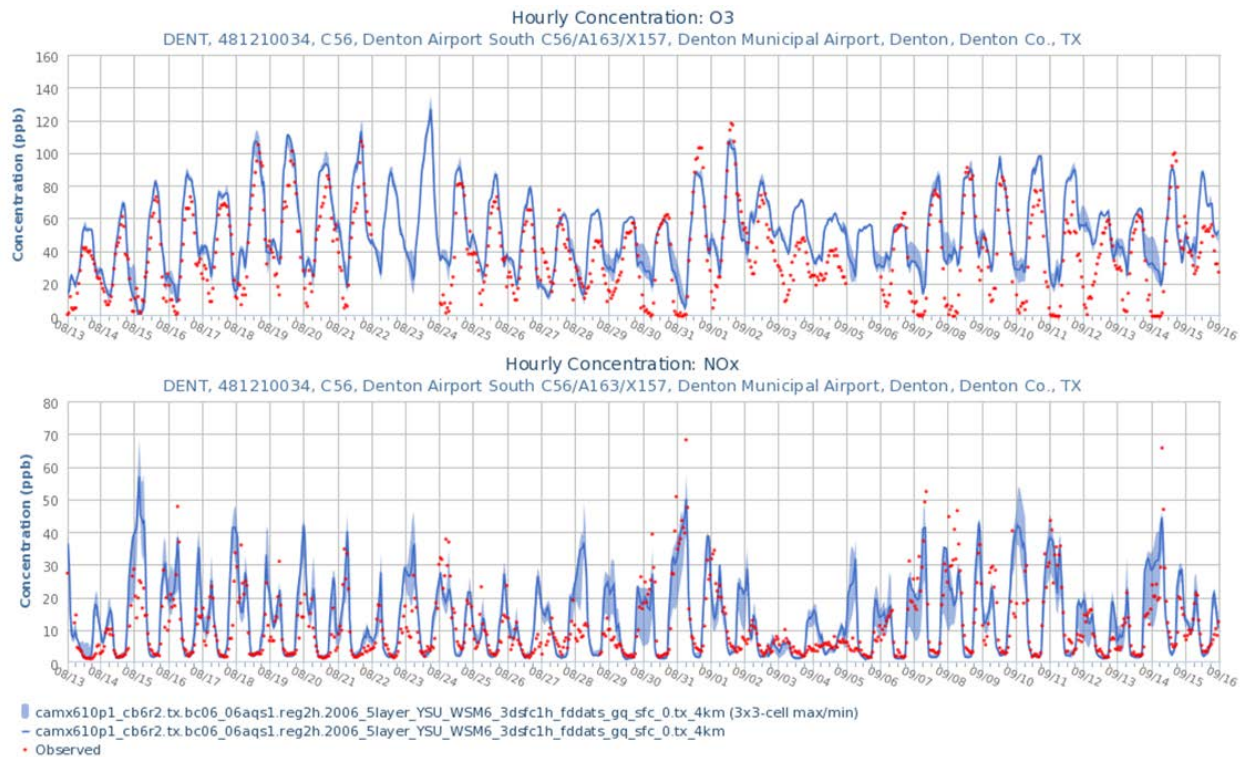


Figure 4-20: Time series showing observed ozone (top) and NO_x (center) at Denton Airport C56 for the August-September 2006 episode. Shaded bands indicate the minimum and maximum concentrations within the 3×3 array of grid cells centered on the monitor. Also shown are scatter plots of the same data (bottom), overlaid with Q-Q plots.

4.5.1.5. Eagle Mountain Lake

The Eagle Mountain Lake C75 (EMTL) is distinguished by showing the highest monitored MDA8 ozone design value in 2006 at 96 ppb (Denton Airport was a close second at 95 ppb). The site is in a relatively rural area but is within a mile of a large church and thus its observations may be inordinately influenced by weekend activity. It also lies near a private airport and is proximate to a number of gas wells, which were mostly in place during the 2006 episodes. Some drilling activity appears to have been going on during that time period as well. *Figure 4-21: Time series showing observed ozone at Eagle Mountain Lake C75 for the June (top) and August-September (center) episodes. Shaded bands indicate the minimum and maximum concentrations within the 3×3 array of grid cells centered on the monitor. Also shown are scatter plots of the same data (bottom), overlaid with Q-Q plots.* shows time series and scatter plots for ozone during both episodes (NO_x was not monitored at this location in 2006).

The figure shows that ozone was simulated very well in June with little bias evident across the spectrum of monitored values, although in the August-September period the model does exhibit a modest positive bias, which increases with higher observed concentrations.

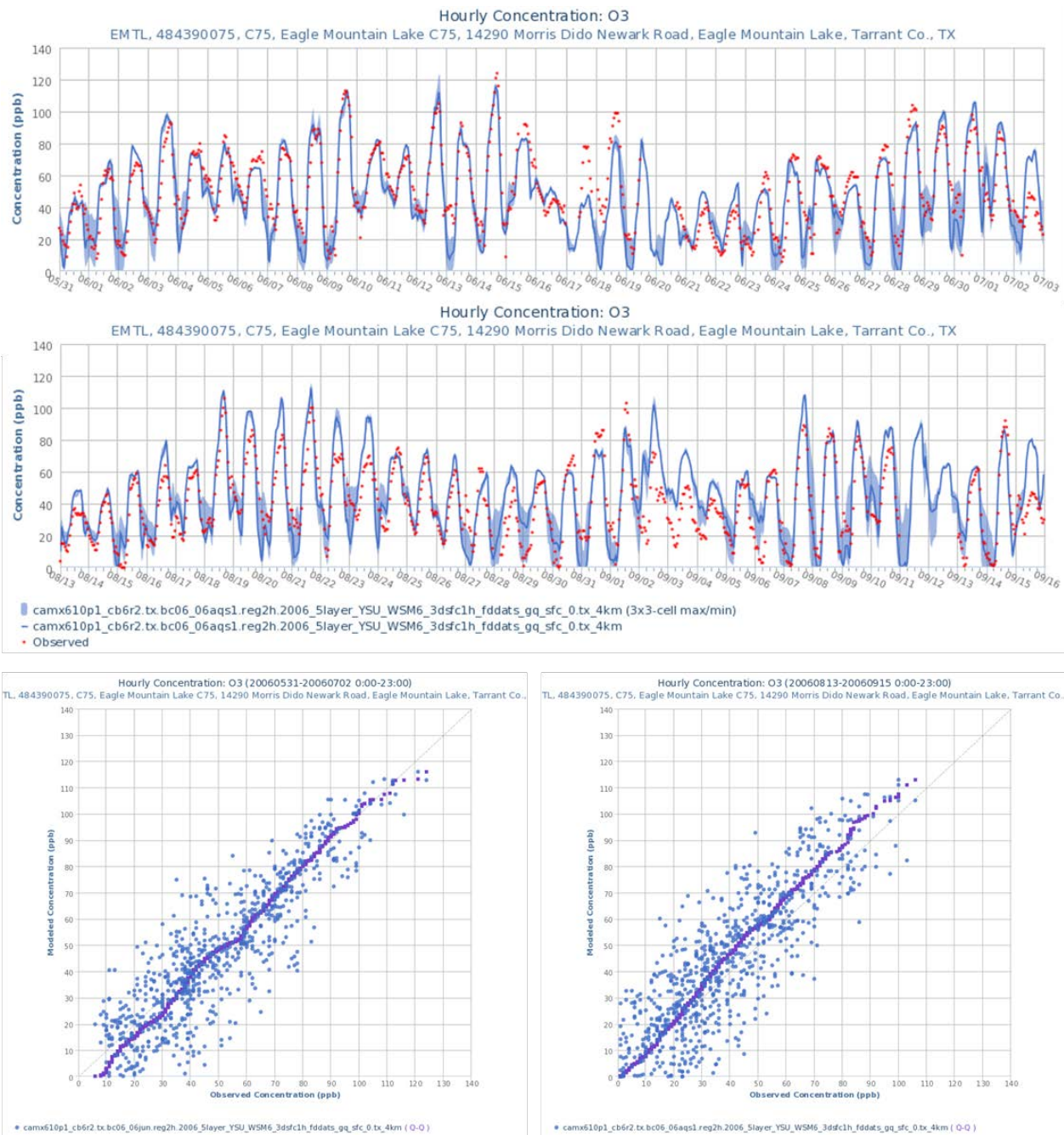


Figure 4-21: Time series showing observed ozone at Eagle Mountain Lake C75 for the June (top) and August-September (center) episodes. Shaded bands indicate the minimum and maximum concentrations within the 3×3 array of grid cells centered on the monitor. Also shown are scatter plots of the same data (bottom), overlaid with Q-Q plots.

4.5.2. Peak Ozone Tile Plots

Along with time series and scatter plots, the TCEQ employs several additional graphical analysis techniques, including cumulative density plots, hourly ozone animations, and customized graphics. One of the most intuitive graphics is a plot showing the daily peak ozone across the modeling domain. This plot is akin to the contour plots often used to display terrain elevations,

and is a good tool for visually comparing the modeled peak ozone across the domain with observations. It is important to note that the plots below are not snapshots in time, but show the maximum value per grid cell (in this case, peak daily eight-hour ozone) regardless of when it occurred during the day. Areas downwind of the urban core will generally have peaks that occur later in the day than upwind areas.

Figure 4-22: Modeled and observed MDA8 ozone on June 3 and 4, 2006. On both days the model predicted the location and magnitude of the urban plume quite well, but on June 3 over-predicted the MDA8 concentrations outside the plume by a modest amount. through *Figure 4-38: Modeled and observed MDA8 ozone on September 14, 2006.* On this day the model shows generally good performance, with a small under-predictive bias. depict modeled and measured MDA8 ozone concentrations for every episode day with observed MDA8 ozone > 75 ppb. The figure captions provide a brief summary of model performance relative to peak MDA8 ozone for each day. Observed MDA8 ozone concentrations are represented by small circles at the monitor locations. When the color of the dot matches closely the surrounding colors, the model is predicting the observed MDA8 value well.

In general, the model performs very well during the June 2006 episode with only a few days having questionable performance. On the other hand, the August-September 2006 episode is characterized by over-prediction, particularly in August and early September. However, a few days in this latter episode do show good performance. In both episodes, with few exceptions, the model locates the plumes of highest ozone concentration very well.

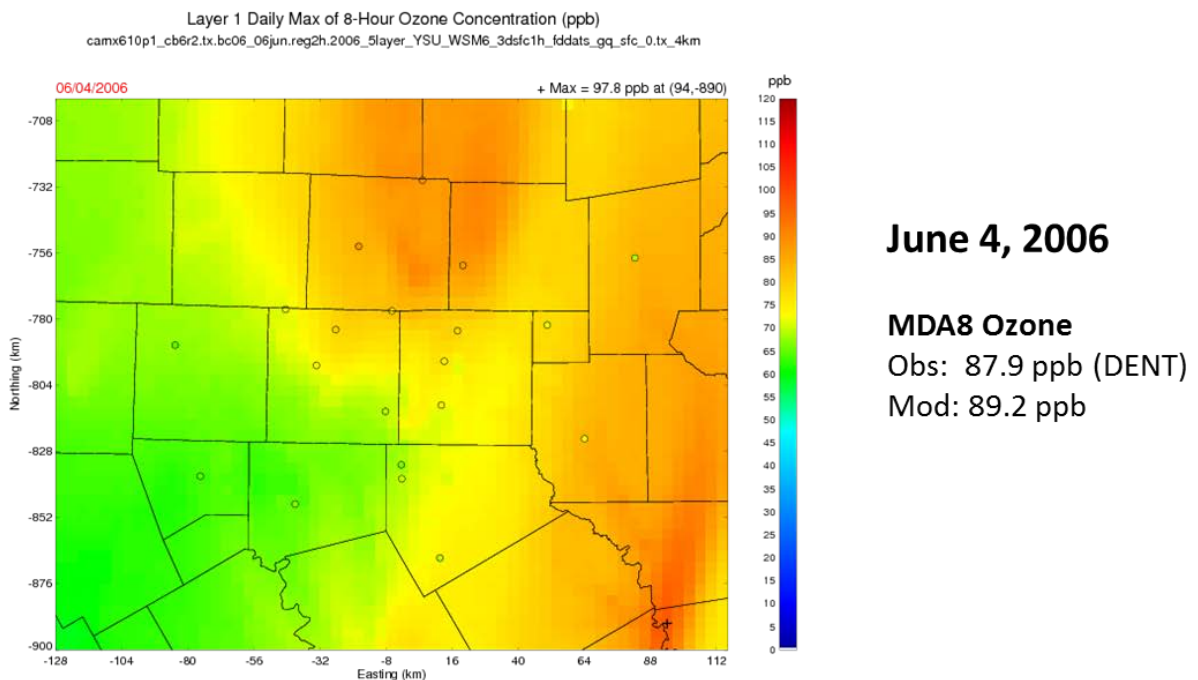
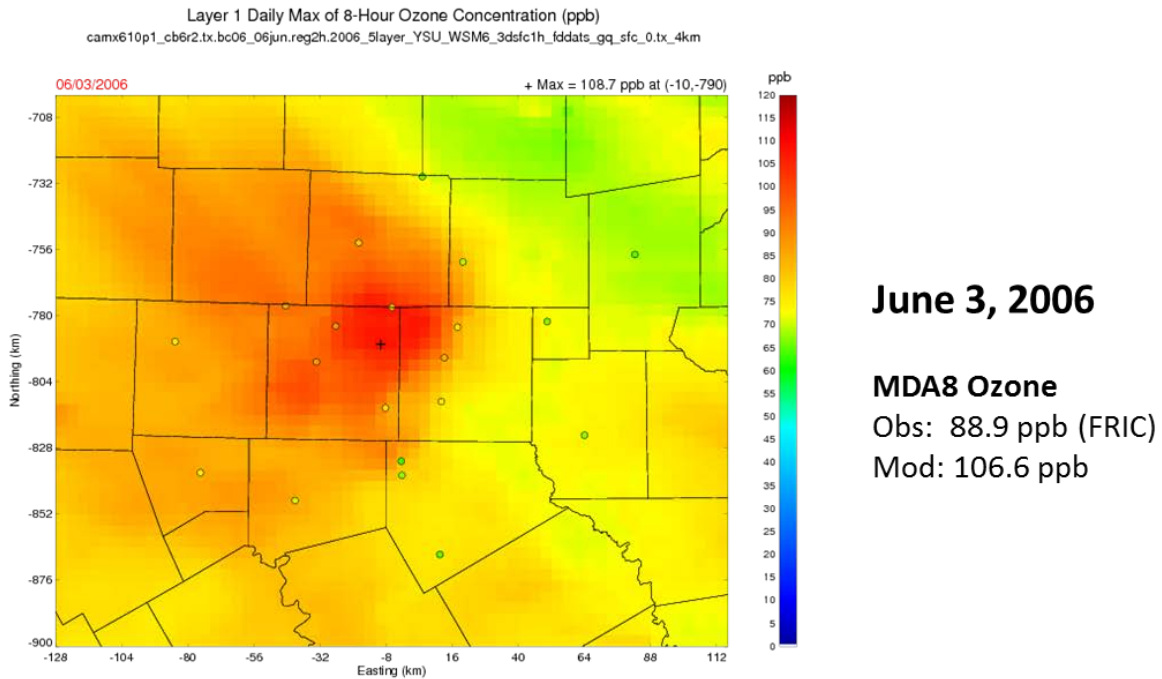


Figure 4-22: Modeled and observed MDA8 ozone on June 3 and 4, 2006. On both days the model predicted the location and magnitude of the urban plume quite well, but on June 3 over-predicted the MDA8 concentrations outside the plume by a modest amount.

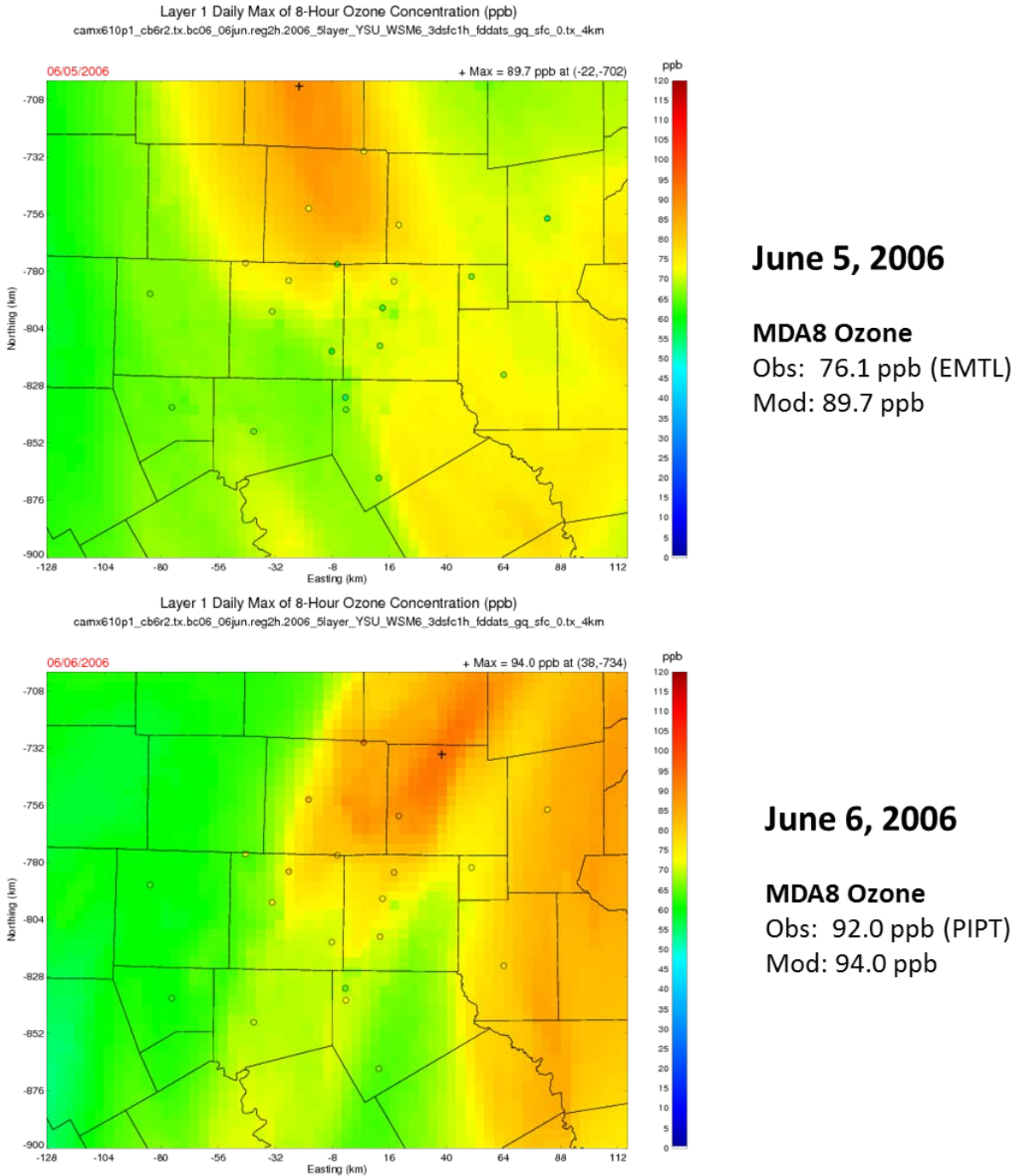


Figure 4-23: Modeled and observed MDA8 ozone on June 5 and 6, 2006. On June 5 the model over-predicted concentrations across the DFW area although the higher modeled concentrations were located in the right places. The modeled concentrations matched the observations very well on June 6.

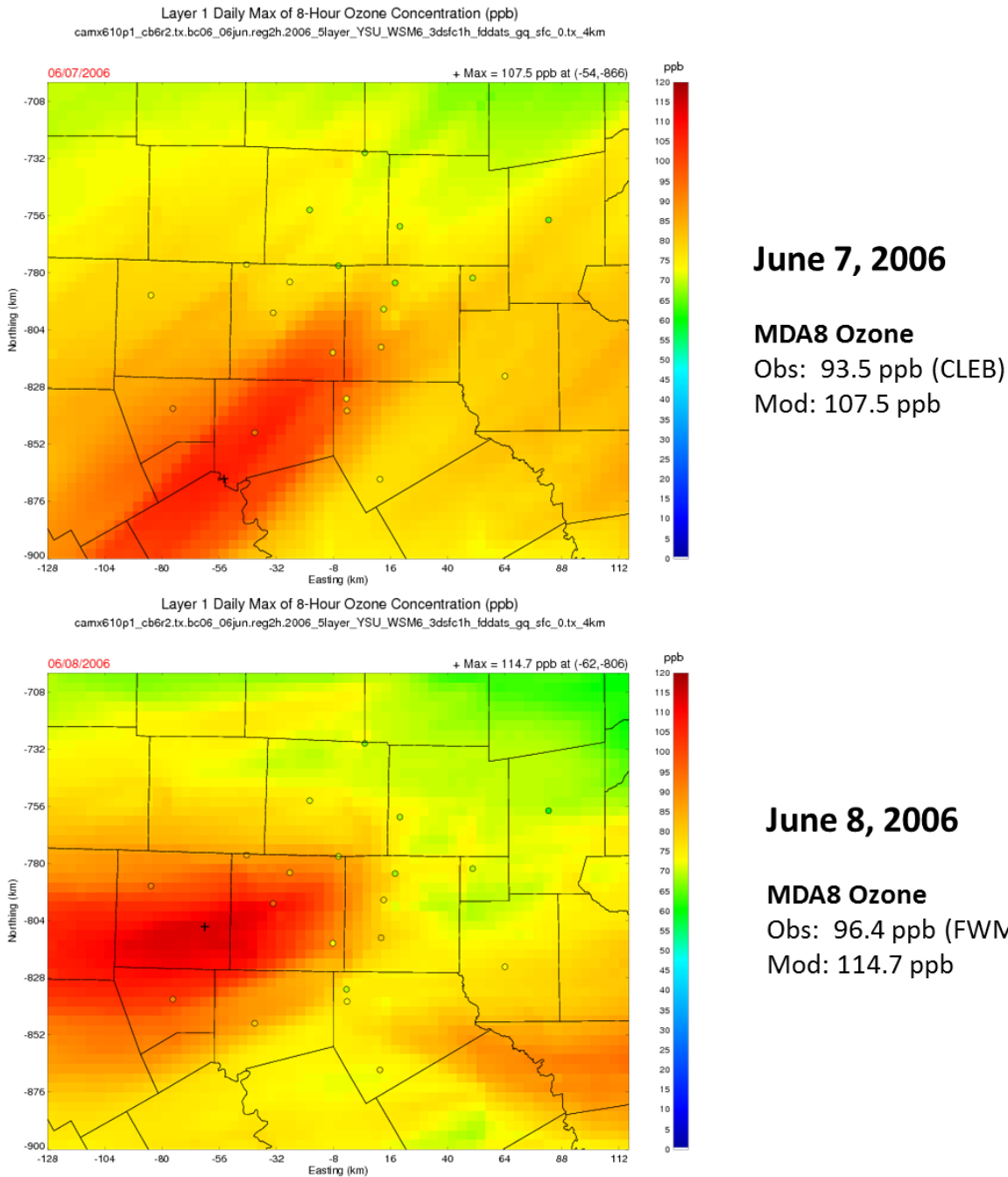
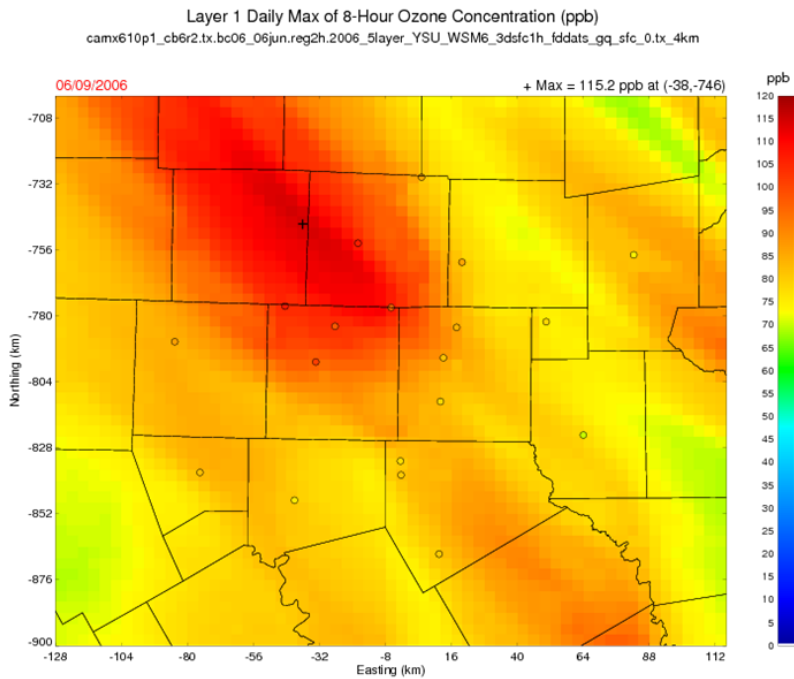


Figure 4-24: Modeled and observed MDA8 ozone on June 7 and 8, 2006. On June 7 the model over-predicted concentrations across much of the DFW area, but the modeled plume is located appropriately. The modeled concentrations matched the observations well on June 8 although may be over-predicting the highest areas slightly. The modeled peak is not located near a monitor but because the surrounding monitors are modeled fairly accurately, it is likely that the modeled peak is located appropriately.

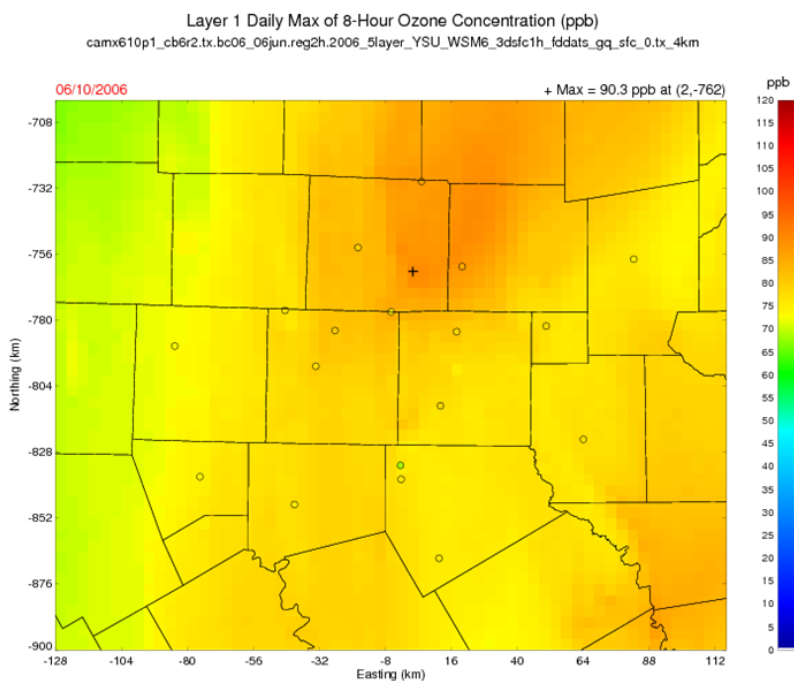


June 9, 2006

MDA8 Ozone

Obs: 106.8 ppb (EMTL)

Mod: 115.2 ppb



June 10, 2006

MDA8 Ozone

Obs: 86.0 ppb (FRIC)

Mod: 90.3 ppb

Figure 4-25: Modeled and observed MDA8 ozone on June 9 and 10, 2006. Model performance is very good on both these days, both in location and magnitude of the ozone plume.

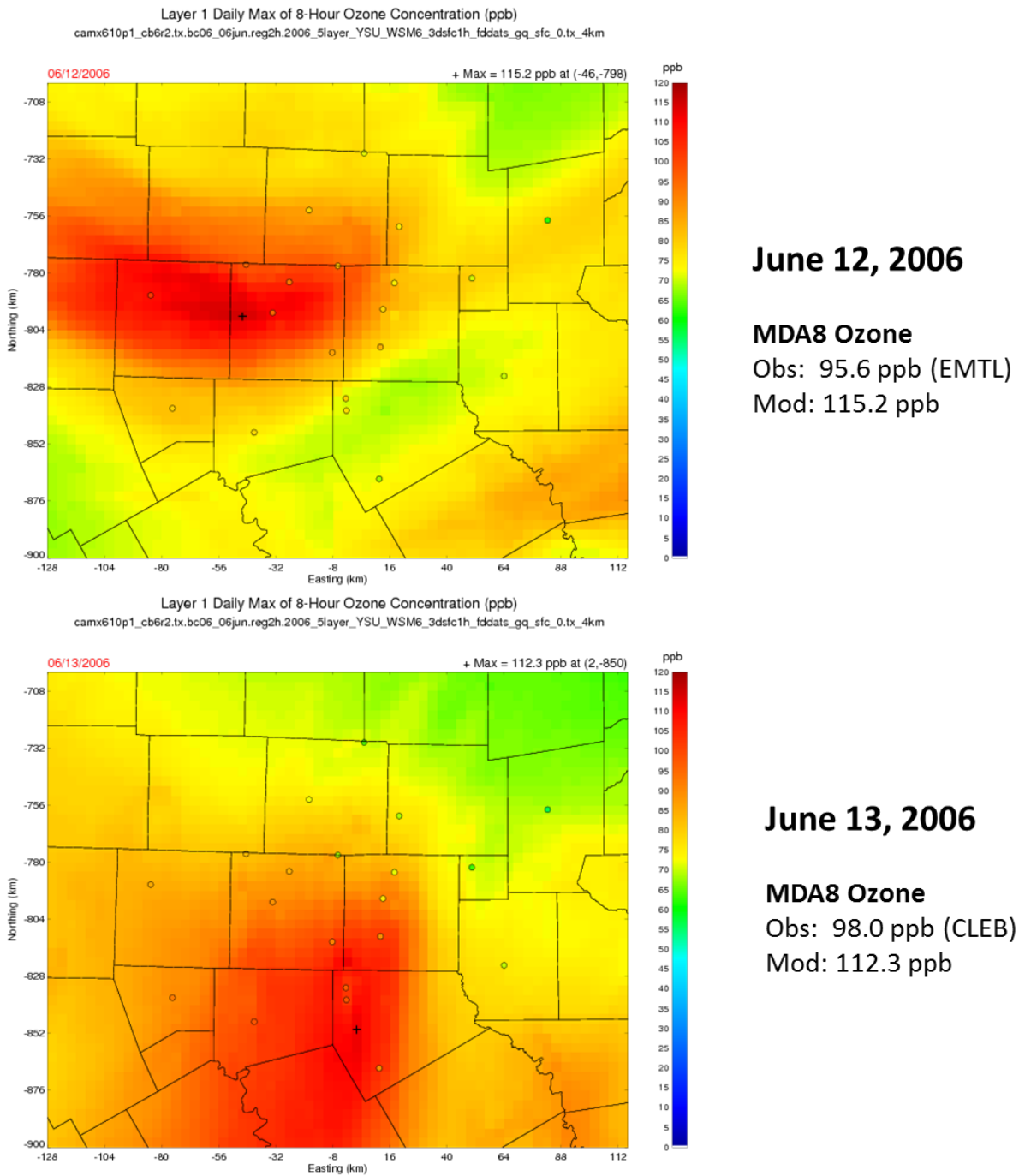
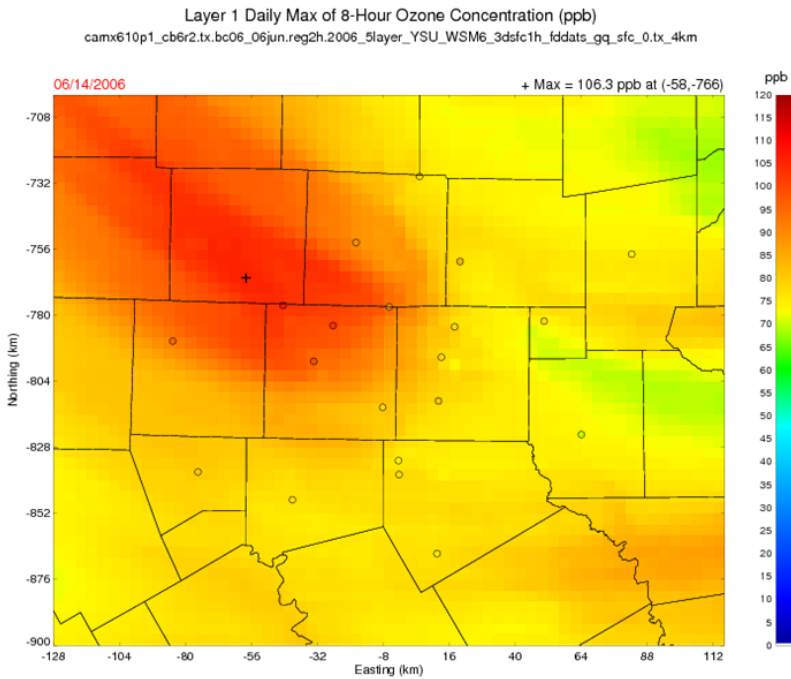


Figure 4-26: Modeled and observed MDA8 ozone on June 12 and 13, 2006. On June 12 the model shows a small overall positive bias but locates the observed plume very well. The model also exhibits some positive bias on June 13, but once again accurately places the plume of highest concentrations.

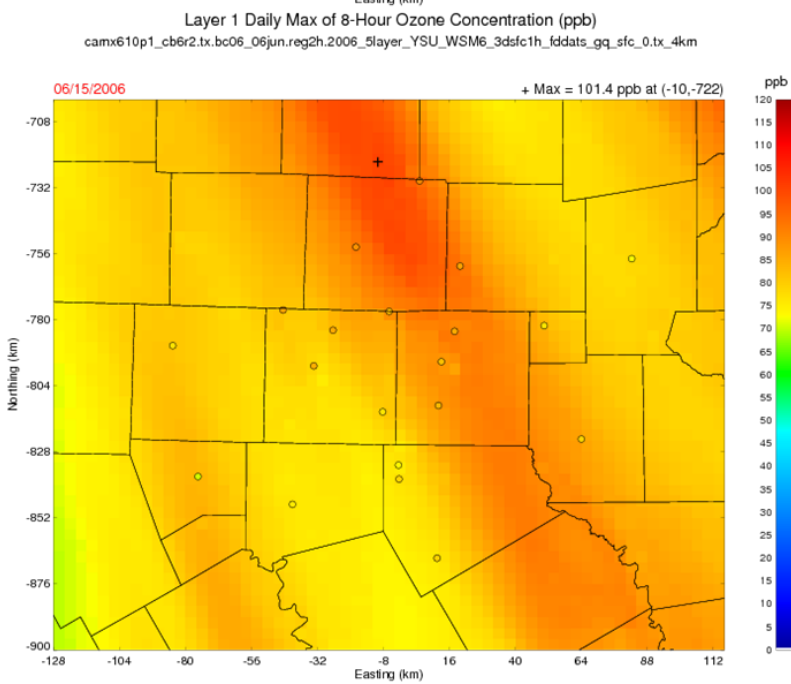


June 14, 2006

MDA8 Ozone

Obs: 107.5 ppb (EMTL)

Mod: 106.3 ppb



June 15, 2006

MDA8 Ozone

Obs: 89.8 ppb (PIPT)

Mod: 101.4 ppb

Figure 4-27: Modeled and observed MDA8 ozone on June 14 and 15, 2006. Model performance on June 14 is very good, but on June 15 the model produced a notable positive bias across the DFW area.

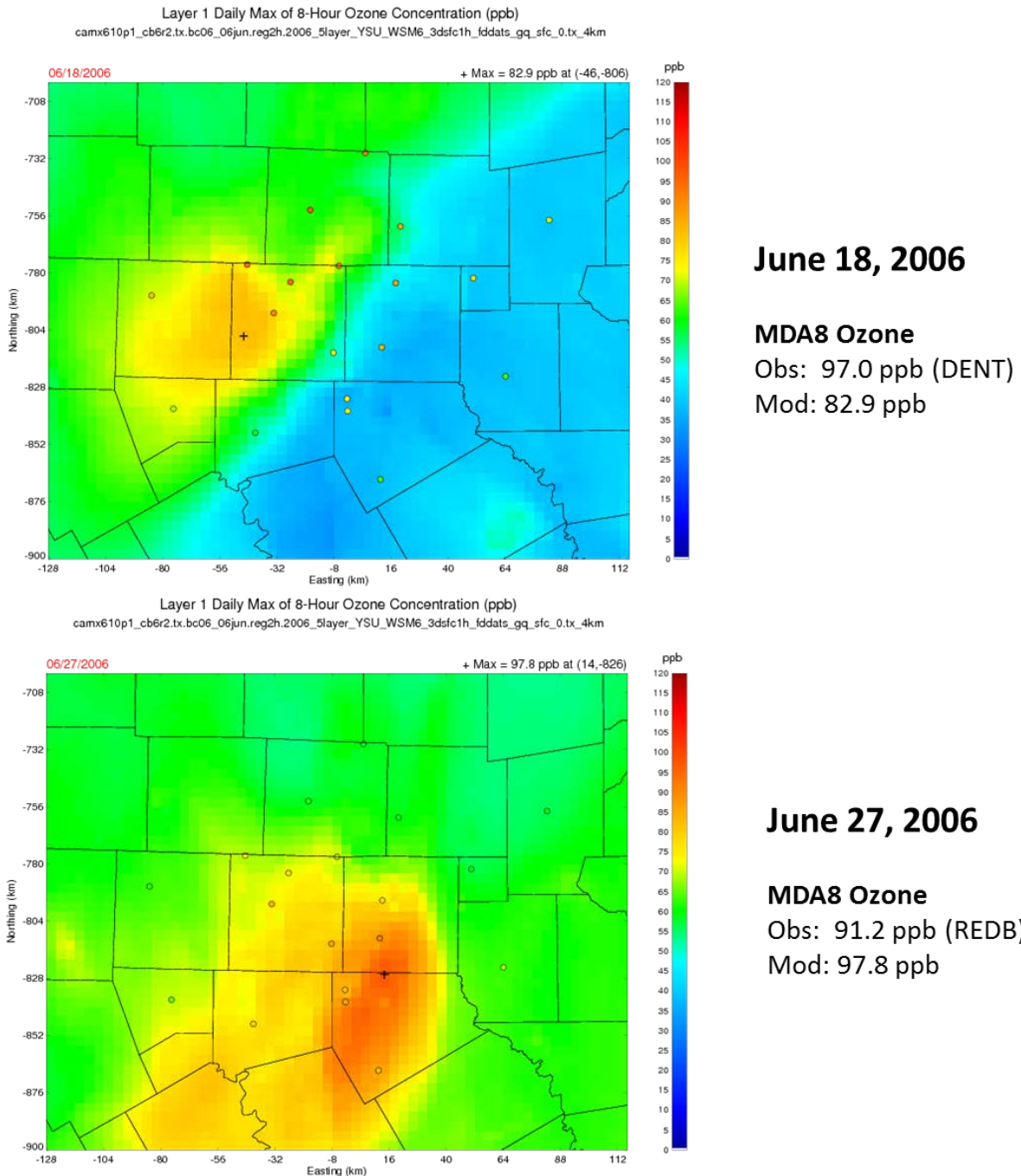
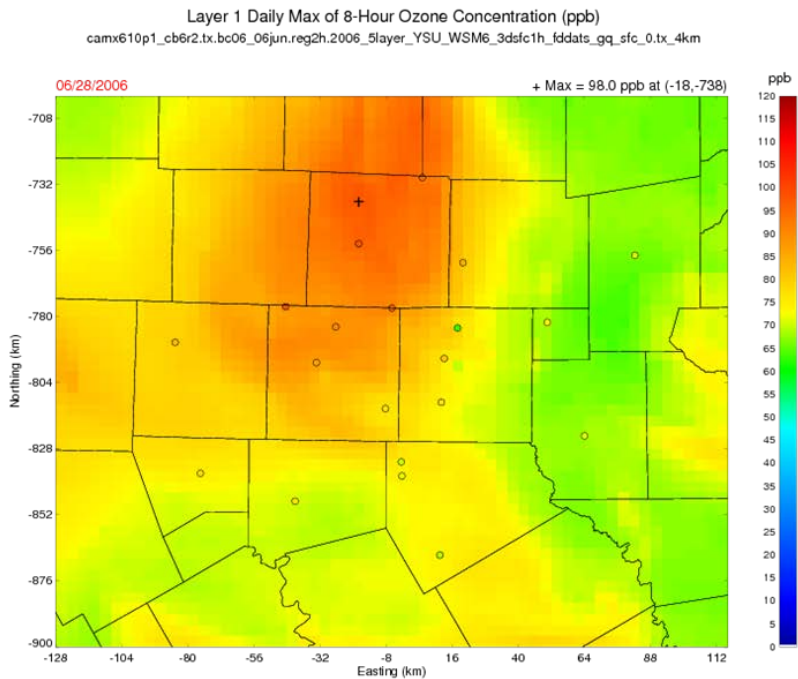


Figure 4-28: Modeled and observed MDA8 ozone on June 18 and 27, 2006. On June 18 the model strongly under-predicts MDA8 ozone concentrations. On this day, the hourly ozone animation shows cyclonic flow centered near Waco bringing clean air from Southeast Texas into the region, accounting for the striking discontinuity in ozone concentrations. Most likely WRF pushed the clean air into the region too early, preventing the model from producing enough ozone. On June 27, the model performs well in terms of placement, but over-predicts ozone concentrations in Ellis County by a few ppb.

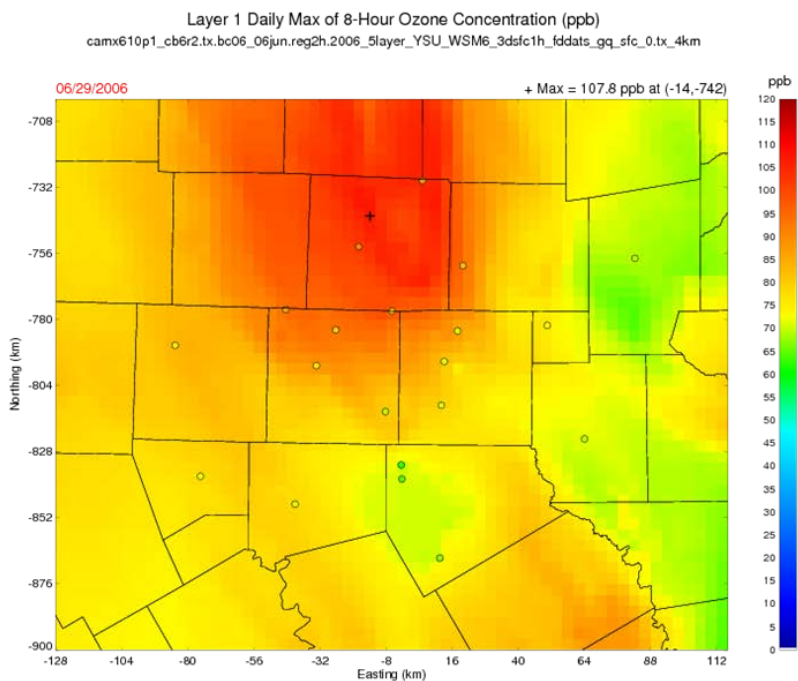


June 28, 2006

MDA8 Ozone

Obs: 98.1 ppb (EMTL)

Mod: 98.0 ppb



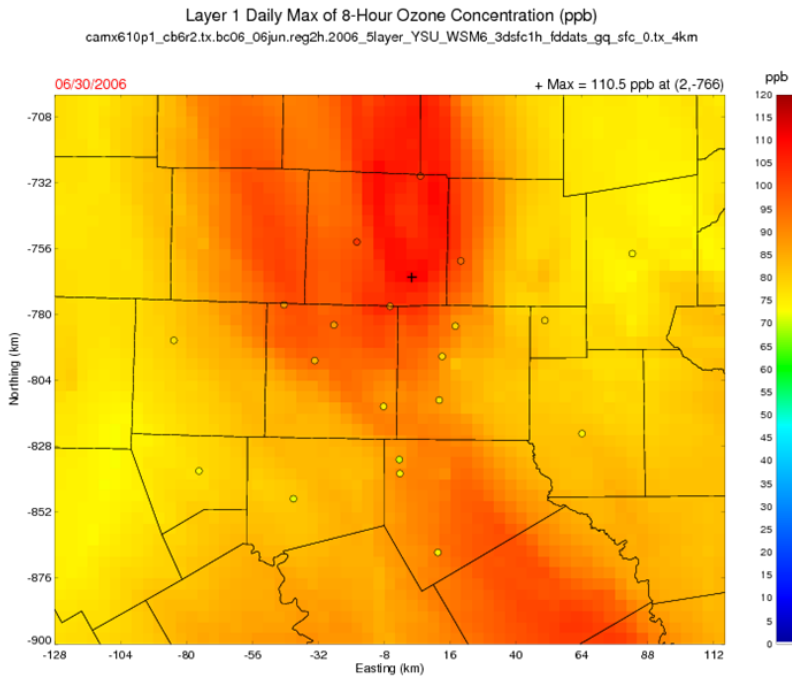
June 29, 2006

MDA8 Ozone

Obs: 91.2 ppb (DENT)

Mod: 107.8 ppb

Figure 4-29: Modeled and observed MDA8 ozone on June 28 and 29, 2006. On June 28 the model places the plume very well, but in this case generally under-predicts MDA8 ozone concentrations by a few ppb. The model makes up for this under-prediction on the following day by over-predicting ozone concentrations across the DFW area, though again the model places the plume accurately.

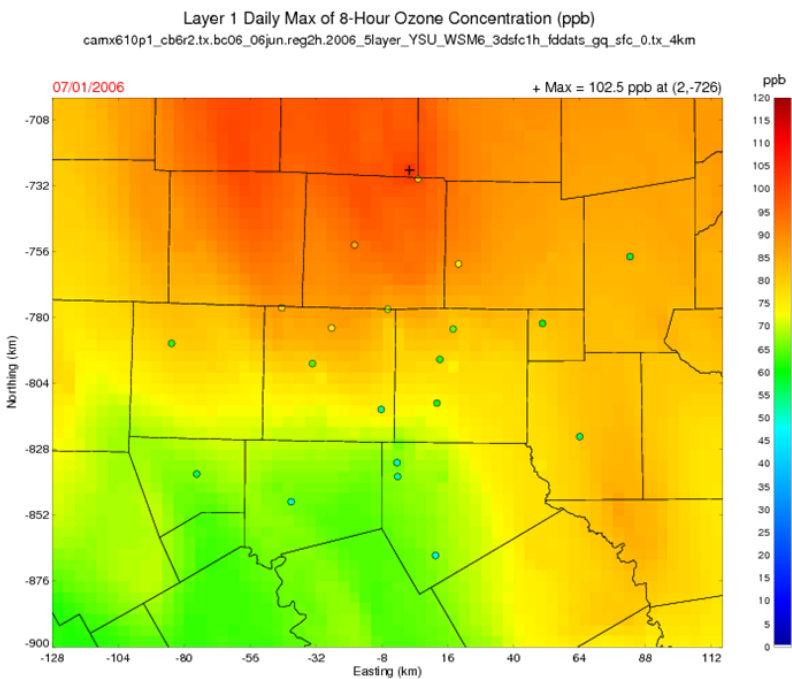


June 30, 2006

MDA8 Ozone

Obs: 102.5 ppb (DENT)

Mod: 110.5 ppb



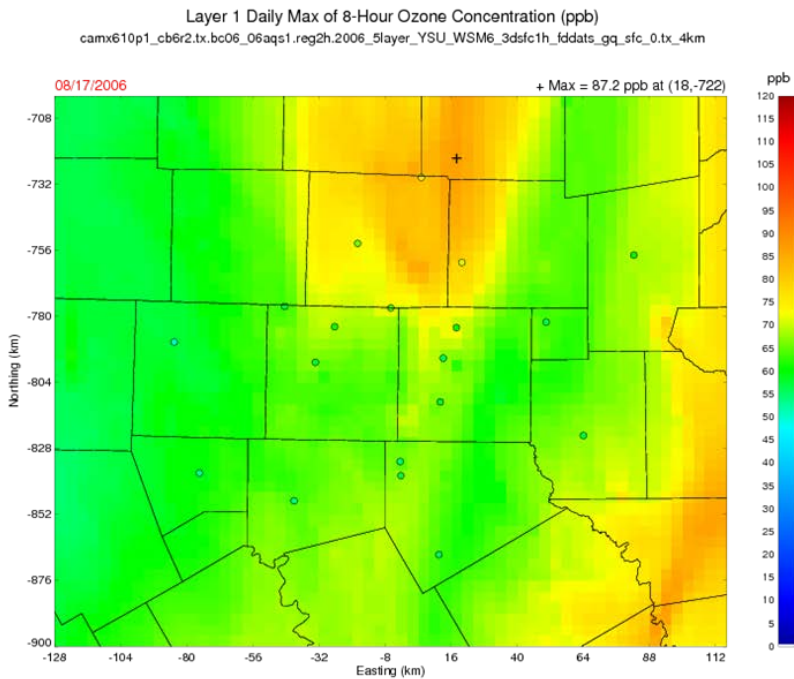
July 1, 2006

MDA8 Ozone

Obs: 85.1 ppb (DENT)

Mod: 102.5 ppb

Figure 4-30: Modeled and observed MDA8 ozone on June 30 and July 1, 2006. On June 30 the model over-predicts ozone except in the area of highest concentrations – Denton and Collin Counties – but performs quite well in that area. On July 1 the model’s ozone contours follow the monitoring network, but over-predict the observed concentrations everywhere.

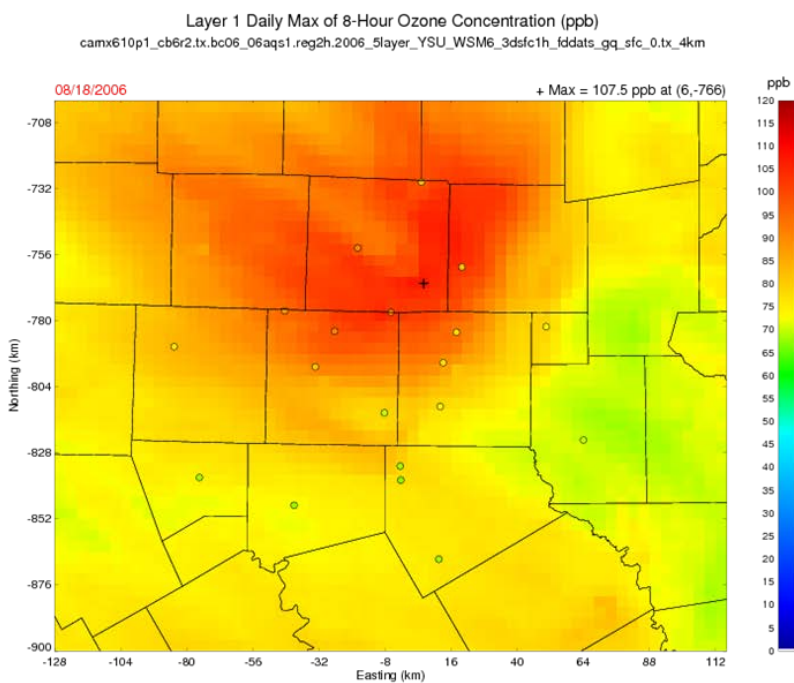


August 17, 2006

MDA8 Ozone

Obs: 75.0 ppb (PIPT)

Mod: 87.2 ppb



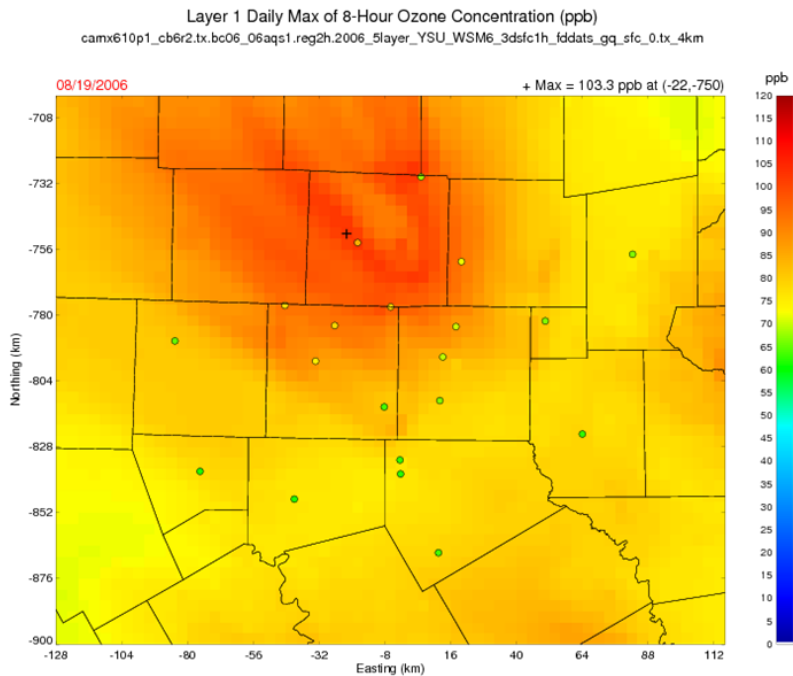
August 18, 2006

MDA8 Ozone

Obs: 91.2 ppb (GRAP)

Mod: 107.5 ppb

Figure 4-31: Modeled and observed MDA8 ozone on August 17 and 18, 2006. Both of these days embody the model's tendency towards over-prediction in the August-September episode. In both days the model places the ozone plume fairly accurately, but shows a notable positive bias in both.

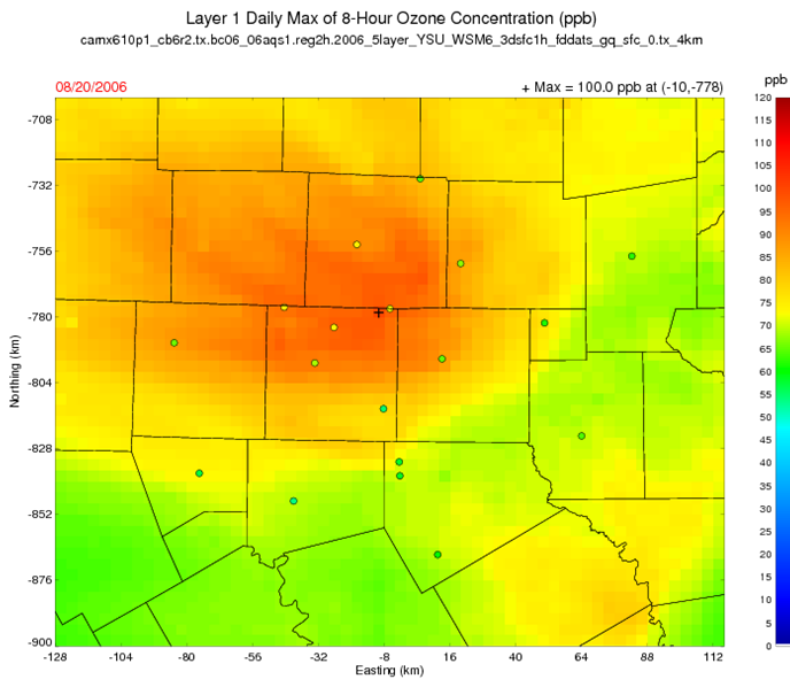


August 19, 2006

MDA8 Ozone

Obs: 84.1 ppb (DENT)

Mod: 103.3 ppb



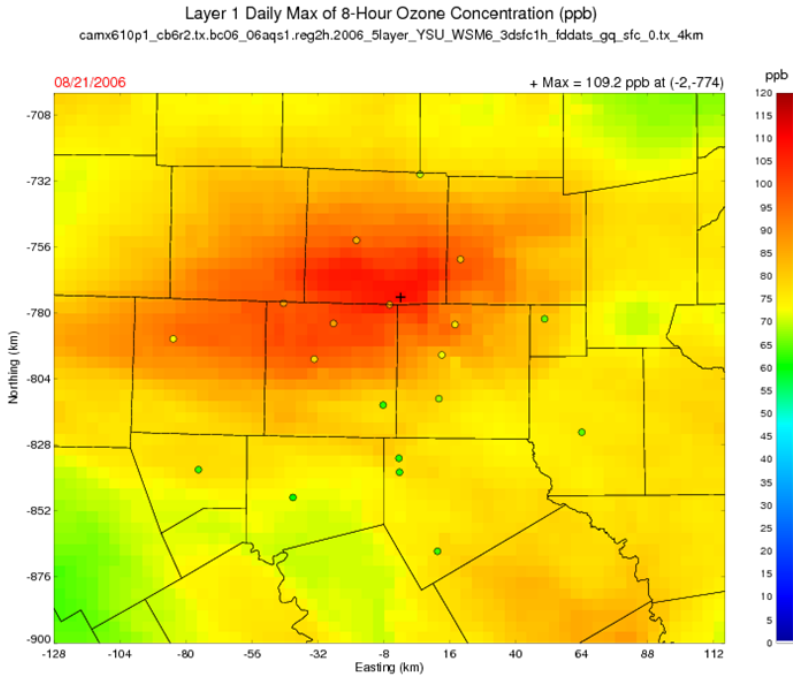
August 20, 2006

MDA8 Ozone

Obs: 75.8 ppb (EMTL)

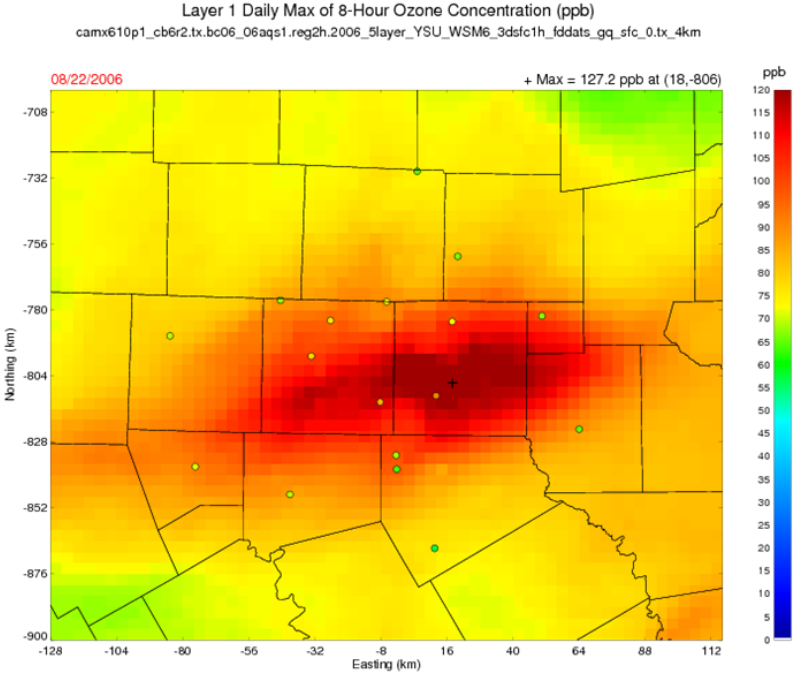
Mod: 100.0 ppb

Figure 4-32: Modeled and observed MDA8 ozone on August 19 and 20, 2006. Again, the model predicts well the highest concentrations, but significantly over-predicts the observed MDA8 ozone concentrations universally.



August 21, 2006

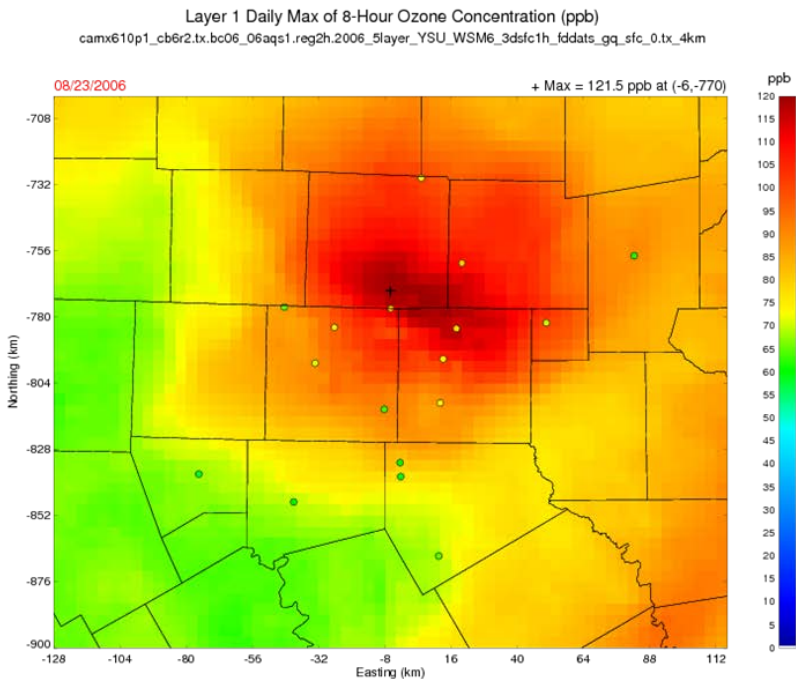
MDA8 Ozone
Obs: 88.2 ppb (GRAP)
Mod: 109.2 ppb



August 22, 2006

MDA8 Ozone
Obs: 91.2 ppb (REDB)
Mod: 127.2 ppb

Figure 4-33: Modeled and observed MDA8 ozone on August 21 and 22, 2006. Again the plumes are well-located, but ozone is significantly over-predicted.

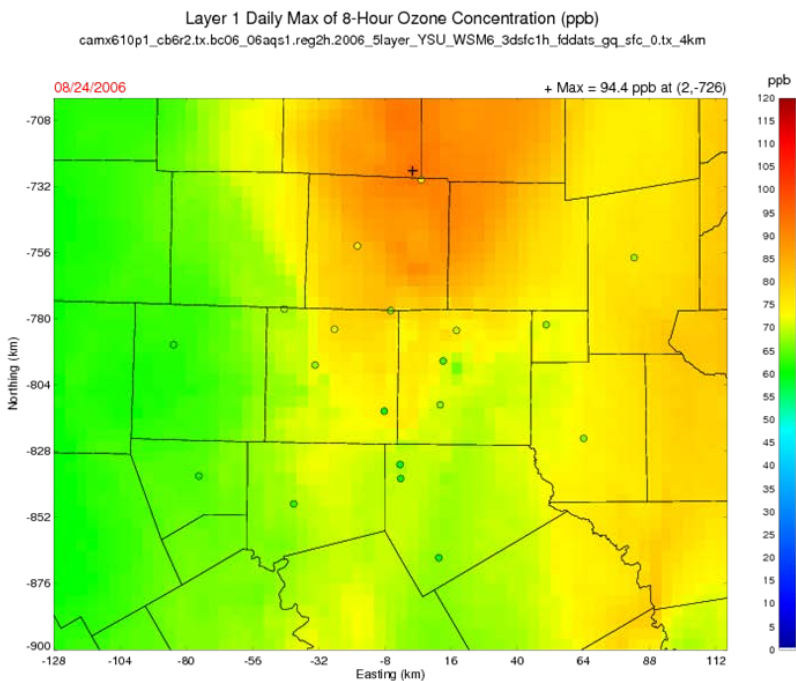


August 23, 2006

MDA8 Ozone

Obs: 83.1 ppb (GRAP)

Mod: 121.5 ppb



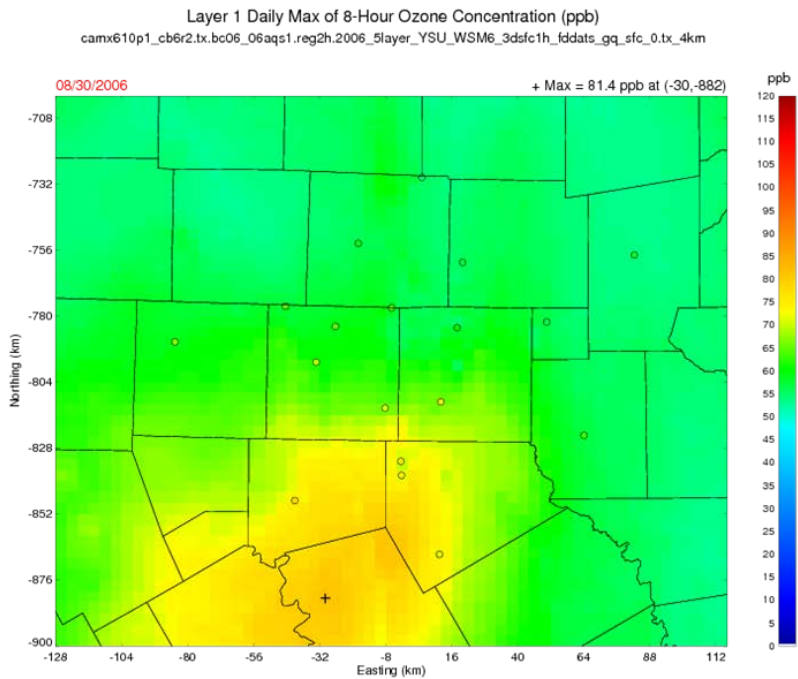
August 24, 2006

MDA8 Ozone

Obs: 75.4 ppb (PIPT)

Mod: 94.4 ppb

Figure 4-34: Modeled and observed MDA8 ozone on August 23 and 24, 2006. On August 23 the model grossly over-predicts ozone, and significantly over-predicts ozone on August 24. The plumes are located appropriately.

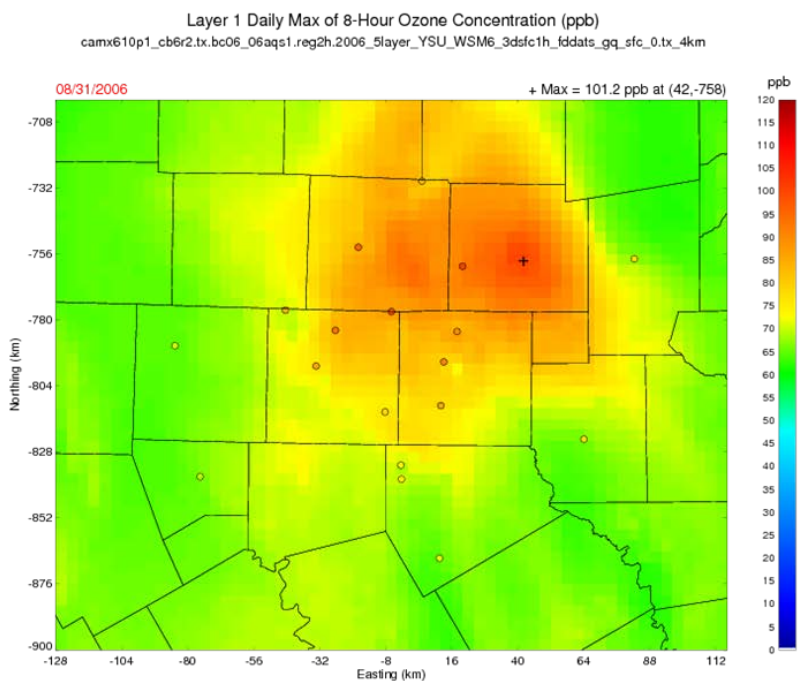


August 30, 2006

MDA8 Ozone

Obs: 76.8 ppb (CLEB)

Mod: 81.3 ppb



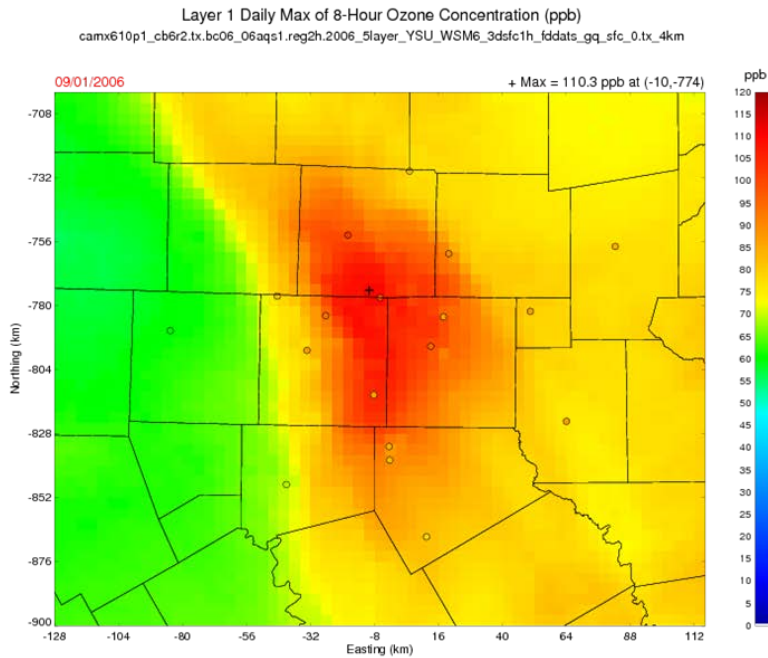
August 31, 2006

MDA8 Ozone

Obs: 101.0 ppb (FRIC)

Mod: 101.2 ppb

Figure 4-35: Modeled and observed MDA8 ozone on August 30 and 31, 2006. On August 30 the model shows fairly good performance but the ozone plume appears to be located a little too far south. On August 31 the model again performs fairly well, but under-predicts ozone concentrations by a few ppb nearly everywhere.

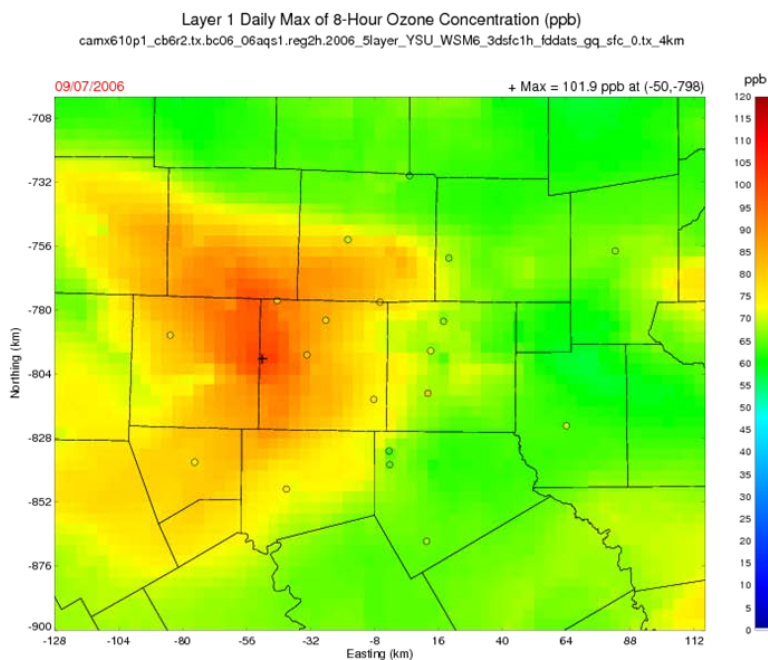


September 1, 2006

MDA8 Ozone

Obs: 102.4 ppb (DENT)

Mod: 110.3 ppb



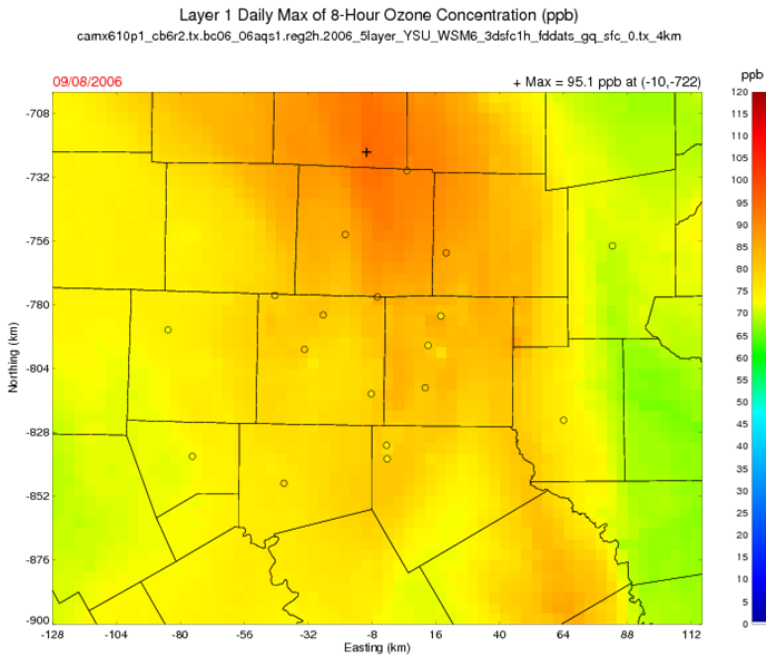
September 7, 2006

MDA8 Ozone

Obs: 82.2 ppb (FWMC)

Mod: 101.9 ppb

Figure 4-36: Modeled and observed MDA8 ozone on September 1 and 7, 2006. The model shows very good performance on September 1, reproducing well the sharp concentration gradient seen in the monitoring data on that day. The model similarly reproduces the less well-defined concentration gradient on September 7, but over-predicts ozone concentrations in Tarrant and Wise counties.

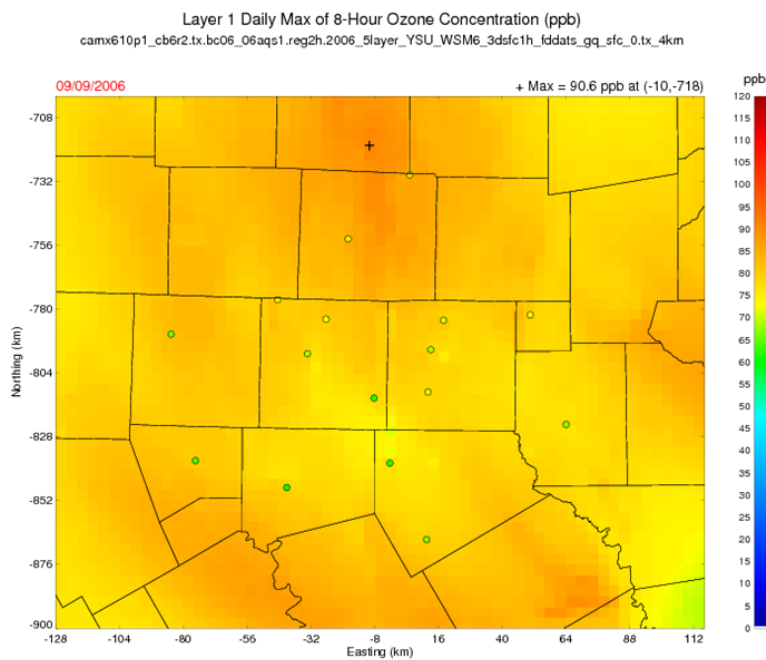


September 8, 2006

MDA8 Ozone

Obs: 87.8 ppb (PIPT)

Mod: 95.1 ppb



September 9, 2006

MDA8 Ozone

Obs: 76.9 ppb (PIPT)

Mod: 90.6 ppb

Figure 4-37: Modeled and observed MDA8 ozone on September 8 and 9, 2006. Model performance on September 8 is quite good, but the model over-predicts observed ozone concentrations on September 9 across the entire area.

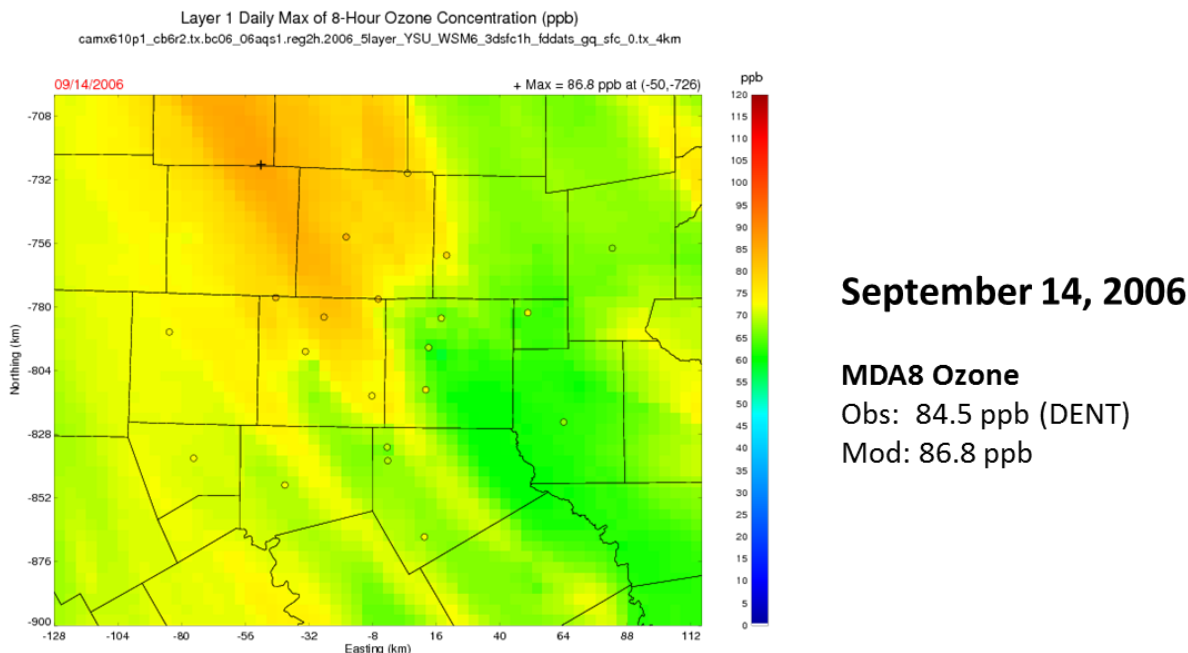


Figure 4-38: Modeled and observed MDA8 ozone on September 14, 2006. On this day the model shows generally good performance, with a small under-predictive bias.

4.5.3. Summary

This section provided an in-depth analysis of model performance in the DFW area for two episodes. Overall the model showed very good agreement with observed MDA8 ozone concentrations for the June episode, but over-predicted ozone for much of the August-September episode. However, even in the latter episode the model located well the plumes of highest ozone concentrations. At most sites one-hour ozone concentrations at all levels are predicted well in the June episode with a positive bias in August-September, but at the rural Kaufman C71 site the model generally over-predicted one-hour ozone concentrations. The Kaufman C71 site, conversely, under-predicted NO_x especially during the August-September episode. At the more urban locations the tendency was towards over-prediction of NO_x concentrations, particularly in the mid-range of observed concentrations from around 10 ppb to around 25 ppb. The modeled concentrations of HRVOC species was much higher than observed at Hinton Street C401 and at Fort Worth Northwest C13. An analysis discussed later in this chapter addresses the sensitivity of modeled ozone concentrations to increased HRVOC emissions.

4.6. Background Model Performance Evaluation

An important aspect of ozone modeling is characterizing pollutant concentrations upwind of the area of interest. In this section we look at how well the model predicts ozone concentrations at selected rural sites that characterize background values for the DFW area. The four sites analyzed are: Italy High School C60 (ITHS), a non-regulatory site in Ellis County about 30 miles south of Dallas; Palestine C647 (PLTN), a 2005-2006 Texas Air Quality Study (TexAQS II) field study site about 80 miles southeast of Dallas; San Augustine C646 (SAGA), a TexAQS II site near the Louisiana border about 160 miles ESE of Dallas; and Clarksville C648 (CLVL), a TexAQS II site located about 100 miles northeast of Dallas. All four sites are relatively rural and far from major highways except for Italy High School C60, which sits a couple of miles east of Interstate 35 East. These locations are good for measuring incoming ozone concentrations from

the south and east of the DFW area, as shown with red circles in *Figure 4-39: Sites used for DFW background model performance evaluation.* The figure also shows two sites, in yellow squares, where ozonesondes (instrumented balloons) were launched during the June 2006 episode.

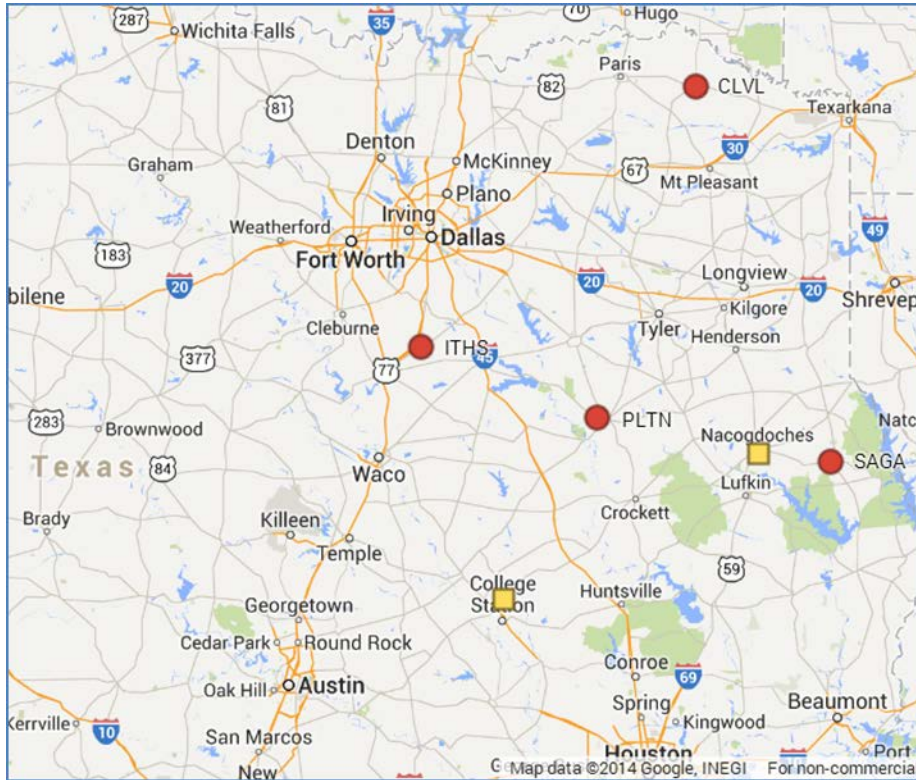


Figure 4-39: Sites used for DFW background model performance evaluation.

Figure 4-40: Modeled and measured ozone concentrations at four sites that characterize background for the DFW area in the June 2006 episode shows observed and modeled ozone at the four sites selected for the June 2006 episode. The model predicts the observed peak ozone concentrations at Italy High School C60 and Clarksville C648 quite well during this episode with a few exceptions, but shows a moderate over-prediction for peak concentrations at Palestine C647 and San Augustine C646 on several days. Generally the model over-predicts nighttime/early morning concentrations at all four sites, probably the result of too-vigorous vertical mixing in the nocturnal boundary layer by the model, resulting in excessive NO_x titration.

Figure 4-41: Modeled and measured ozone concentrations at four sites that characterize background for the DFW area in the August-September 2006 episode shows a similar picture for the August-September 2006 episode. The model generally predicts peak ozone concentrations well at Italy High School C60, but shows somewhat enhanced over-predictive tendencies at the remaining three sites. Again, overnight/early morning ozone concentrations are over-predicted almost universally.

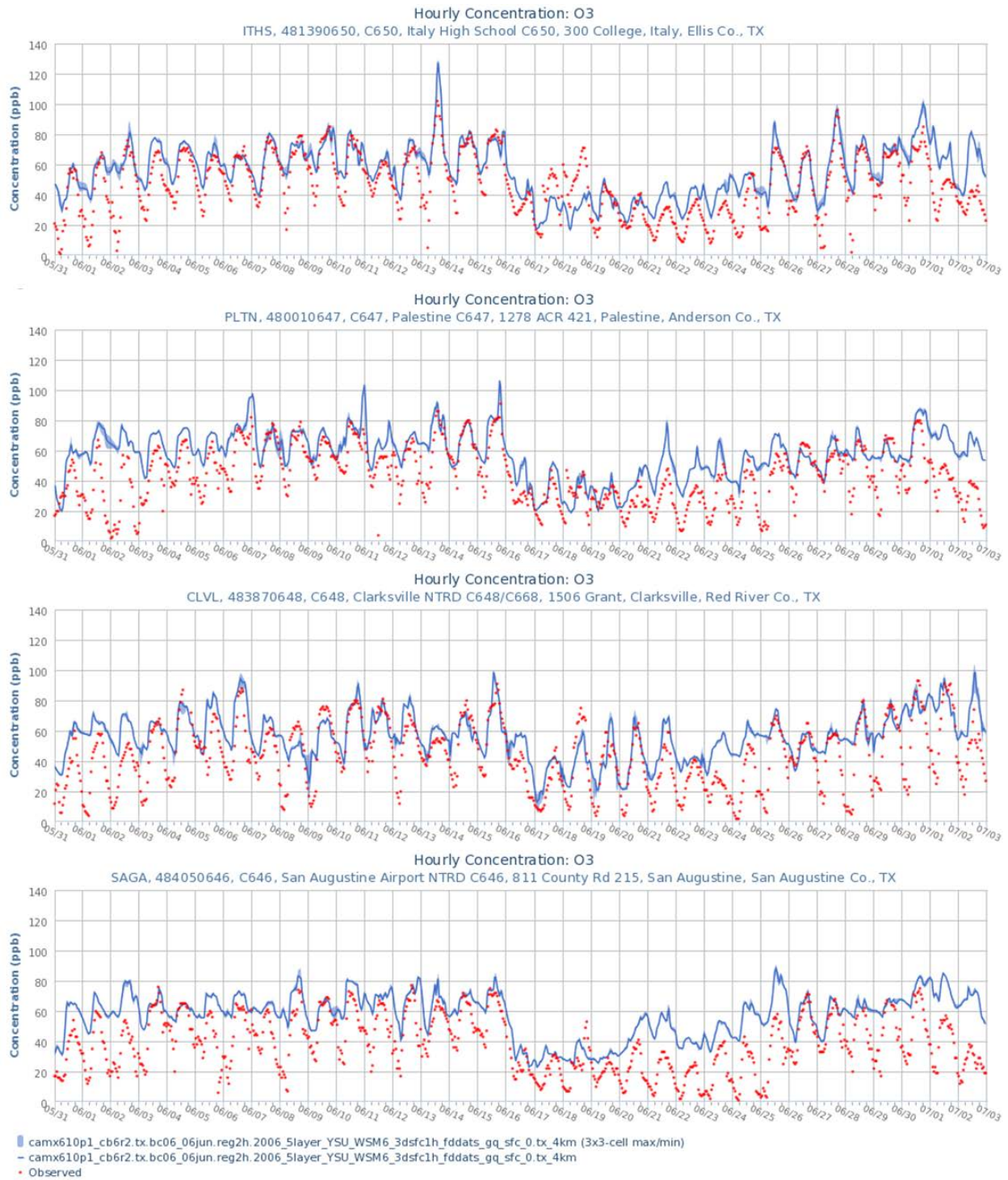


Figure 4-40: Modeled and measured ozone concentrations at four sites that characterize background for the DFW area in the June 2006 episode

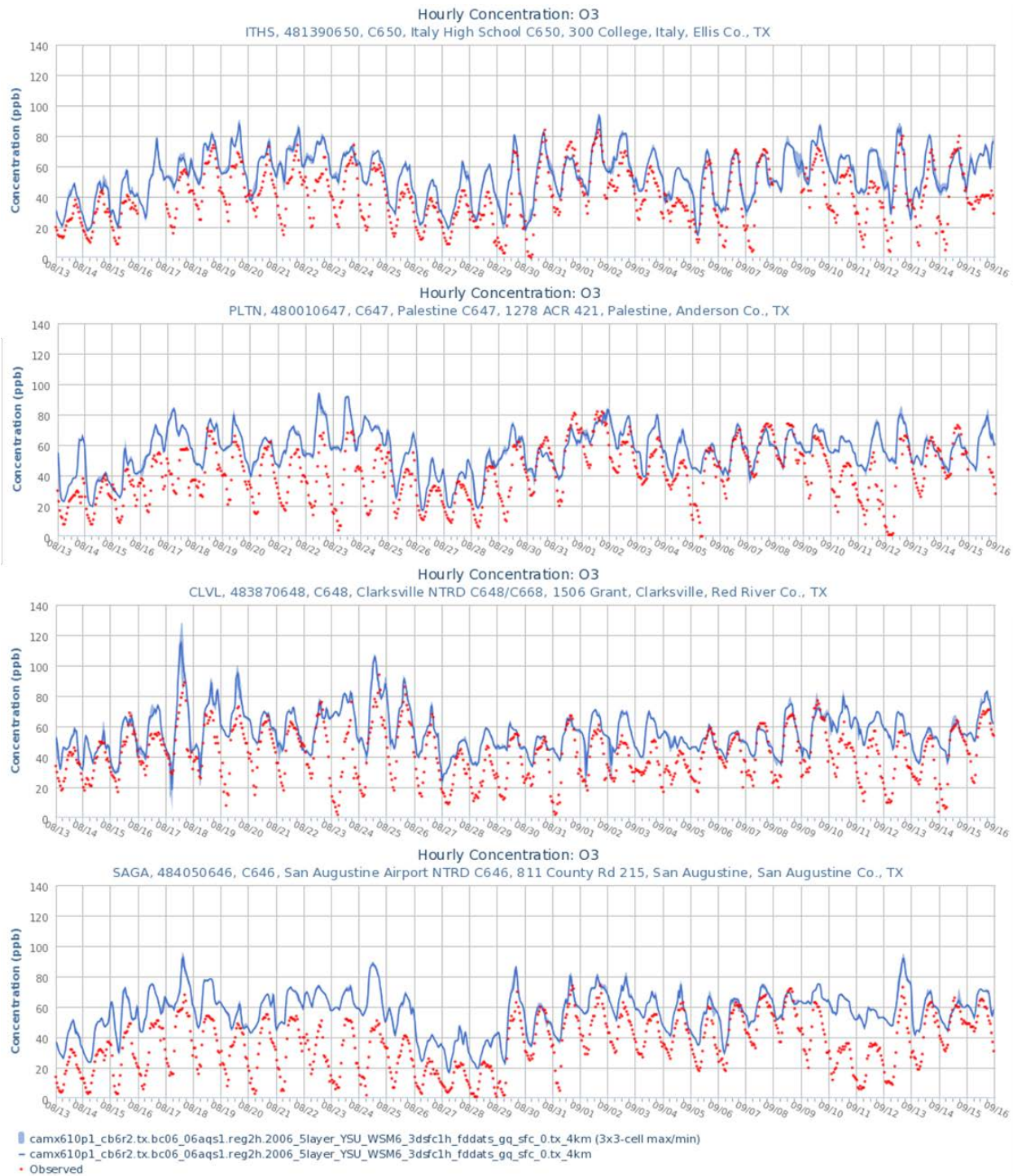


Figure 4-41: Modeled and measured ozone concentrations at four sites that characterize background for the DFW area in the August-September 2006 episode

Figure 4-42: Modeled and measured NO_x concentrations at San Augustine C646 in the June and August-September 2006 episodes. shows observed and modeled NO_x concentrations at San Augustine C646 for both episodes, and the model seems to maintain about the right levels of NO_x at this site, although modeled daytime concentrations are typically too low. Overall both measured and modeled concentrations are quite low.

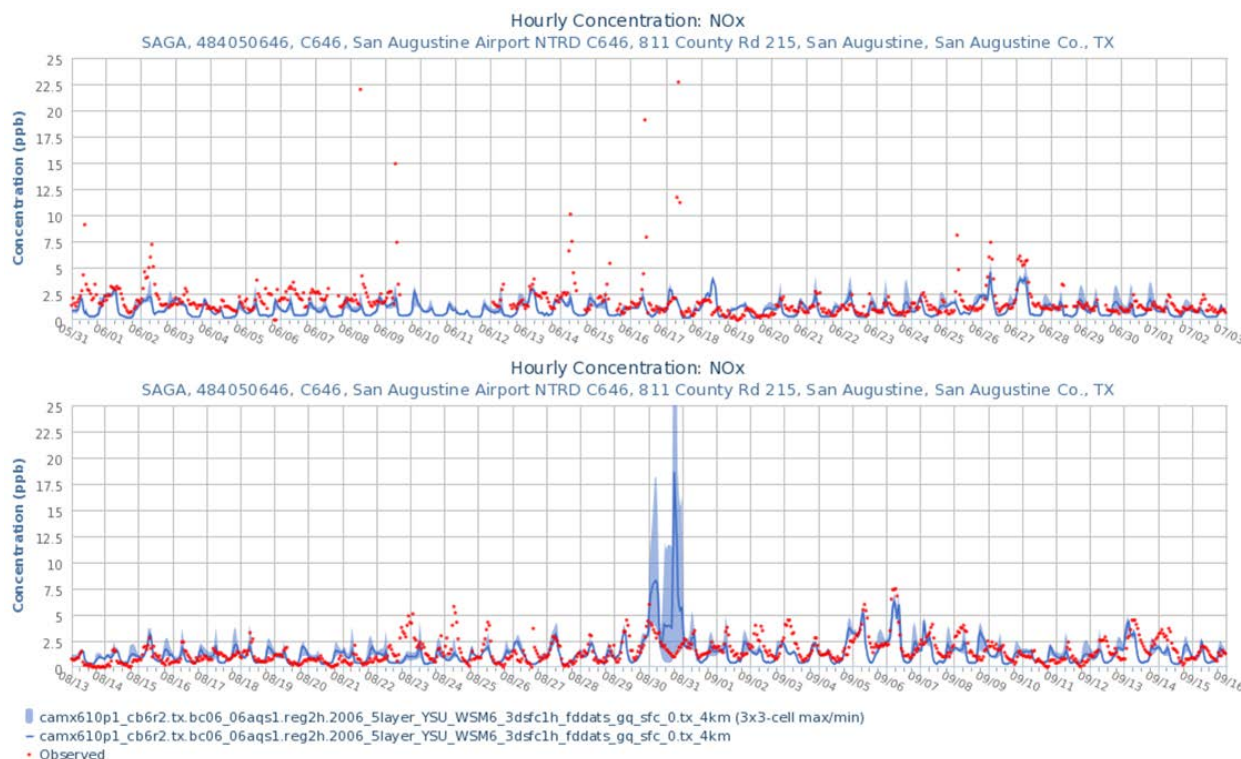


Figure 4-42: Modeled and measured NO_x concentrations at San Augustine C646 in the June and August-September 2006 episodes.

An additional opportunity to study modeled background arises from two ozonesonde launches that were made during the June 2006 episode from semi-rural locations in East Texas, one from College Station and the other from Nacogdoches. Many additional launches were made during the two episodes, but all the rest were performed in either the Houston area or in the Gulf of Mexico from the fantail of the Research Vessel Ronald H. Brown during the TexAQS II intensive period, and are not particularly relevant to DFW background.

Figure 4-43: Observed and modeled ozone concentrations for two ozonesonde launches (L) from College Station at 12:00 on June 15, 2006, and (R) Nacogdoches at 12:00 on June 27, 2006. shows modeled and observed ozone concentrations as the sondes rose through the atmosphere on two days: June 15 (launch at College Station) and June 23 (launch at Nacogdoches), both at noon CST. The left-hand plot shows that on June 15 ozone was fairly uniformly mixed through the first 3000 m, which likely defines the top of the planetary boundary layer (PBL) at this location and time. The plot shows that the model similarly showed ozone well-mixed to a similar depth. The model tracks the observed ozone through about 6000 m, where it diverges from the observations. On June 23, modeled ozone at the surface exceeds the observed concentration by about 15 ppb, and then decreases up to around 1500 m, while

observed ozone increases through the same column until the two converge at what is probably the top of the PBL on that day. Above that point both modeled and observed ozone increase up to 7000 m, though not monotonically and somewhat asynchronously. Above 7000 m the model increases more rapidly than the observations. For both launches, much of the disparity between modeled and observed ozone concentrations aloft may be due to very coarse vertical resolution of modeled layers above 3000 m.

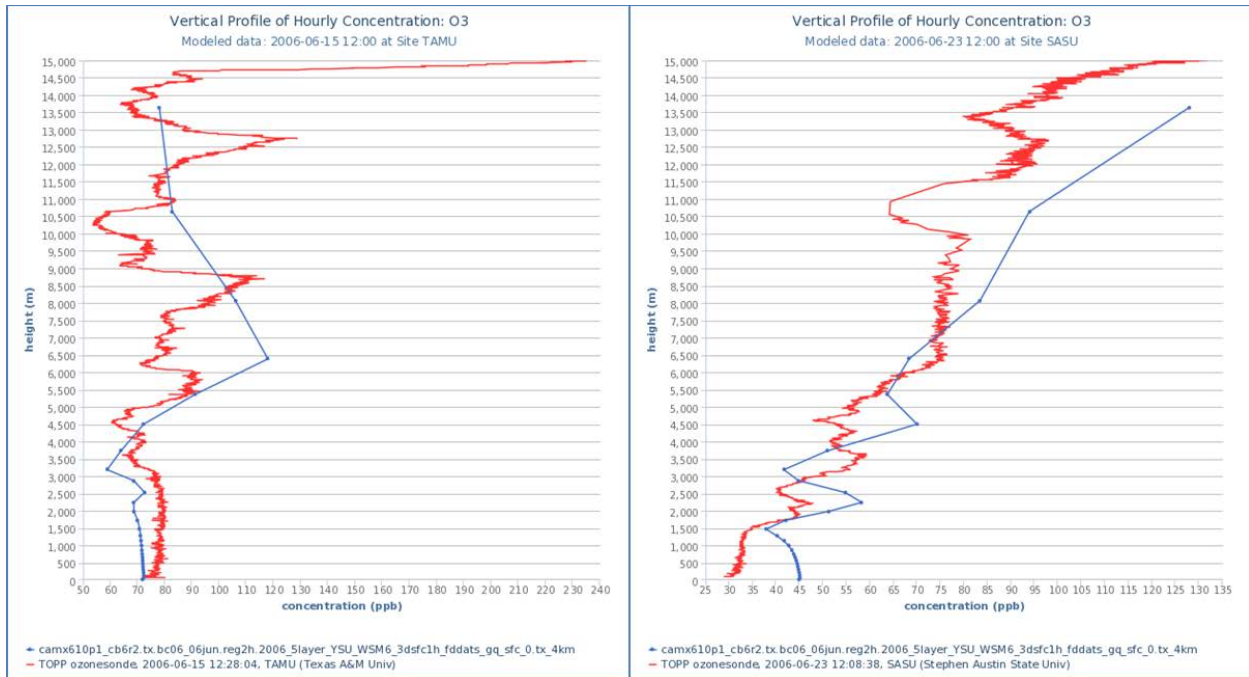


Figure 4-43: Observed and modeled ozone concentrations for two ozonesonde launches (L) from College Station at 12:00 on June 15, 2006, and (R) Nacogdoches at 12:00 on June 27, 2006.

4.6.1. Summary and Conclusions

Modeled ozone at rural surface monitors generally predicted peak ozone concentrations well, with only minor over-prediction on some days at a couple of sites. The over-prediction was notably greater in the August-September episode although the model predicted the peaks on some days well. In general, the model over-predicted overnight/early morning ozone concentrations. The modeled and observed NO_x concentrations at San Augustine were both generally very low.

The ozonesonde data provided a unique and valuable means for assessing the model's performance. Besides simply allowing modeled concentrations to be compared with measurements aloft, the detailed profiles provide insight into how the model characterizes vertical mixing compared to the real atmosphere.

The most striking difference between observed and modeled vertical ozone profiles is the wide variability in ozone concentrations with altitude, observed on most days. The model, meanwhile, tends to vary much more slowly, which is not unexpected as it tends to organize wind flow and vertical motion, and because the model's vertical resolution becomes coarser the higher up it goes.

4.7. Aircraft Model Performance Evaluation

The TexAQS II intensive period was nominally between August 15 and September 15, 2006, although a variety of measurements were made before and after this period. Because the National Oceanic and Atmospheric Administration (NOAA) WP-3D Orion aircraft was not fully deployed until September and was primarily focused on Houston, only a single flight provided meaningful data for the DFW area. *Figure 4-44: Flight path of the NOAA WP3D Orion over the DFW area on September 13, 2006.* Observed ozone concentrations and measured winds are displayed. shows the flight path on September 13, 2006 when the aircraft made a series of overflights of the DFW area before returning to Houston. The aircraft maintained an altitude of around 500 m and encountered relative light winds that were mostly southwesterly but showed some local variations.

NOAA P3 Measured O3 Mixing Ratio
13SEP 13:30 to 13SEP 16:00, 1 Minute Averages

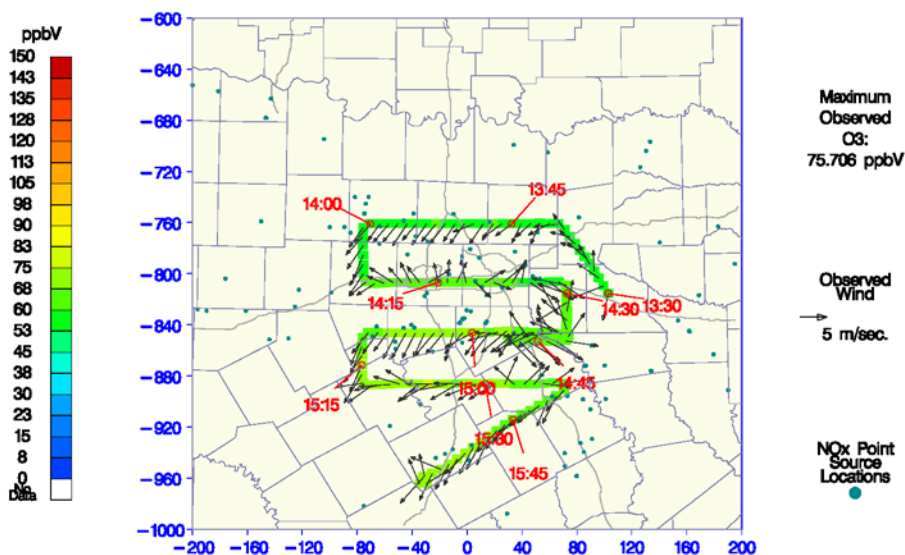


Figure 4-44: Flight path of the NOAA WP3D Orion over the DFW area on September 13, 2006. Observed ozone concentrations and measured winds are displayed.

Figure 4-45: Modeled ozone concentrations and winds along the flight path of the NOAA WP3D Orion over the DFW area on September 13, 2006 **Error! Reference source not found.** shows modeled ozone along the same flight track as Figure 4-44. The model predicts the observed ozone quite well except for a small over-prediction as the aircraft passed through the urban plume downwind of the DFW metropolitan area. The modeled winds are more southerly than the observations and show very little variability through the sampling period.

Figure 4-46: Time series of modeled and aircraft-monitored ozone concentrations, 13:30 to 16:00, September 13, 2006 plots the same data as in the preceding two figures as a time series. The transects of the urban plume are easily discerned by the “bumps” seen in both the modeled and observed ozone concentrations (left y-axis), which track together very well. The altitude is shown as the thin black line, using the right y-axis. The aircraft descended to an altitude of approximately 500 m shortly after 13:30, then maintained this altitude fairly consistently until it ascended for its return to Houston just prior to 16:00.

CAMx Reg2h Modeled O3 Mixing Ratio
13SEP 13:30 to 13SEP 16:00, 1 Minute Averages

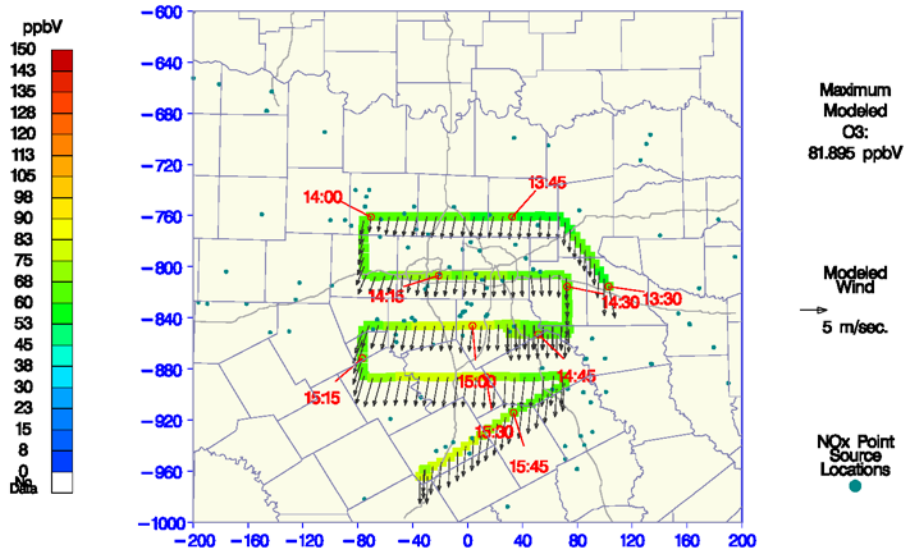


Figure 4-45: Modeled ozone concentrations and winds along the flight path of the NOAA WP3D Orion over the DFW area on September 13, 2006

Observed and Modeled O3 Mixing Ratios
13SEP 13:30 to 13SEP 16:00, 1 Minute Averages

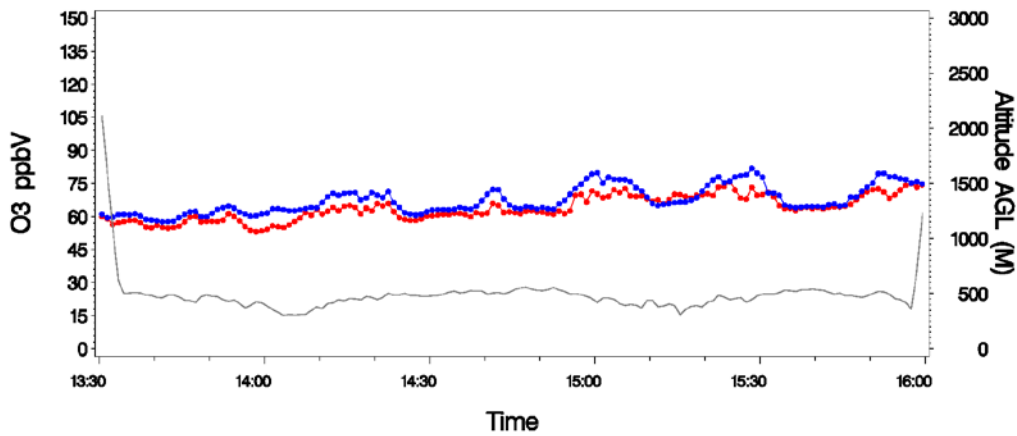


Figure 4-46: Time series of modeled and aircraft-monitored ozone concentrations, 13:30 to 16:00, September 13, 2006

Figure 4-47: Modeled and aircraft monitored concentrations of CO, formaldehyde (FORM), nitric acid (HNO₃), isoprene, NO, NO₂, NO_y, PAN, toluene (TOL), and xylene (XYL) over the DFW area on September 13, 2006 shows time series for 10 pollutants measured during the same

flight over the DFW area. Because this was one of the first flights of the TexAQS II campaign, not all equipment was operating (including the continuous ethylene monitoring), and no canister samples were taken, which would have provided information on many additional hydrocarbons. However, the available measurements are quite useful for evaluating the model's performance aloft. Each plot in the figure (except isoprene (ISOP)) shows clearly the urban plume transects, and all show fairly good agreement between modeled and observed concentrations. Modeled background CO is lower than observed, but agrees well with observed values within the urban plume, while modeled formaldehyde (FORM) is about 20% below the observed concentrations both in and outside of the plume. Modeled nitric acid (HNO₃) background values are a little high, but the model agrees very well with observations in the urban plume.

Modeled isoprene is lower than measured except for a short period when the aircraft was southeast of Dallas. Both NO and NO₂ have modeled and observed backgrounds near zero, and the model shows some under-prediction within the urban plume. Similarly, modeled NO_y shows a small negative bias, but otherwise tracks very well with the observations. Background values of nitrous acid (PAN) are simulated well for much of the flight but have some under-prediction southeast of Dallas coincident with the location of the isoprene over-prediction noted above.

Finally, the model simulates toluene very well, but under-predicts xylene.

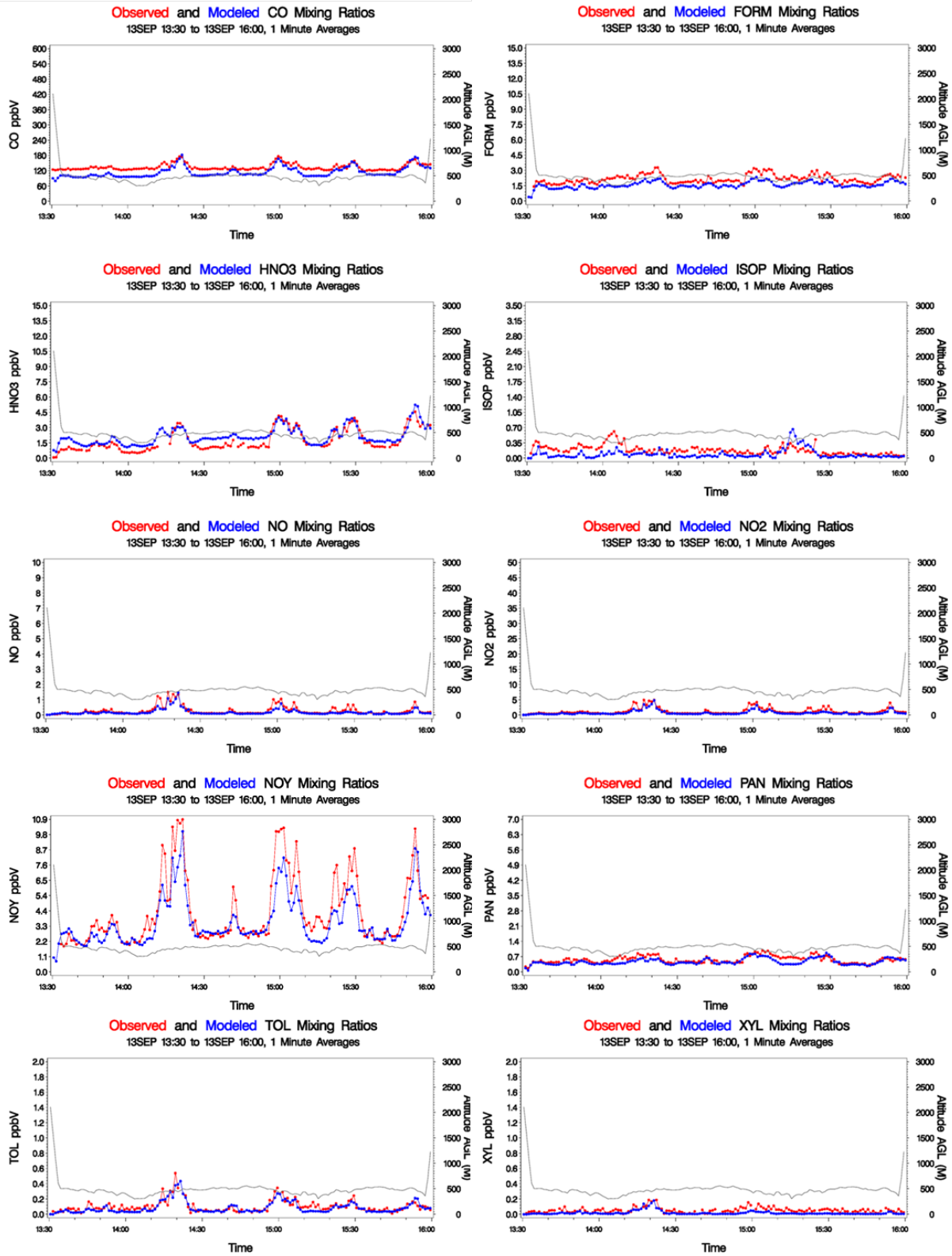


Figure 4-47: Modeled and aircraft monitored concentrations of CO, formaldehyde (FORM), nitric acid (HNO₃), isoprene, NO, NO₂, NOY, PAN, toluene (TOL), and xylene (XYL) over the DFW area on September 13, 2006

5. DIAGNOSTIC EVALUATIONS

5.1. Sensitivity Analyses

Besides comparing the 2014 and 2011 modeling platforms, the TCEQ conducted several sensitivity runs wherein two CAMx model runs that differed from one another by a single input were compared. The sensitivity of the modeled ozone concentrations to this difference was assessed. Sensitivity analyses help to identify the factors most relevant to ozone production and therefore most important to improving model performance. Because the evolution of the 2014 modeling platform involved several incremental steps, some of the sensitivity analyses presented here were performed on configurations slightly different from the final base case, but the differences are small enough for the results to still be applicable.

5.1.1. Alternative Chemistry Mechanisms: CB05 vs. CB6r2d3

A major difference between the 2011 and 2014 modeling platforms was changing from the older CB05 chemical mechanism to the more advanced CB6 mechanism. Emissions were processed through EPS3 to produce inputs appropriate for both mechanisms, and the two sets of emissions were run for each episode using the appropriate chemical processor. CAMx was run using the stock CB6 chemistry, but the modeled ozone concentrations exhibited significant over-predictive bias. The CB6r2d3 chemical mechanism, a non-public test version, generally produced higher ozone peaks than CB05, but not as high as CB6. The runs described in this sensitivity provide only a comparison between CB6r2d3 and the version used in the 2011 attainment demonstration, CB05. The model runs used in this comparison were performed in September and October of 2013 using the Reg2e base emission inventory. Note that the chemical mechanism used in the final attainment demonstration is CB6r2, which produces slightly lower (generally < 1 ppb) ozone concentrations than CB6r2d3.

Besides comparing the models' ability to replicate base year ozone concentrations, these runs were made to see if the different chemical mechanisms would respond differentially to projected changes in emissions between 2006 and 2018. Because the attainment test is based on relative model response, assessing the sensitivity of the relative response factors (RRFs) to model configuration changes is as important (if not more so) than assessing the sensitivity of model performance to these changes. To preserve comparability with the 2018 future case, these sensitivity analyses were conducted using the 2006 baseline instead of the base case emissions.

The sensitivity of the model to a change in chemistry processors can be easily visualized using the "soccer goal" plot which plots relative error against relative bias for both runs, and scatter plots of each run's peak predicted ozone concentration against the domain-wide observed maximum. One-hour ozone bias and error are calculated for each episode day using all model-observation pairs with observed ozone ≥ 60 ppb. For eight-hour ozone, only the maximum daily average eight-hour ozone concentrations (MDA8) are used, provided the observed MDA8 value is ≥ 40 ppb. Hence the one-hour statistics can include up to 24 model-observation pairs for every site on a given day, but the 8-hour statistics can include no more than one pair per monitor on a given day.

Figure 5-1: One and eight-hour relative bias, error, and domain-wide peak ozone for the June 2006 episode for CB05 and CB6r2d3 shows bias, error, and peak ozone predictions for two model runs, both using CAMx v6.0 and otherwise identical inputs, but one with CB05 and the other with CB6r2d3, for the June 2006 episode. The left-hand soccer goal plots indicate the recommended error tolerances of 15% and 30% for relative bias and error for one-hour ozone. Although EPA has not established similar tolerances for eight-hour ozone, the goal box is shown on the eight-hour plots for reference.

Both the CB05 and CB6r2d3 runs show most days falling within the recommended ranges for bias and error for one-hour ozone, although the latter runs shows some shift towards the right-hand side of the graph, indicating some over-prediction bias. Three more days move outside the recommended error tolerances. Peak one-hour ozone over-prediction is increased somewhat with CB6r2d3, but as explained earlier, over-prediction of the peak concentration may be simply the result of modeling every location while only a relatively few locations are monitored. Similarly, the statistics for MDA8 ozone also show a shift towards over-prediction with CB6r2d3.

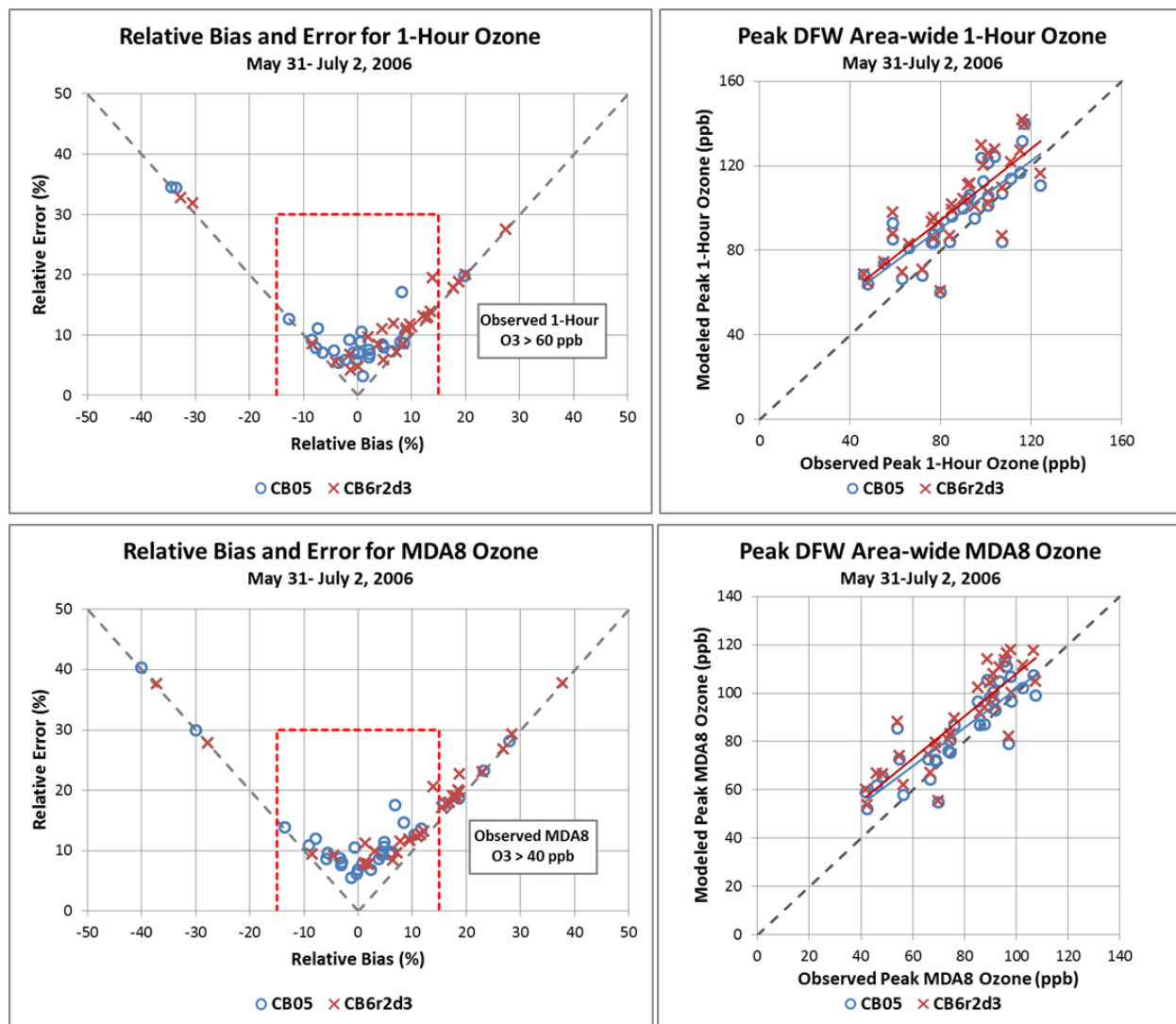


Figure 5-1: One and eight-hour relative bias, error, and domain-wide peak ozone for the June 2006 episode for CB05 and CB6r2d3.

Figure 5-2: One and eight-hour relative bias, error, and domain-wide peak ozone for the August-September 2006 episode for CB05 and CB6r2d3. shows similar plots for the August-September episode. In this case, both chemical mechanisms indicate a tendency towards over-prediction, more so with CB6r2d3 than with CB05, although the change is less pronounced than for the June episode, and in fact is minimal for the domain wide peaks.

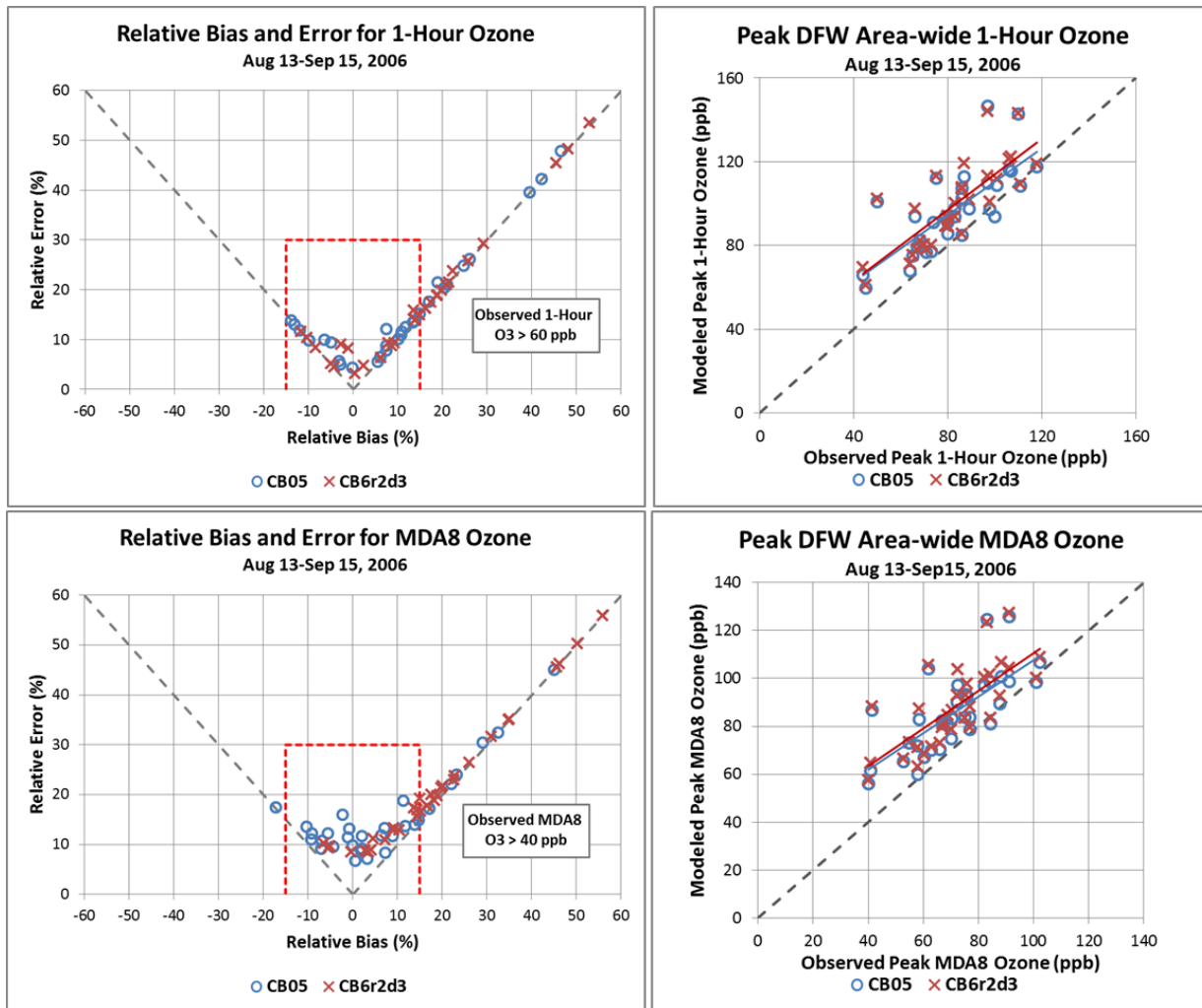


Figure 5-2: One and eight-hour relative bias, error, and domain-wide peak ozone for the August-September 2006 episode for CB05 and CB6r2d3.

To examine the differences between CB05 and CB6r2d3 more thoroughly, *Figure 5-3: Time series at four DFW monitors for August 18-23, 2006 comparing modeled ozone concentrations using CB6r2d3 (blue) with those using CB05 (green)* shows time series plots for five days in August 2006 where moderate to high ozone was recorded in the north and northwestern part of the DFW area. Four monitors in this area are shown: Denton C56 (DENT), Eagle Mountain Lake C75 (EMTL), Grapevine C70 (GRAP), and Keller C17 (KELC). For four of the five days CB6r2d3 (blue) created higher peak ozone concentrations than did CB05 (green), but in most cases the modeled peaks were slightly higher than the observations (red). On a few of the higher ozone days (August 18 at Denton C56, Eagle Mountain Lake C75, and Keller C17, and August 21 at Denton C56) CB6r2d3 predicted the maximum better than did CB05. While on some other days, CB05 matched the observations better. Overall, however, both chemical mechanisms do a credible job of predicting both the peak and diurnal variation of ozone concentrations.

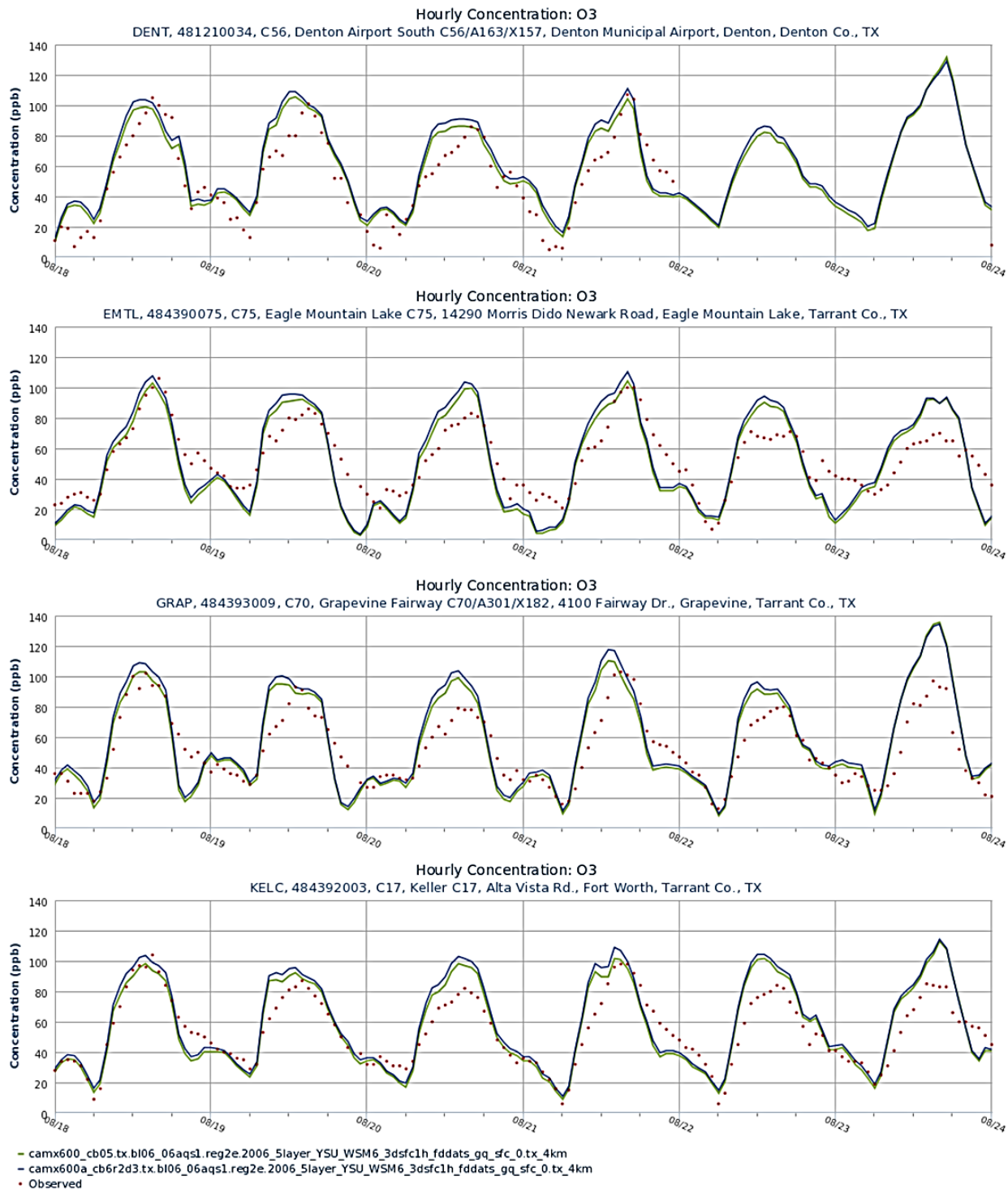


Figure 5-3: Time series at four DFW monitors for August 18-23, 2006 comparing modeled ozone concentrations using CB6r2d3 (blue) with those using CB05 (green)

Additional insight can be gained by looking at the same data through a different lens. Figure 5-4 shows scatter plots of observed and modeled one-hour ozone concentrations at four different locations for the August-September episode. Denton C56 (upper-left) and Eagle Mountain Lake

C75 (upper right) are shown, along with two monitors on the outskirts of the DFW area, Greenville C1006 (lower left) and Kaufman C71 (lower right). Besides the paired observations for modeling conducted with the CB05 (green) and CB6r2d3 (blue) mechanisms, the modeling shows the quantile-quantile (QQ) plots, which show graphically how the modeled concentrations for the two distributions (orange and purple, respectively) compare. All four graphics show a modest increase in ozone concentrations from CB05 to CB6r2d3, but in every case both mechanisms exhibit good performance for the higher range of observed ozone concentrations.

Note that the increase in ozone concentrations between CB05 and CB6r2d3 is very similar among all four monitors. If CB6r2d3 produced ozone significantly faster than CB05, there would be a more pronounced difference for the two monitors downwind of the urban areas (Denton C56 and Eagle Mountain Lake C75). Because this is not the case, it appears that CB06r2d3 creates more ozone regionally, not just within urban plumes.

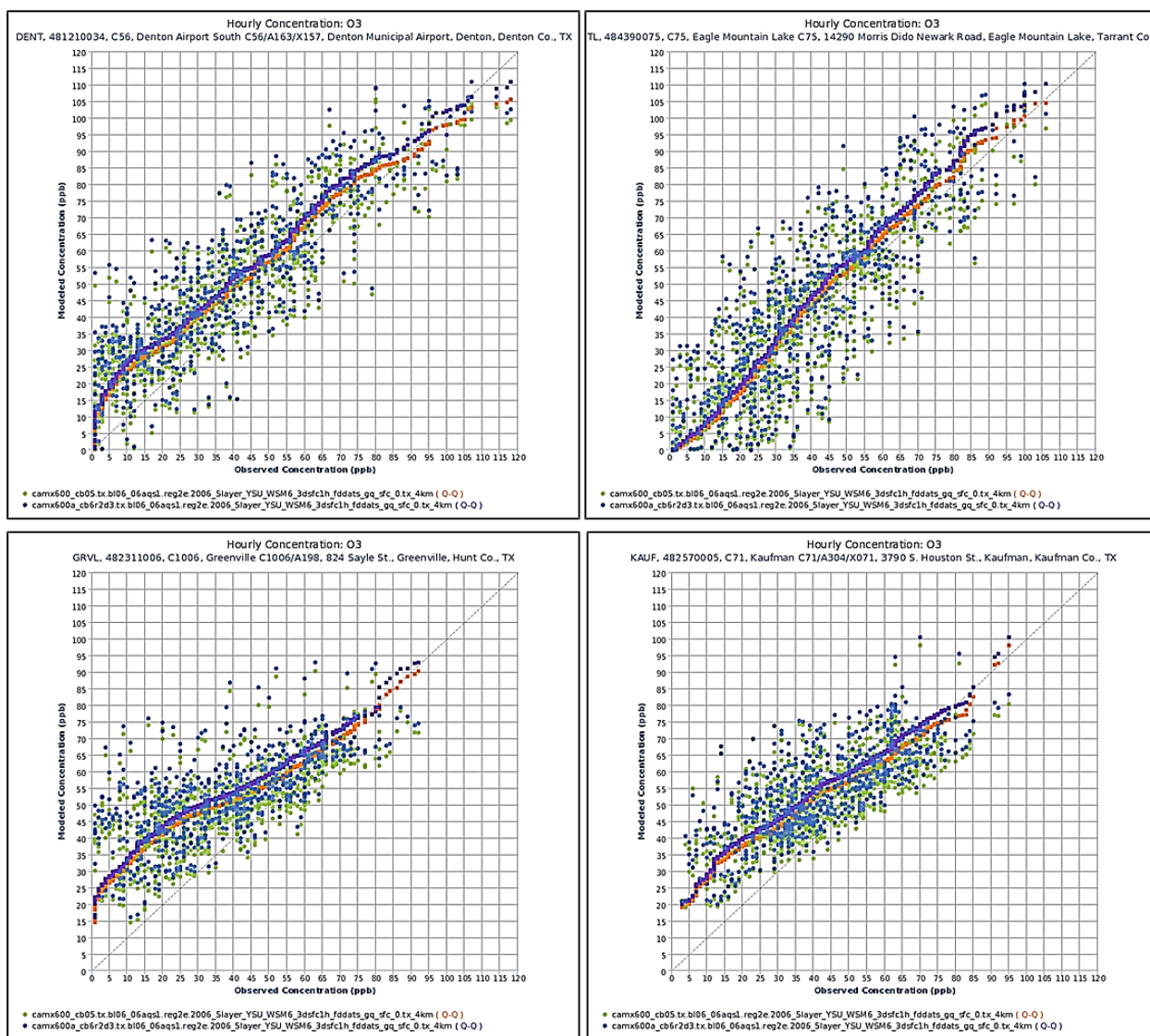


Figure 5-4: Scatter plots of observed and modeled ozone concentrations at four DFW area monitors comparing CB05 (green) with CB6r2d3 (blue) ozone concentrations. QQ plots for the two chemical mechanisms are shown in orange and purple, respectively.

Finally, the primary purpose of this sensitivity analysis was to compare the responsiveness of CAMx with the two chemical mechanisms. The modeled attainment test calculates future design values using RRFs, so comparing the RRFs between the two mechanisms is directly related to the attainment test. The modeled 2006 to 2018 RRFs for the two chemical mechanisms are shown in *Table 5-1: Comparison of 2006 to 2018 RRFs between CAMx runs using CB05 and CB6r2d3*.

Table 5-1: Comparison of 2006 to 2018 RRFs between CAMx runs using CB05 and CB6r2d3

Monitor ID	Monitor Name	CB05 RRF	CB6r2d3 RRF
ARLA	Arlington Municipal Airport C61	0.828	0.833
CLEB	Cleburne Airport C77	0.816	0.827
DALN	Dallas North C63	0.827	0.839
DENT	Denton Airport South C56	0.811	0.821
DHIC	Dallas Hinton Street C401	0.825	0.837
EMTL	Eagle Mountain Lake C75	0.803	0.812
FRIC	Frisco C31	0.819	0.832
FWMC	Fort Worth Northwest C13	0.815	0.824
GRAN	Granbury C73	0.816	0.819
GRAP	Grapevine C70	0.822	0.834
GRVL	Greenville C1006	0.846	0.840
KAUF	Kaufman C71	0.850	0.842
KELC	Keller C17	0.813	0.824
MDLO	Midlothian OFW C52	0.830	0.837
MDLT	Midlothian Tower C94	0.831	0.837
PIPT	Pilot Point C1032	0.811	0.821
REDB	Dallas Executive Airport C402	0.830	0.833
RKWL	Rockwall Heath C69	0.835	0.841
WTFD	Parker County c76	0.809	0.813
Average RRF		0.823	0.830

The responsiveness of CB6r2d3 is slightly less than that of CB05 (a smaller RRF is more responsive, which yields a higher DV_F), at least for the modeled emission differences between 2006 and 2018. Only two monitors outside the main urban areas, Kaufman C71 and Greenville C1006, showed more responsiveness with CB6r2d3, while the converse is true for the seventeen remaining monitors. Despite the small numerical difference, a two-sample t-test showed that the difference was statistically highly significant (p = 0.00029).

5.1.2. MEGAN vs. GloBEIS biogenic emissions

One significant scientific advancement between the 2011 modeling platform and the 2014 platform is use of the Model of Emissions of Gases and Aerosols from Nature (MEGAN) version 2.1 instead of the previously used Global Biosphere Emissions and Interactions System (GloBEIS). The TCEQ had relied on GloBEIS instead of EPA's Biogenic Emissions Inventory System (BEIS) primarily because GloBEIS accepted user-provided Land Use/Land Cover (LULC) data instead of relying on stock LULC databases provided with BEIS. However, MEGAN is much more widely used than GloBEIS and is updated more frequently. It also is amenable to user-supplied LULC data.

The sensitivity test described here was run in June and July 2013 using the Reg2c base case. An additional difference between the runs here is that the MEGAN runs used photosynthetically active radiation (PAR) from the WRF model, while the GloBEIS run used PAR measured by the Geosynchronous Operational Environmental Satellites (GOES). Subsequent sensitivity tests found that MEGAN achieved slightly better predictions of isoprene using PAR from GOES, so the final base case used in the attainment demonstration (Reg2h) uses GOES PAR. *Figure 5-5: Comparison of biogenic isoprene emissions using (left) GloBEIS with GOES PAR and (right) MEGAN with WRF PAR compares biogenic emissions for June 19, 2006 using GloBEIS (with GOES PAR) with emissions using MEGAN (with WRF PAR).*

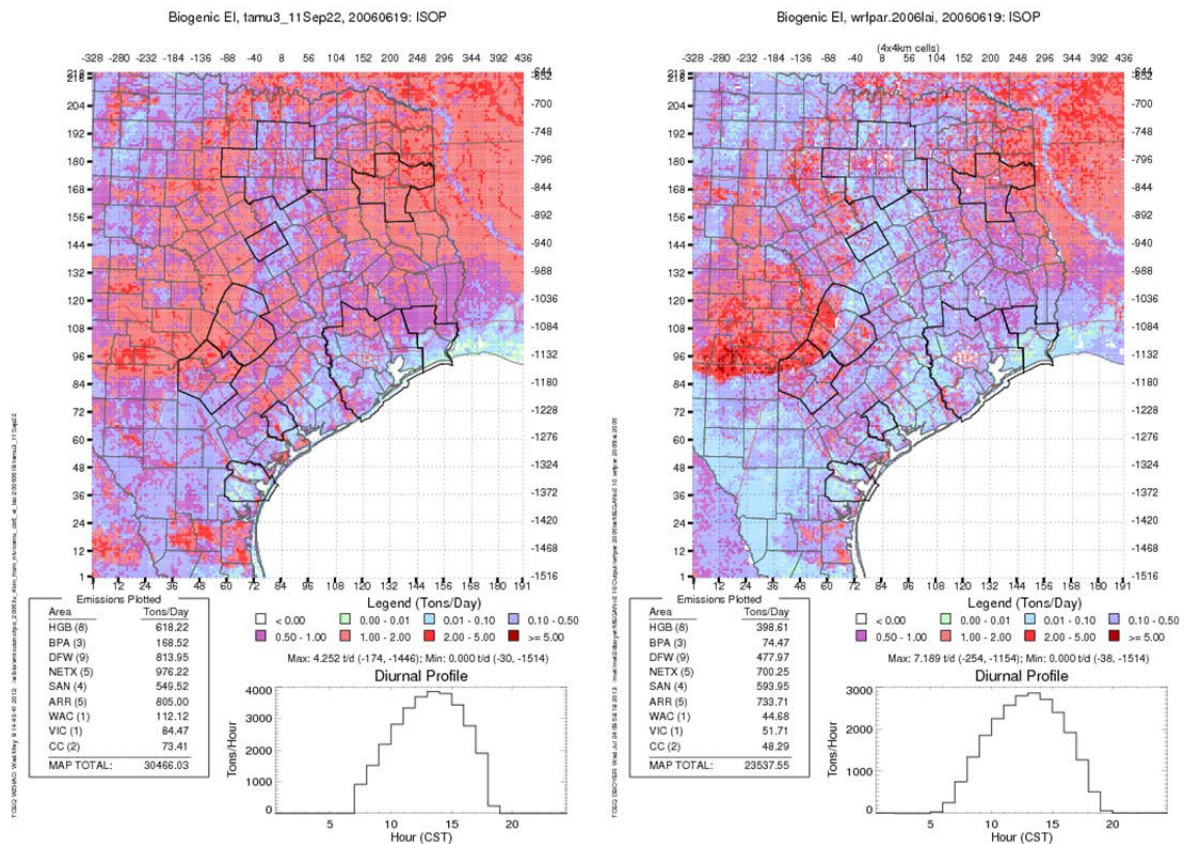


Figure 5-5: Comparison of biogenic isoprene emissions using (left) GloBEIS with GOES PAR and (right) MEGAN with WRF PAR

For this sensitivity analysis, we first compare modeled isoprene concentrations between the two base cases with observations in the DFW area. *Figure 5-6: Predicted and observed isoprene concentrations using MEGAN and GloBEIS at Hinton Street C401 (DHIC) and Fort Worth Northwest C13 (FWMC) sites for June 2006 (top) and Aug-Sep 2006 (bottom) episodes* shows time series plots of the two configurations at Hinton Street C401 (DHIC) and at Fort Worth Northwest C13 (FWMC) compared with hourly Auto-GC measurements for both the June and August-September episodes. Clearly MEGAN (blue line) does a better job predicting isoprene concentrations at Hinton Street than does GloBEIS (green line), although both over-predict isoprene concentrations poorly at Fort Worth Northwest.

Because the Aug-Sep episode coincided with part of the 2006 Texas Air Quality Study (TexAQS II), there was a limited amount of aircraft observation data available for the DFW area and for some upwind areas. The only modeled day coincident with a flight of the NOAA P3 aircraft was September 13, depicted in *Figure 5-7: DFW area NOAA P3 isoprene data for September 13, 2006*. Top Row -Left: Observed isoprene for full flight, - Right Observed isoprene in DFW area; Middle Row – Left: Modeled isoprene along DFW flight path with GloBEIS/GOES, - Right: Modeled isoprene along DFW flight path with MEGAN/WRF; Bottom Row – Left: Time series of observed and modeled isoprene with GloBEIS/GOES, - Right: Time series of observed and modeled isoprene with MEGAN/WRF.. The top left inset shows the flight path on that day with several E-W transects of the DFW area and the top right inset shows a blow-up of the isoprene data collected within the DFW area. The next row of the figure shows (left to right) modeled isoprene concentrations using GloBEIS and using MEGAN. While both modeled and observed isoprene concentrations are generally low, the concentrations with GloBEIS show a definite positive bias, while MEGAN produces isoprene concentrations similar to those observed. The bottom row presents time-series comparisons of GloBEIS and MEGAN. These show a slight negative bias for MEGAN until the aircraft exits the DFW metropolitan area to the south, while GloBEIS shows a strong positive bias over much of the flight path.

The only other modeled days on which the P3 flew were August 31 and September 11 and 15. On the first two days the aircraft did not venture north of the Houston urban core. The aircraft did sample downwind of Houston on September 15, but stayed well south of the DFW area. On that day, also, the modeling with MEGAN showed some negative bias while that with GloBEIS showed a larger positive bias. Note that the shift from a positive bias at ground level to a negative bias aloft for the MEGAN-based modeled concentrations may be related to any of several issues including vertical mixing, reaction rates, or sparse observational data.

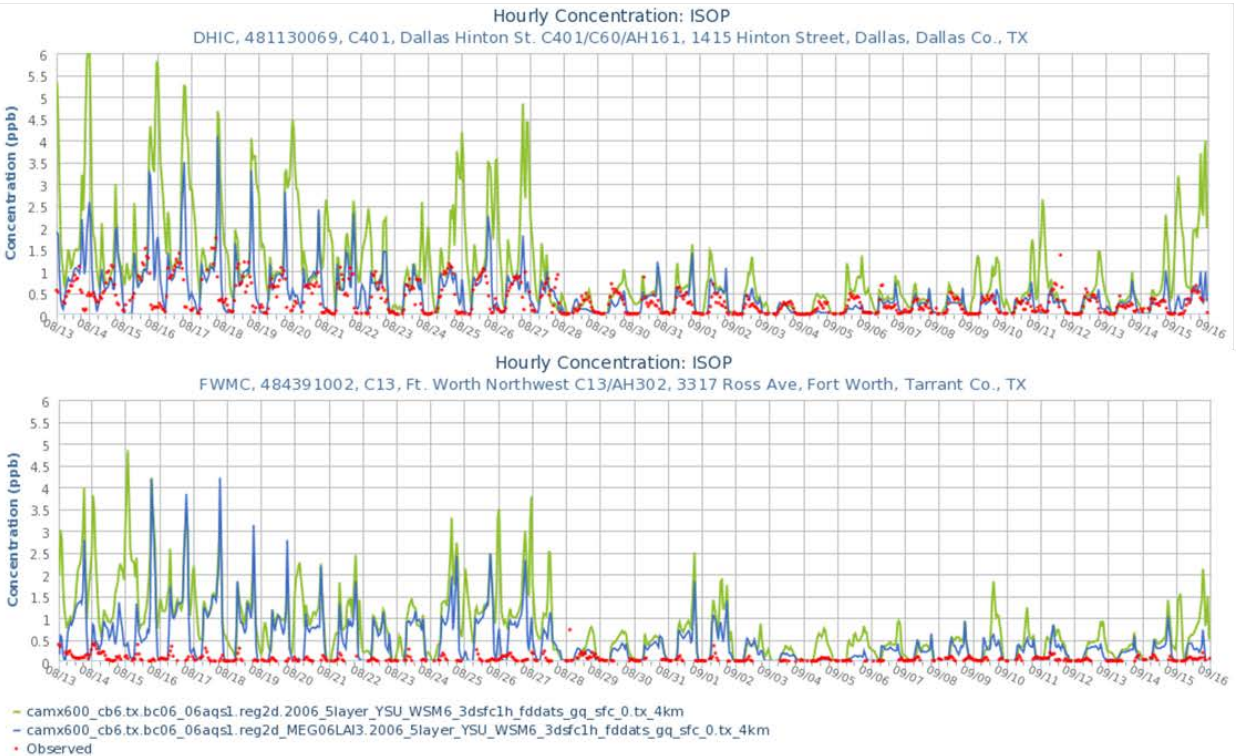
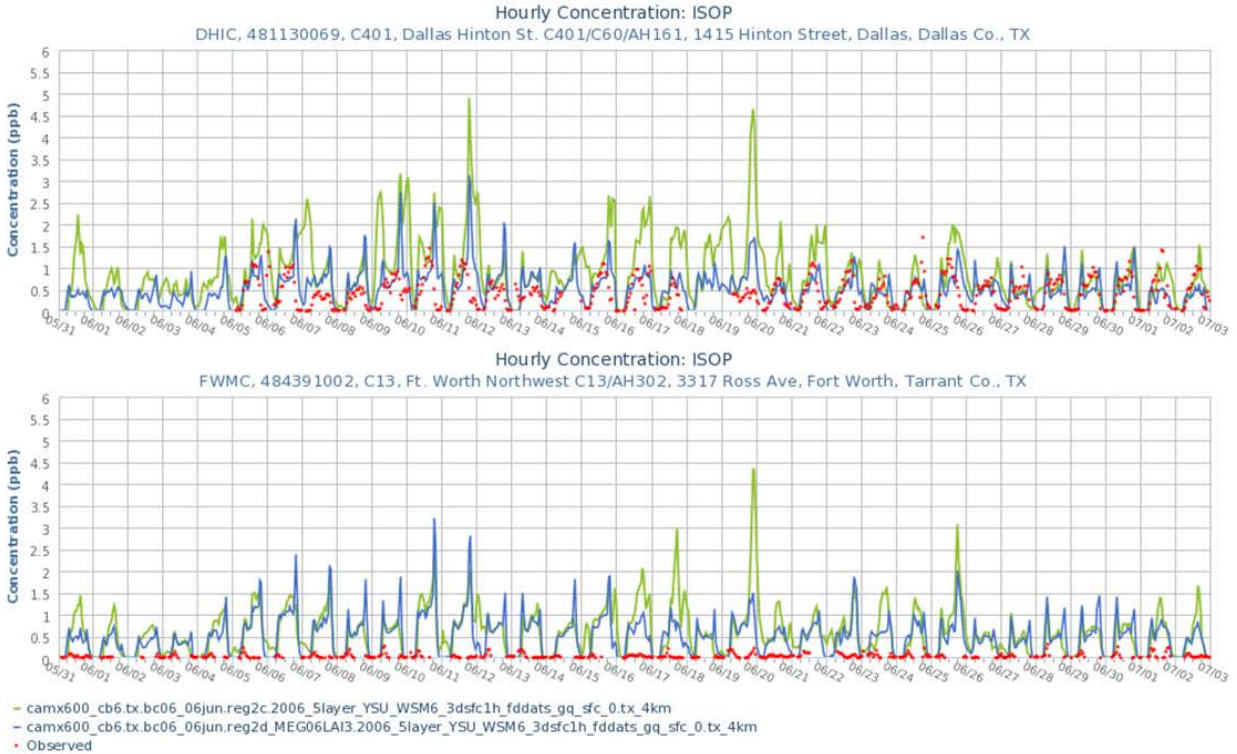


Figure 5-6: Predicted and observed isoprene concentrations using MEGAN and GloBEIS at Hinton Street C401 (DHIC) and Fort Worth Northwest C13 (FWMC) sites for June 2006 (top) and Aug-Sep 2006 (bottom) episodes

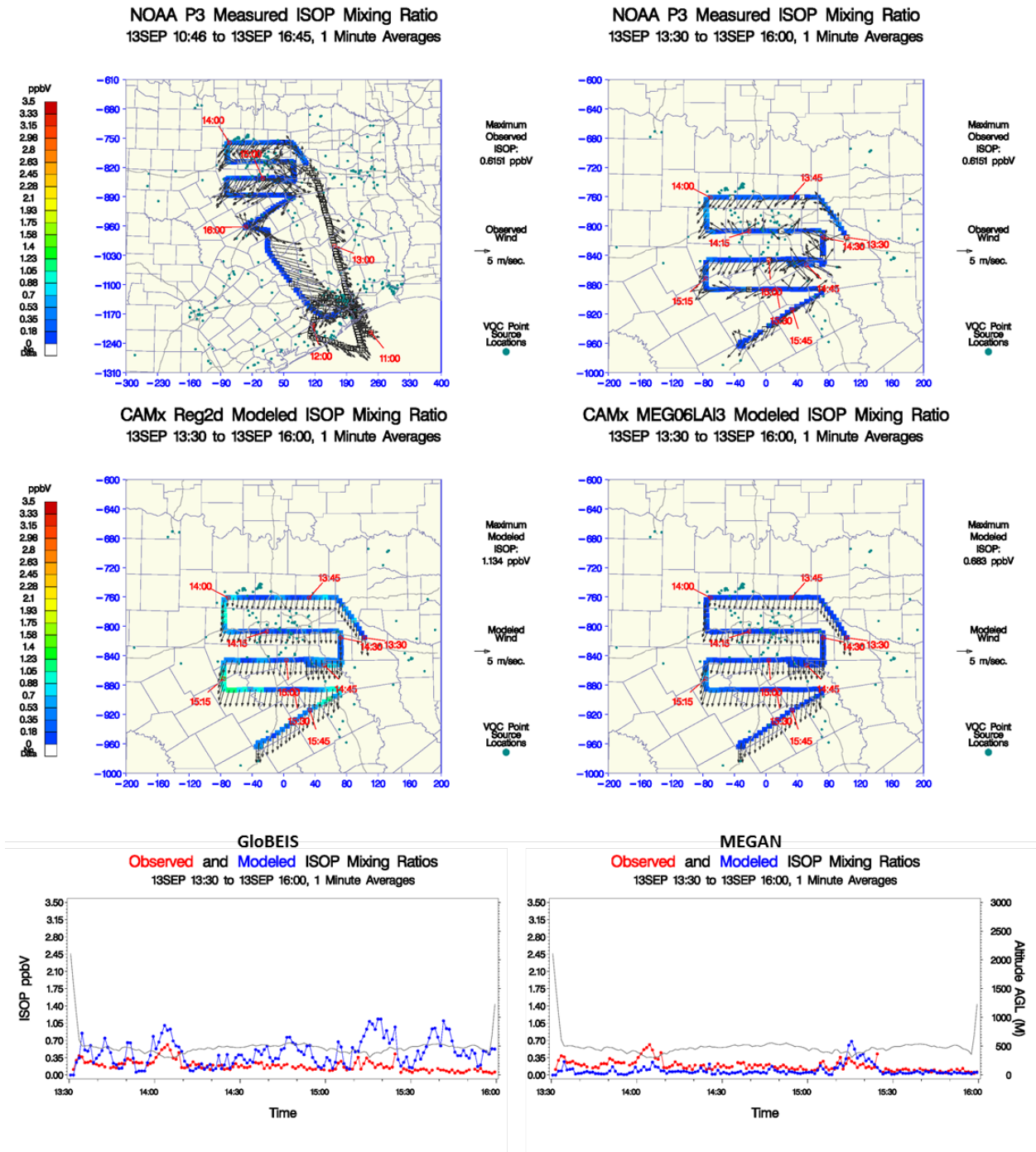


Figure 5-7: DFW area NOAA P3 isoprene data for September 13, 2006. Top Row -Left: Observed isoprene for full flight, - Right Observed isoprene in DFW area; Middle Row – Left: Modeled isoprene along DFW flight path with GloBEIS/GOES, - Right: Modeled isoprene along DFW flight path with MEGAN/WRF; Bottom Row – Left: Time series of observed and modeled isoprene with GloBEIS/GOES, - Right: Time series of observed and modeled isoprene with MEGAN/WRF.

The effects of using MEGAN with WRF PAR instead of GloBEIS with GOES PAR on ozone are shown in *Figure 5-8: One and 8-hour relative bias, error, and domain-wide peak ozone for the June 2006 episode for biogenic emissions using GloBEIS with GOES PAR and MEGAN with WRF PAR.* and *Figure 5-9: One and 8-hour relative bias, error, and domain-wide peak ozone for the August-September 2006 episode for biogenic emissions using GloBEIS with GOES PAR and MEGAN with WRF PAR.* below. The reduction in biogenic isoprene emissions and concentrations translates into improved ozone performance by reducing the over-predictive bias and moving more days into the “goal” box on the soccer-goal plots for both one-hour and MDA8 ozone, and also reducing one-hour and MDA8 peaks.

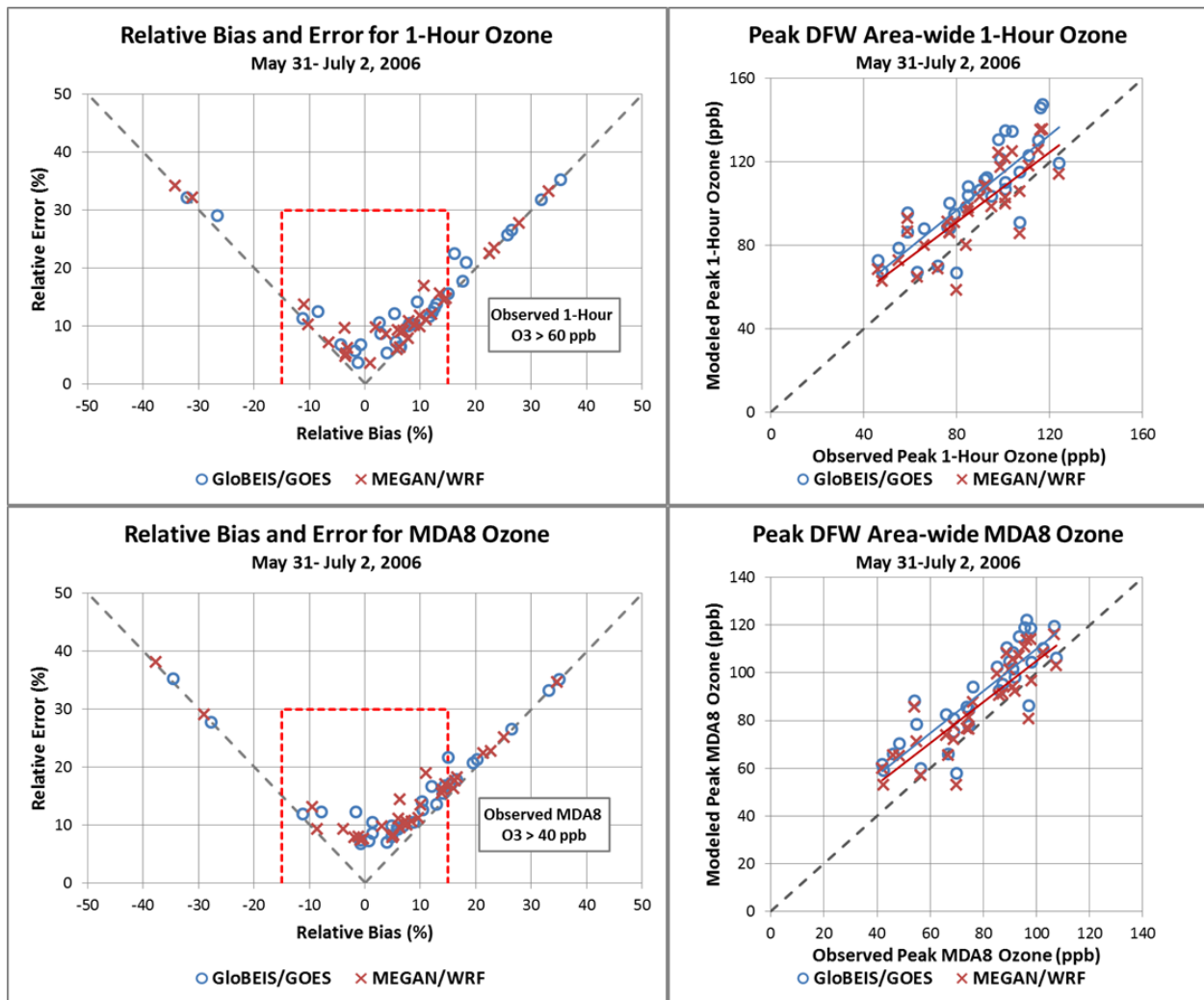


Figure 5-8: One and 8-hour relative bias, error, and domain-wide peak ozone for the June 2006 episode for biogenic emissions using GloBEIS with GOES PAR and MEGAN with WRF PAR.

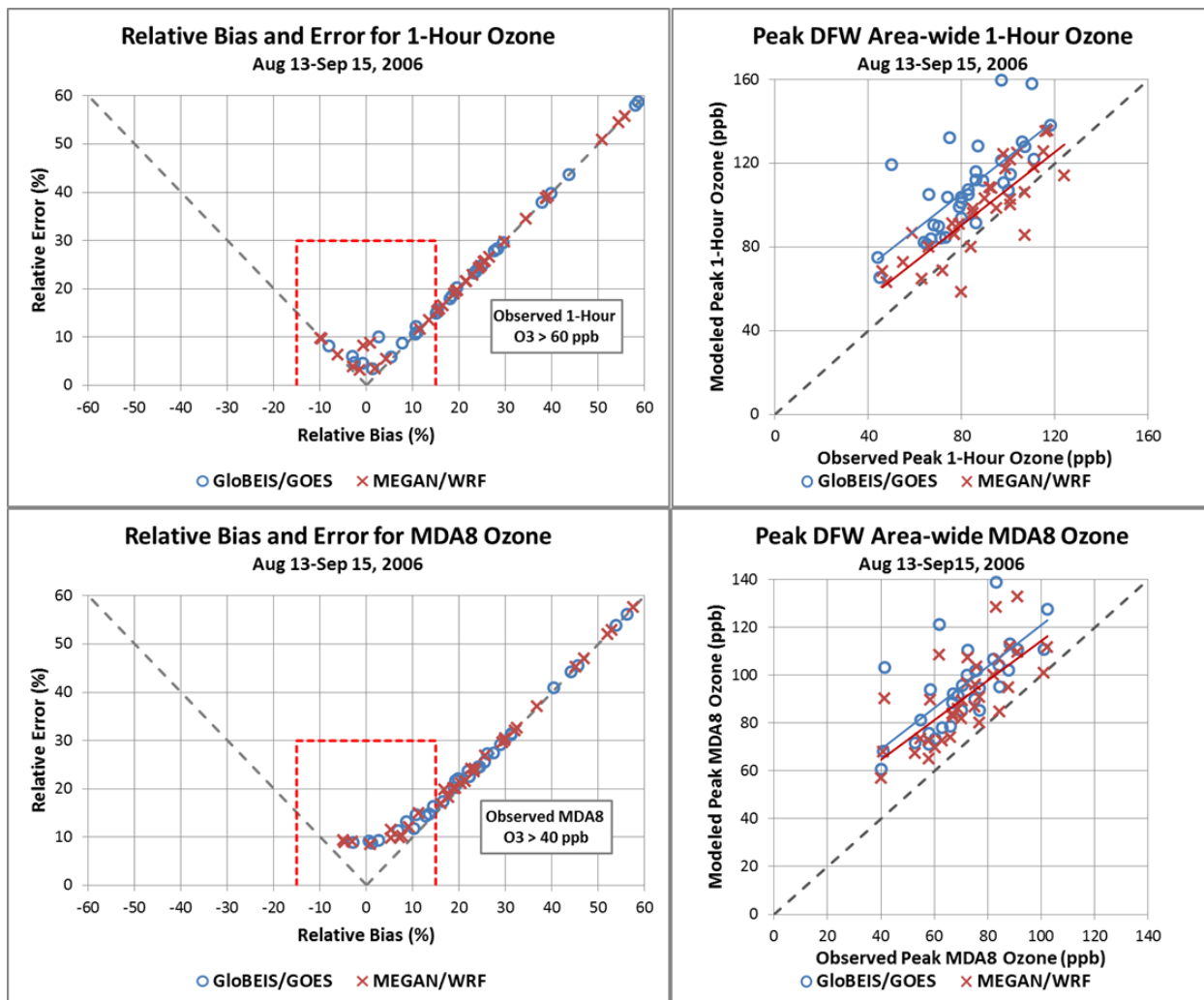


Figure 5-9: One and 8-hour relative bias, error, and domain-wide peak ozone for the August-September 2006 episode for biogenic emissions using GloBEIS with GOES PAR and MEGAN with WRF PAR.

Overall, MEGAN appears to produce modeled isoprene concentrations closer to the observations than does GloBEIS, though the observational data base is fairly small. Using the MEGAN biogenic emissions, the predicted ozone concentration bias and error statistics are reduced compared to using GloBEIS emissions. As we develop newer episodes, additional opportunities to evaluate biogenic emissions estimation will be available.

5.1.3. Highly-Reactive VOC Sensitivity

As discussed in Section 4.5, modeled concentrations of the ETH and OLE CB06 HRVOC species are very high compared with observations at the Hinton Street C401 and Fort Worth Northwest C13 auto-GCs, and also compared with concentrations observed in the previous SIP revision. Two factors which contributed to the increase in HRVOCs have been found:

1. The MEGAN biogenic emission model, while reducing isoprene emissions, increases the relative fraction of hydrocarbons forming the ETH and OLE CB6 species.
2. The updated speciation profiles for mobile sources are richer in hydrocarbons forming ETH and OLE. While the absolute amounts of additional emissions are fairly small, even small amounts of these emissions can contribute significantly to ozone production under certain circumstances, so there is some cause for concern.

We conducted a sensitivity analysis to quantify the effect of the increased HRVOC emissions on ozone concentrations. The emissions modifications were applied as follows: 1) All MEGAN-generated biogenic emissions of ETH, OLE, and IOLE (internal olefins) were set to zero; and 2) All anthropogenic emissions of ETH and OLE were reduced by half.

Figure 5-10: One hour ozone comparison of two model runs: reg2h (blue) and reg2h with zero biogenic HRVOC and 50% anthropogenic HRVOC emissions (green) for the June Episode. Observed concentrations are shown in red. Top: Hinton Street C401 ETH; Second from top: Hinton Street C401 OLE; Third from top: Fort Worth Northwest C13 ETH; Bottom Fort Worth Northwest C13 OLE. compares the modeled concentrations of the modified model configuration with the reg2h base case at Hinton Street C401 and Fort Worth Northwest C13 for the June 2006 episode (the sensitivity was only performed for this episode). From the figure it is apparent that the emissions modifications caused the modeled OLE and ETH concentrations at both locations to agree much better with the observations.

Figure 5-11: Comparison of modeled MDA8 ozone for two model runs: reg2h and reg2h with zero biogenic HRVOC and 50% anthropogenic HRVOC emissions at (left) Denton C56 and (right) Eagle Mountain Lake C75. shows modeled MDA8 ozone concentrations with and without the ozone reductions at the Denton C56 and Eagle Mountain Lake C75 monitors. While reducing the HRVOC emissions clearly affects modeled ozone concentrations, the effect is relatively small even for the highest modeled ozone concentrations.



Figure 5-10: One hour ozone comparison of two model runs: reg2h (blue) and reg2h with zero biogenic HRVOC and 50% anthropogenic HRVOC emissions (green) for the June Episode. Observed concentrations are shown in red. Top: Hinton Street C401 ETH; Second from top: Hinton Street C401 OLE; Third from top: Fort Worth Northwest C13 ETH; Bottom Fort Worth Northwest C13 OLE.

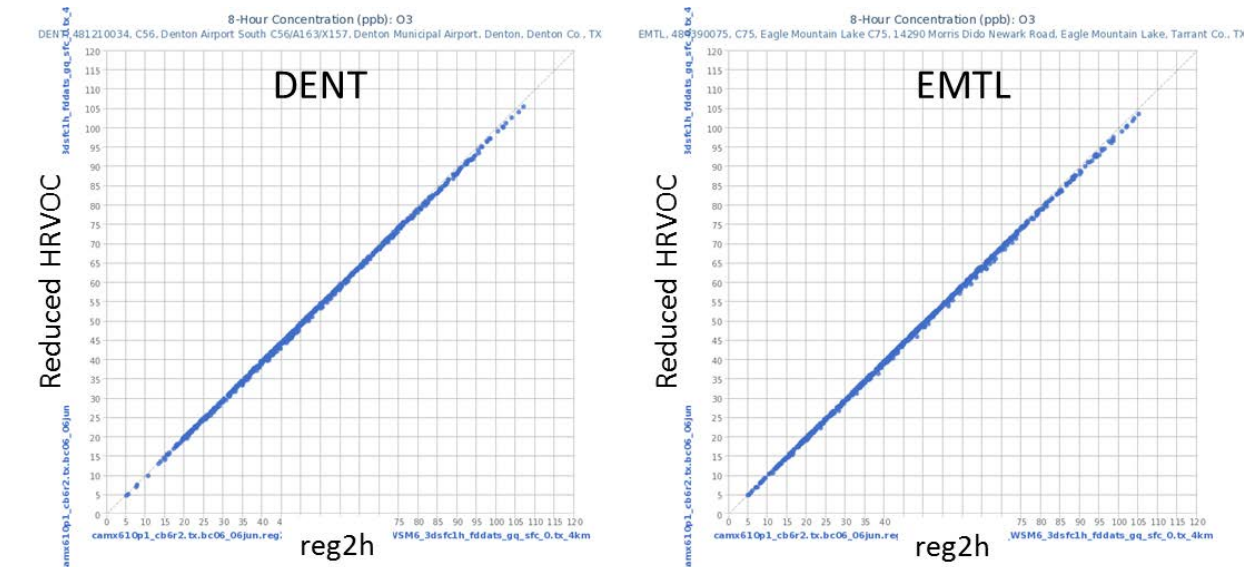


Figure 5-11: Comparison of modeled MDA8 ozone for two model runs: reg2h and reg2h with zero biogenic HRVOC and 50% anthropogenic HRVOC emissions at (left) Denton C56 and (right) Eagle Mountain Lake C75.

These analyses indicate the impact on ozone concentrations from ETH and OLE appear to be small and not likely to influence ozone production substantially in the DFW area. Replicating ETH and OLE concentrations well is important though and we plan to investigate both of the factors discussed above in future work. Time constraints did not allow for additional analysis before the proposed SIP revision was finalized.

5.2. Diagnostic Analyses

Diagnostic analyses were conducted to focus more specifically on the change in model-predicted ozone to changes in the ozone precursor emissions as compared to observed changes in ozone resulting from changes in emissions. The TCEQ conducted several diagnostic analyses, including retrospective modeling, observational modeling and source apportionment analysis.

5.2.1. Retrospective Modeling – 2012

The purpose of this diagnostic analysis is to test the model in a forecast mode, where the answer is known in advance. In previous AD SIP revisions the model was used in a truly retrospective mode to estimate ozone concentrations for a year prior to the base case. In those cases, we had performed modeling for those earlier years for prior SIP revisions so were able to develop emissions fairly easily. In the previous DFW AD SIP revision, we back-cast ozone concentrations to 1999. In this AD, however, we have a unique opportunity to test the model's ability to forecast to a year after the base case. Since the area's attainment year for the 1997 ozone standard was 2012, the 2011 AD SIP revision forecast ozone production to that year. Using a 2012 forecast year had the added advantage of providing an opportunity to see how the new modeling platform stacks up against that used in the 2011 AD SIP.

Since the model predictions of a typical future design value is based on a DV_B , which is the average of three regulatory design values (EPA, 2007), the quantity forecast in this test is not a specific future year's design value but rather the average of three years. So the actual forecast

DV_F is the three-year average of the 2012, 2013, and 2014 design values. At the time this analysis was conducted the 2014 ozone season was not finished, so the future year comparison was based on the two-year average of 2012 and 2013. Because of continuing declines in emissions and observed ozone concentrations in the area, it is likely that the three-year averages containing 2014 will be lower than the two-year averages used in this analysis. Table 5-2: Observed Design Values for Retrospective 2012 Analysis (all values in ppb) shows the baseline DV along with the 2012 and 2013 DVs and the observed future DV (average of 2012 and 2013) at 18 area monitors (the Midlothian Tower C94 monitor was deactivated prior to 2012).

Table 5-2: Observed Design Values for Retrospective 2012 Analysis (all values in ppb)

Monitor	2006 DV _B (2006-8 Avg.)	2012 DV	2013 DV	2012-2013 Average DV
Arlington C61	83.33	83	80	81.5
Cleburne C77	85	79	79	79
Dallas Exec Airport C402	85	81	80	80.5
Dallas North C63	85	81	83	82
Denton C56	93.33	83	87	85
Eagle Mountain Lake C75	93.33	82	81	81.5
Fort Worth Northwest C13	89.33	80	81	80.5
Frisco C31	87.67	83	84	83.5
Granbury C73	83	77	77	77
Grapevine C70	90.67	86	86	86
Greenville C1006	75	72	74	73
Hinton Street C401	81.67	82	84	83
Kaufman C71	74.67	70	74	72
Keller C17	91	87	85	86
Midlothian OFW C52	75	76	77	76.5
Pilot Point C1032	81	82	84	83
Rockwall C69	77.67	77	77	77
Weatherford C76	87.67	78	79	78.5

The modeling inventory for 2012 was developed in a manner analogous to the 2018 future case, but had the advantage of requiring little (or in some cases no) projection. For example, point sources were modeled using reported 2012 emissions, and on-road mobile sources were based on 2012 travel-demand modeling that included 2012 traffic counts. Other facets of the inventory were based on the best available inventories and were projected to 2012 if necessary.

Once the model was run with the 2012 emissions, the 2012 “future” design value, or DV_F, of each monitor was calculated as per EPA guidance. The process was the same as used to predict the 2018 DV_F for the monitors as described in Chapter 3 of the SIP. **Table 5-3: Predicted 2006-12 RRF and DV_F (all values except RRF are in ppb)** shows the RRF for each monitor and the resulting DV_F, compared with the observed 2012-2013 average DV.

Table 5-3 indicates that the model shows a tendency to under-predict the 2012-13 average DV, but predicts well the high design values observed at Denton C56 (83.56 ppb compared with observed 85 ppb) and Eagle Mountain Lake C75 (82.65 ppb compared with 81.5 ppb), and the modeled area-wide 2012 DV 83.56 ppb compares well with the observed 2012-13 average DV of 86 ppb at Grapevine C70, especially considering that the 2012-14 average DV is likely to be lower than the 2012-13 average.

Table 5-3: Predicted 2006-12 RRF and DV_F (all values except RRF are in ppb)

Monitor	2006 DV _B (2006-8 Avg.)	2006-12 RRF	2012 DV _F	2012-2013 Average DV
Arlington C61	83.33	0.895	74.60	81.5
Cleburne C77	85.00	0.893	75.91	79.0
Dallas Exec Airport C402	85.00	0.901	76.62	80.5
Dallas North C63	85.00	0.908	77.17	82.0
Denton C56	93.33	0.894	83.46	85.0
Eagle Mountain Lake C75	93.33	0.886	82.65	81.5
Fort Worth Northwest C13	89.33	0.894	79.87	80.5
Frisco C31	87.67	0.902	79.05	83.5
Granbury C73	83.00	0.886	73.53	77.0
Grapevine C70	90.67	0.903	81.84	86.0
Greenville C1006	75.00	0.894	67.06	73.0
Hinton Street C401	81.67	0.906	73.98	83.0
Kaufman C71	74.67	0.896	66.92	72.0
Keller C17	91.00	0.895	81.43	86.0
Midlothian OFW C52	75.00	0.897	67.29	76.5
Pilot Point C1032	81.00	0.895	72.49	83.0
Rockwall C69	77.67	0.905	70.32	77.0
Weatherford C76	87.67	0.887	77.78	78.5

It is of interest to see how well the current modeling platform's 2012 predictions compare with those made in the 2011 AD SIP revision. Table 5-4: Predicted 2006-12 DV_F in 2011 and Current AD SIP Revisions (all values are in ppb) gives a side-by-side comparison of the two predictions, and *Figure 5-12: Predicted and Observed DFW Ozone Design Values for 2012 Using the 2011 and Current Modeling Platforms, Compared with Average 2012-13 Observed Design Values* gives a graphical comparison of predictions made with the two modeling platforms. Clearly the current modeling platform mimics the observed response much better than the 2011 platform.

Table 5-4: Predicted 2006-12 DV_F in 2011 and Current AD SIP Revisions (all values are in ppb)

Monitor	2011 AD SIP DV _F	Current AD SIP DV _F	2012-2013 Average DV
Arlington C61	70.32	74.60	81.5
Cleburne C77	70.85	75.91	79.0
Dallas Exec Airport C402	70.58	76.62	80.5
Dallas North C63	71.15	77.17	82.0
Denton C56	77.03	83.46	85.0
Eagle Mountain Lake C75	78.06	82.65	81.5
Fort Worth Northwest C13	75.36	79.87	80.5
Frisco C31	74.45	79.05	83.5
Granbury C73	69.66	73.53	77.0
Grapevine C70	76.17	81.84	86.0
Greenville C1006	59.96	67.06	73.0
Hinton Street C401	67.89	73.98	83.0
Kaufman C71	60.42	66.92	72.0
Keller C17	76.45	81.43	86.0
Midlothian OFW C52	62.24	67.29	76.5
Pilot Point C1032	67.35	72.49	83.0
Rockwall C69	63.27	70.32	77.0
Weatherford C76	72.71	77.78	78.5

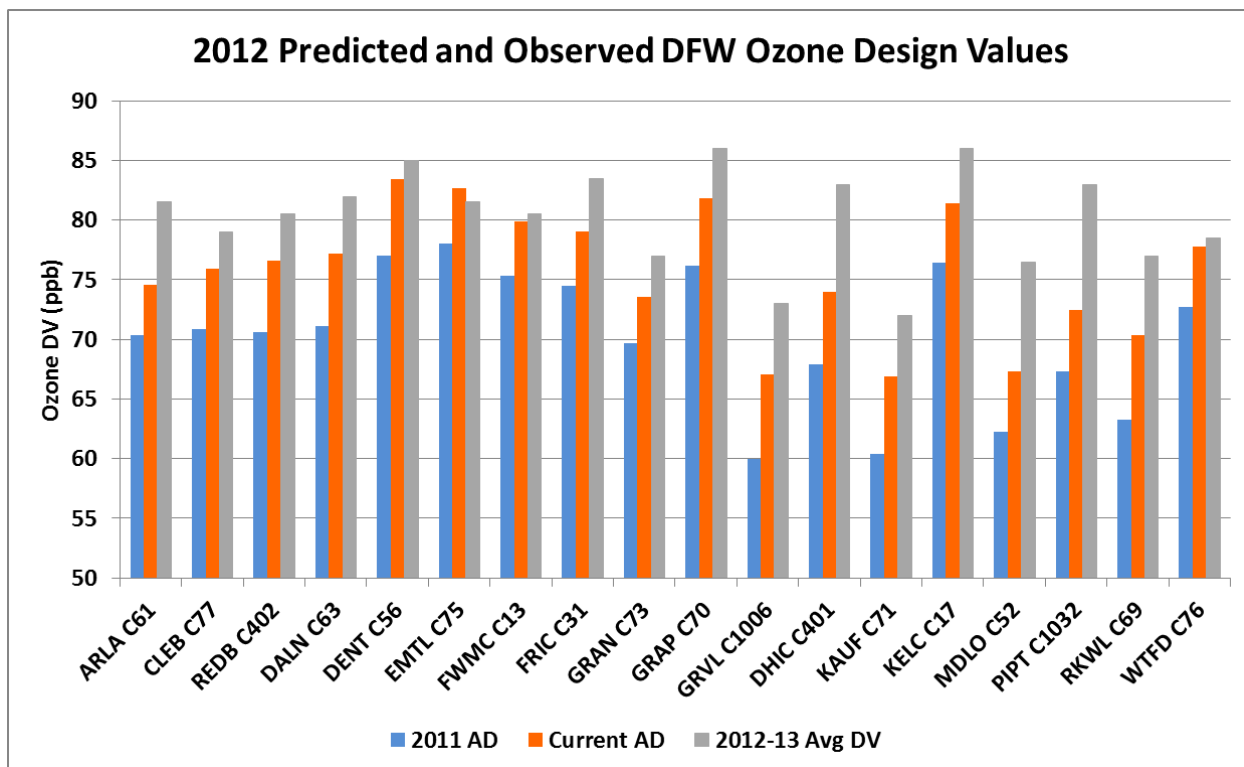


Figure 5-12: Predicted and Observed DFW Ozone Design Values for 2012 Using the 2011 and Current Modeling Platforms, Compared with Average 2012-13 Observed Design Values

5.2.2. Observational Modeling – Weekday/Weekend

Weekend emissions of NO_x in urban areas tend to be lower than weekday emissions because of fewer vehicle miles driven. The effect is most pronounced on weekend mornings, especially Sundays, since commuting is much lower than weekdays. Figure 5-13: *Comparison of modeled 6 AM NO_x and VOC emissions for Wednesdays, Saturdays, and Sundays***Error! Reference source not found.** shows a comparison of modeled 6 AM NO_x and VOC emissions for Wednesdays, Saturdays, and Sundays. Early morning emissions tend to be especially important in determining peak eight-hour ozone levels (MacDonald, 2010), so the weekday-weekend differences should manifest themselves noticeably in the relative levels of weekday and weekend ozone concentrations.

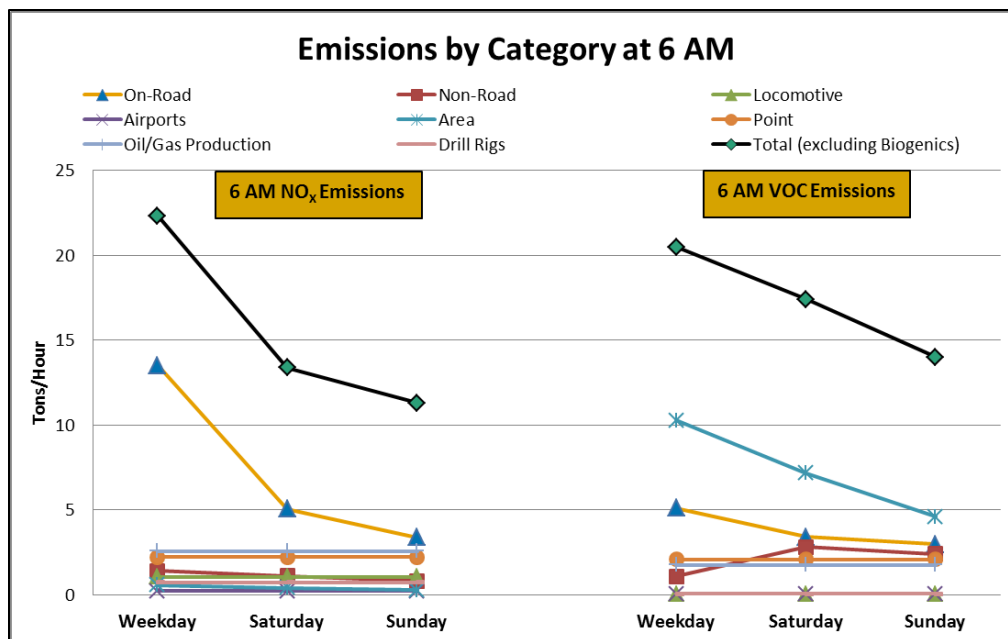


Figure 5-13: Comparison of modeled 6 AM NO_x and VOC emissions for Wednesdays, Saturdays, and Sundays

Because there are relatively few Saturdays, Sundays, and Wednesdays (chosen to represent typical weekdays) in the two episodes, the TCEQ employed a novel approach which allowed each day of the episode to be treated as a Saturday, Sunday, and Wednesday, providing a total of 65 of each day type. This approach is possible since meteorology is independent of day-of-week, so replacing the emissions of any episode day with Saturday (or Sunday or Wednesday) emissions creates an appropriate representation of that day. The modeling procedure involved a series of runs using the 2006 baseline, designed to ensure that each day-type was preceded by the appropriate predecessor day-type, i.e., each Sunday was modeled following a Saturday, each Saturday followed a Friday, and each Wednesday followed a Wednesday (baseline modeled Tuesday emissions are very similar to Wednesdays).

For comparison with the modeled emissions, median monitored 6:00 AM NO_x concentrations were calculated for every Wednesday, Saturday, and Sunday for the summer timeframe of May 15 through October 15 for the years 2004 through 2008. A total of 79 to 133 observations were obtained for each monitor-day combination, depending on monitor operations, in the May 15 to October 15 timeframe for the years 2004 through 2008 for 11 NO_x monitoring sites in DFW.

Figure 5-14: *Modeled and Observed NO_x Concentrations at DFW Monitors as a Percentage of Wednesdays* shows observed and modeled 6 AM NO_x concentrations at 11 sites in the DFW area. All sites show modeled and observed NO_x concentrations that decline monotonically from Wednesday through Saturday to Sunday. The modeled values replicate their observed counterparts well, with all sites having modeled decreases between 37% and 67% from Wednesday to Sunday; while the observed decreases at all sites were in the range of 40% and 70%.

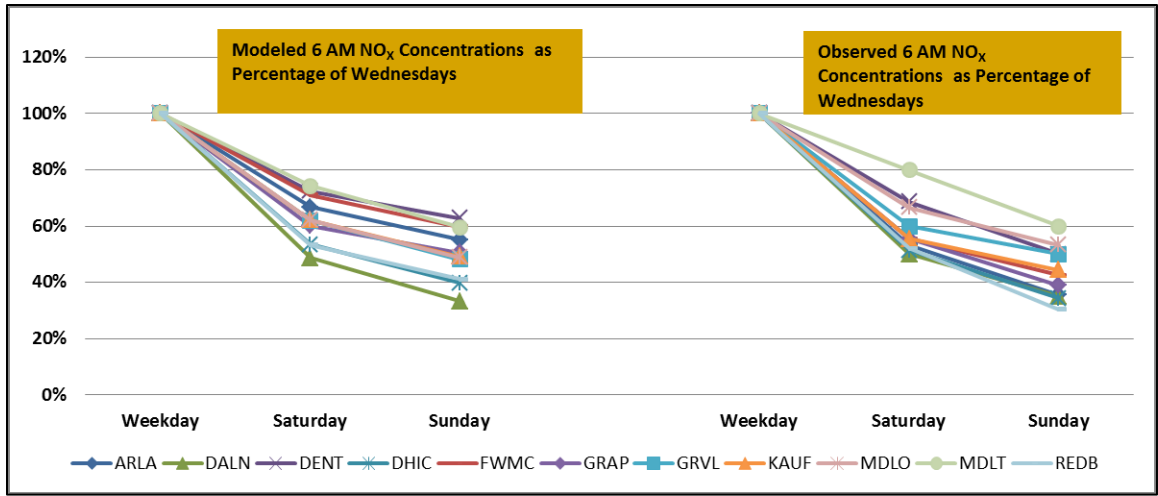


Figure 5-14: Modeled and Observed NO_x Concentrations at DFW Monitors as a Percentage of Wednesdays

Figure 5-15: *Observed and Modeled Daily Peak Eight-Hour Ozone Concentrations as a Percentage of Wednesdays* shows observed and modeled median daily peak eight-hour ozone concentrations as a percentage of Wednesdays for 19 DFW-area monitoring sites. The observed Saturday ozone concentrations (as a percent of Wednesday) are spread between a 7% increase and a 13% decrease, with 9 sites increasing and 10 sites decreasing. Observed Sunday concentrations ranged between a 2% increase and a 15% decrease from Wednesday, with all but four sites showing a decrease. The modeled values showed less variability with the modeled Saturday concentrations being spread between an increase of 3% and a decrease of 3% with the increases observed only at 2 sites, while Sunday concentrations were between a 1% increase and 6% decrease with increases observed again at 2 sites.

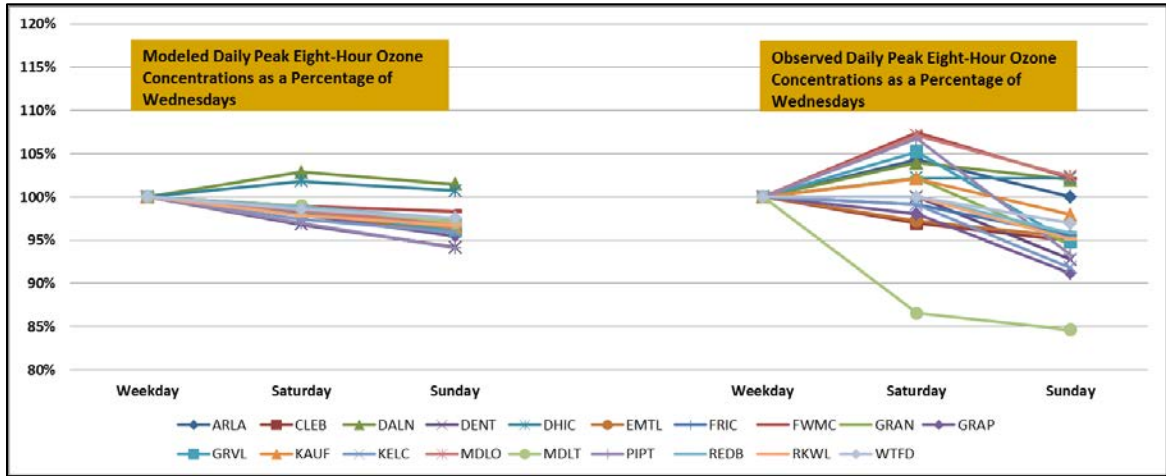


Figure 5-15: Observed and Modeled Daily Peak Eight-Hour Ozone Concentrations as a Percentage of Wednesdays

Part of the apparent discrepancy between the observed and modeled concentrations can be attributed to the comparison of observations from the entire ozone season with modeled

episodes, which were selected specifically to represent a period of especially high ozone concentrations. When the observed and modeled concentrations are replaced with 95th percentile concentrations (representing high ozone days), the behavior of the observed and modeled concentrations is more consistent as seen in Figure 5-16: *Observed and Modeled 95th Percentile Daily Peak Eight-Hour Ozone Concentrations as a Percentage of Wednesdays***Error! Reference source not found.** The observed 95th percentile concentrations range between a 1% increase to a 10% decrease on Saturday (compared with Wednesday), while on Sunday, the observed concentration changes (compared to Wednesday) decreased across all monitors with a range of a 6% to 16%. The modeled values showed changes for Saturday (compared to Wednesday) between a 2% increase and 6% decrease, while for Sunday it showed a decrease across all monitors with a range between 2% to 11%. The model is successfully replicating the observed weekday-weekend trends, especially for the higher ozone days.

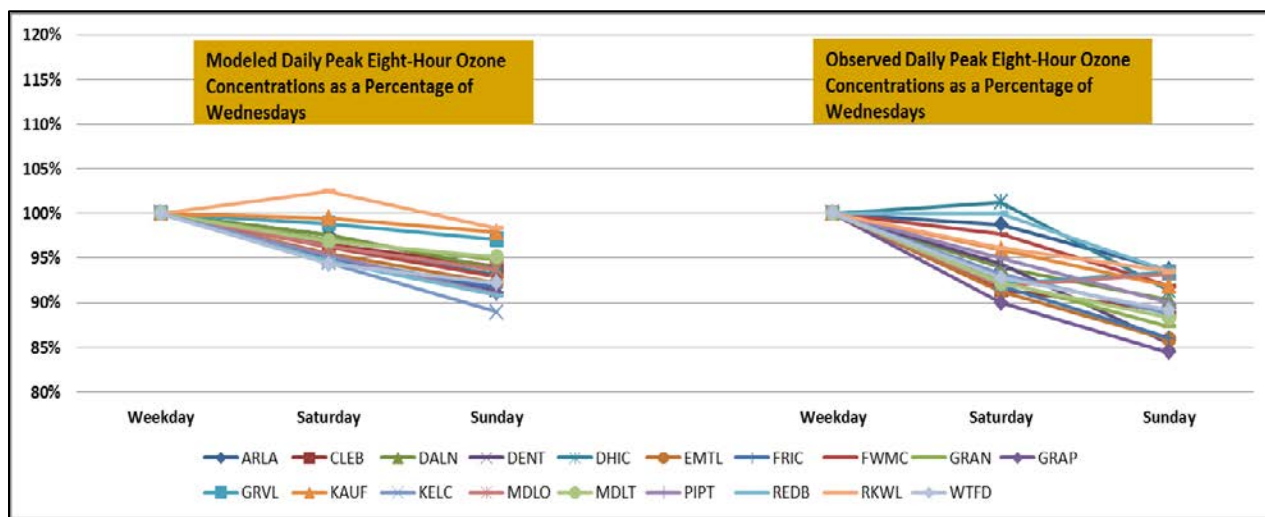


Figure 5-16: Observed and Modeled 95th Percentile Daily Peak Eight-Hour Ozone Concentrations as a Percentage of Wednesdays

Finally, the modeled concentrations exhibit very little site-to-site variability compared to the observations. This is because the modeling procedure applied Wednesday, Saturday, and Sunday emissions to exactly the same set of days. The day-to-day and site-to-site meteorological variability, which clearly affects the observed concentrations, is absent in the modeled concentrations. This modeling technique isolated the model response to weekday-weekend emission changes from the meteorological variability, allowing a clean assessment of the model's response to the emission variability.

5.2.3. Process Analysis

Process analysis is a valuable modeling tool that allows modelers to analyze the internal workings of the model in detail. In a standard photochemical grid modeling run, the output of the model is composed of concentration fields for different chemicals such as ozone and nitrogen dioxide. In a process analysis modeling run, the rates of chemical production and destruction are preserved as well as the concentrations, so that it is easier to trace the pathway by which ozone is formed.

In previous modeling projects, including the 2011 DFW attainment SIP revision, the TCEQ has used process analysis to examine radical budgets, in an effort to determine why simulated ozone concentrations were not as high as observed in Houston industrial plumes. Process analysis has also been used to evaluate relative rates of VOC-sensitive and NO_x-sensitive ozone formation, VOC reactivity and OH radical loss rates, and the role of photolysis on ozone formation rates (TCEQ, 2011). For the previous DFW AD SIP revision process analysis was primarily used to evaluate the relative roles of local ozone production and regional background ozone, and to examine the sensitivity of ozone formation in DFW to VOC and NO_x concentrations.

At this time CAMx 6.1 does not support process analysis, so it is not possible to apply this diagnostic tool to the current modeling platform. If a process analysis or equivalent feature is included in a forthcoming release of CAMx, we will consider including it in future modeling analyses such as the adoption package for this SIP revision.

5.2.4. Source Apportionment Analysis-Anthropogenic Precursor Culpability Assessment (APCA)/Ozone Source Apportionment Technology (OSAT)

The source apportionment analysis was conducted on the future 2018 year modeling. Two techniques, Anthropogenic Precursor Culpability Assessment (APCA) and Ozone Source Apportionment Technology (OSAT), were used to analyze contributions by different emission source categories in selected regions to the 2018 modeled ozone concentration. APCA and OSAT keeps track of the origin of the NO_x and VOC precursors creating the ozone during the model run, which can then be apportioned to specific user-defined source groups and regions. A key difference between APCA and OSAT is that APCA recognizes that the biogenic source category is not controllable. Where OSAT would apportion ozone production to biogenic emissions, APCA reallocates that ozone production to the controllable or anthropogenic emissions that combined with the biogenic emissions to create ozone. Only ozone created from both biogenic NO_x and VOC precursors is apportioned to the biogenic emission source group by APCA. For the source apportionment analysis, three geographic regions - Ten-County DFW, Texas Outside of DFW, and Outside Texas were chosen. Figure 5-17: *APCA/OSAT Region Categories* shows the geographic regions used in the APCA/OSAT analysis. Below is a list of the eleven emission sources categories selected for the APCA/OSAT source apportionment analysis.

- Biogenic
- Point – Elevated – Electric Generating Units (EGUs)
- Point – Elevated - Cement Kilns
- Point – Elevated – Other
- Area (excluding Non-road/Off-road, Oil and Gas)
- On-Road
- Off-Road
- Non-Road (Airports, Locomotive, Shipping)
- Oil and Gas - Drilling and Production – Barnett Shale
- Oil and Gas - Drilling and Production – Other Texas
- Point - Low Level (Leftover)

Texas Ozone Modeling Domain and APCA Regions

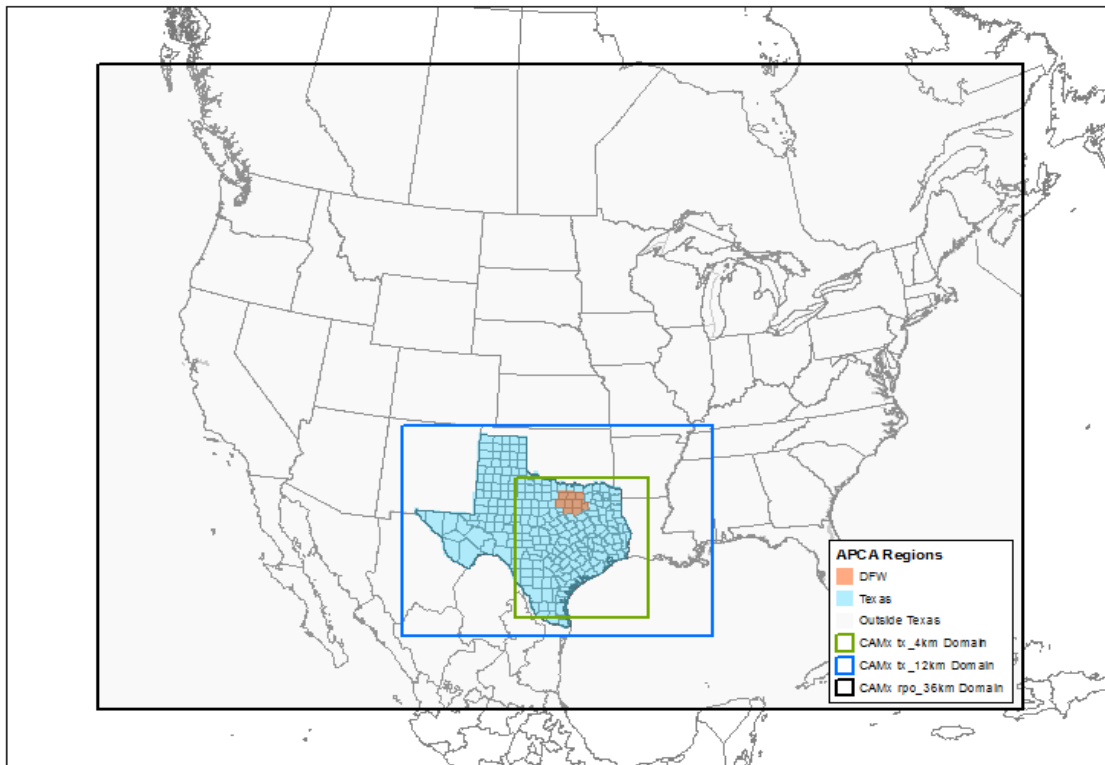


Figure 5-17: APCA/OSAT Region Categories

Model runs were done with the APCA/OSAT probing tools for the future year for both the June (5/31-7/2) and Aqs1 (8/13-9/15) episodes. The output of the APCA/OSAT runs provides the eight-hour average ozone contribution for each hour of the episodes in ppb for 44 source category-region combinations, the 33 region-source combinations based on the three regions and 11 source categories listed above plus five (west, east, north, south, and top) boundary conditions and initial condition.

5.2.4.1. APCA Analysis

The source apportionment analysis of the modeled 2018 eight-hour average ozone was focused on three monitors: Denton Airport South (DENT CAMS 56), Parker County (WTFD CAMS 76) and Kaufman (KAUF CAMS 71). The Denton Airport South (DENT CAMS 56) was chosen as it had the peak modeled future design value at 76.0 ppb, Parker County (WTFD CAMS 76) was chosen to analyze impacts of oil and gas activities in the Barnett Shale development on the western part of DFW area, and Kaufman (KAUF CAMS 71) was chosen to evaluate upwind contributions. The results are graphed as layered area plots for every rolling eight-hour average. While all the emission source categories for the ten-county DFW region are represented by individual layers the graphs, some source categories for the other two regions were combined. The combinations were selected such that the graphs have a more refined representation for ten-county DFW emission source categories with progressively broader representation of the emission source categories as we move away from the DFW area. *Table 5-5: APCA/OSAT Region-Source Category Combinations* presents the region-source category combinations

represented by the different layers of the graphs (top to bottom) along with the abbreviations used to reference the different layers in figure legend.

Table 5-5: APCA/OSAT Region-Source Category Combinations

Figure Legend Abbreviation	APCA/OSAT Region-Source Combinations
DFW On-Road	Ten-County DFW On-Road
DFW Non-Road	Ten-County DFW Non-Road
DFW Off-Road –Airports and Locomotives	Ten-County DFW Off-Road – Airports and Locomotives
DFW Area Sources	Ten-County DFW Area Sources
DFW Oil/Gas Drilling and Production	Ten-County DFW Oil/Gas Drilling and Production
DFW Point - Electric Utilities	Ten-County DFW Point - Electric Utilities
DFW Point - Cement Kilns	Ten-County DFW Point - Cement Kilns
DFW Point - Other	Ten-County DFW Point - Other
Non-DFW TX On-Road	Texas Outside of DFW TX On-Road
Non-DFW TX Non-Road, Off-Road, & Area	Texas Outside of DFW Non-Road, Off-Road, & Area
Non-DFW TX Oil/Gas Drilling and Production	Texas Outside of DFW Oil/Gas Drilling and Production
Non-DFW TX Point - Electric Utilities	Texas Outside of DFW Point - Electric Utilities
Non-DFW TX Point - Kilns, Oil/Gas, and Other	Texas Outside of DFW Point – Kilns, Oil/Gas, and Other
Non-TX Anthropogenic	Outside of Texas Anthropogenic
Biogenic	Biogenic –All Geographic Areas
Boundary Conditions	Boundary Conditions
Initial Conditions	Initial Conditions

The APCA results for days when the modeled baseline maximum daily eight-hour average value was greater than 75 ppb were used to obtain the contribution by each region-source category combination towards the 2018 future design value for each of the three monitors.

5.2.4.1.1. Denton Airport South

The Denton Airport South (DENT CAMS 56) was chosen as it had the peak modeled future design value at 76.7 ppb. *Figure 5-18: 2018 Denton Airport South (C56) Eight-Hour APCA Results for the June Episode (5/31-6/16)* and *Figure 5-19: 2018 Denton Airport South (C56) Eight-Hour APCA Results for the June Episode (6/17-7/2)*, presents the layered area plot for the June episode APCA source apportionment at the Denton Airport South site, while *Figure 5-20: 2018 Denton Airport South (C56) Eight-Hour APCA Results for the Aqs1 Episode (8/13-8/27)* and *Figure 5-21: 2018 Denton Airport South (C56) Eight-Hour APCA Results for the Aqs1 Episode (8/28-9/15)* presents the layered area plot for the Aqs1 episode APCA source apportionment at the Denton Airport South site.

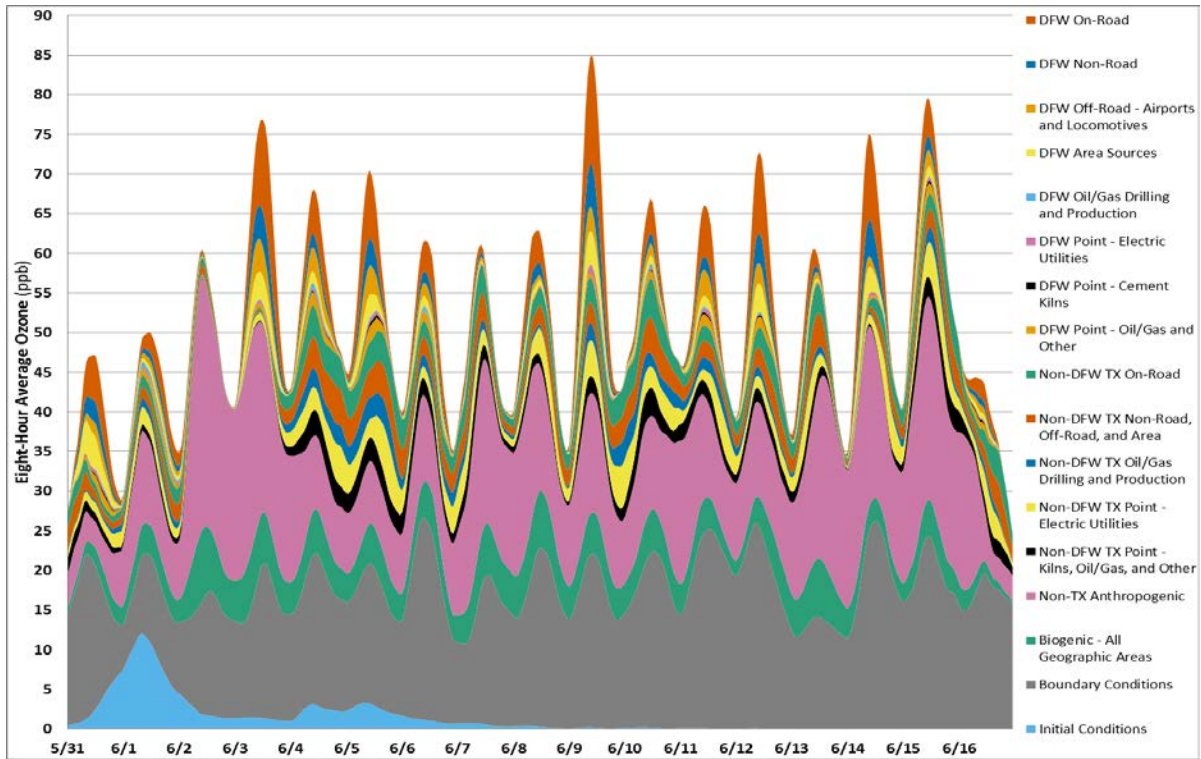


Figure 5-18: 2018 Denton Airport South (C56) Eight-Hour APCA Results for the June Episode (5/31-6/16)

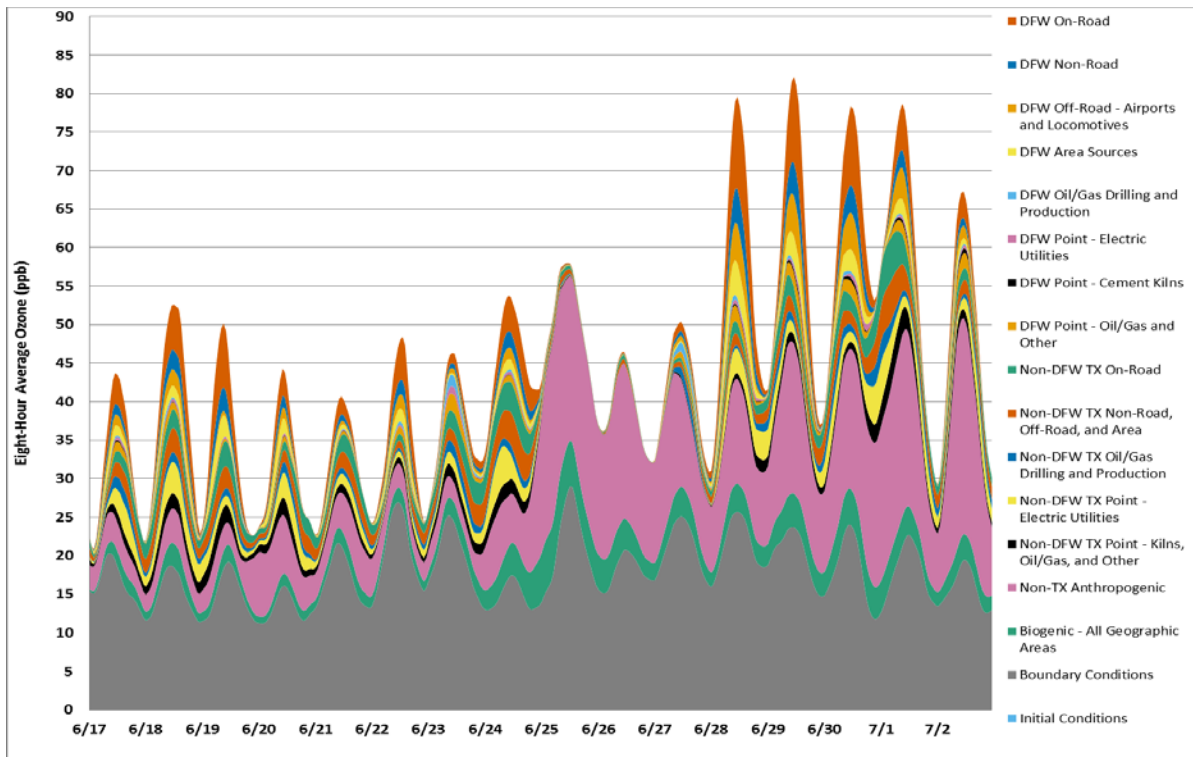


Figure 5-19: 2018 Denton Airport South (C56) Eight-Hour APCA Results for the June Episode (6/17-7/2)

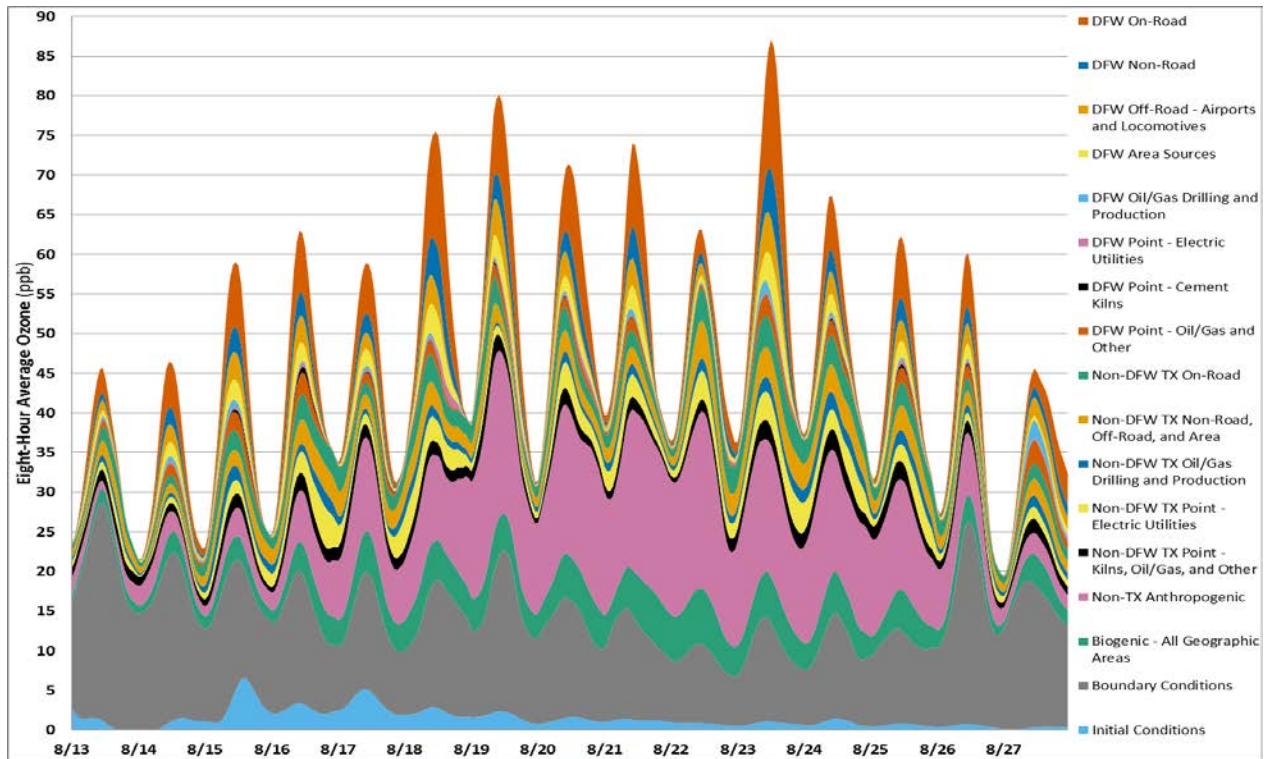


Figure 5-20: 2018 Denton Airport South (C56) Eight-Hour APCA Results for the Aqsl Episode (8/13-8/27)

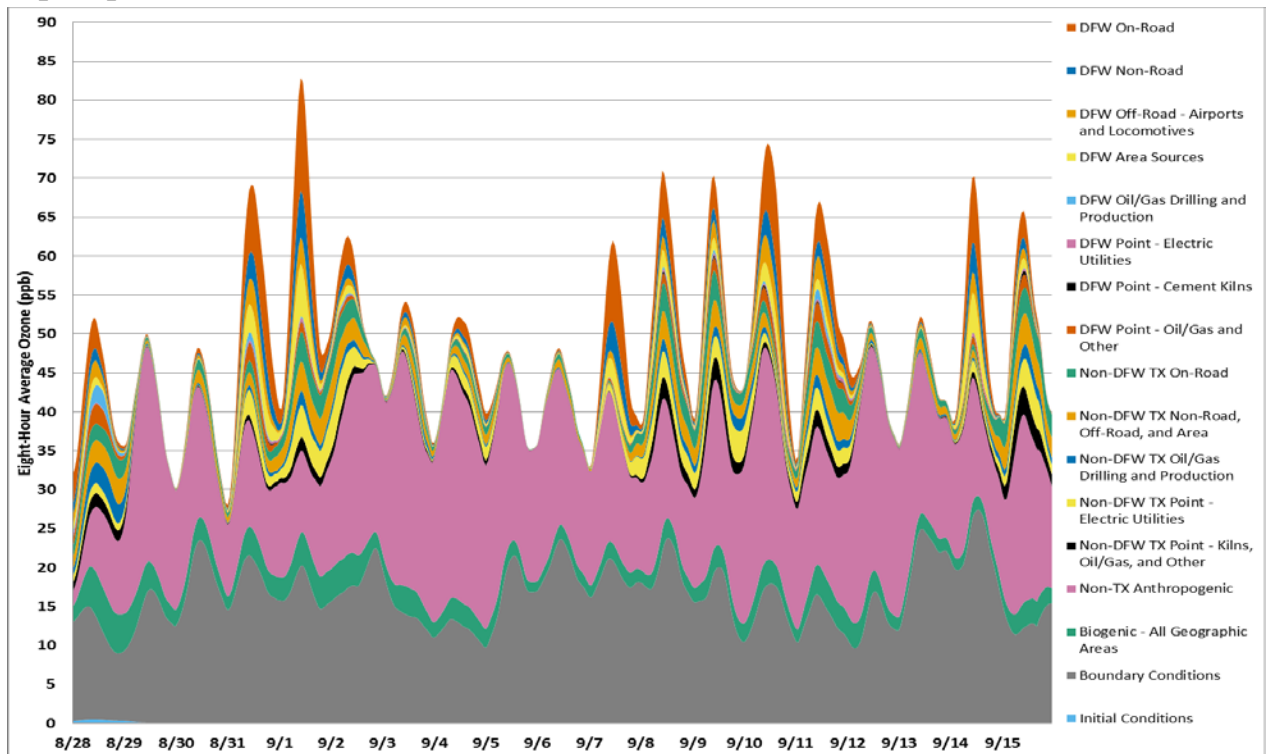


Figure 5-21: 2018 Denton Airport South (C56) Eight-Hour APCA Results for the Aqsl Episode (8/28-9/15)

Among local emission source categories in the ten-county DFW region, the on-road emission source category had the largest contribution with 10.99% followed by non-road at 4.21% and off-road and area sources at 3.86% and 3.54%, at the Denton Airport County site. The total contribution from all local DFW sources at the Denton Airport South site equals 25.81%, exceeded only Boundary Conditions at 27.13%. *Table 5-6: APCA Source Apportionment Contributions at Denton Airport South (C56) for Days with a Modeled Baseline Greater than 75 ppb* shows the percentage contribution and maximum contribution in ppb across all the baseline days modeled above 75 ppb.

Table 5-6: APCA Source Apportionment Contributions at Denton Airport South (C56) for Days with a Modeled Baseline Greater than 75 ppb

APCA Region-Source Category Combination	Percentage Contribution	Maximum Contribution (ppb)
Initial Conditions	1.00%	3.43
Boundary Conditions	27.13%	27.00
Biogenic	6.42%	7.02
Non-TX Anthropogenic	24.42%	28.03
Non-DFW TX Point - Cement Kilns and Other	2.59%	3.59
Non-DFW TX Point - Electric Utilities	3.50%	4.49
Non-DFW TX Oil & Gas Drilling/Production	1.70%	2.75
Non-DFW TX Non-Road, Off-Road, & Area	3.72%	4.77
Non-DFW TX On-Road	3.72%	4.97
DFW Point - Other	1.92%	2.63
DFW Point - Cement Kilns	0.28%	0.67
DFW Point - Electric Utilities	0.54%	1.10
DFW Oil & Gas Drilling/Production	0.46%	1.34
DFW Area Sources	3.54%	6.77
DFW Off-Road	3.86%	5.24
DFW Non-Road	4.21%	6.22
DFW On-Road	10.99%	16.30

5.2.4.1.2. Parker County

The Parker County (WTFD CAMS 76) was chosen to analyze impacts of oil and gas activities in the Barnett Shale development on the western part of DFW area. *Figure 5-22: 2018 Parker County (C76) Eight-Hour APCA Results for the June Episode (5/31-6/16)* and *Figure 5-23: 2018 Parker County (C76) Eight-Hour APCA Results for the June Episode (6/17-7/2)*, presents the layered area plot for the June episode APCA source apportionment at the Parker County site, while *Figure 5-24: 2018 Parker County (C76) Eight-Hour APCA Results for the Aqs1 Episode (8/13-8/27)* and *Figure 5-25: 2018 Parker County (C76) Eight-Hour APCA Results for the Aqs1 Episode (8/28-9/15)* presents the layered area plot for the Aqs1 episode APCA source apportionment at Parker County site.

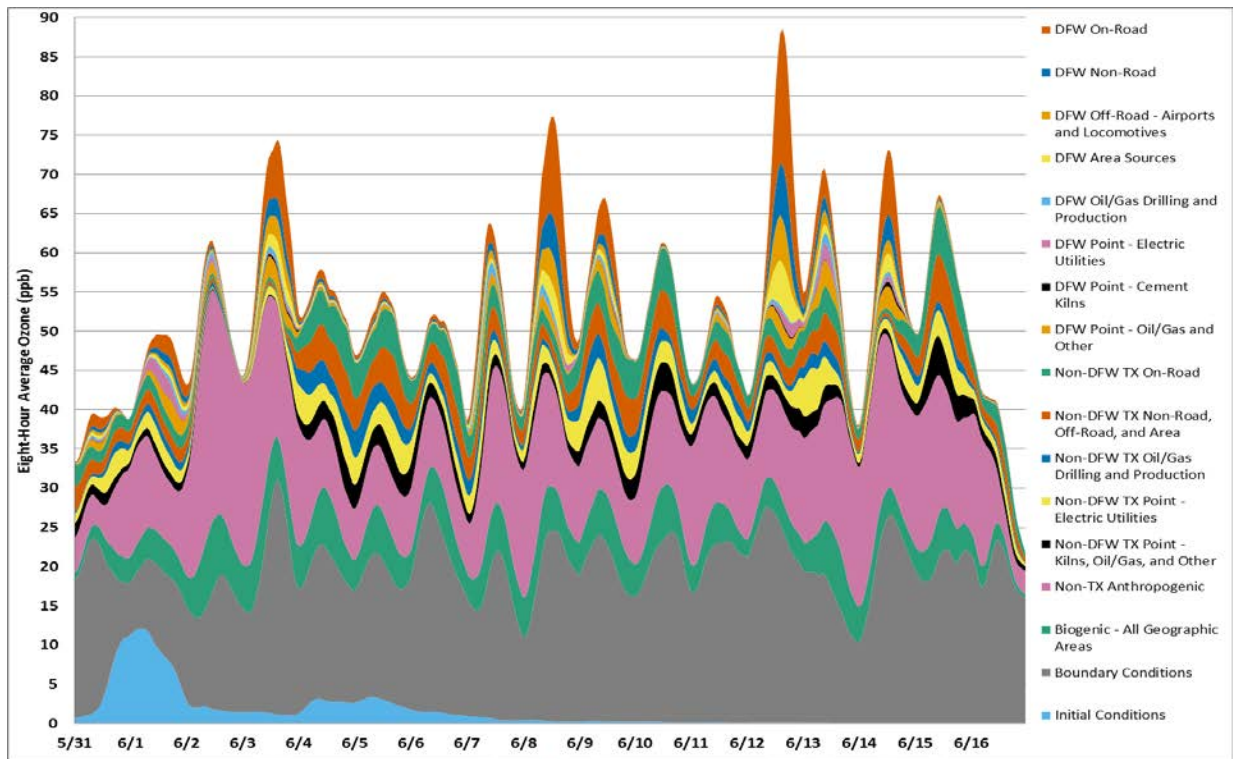


Figure 5-22: 2018 Parker County (C76) Eight-Hour APCA Results for the June Episode (5/31-6/16)

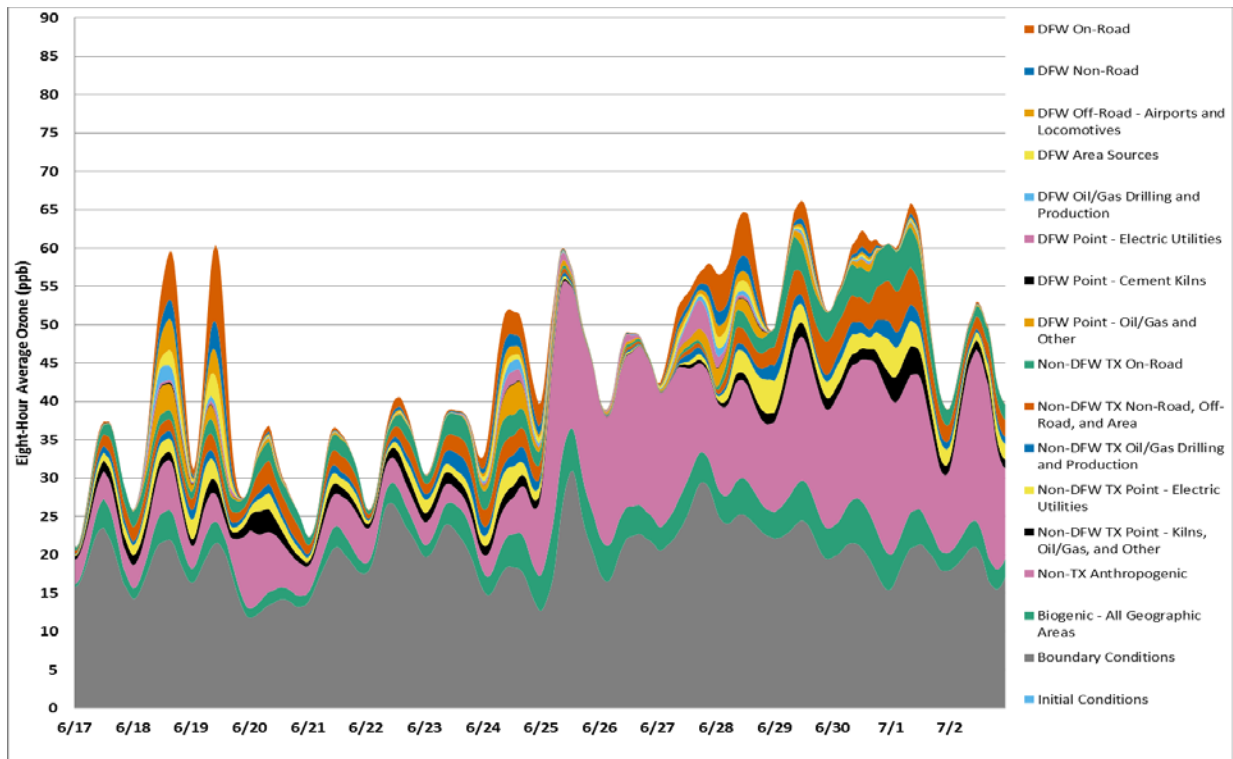


Figure 5-23: 2018 Parker County (C76) Eight-Hour APCA Results for the June Episode (6/17-7/2)

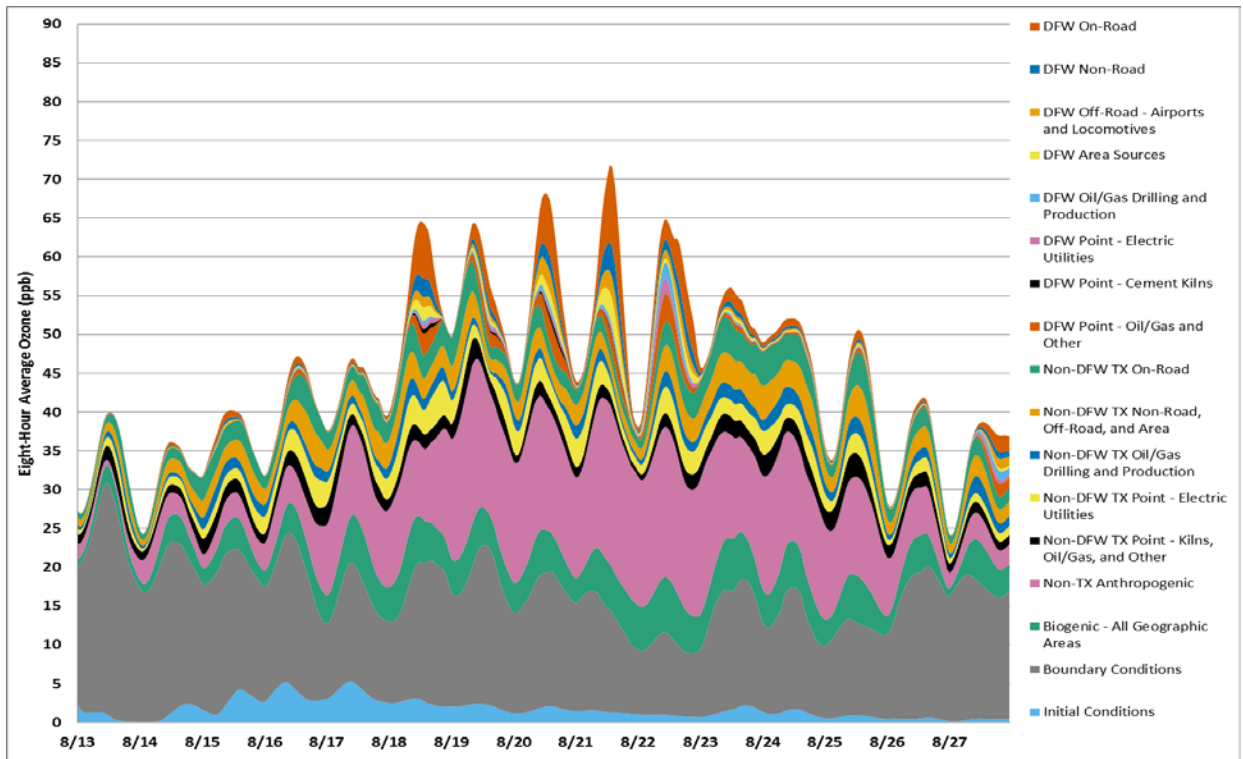


Figure 5-24: 2018 Parker County (C76) Eight-Hour APCA Results for the Aqs1 Episode (8/13-8/27)

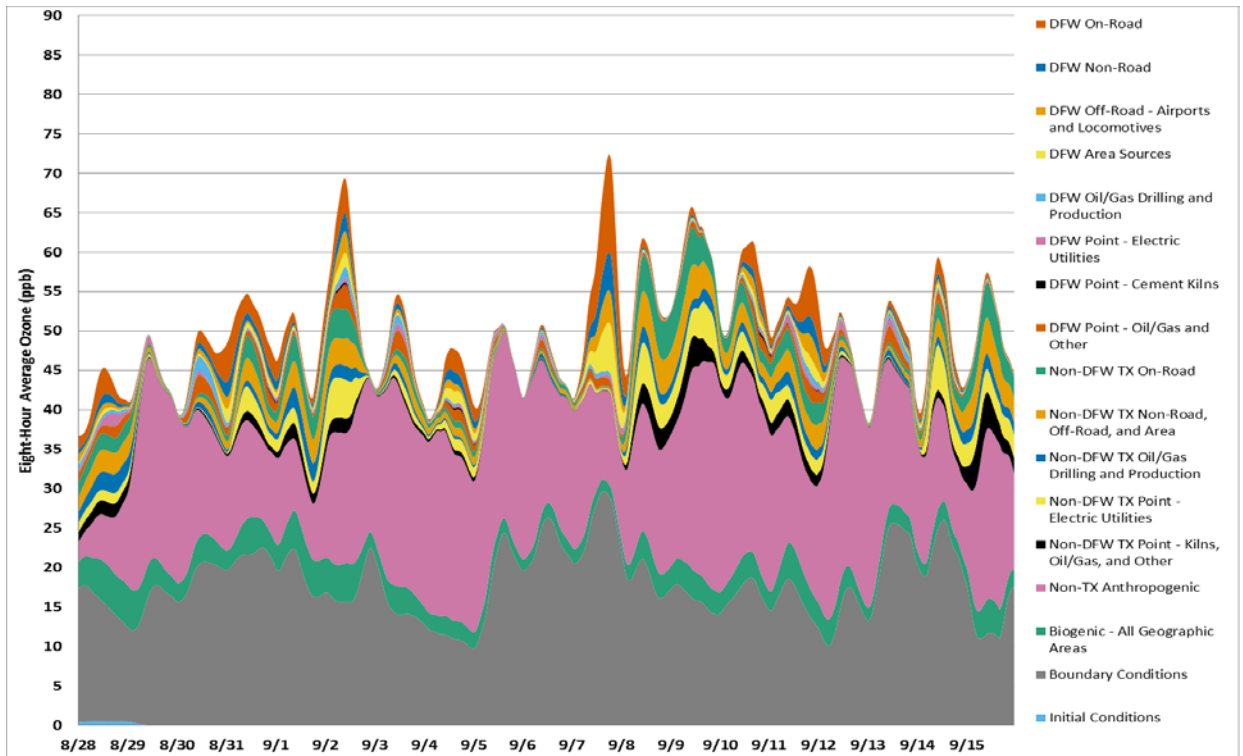


Figure 5-25: 2018 Parker County (C76) Eight-Hour APCA Results for the Aqs1 Episode (8/28-9/15)

The Parker County site shows a similar source apportionment distribution to the Denton Airport South site with the on-road emission source category having the largest contribution with 8.34% followed by non-road at 3.16% and off-road and area sources at 2.56% and 2.47% among the local (DFW area) emission source categories. The total contribution from all local DFW sources at the Parker County site equals 21.26%, which is less than at the Denton Airport South site. Due to its location in relation to the Barnett Shale, the Parker County shows a slightly higher contribution from the DFW Oil & Gas Drilling/Production category at 1.00% compared to the 0.46% at the Denton Airport South site. *Table 5-7: APCA Source Apportionment Contributions at Parker County (C76) for Days with a Modeled Baseline Greater than 75 ppb* shows the contribution percentage and maximum contribution in ppb across all the baseline days modeled above 75 ppb.

Table 5-7: APCA Source Apportionment Contributions at Parker County (C76) for Days with a Modeled Baseline Greater than 75 ppb

APCA Region-Source Category Combination	Contribution Percentage	Maximum Contribution (ppb)
Initial Conditions	0.88%	2.98
Boundary Conditions	30.17%	29.94
Biogenic	7.52%	7.15
Non-TX Anthropogenic	23.63%	24.97
Non-DFW TX Point - Cement Kilns and Other	2.80%	4.97
Non-DFW TX Point - Electric Utilities	3.73%	4.88
Non-DFW TX Oil & Gas Drilling/Production	1.72%	2.56
Non-DFW TX Non-Road, Off-Road, & Area	4.02%	6.13
Non-DFW TX On-Road	4.25%	6.02
DFW Point - Other	2.74%	3.53
DFW Point - Cement Kilns	0.24%	0.62
DFW Point - Electric Utilities	0.74%	2.04
DFW Oil & Gas Drilling/Production	1.00%	2.09
DFW Area Sources	2.47%	6.21
DFW Off-Road	2.56%	5.65
DFW Non-Road	3.16%	6.90
DFW On-Road	8.34%	17.33

5.2.4.1.3. Kaufman

Kaufman (KAUF CAMS 71) was chosen as it is upwind of the DFW urban core and can be indicative of background air entering the DFW area. *Figure 5-26: 2018 Kaufman (C71) Eight-Hour APCA Results for the June Episode (5/31-6/16)* and *Figure 5-27: 2018 Kaufman (C71) Eight-Hour APCA Results for the June Episode (6/17-7/2)*, presents the layered area plot for the June episode APCA source apportionment at the Parker County site, while *Figure 5-28: 2018 Kaufman (C71) Eight-Hour APCA Results for the Aqs1 Episode (8/13-8/27)* and *Figure 5-29: 2018 Kaufman (C71) Eight-Hour APCA Results for the Aqs1 Episode (8/28-9/15)* presents the layered area plot for the Aqs1 episode APCA source apportionment at Parker County site.

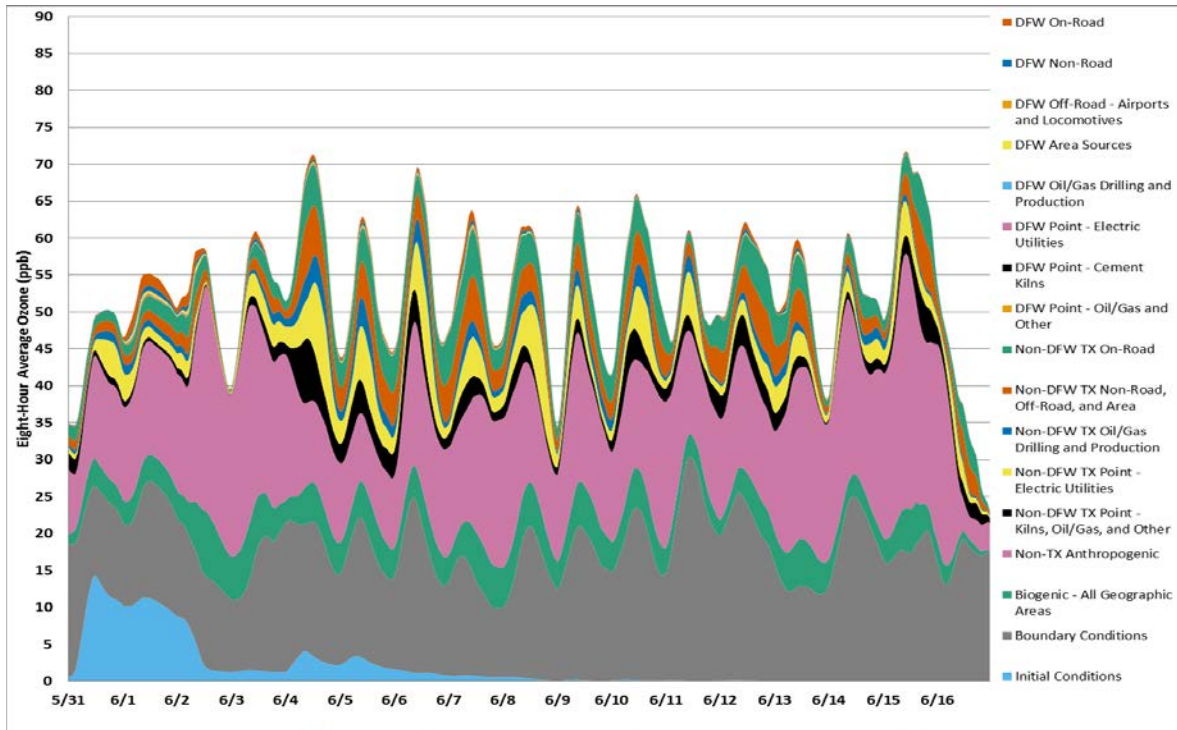


Figure 5-26:2018 Kaufman (C71) Eight-Hour APCA Results for the June Episode (5/31-6/16)

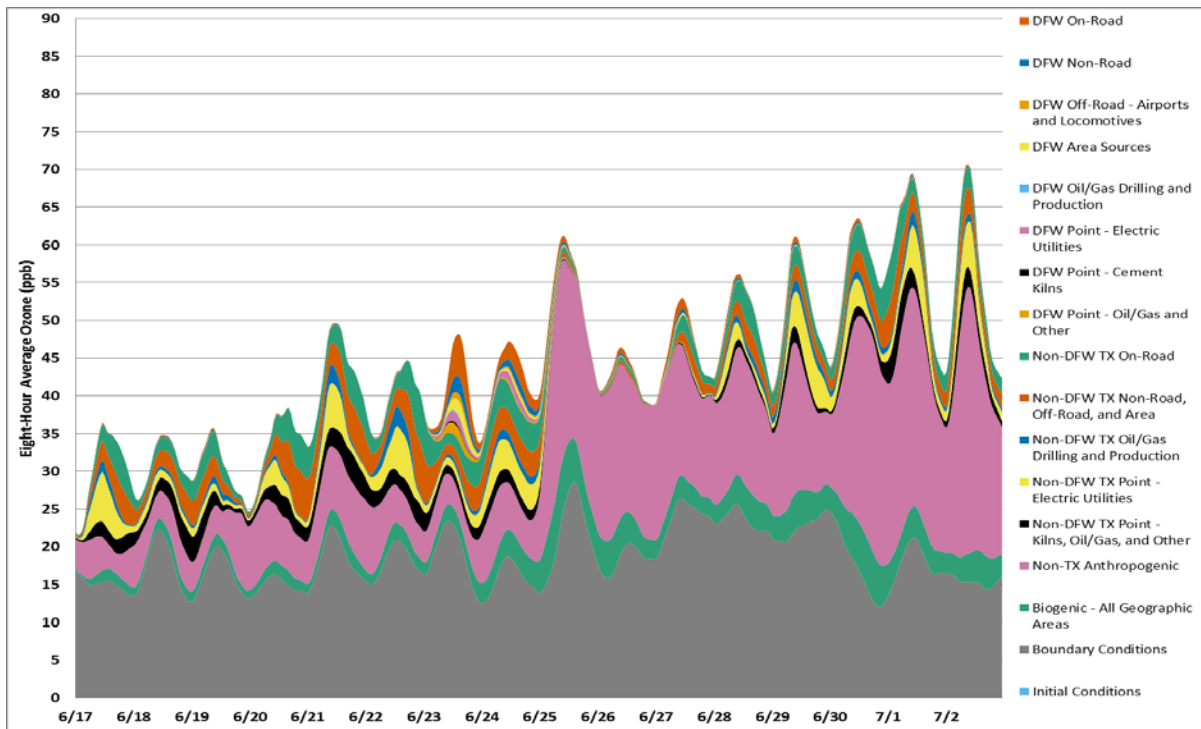


Figure 5-27:2018 Kaufman (C71) Eight-Hour APCA Results for the June Episode (6/17-7/2)

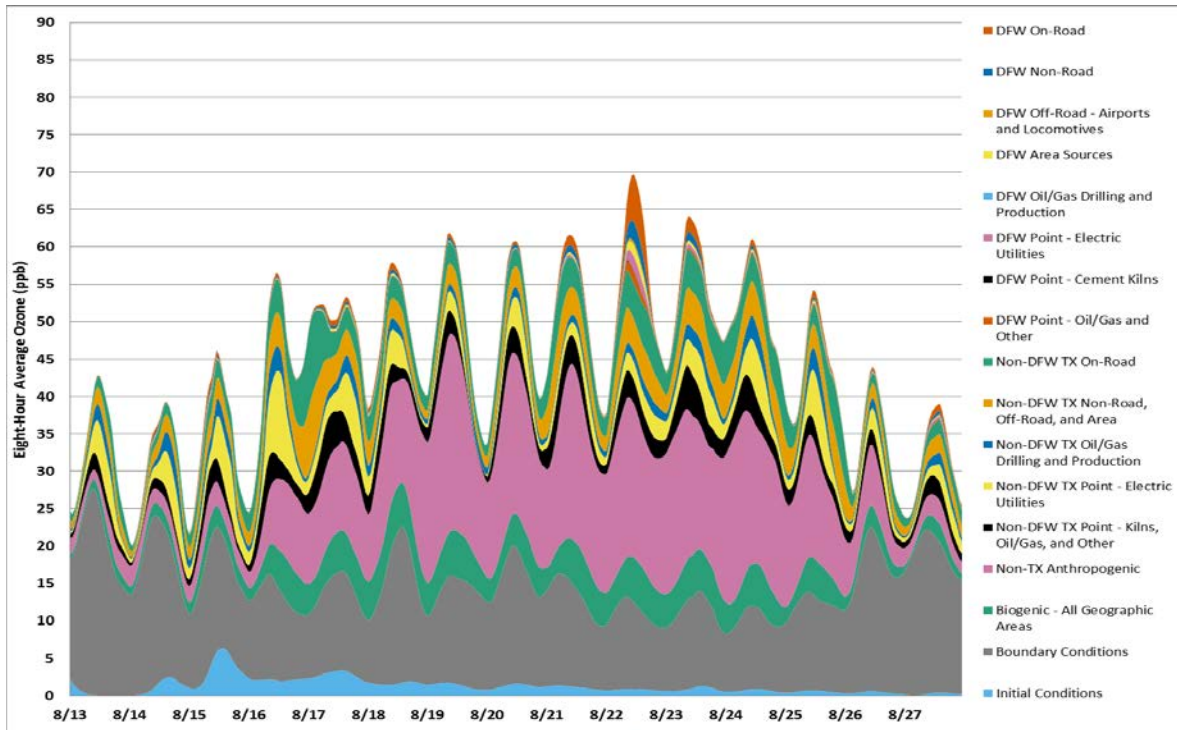


Figure 5-28:2018 Kaufman (C71) Eight-Hour APCA Results for the Aqs1 Episode (8/13-8/27)

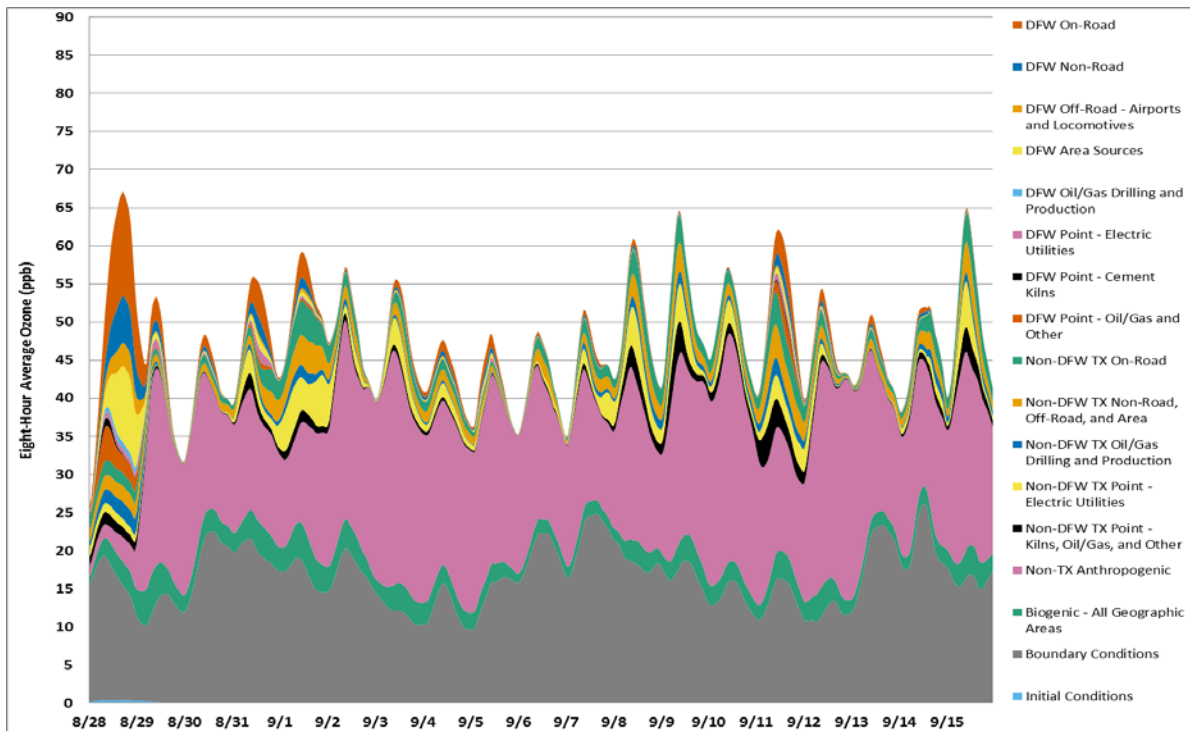


Figure 5-29:2018 Kaufman (C71) Eight-Hour APCA Results for the Aqs1 Episode (8/28-9/15)

Indicative of its location as an upwind monitor, the total source contribution from emission sources within the DFW area was only 4.07% compared to 60.61% contribution from sources outside the DFW area with 33.9% coming from outside of Texas (Non-TX Anthropogenic). Among the local source categories the on-road emission source category still had the largest contribution at 1.88%. *Table 5-8: APCA Source Apportionment Contributions at Kaufman (C71) for Days with a Modeled Baseline Greater than 75 ppb* shows the contribution percentage and maximum contribution in ppb across all the baseline days modeled above 75 ppb.

Table 5-8: APCA Source Apportionment Contributions at Kaufman (C71) for Days with a Modeled Baseline Greater than 75 ppb

APCA Region-Source Category Combination	Contribution Percentage	Maximum Contribution (ppb)
Initial Conditions	0.90%	3.45
Boundary Conditions	26.41%	23.37
Biogenic	8.01%	7.13
Non-TX Anthropogenic	33.90%	35.46
Non-DFW TX Point - Cement Kilns and Other	4.77%	7.24
Non-DFW TX Point - Electric Utilities	7.34%	8.53
Non-DFW TX Oil & Gas Drilling/Production	2.71%	3.57
Non-DFW TX Non-Road, Off-Road, & Area	5.99%	7.06
Non-DFW TX On-Road	5.90%	6.20
DFW Point - Other	0.35%	1.76
DFW Point - Cement Kilns	0.04%	0.26
DFW Point - Electric Utilities	0.33%	1.98
DFW Oil & Gas Drilling/Production	0.03%	0.07
DFW Area Sources	0.37%	1.48
DFW Off-Road	0.17%	0.45
DFW Non-Road	0.91%	2.69
DFW On-Road	1.88%	6.36

5.2.4.2. OSAT-APCA Comparison

The APCA and OSAT source apportionment results were compared to determine the relative impact of Biogenic emissions on ozone formation. The difference, in ppb, between the ozone attributed by OSAT to a region-source combination and the ozone attributed by APCA to the same region-source combination was calculated for days with modeled baseline maximum daily eight-hour average greater than 75 ppb. The total ozone formed for each episode day (for both the June and Aqs1 episodes) in the future year remained the same for both the OSAT and APCA model runs with the only difference between the two model runs being how much ozone formed at a site is attributed to the Biogenic emissions source category.

Figure 5-30: Difference between OSAT and APCA Source Apportionment at Denton Airport South (C56) shows the difference in each region-source combination's contribution to Denton Airport South's 2018 design value when using OSAT compared to APCA.

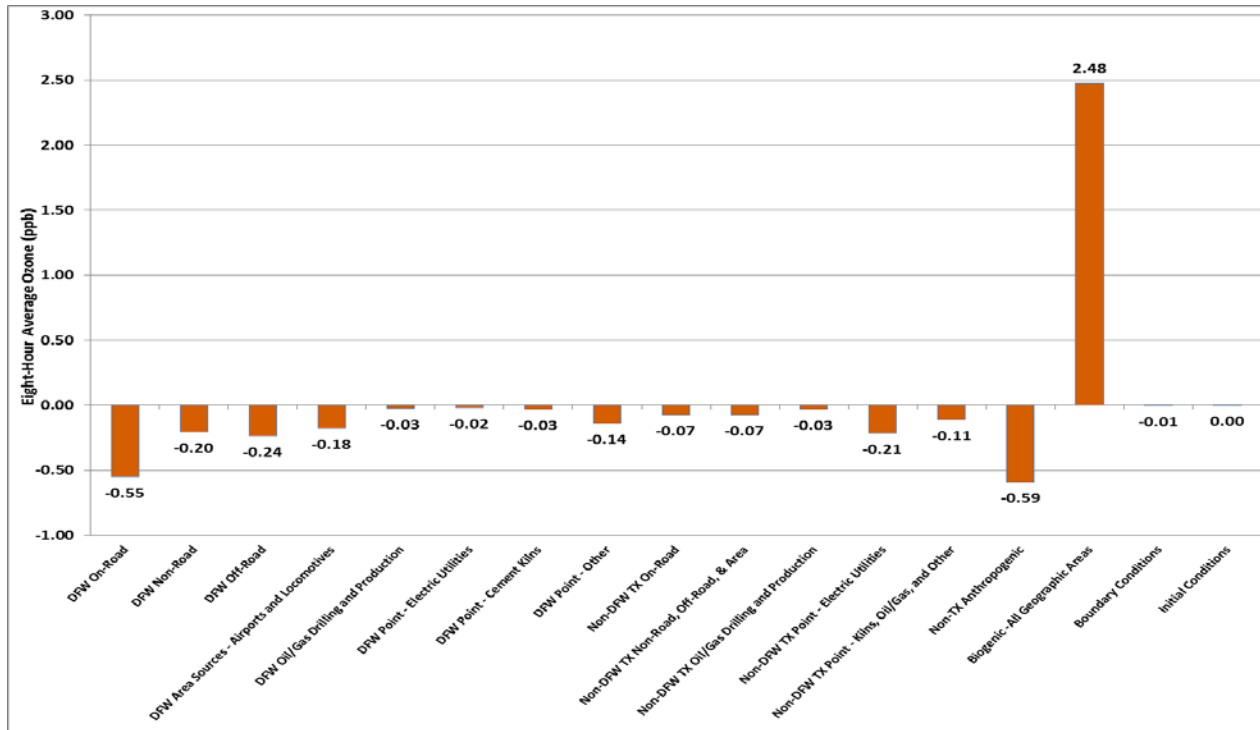


Figure 5-30: Difference between OSAT and APCA Source Apportionment at Denton Airport South (C56)

In Figure 5-30 the contribution attributed to the Biogenic category was greater in OSAT by 2.48 ppb with the largest decreases in contribution being from the Non-TX Anthropogenic region-source combination (at 0.59 ppb) followed by the DFW On-Road region-source combination (at 0.51 ppb). The average increase in ozone contribution attributed to the Biogenic category by OSAT across all hours and days of the episode was 1.64 ppb.

Figure 5-31: *Difference between OSAT and APCA Source Apportionment at Parker County (C76)* shows the difference in each region-source combination’s contribution to Parker County’s 2018 design value when using OSAT compared to APCA. At the Parker County site, the contribution attributed to the Biogenic category was greater in OSAT by 1.45 ppb with the largest decreases in contribution being from the Non-TX Anthropogenic category at 0.51 ppb followed by the DFW On-Road at 0.20 ppb. The average increase in ozone contribution by the Biogenic category across all hours and days of the episode was 1.14 ppb.

Figure 5-32: *Difference between OSAT and APCA Source Apportionment at Kaufman (C71)* shows the difference in each region-source combination’s contribution to Kaufman’s 2018 design value when using OSAT compared to APCA. The contribution attributed to the Biogenic category was greater in OSAT by 1.53 ppb with the largest decreases in contribution being from the Non-TX Anthropogenic category at 0.68 ppb. The average increase in ozone contribution by the Biogenic category across all hours and days of the episode was 1.35 ppb.

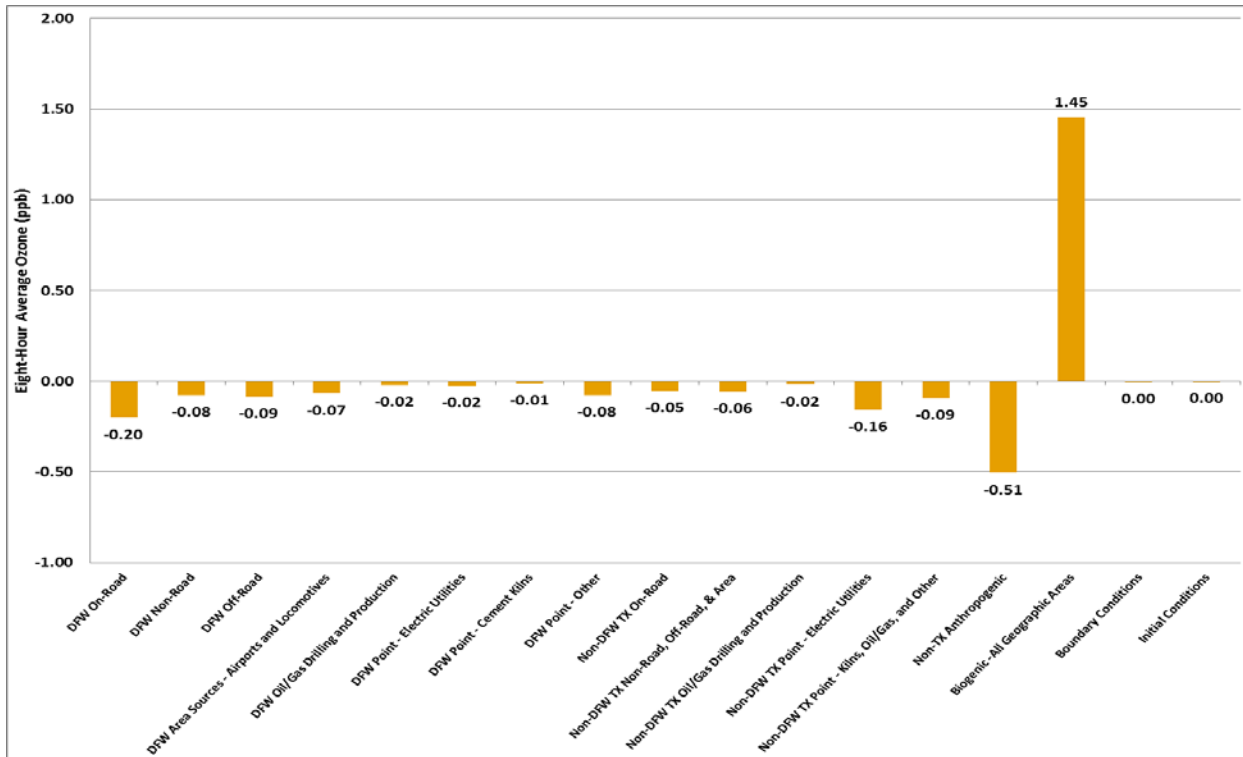


Figure 5-31: Difference between OSAT and APCA Source Apportionment at Parker County (C76)

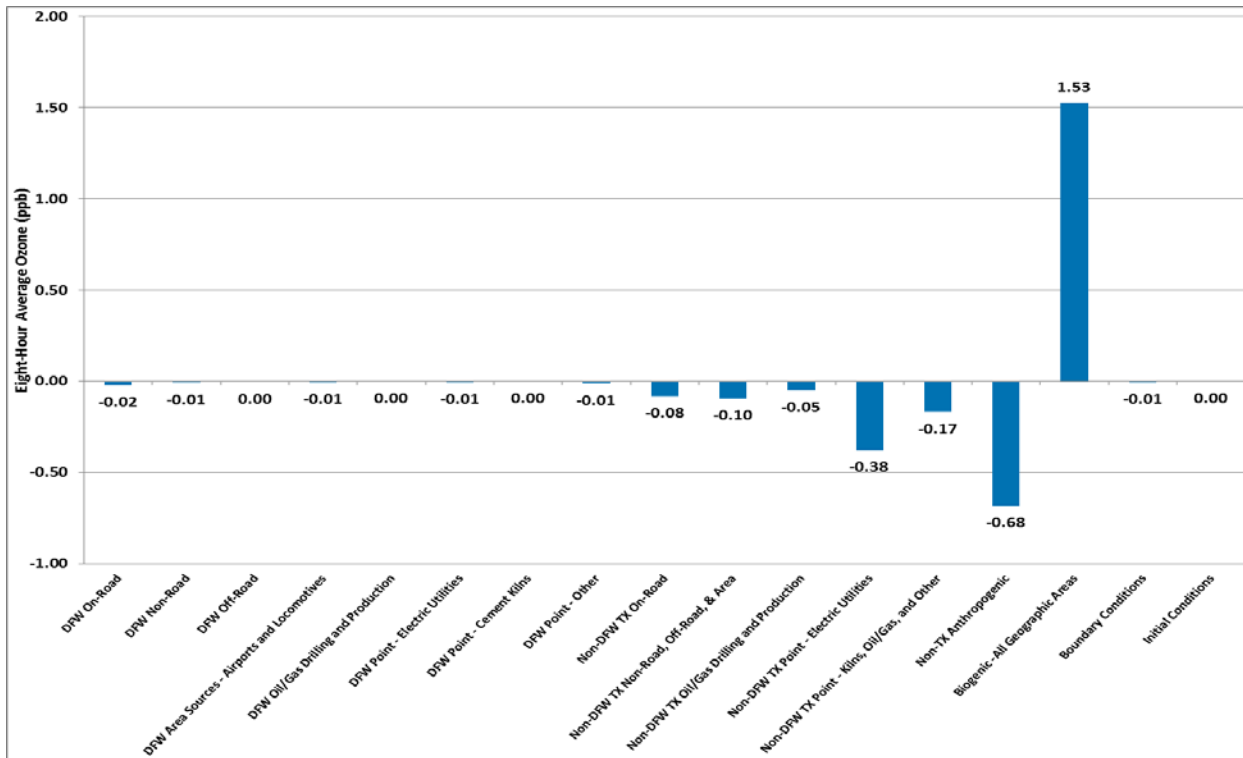


Figure 5-32: Difference between OSAT and APCA Source Apportionment at Kaufman County (C71)

Unlike Denton Airport South and Parker County, at Kaufman the largest decrease after the Non-TX Anthropogenic category is the Non-DFW TX Point-Electric Utilities category. This is in line with the contribution profile detailed in Table 5-8 for the Kaufman site with the Non-DFW TX Point-Electric Utilities category being the second largest contributor. Similarly, both the Denton Airport South site and Parker County site showed the second largest decrease in the DFW On-Road category in line with their contribution profiles detailed in Table 5-6 and Table 5-7, respectively.

6. BASELINE (2006) AND FUTURE CASE (2018) MODELING

6.1. Baseline Modeling

The TCEQ used 2006 as the baseline year for conducting the attainment modeling. Two features of the baseline year are used. First, the baseline year identifies the three consecutive years with design values (DVs) that include the fourth high of the baseline year. These three DVs are averaged to calculate the DV_B, as previously illustrated in Figure 1-1, for each of the regulatory monitors. Second, the baseline year is used to develop the typical ozone-season-day (OSD) modeling emissions as shown in Table 6-1: *2006 Summer Baseline Anthropogenic Emissions for the Ten-County DFW Nonattainment Area*

DFW Area Source Type	NO _x (tpd)	VOC (tpd)	CO (tpd)
On-Road	265.87	113.15	1,237.75
Non-Road	88.75	63.84	802.52
Area Sources	29.02	290.46	85.59
Off-Road – Locomotives	29.97	1.72	4.12
Off-Road – Airports	12.78	4.46	48.09
Oil and Gas – Production	61.84	43.72	20.09
Oil and Gas – Drill Rigs	18.23	1.16	3.57
Point – Oil and Gas	11.53	21.82	8.74
Point – EGUs (Ozone Season Average)	9.63	1.03	4.77
Point – Cement Kilns	22.08	1.94	17.45
Point – Other	14.31	25.65	17.26
Total	564.01	568.95	2,249.95

Table 6-1: 2006 Summer Baseline Anthropogenic Emissions for the Ten-County DFW Nonattainment Area

DFW Area Source Type	NO _x (tpd)	VOC (tpd)	CO (tpd)
On-Road	265.87	113.15	1,237.75
Non-Road	88.75	63.84	802.52
Area Sources	29.02	290.46	85.59
Off-Road – Locomotives	29.97	1.72	4.12
Off-Road – Airports	12.78	4.46	48.09

DFW Area Source Type	NO _x (tpd)	VOC (tpd)	CO (tpd)
Oil and Gas – Production	61.84	43.72	20.09
Oil and Gas – Drill Rigs	18.23	1.16	3.57
Point – Oil and Gas	11.53	21.82	8.74
Point – EGUs (Ozone Season Average)	9.63	1.03	4.77
Point – Cement Kilns	22.08	1.94	17.45
Point – Other	14.31	25.65	17.26
Total	564.01	568.95	2,249.95

The baseline modeling results are used to calculate the denominator of the RRF (RRF_D) for each of the regulatory monitors. The RRF_D is calculated as the average of the modeled daily maximum eight-hour ozone concentrations above 75 ppb within the 3 x 3 grid cell array about the monitor (Figure 6-1: *Near Monitoring Site Grid Cell Array Size*).

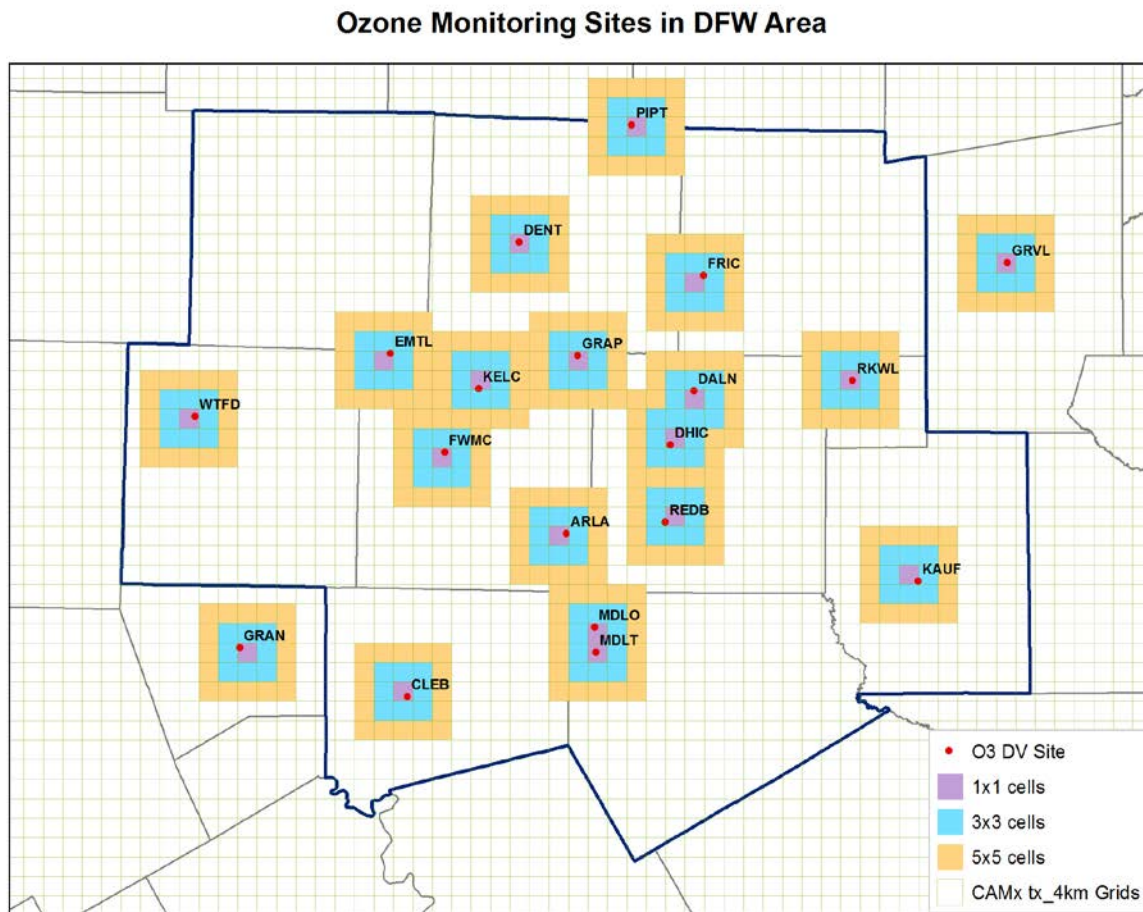


Figure 6-1: Near Monitoring Site Grid Cell Array Size

Per the EPA's modeling guidance, if there are fewer than 10 days with 2006 baseline modeled concentrations greater than 84 ppb, then days with modeled concentrations greater than or equal to 70 ppb can be used in the average. The same approach was taken for the 2008 eight-hour standard using days greater than 75 ppb with the 70 ppb lower cutoff. The DV_B and the RRF_D for the DFW monitors from the June and August-September 2006 episodes are summarized in Table 6-2: 2006 DV_B, RRF_D, and Number of Baseline Modeled Days Averaged over the June and August-September 2006 Episodes.

Table 6-2: 2006 DV_B, RRF_D, and Number of Baseline Modeled Days Averaged over the June and August-September 2006 Episodes

Site	Monitor	2006 DV _B (ppb)*	RRF _D (ppb)	Modeled Days
DENT	Denton C56	93.33	89.04	37
EMTL	Eagle Mountain Lake C75	93.33	88.32	31
KELC	Keller C17	91.00	91.06	32
GRAP	Grapevine Fairway C70	90.67	91.68	35
FWMC	Fort Worth Northwest C13	89.33	89.87	30
FRIC	Frisco C31	87.67	87.42	37
WTFD	Weatherford Parker County C76	87.67	86.33	20
CLEB	Cleburne C77	85.00	83.41	19
DALN	Dallas North C63	85.00	87.07	32
REDB	Dallas Exec Airport C402	85.00	84.93	29
ARLA	Arlington C61	83.33	86.34	31
GRAN [#]	Granbury C73 [#]	83.00 [#]	83.40	20
DHIC	Dallas Hinton C401	81.67	87.00	33
PIPT [†]	Pilot Point C1032 [†]	81.00 [†]	88.03	33
MDLT [†]	Midlothian Tower C94 [†]	80.50 [†]	82.82	26
RKWL	Rockwall Heath C69	77.67	82.99	26
GRVL [#]	Greenville C1006 [#]	75.00 [#]	79.12	18
MDLO [†]	Midlothian OFW C52 [†]	75.00 [†]	83.19	28
KAUF	Kaufman C71	74.67	79.74	19

* DV_B values 76 ppb or greater are shown in red.

† PIPT, MDLT, and MDLO did not measure enough data from 2004 through 2008 to calculate a complete DV_B. The DV_B shown uses all available data.

[#] Granbury C73 and Greenville C1006 are outside the 2008 eight-hour ozone NAAQS DFW nonattainment area.

6.2. Future Baseline Modeling

Similar to the 2006 baseline modeling, the 2018 modeling was conducted for each of the episode days using the projected 2018 ozone season day emissions. The 2018 anthropogenic modeling emissions for the DFW 10-county area are shown in Table 6-3: 2018 Future Case Anthropogenic Emissions for the Ten-County DFW Nonattainment Area.

Table 6-3: 2018 Future Case Anthropogenic Emissions for the Ten-County DFW Nonattainment Area

DFW Area Source Type	NO _x (tpd)	VOC (tpd)	CO (tpd)
On-Road	113.36	55.63	671.77
Non-Road	39.87	32.80	577.61
Area Sources	30.76	284.94	78.09
Off-Road – Locomotives	18.90	0.93	4.10
Off-Road – Airports	13.06	3.55	34.07
Oil and Gas – Production	7.15	23.79	5.41
Oil and Gas – Drill Rigs	2.82	0.21	0.45
Point – Oil and Gas	16.37	26.02	12.75
Point – EGUs (Peak Ozone Season Average)	16.91	4.44	20.61
Point – Cement Kilns	17.64	0.78	11.45
Point – Other	6.62	20.43	17.14
Total	283.46	453.52	1,433.45

Figure 6-2: 2006 Baseline and 2018 Future Modeling Emissions for the DFW Nonattainment Area exhibits a comparison between 2006 and 2018 modeling emissions. From 2006 to 2018, NO_x emissions decrease from most source categories, notably from on-road, non-road, and oil and gas production sources. VOC emissions decrease as well, with the largest projected cuts from on-road, non-road, and oil and gas production sources.

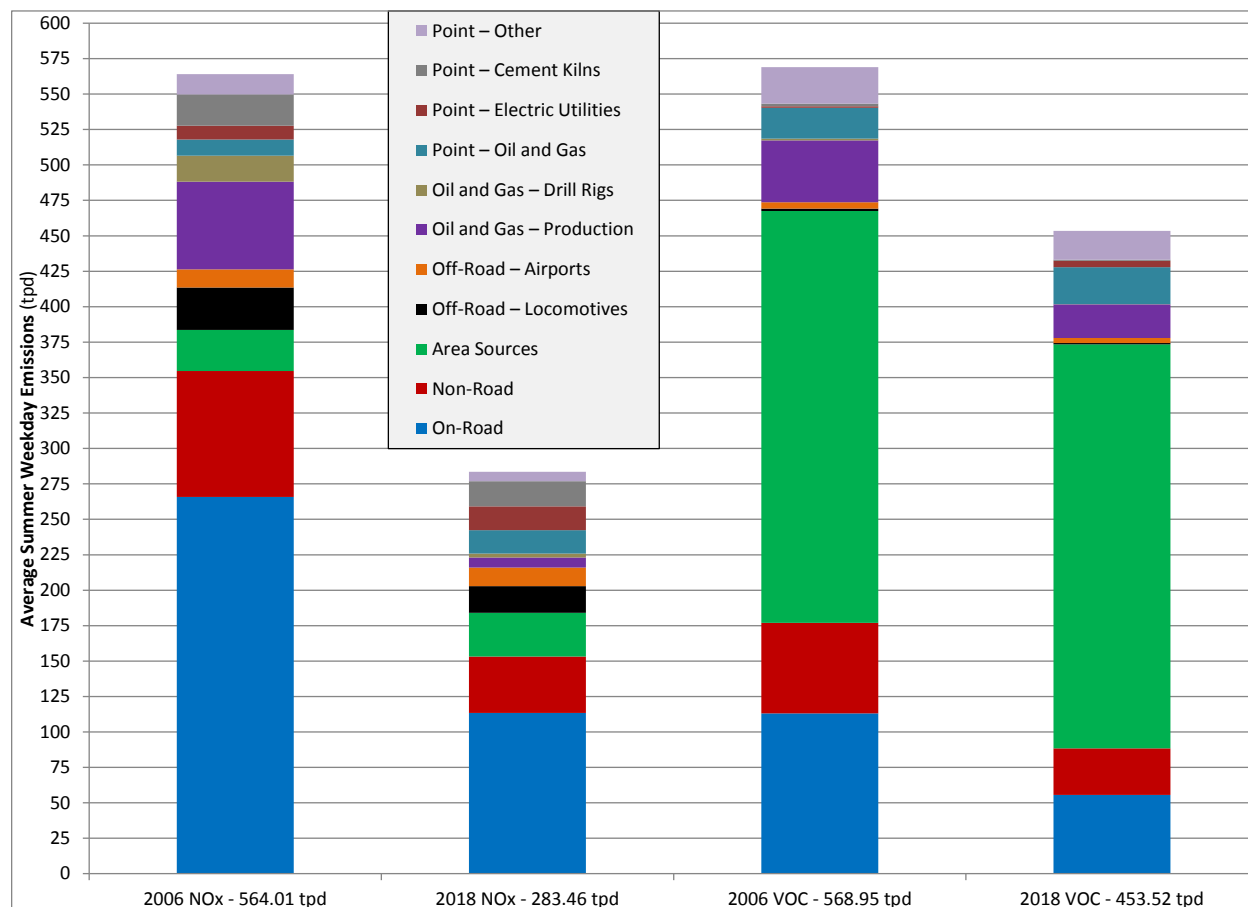


Figure 6-2: 2006 Baseline and 2018 Future Modeling Emissions for the DFW Nonattainment Area

Using the same days as used in the 2006 baseline modeling to calculate the RRF_D, an RRF numerator (RRF_N) was calculated as the average of the of the 2018 modeled maximum daily eight-hour ozone concentrations within the 3 x 3 grid cell array about each monitor (Figure 6-1). The RRF at each monitor was calculated as the ratio RRF_N / RRF_D, and the 2018 future design value (DV_F) at each monitor was estimated as per EPA’s modeling guidance by multiplying the 2006 DV_B by the RRF. Table 6-4: *Summary of the RRF and 2018 Future Design Values* summarizes the 2006 DV_B, RRF and 2018 DV_F at each of the regulatory monitors.

Table 6-4: Summary of the RRF and 2018 Future Design Values

Site	Monitor	2006 DV _B (ppb)*	RRF	2018 DV _F (ppb)*
DENT	Denton C56	93.33	0.821	76.67

Site	Monitor	2006 DV _B (ppb)*	RRF	2018 DV _F (ppb)*
EMTL	Eagle Mountain Lake C75	93.33	0.813	75.90
KELC	Keller C17	91.00	0.824	74.96
GRAP	Grapevine Fairway C70	90.67	0.836	75.78
FWMC	Fort Worth Northwest C13	89.33	0.823	73.48
FRIC	Frisco C31	87.67	0.834	73.10
WTFD	Weatherford Parker County C76	87.67	0.812	71.18
CLEB	Cleburne C77	85.00	0.827	70.26
DALN	Dallas North C63	85.00	0.842	71.54
REDB	Dallas Exec Airport C402	85.00	0.833	70.84
ARLA	Arlington C61	83.33	0.833	69.39
GRAN [#]	Granbury C73 [#]	83.00 [#]	0.817 [#]	67.84 [#]
DHIC	Dallas Hinton C401	81.67	0.839	68.54
PIPT [†]	Pilot Point C1032 [†]	81.00 [†]	0.822 [†]	66.60 [†]
MDLT [†]	Midlothian Tower C94 [†]	80.50 [†]	0.838 [†]	67.45 [†]
RKWL	Rockwall Heath C69	77.67	0.845	65.64
GRVL [#]	Greenville C1006 [#]	75.00 [#]	0.833 [#]	62.46 [#]
MDLO [†]	Midlothian OFW C52 [†]	75.00 [†]	0.840 [†]	62.99 [†]
KAUF	Kaufman C71	74.67	0.833	62.18

* DV_B and DV_F values 76 ppb or greater are shown in red.

† PIPT, MDLT, and MDLO did not measure enough data from 2004 through 2008 to calculate a complete DV_B. The DV_B shown uses all available data, which was used to calculate the RRF and DV_F.

Granbury C73 and Greenville C1006 are outside the 2008 eight-hour ozone NAAQS DFW nonattainment area.

The 2018 baseline attainment modeling projects only one regulatory monitor with a DV_F 76 ppb or greater.

6.2.1. Alternative Future Design Value Calculations

The attainment test applied above was based on the EPA's guidance (EPA, 2007), which was documented in the modeling protocol supplied to the EPA. However, the calculation of RRFs using different methods may provide information about the sensitivity of the model.

6.2.1.1. Daily RRF Analysis:

The EPA's guidance states to calculate the RRF by dividing the averaged future case concentrations by the averaged baseline concentrations over the same modeled days using the minimum threshold discussed above (Ratio of Means). An alternative calculation can be made by dividing the future by the baseline for each day and then averaging the resulting daily RRFs (Mean of Ratios). Table 6-5, Table 6-6, Table 6-7, and Table 6-8 below show the daily RRFs at each monitor throughout the June and August-September episodes. Using the same days above 75 ppb as in the official attainment test, the DV_Fs are very similar as shown in Table 6-9: Summary of the RRF and 2018 Future Design Values Calculated by Ratio of Means and Mean of Ratios.

Table 6-5: May 31 – June 17 Daily RRFs

Site	5/31	6/1	6/2	6/3	6/4	6/5	6/6	6/7	6/8	6/9	6/10	6/11	6/12	6/13	6/14	6/15	6/16	6/17
ARLA	0.870	0.958	0.846	0.806	0.852	0.868	0.866	0.837	0.827	0.824	0.852	0.896	0.835	0.828	0.821	0.890	0.926	0.863
CLEB	0.887	0.903	0.829	0.794	0.861	0.821	0.865	0.814	0.823	0.808	0.859	0.878	0.870	0.789	0.849	0.841	0.917	0.838
DALN	0.920	0.997	0.854	0.797	0.845	0.861	0.872	0.835	0.840	0.839	0.839	0.891	0.849	0.805	0.848	0.874	0.992	0.957
DENT	0.966	0.844	0.839	0.824	0.819	0.835	0.815	0.821	0.832	0.798	0.818	0.844	0.847	0.800	0.822	0.857	0.926	0.908
DHIC	0.925	1.014	0.854	0.796	0.851	0.869	0.875	0.839	0.842	0.836	0.847	0.893	0.849	0.808	0.860	0.878	0.975	0.953
EMTL	1.014	0.850	0.819	0.818	0.826	0.818	0.873	0.806	0.814	0.789	0.828	0.837	0.827	0.796	0.804	0.844	0.921	0.863
FRIC	0.885	0.846	0.837	0.813	0.827	0.849	0.840	0.822	0.837	0.836	0.822	0.873	0.869	0.805	0.841	0.864	0.935	0.932
FWMC	0.948	0.881	0.814	0.852	0.829	0.844	0.855	0.850	0.830	0.806	0.839	0.865	0.823	0.808	0.816	0.856	0.929	0.871
GRAN [#]	0.869	0.859	0.801	0.800	0.867	0.836	0.892	0.860	0.808	0.815	0.866	0.873	0.835	0.795	0.812	0.837	0.925	0.892
GRAP	0.925	0.878	0.843	0.821	0.847	0.845	0.837	0.845	0.847	0.811	0.835	0.865	0.847	0.834	0.827	0.867	0.947	0.942
GRVL [#]	0.915	0.858	0.841	0.831	0.844	0.828	0.864	0.819	0.828	0.818	0.844	0.934	0.851	0.822	0.840	0.813	0.931	0.832
KAUF	0.871	0.857	0.840	0.812	0.845	0.860	0.879	0.800	0.812	0.858	0.867	0.940	0.864	0.798	0.831	0.845	0.933	0.882
KELC	0.924	0.876	0.831	0.823	0.817	0.832	0.831	0.833	0.843	0.798	0.832	0.849	0.831	0.820	0.822	0.867	0.929	0.898
MDLO [†]	0.854	0.958	0.853	0.861	0.846	0.869	0.861	0.821	0.838	0.854	0.852	0.934	0.871	0.800	0.847	0.892	0.910	0.878
MDLT [†]	0.851	0.955	0.853	0.856	0.843	0.865	0.860	0.822	0.843	0.859	0.852	0.934	0.887	0.799	0.839	0.892	0.910	0.875
PIPT [†]	0.869	0.845	0.844	0.828	0.835	0.832	0.821	0.812	0.822	0.831	0.819	0.859	0.852	0.816	0.827	0.849	0.911	0.909
REDB	0.884	1.022	0.867	0.801	0.850	0.858	0.868	0.820	0.855	0.836	0.847	0.901	0.857	0.785	0.831	0.876	0.947	0.935
RKWL	0.869	0.881	0.843	0.819	0.856	0.857	0.890	0.813	0.843	0.849	0.862	0.929	0.862	0.820	0.855	0.837	0.930	0.906
WTFD	0.892	0.858	0.862	0.870	0.855	0.830	0.863	0.808	0.801	0.791	0.853	0.840	0.818	0.837	0.806	0.837	0.925	0.933
Mean	0.902	0.902	0.841	0.822	0.843	0.846	0.859	0.825	0.831	0.824	0.844	0.886	0.850	0.809	0.832	0.859	0.933	0.898

[†] PIPT, MDLT, and MDLO did not measure enough data from 2004 through 2008 to calculate a complete DV_B. A DV_B was calculated using all available data for the RRF and DV_F shown.

[#] Granbury C73 and Greenville C1006 are outside the 2008 eight-hour ozone NAAQS DFW nonattainment area.

Table 6-6: June 18 through July 2 Daily RRFs

Site	6/18	6/19	6/20	6/21	6/22	6/23	6/24	6/25	6/26	6/27	6/28	6/29	6/30	7/1	7/2
ARLA	0.887	0.842	0.960	0.849	0.901	0.891	0.854	0.874	0.865	0.855	0.843	0.839	0.812	0.868	0.898
CLEB	0.923	0.863	0.879	0.885	0.888	0.880	0.837	0.848	0.877	0.841	0.888	0.834	0.821	0.880	0.873
DALN	0.955	0.852	0.916	0.928	0.930	0.928	0.868	0.895	0.896	0.893	0.848	0.821	0.809	0.860	0.893
DENT	0.873	0.857	0.925	0.858	0.874	0.861	0.811	0.899	0.855	0.829	0.836	0.804	0.812	0.844	0.881
DHIC	0.953	0.869	0.926	0.891	0.927	0.932	0.862	0.886	0.896	0.892	0.845	0.822	0.803	0.861	0.894
EMTL	0.836	0.863	0.916	0.852	0.885	0.859	0.821	0.900	0.886	0.846	0.828	0.804	0.779	0.838	0.848
FRIC	0.884	0.844	0.894	0.883	0.904	0.833	0.826	0.897	0.872	0.857	0.860	0.816	0.799	0.842	0.878
FWMC	0.848	0.869	0.958	0.869	0.906	0.854	0.827	0.869	0.873	0.817	0.838	0.831	0.800	0.855	0.871
GRAN [#]	0.852	0.836	0.894	0.909	0.946	0.844	0.816	0.888	0.899	0.817	0.814	0.846	0.825	0.870	0.889
GRAP	0.887	0.879	0.939	0.876	0.878	0.820	0.840	0.880	0.850	0.798	0.838	0.818	0.799	0.859	0.887
GRVL [#]	0.880	0.812	0.878	0.888	0.932	0.865	0.814	0.906	0.886	0.886	0.837	0.866	0.817	0.858	0.873
KAUF	0.893	0.816	0.855	0.884	0.868	0.852	0.842	0.874	0.886	0.850	0.818	0.857	0.806	0.866	0.887
KELC	0.879	0.877	0.941	0.874	0.879	0.823	0.817	0.873	0.855	0.795	0.832	0.803	0.793	0.844	0.876
MDLO [†]	0.980	0.847	0.924	0.837	0.884	0.876	0.839	0.867	0.879	0.852	0.851	0.879	0.818	0.840	0.893
MDLT [†]	0.977	0.847	0.921	0.837	0.883	0.877	0.841	0.865	0.886	0.843	0.849	0.901	0.816	0.840	0.893
PIPT [†]	0.850	0.828	0.881	0.890	0.877	0.842	0.815	0.909	0.866	0.845	0.821	0.801	0.786	0.821	0.860
REDB	0.951	0.821	0.920	0.885	0.924	0.916	0.859	0.873	0.894	0.887	0.826	0.829	0.860	0.871	0.889
RKWL	0.879	0.853	0.907	0.917	0.859	0.885	0.826	0.886	0.869	0.924	0.875	0.878	0.844	0.864	0.887
WTFD	0.842	0.824	0.883	0.879	0.895	0.864	0.813	0.920	0.903	0.912	0.812	0.799	0.784	0.835	0.882
Mean	0.896	0.847	0.911	0.878	0.897	0.868	0.833	0.885	0.879	0.855	0.840	0.834	0.810	0.853	0.882

[†] PIPT, MDLT, and MDLO did not measure enough data from 2004 through 2008 to calculate a complete DV_B. A DV_B was calculated using all available data for the RRF and DV_F shown.

[#] Granbury C73 and Greenville C1006 are outside the 2008 eight-hour ozone NAAQS DFW nonattainment area.

Table 6-7: August 13 through 29 Daily RRFs

Site	8/13	8/14	8/15	8/16	8/17	8/18	8/19	8/20	8/21	8/22	8/23	8/24	8/25	8/26	8/27	8/28	8/29
ARLA	0.902	0.868	0.858	0.835	0.823	0.797	0.825	0.810	0.819	0.795	0.817	0.844	0.834	0.916	0.842	1.018	0.844
CLEB	0.935	0.903	0.851	0.826	0.815	0.818	0.829	0.834	0.821	0.780	0.815	0.840	0.815	0.908	0.880	0.910	0.861
DALN	0.919	0.895	0.871	0.820	0.816	0.798	0.810	0.809	0.801	0.849	0.835	0.851	0.824	0.887	0.887	1.104	0.860
DENT	0.873	0.799	0.815	0.813	0.822	0.779	0.799	0.791	0.768	0.780	0.800	0.824	0.813	0.865	0.771	0.839	0.848
DHIC	0.928	0.888	0.868	0.830	0.836	0.787	0.807	0.807	0.808	0.827	0.819	0.854	0.834	0.890	0.876	1.114	0.863
EMTL	0.894	0.864	0.790	0.794	0.807	0.777	0.791	0.794	0.778	0.750	0.797	0.828	0.808	0.860	0.825	0.881	0.860
FRIC	0.900	0.857	0.860	0.793	0.804	0.786	0.808	0.809	0.805	0.810	0.827	0.823	0.813	0.872	0.855	0.884	0.838
FWMC	0.911	0.860	0.842	0.809	0.820	0.776	0.811	0.787	0.794	0.790	0.811	0.828	0.812	0.877	0.788	0.970	0.851
GRAN [#]	0.969	0.969	0.873	0.851	0.840	0.798	0.822	0.805	0.803	0.771	0.832	0.857	0.833	0.893	0.881	0.872	0.867
GRAP	0.907	0.858	0.882	0.822	0.835	0.781	0.815	0.796	0.797	0.817	0.826	0.837	0.825	0.874	0.809	0.914	0.838
GRVL [#]	0.907	0.876	0.846	0.814	0.819	0.813	0.797	0.832	0.836	0.791	0.800	0.834	0.858	0.894	0.872	0.879	0.841
KAUF	0.920	0.891	0.870	0.832	0.784	0.848	0.803	0.878	0.831	0.787	0.833	0.834	0.856	0.904	0.884	0.987	0.858
KELC	0.902	0.834	0.821	0.806	0.815	0.779	0.806	0.802	0.791	0.771	0.788	0.820	0.813	0.874	0.791	0.907	0.843
MDLO [†]	0.878	0.850	0.851	0.819	0.793	0.842	0.836	0.864	0.850	0.800	0.840	0.839	0.825	0.910	0.862	0.878	0.847
MDLT [†]	0.879	0.851	0.852	0.825	0.793	0.841	0.833	0.866	0.848	0.805	0.830	0.835	0.820	0.899	0.854	0.878	0.847
PIPT [†]	0.881	0.819	0.807	0.798	0.827	0.790	0.801	0.785	0.789	0.820	0.798	0.829	0.808	0.864	0.800	0.842	0.840
REDB	0.908	0.884	0.845	0.855	0.814	0.795	0.821	0.814	0.813	0.801	0.813	0.845	0.817	0.888	0.871	1.056	0.867
RKWL	0.928	0.884	0.904	0.866	0.874	0.842	0.843	0.840	0.831	0.820	0.807	0.857	0.852	0.918	0.844	0.936	0.846
WTFD	0.971	0.893	0.837	0.828	0.847	0.796	0.802	0.791	0.786	0.814	0.802	0.845	0.820	0.889	0.849	0.816	0.876
Mean	0.911	0.871	0.850	0.823	0.820	0.802	0.814	0.817	0.809	0.799	0.815	0.838	0.825	0.889	0.844	0.931	0.852

[†] PIPT, MDLT, and MDLO did not measure enough data from 2004 through 2008 to calculate a complete DV_B. A DV_B was calculated using all available data for the RRF and DV_F shown.

[#] Granbury C73 and Greenville C1006 are outside the 2008 eight-hour ozone NAAQS DFW nonattainment area.

Table 6-8: August 30 through September 15 Daily RRFs

Site	8/30	8/31	9/1	9/2	9/3	9/4	9/5	9/6	9/7	9/8	9/9	9/10	9/11	9/12	9/13	9/14	9/15
ARLA	0.885	0.844	0.840	0.835	0.799	0.871	0.894	0.859	0.844	0.827	0.867	0.835	0.825	0.859	0.912	0.873	0.869
CLEB	0.864	0.843	0.839	0.804	0.810	0.860	0.894	0.844	0.837	0.830	0.882	0.840	0.800	0.844	0.921	0.867	0.826
DALN	0.903	0.860	0.811	0.828	0.822	0.937	0.898	0.865	0.838	0.854	0.860	0.859	0.901	0.863	0.940	0.878	0.872
DENT	0.863	0.828	0.835	0.818	0.797	0.868	0.880	0.864	0.811	0.854	0.840	0.830	0.785	0.846	0.874	0.890	0.872
DHIC	0.904	0.865	0.822	0.828	0.818	0.965	0.899	0.871	0.889	0.853	0.861	0.852	0.863	0.870	0.957	0.894	0.877
EMTL	0.856	0.827	0.884	0.802	0.781	0.929	0.883	0.848	0.844	0.824	0.820	0.823	0.824	0.847	0.883	0.869	0.828
FRIC	0.878	0.861	0.822	0.828	0.810	0.850	0.875	0.845	0.813	0.856	0.842	0.846	0.871	0.838	0.888	0.887	0.855
FWMC	0.819	0.855	0.877	0.810	0.766	0.963	0.883	0.835	0.852	0.836	0.835	0.834	0.801	0.826	0.869	0.879	0.832
GRAN [#]	0.820	0.864	0.858	0.785	0.790	0.852	0.886	0.850	0.828	0.848	0.848	0.826	0.833	0.830	0.873	0.877	0.842
GRAP	0.865	0.880	0.841	0.823	0.801	0.880	0.875	0.846	0.833	0.864	0.850	0.839	0.835	0.837	0.879	0.883	0.876
GRVL [#]	0.875	0.833	0.808	0.841	0.819	0.834	0.874	0.843	0.807	0.821	0.824	0.842	0.836	0.836	0.887	0.832	0.819
KAUF	0.850	0.832	0.796	0.844	0.821	0.851	0.859	0.824	0.829	0.845	0.852	0.871	0.823	0.830	0.868	0.844	0.853
KELC	0.840	0.834	0.847	0.832	0.776	0.892	0.877	0.845	0.890	0.854	0.849	0.837	0.807	0.830	0.870	0.875	0.840
MDLO [†]	0.873	0.871	0.817	0.840	0.795	0.841	0.893	0.861	0.815	0.813	0.842	0.857	0.807	0.874	0.944	0.857	0.862
MDLT [†]	0.870	0.867	0.819	0.835	0.809	0.835	0.899	0.869	0.837	0.809	0.844	0.853	0.825	0.872	0.943	0.847	0.859
PIPT [†]	0.874	0.854	0.817	0.833	0.806	0.832	0.876	0.861	0.799	0.834	0.828	0.826	0.821	0.840	0.905	0.869	0.843
REDB	0.896	0.844	0.806	0.828	0.809	0.895	0.919	0.876	0.856	0.828	0.864	0.847	0.821	0.877	0.977	0.859	0.878
RKWL	0.872	0.810	0.814	0.839	0.818	0.844	0.872	0.846	0.822	0.871	0.859	0.862	0.810	0.839	0.893	0.862	0.850
WTFD	0.847	0.847	0.841	0.791	0.816	0.915	0.875	0.880	0.854	0.834	0.807	0.843	0.882	0.896	0.914	0.837	0.836
Mean	0.866	0.848	0.831	0.823	0.803	0.880	0.885	0.854	0.837	0.840	0.846	0.843	0.830	0.850	0.905	0.867	0.852

[†] PIPT, MDLT, and MDLO did not measure enough data from 2004 through 2008 to calculate a complete DV_B. A DV_B was calculated using all available data for the RRF and DV_F shown.

[#] Granbury C73 and Greenville C1006 are outside the 2008 eight-hour ozone NAAQS DFW nonattainment area.

Table 6-9: Summary of the RRF and 2018 Future Design Values Calculated by Ratio of Means and Mean of Ratios

Site	Monitor	RRF Ratio of Means	2018 DV _F Ratio of Means (ppb)*	RRF Mean of Ratios	2018 DV _F Mean of Ratios (ppb)*
DENT	Denton C56	0.821	76.67	0.823	76.78
EMTL	Eagle Mountain Lake C75	0.813	75.90	0.815	76.03
KELC	Keller C17	0.824	74.96	0.825	75.09
GRAP	Grapevine Fairway C70	0.836	75.78	0.838	75.96
FWMC	Fort Worth Northwest C13	0.823	73.48	0.823	73.55
FRIC	Frisco C31	0.834	73.10	0.835	73.17
WTFD	Weatherford Parker County C76	0.812	71.18	0.812	71.19
CLEB	Cleburne C77	0.827	70.26	0.828	70.41
DALN	Dallas North C63	0.842	71.54	0.843	71.63
REDB	Dallas Exec Airport C402	0.833	70.84	0.835	70.95
ARLA	Arlington C61	0.833	69.39	0.834	69.48
GRAN [#]	Granbury C73 [#]	0.817 [#]	67.84 [#]	0.818 [#]	67.90 [#]
DHIC	Dallas Hinton C401	0.839	68.54	0.841	68.66
PIPT [†]	Pilot Point C1032 [†]	0.822 [†]	66.60 [†]	0.823 [†]	66.68 [†]
MDLT [†]	Midlothian Tower C94 [†]	0.838 [†]	67.45 [†]	0.839 [†]	67.57 [†]
RKWL	Rockwall Heath C69	0.845	65.64	0.846	65.73
GRVL [#]	Greenville C1006 [#]	0.833 [#]	62.46 [#]	0.833 [#]	62.47 [#]
MDLO [†]	Midlothian OFW C52 [†]	0.840 [†]	62.99 [†]	0.841 [†]	63.11 [†]
KAUF	Kaufman C71	0.833	62.18	0.833	62.18

* DV_F values 76 ppb or greater are shown in red.

† PIPT, MDLT, and MDLO did not measure enough data from 2004 through 2008 to calculate a complete DV_B. The DV_B shown uses all available data, which was used to calculate the RRF and DV_F.

[#] Granbury C73 and Greenville C1006 are outside the 2008 eight-hour ozone NAAQS DFW nonattainment area.

6.2.1.2. Grid Cell Array Size Analysis:

The grid cell array size is chosen as an area around a monitor to be spatially representative of that site. For the RRF calculation the maximum concentration in the grid cell array around a monitor from the baseline and future case modeling is used, which may not be at the cell where the monitor is located. The EPA guidance states that this method is beneficial for many reasons, including that the model may displace the peak around a monitor. For the proposed DFW Attainment Demonstration SIP revision a 3x3 grid cell array was chosen. As Figure 6-3: *Grid Cell Array Size Around DFW Monitors* shows, a 5x5 or 7x7 grid cell array causes overlap among many DFW monitors. This contradicts the idea that the grid cell array should be representative of a specific monitoring site and is not preferred. Nevertheless, the RRFs and DV_Fs for the 5x5 and 7x7 grid cell arrays are presented in Table 6-3: *2018 Future Case Anthropogenic Emissions for the Ten-County DFW Nonattainment Area*

DFW Area Source Type	NO _x (tpd)	VOC (tpd)	CO (tpd)
On-Road	113.36	55.63	671.77
Non-Road	39.87	32.80	577.61
Area Sources	30.76	284.94	78.09
Off-Road – Locomotives	18.90	0.93	4.10
Off-Road – Airports	13.06	3.55	34.07
Oil and Gas – Production	7.15	23.79	5.41
Oil and Gas – Drill Rigs	2.82	0.21	0.45
Point – Oil and Gas	16.37	26.02	12.75
Point – EGUs (Peak Ozone Season Average)	16.91	4.44	20.61
Point – Cement Kilns	17.64	0.78	11.45
Point – Other	6.62	20.43	17.14
Total	283.46	453.52	1,433.45

. The maximum DV_F is very similar between the three array sizes. Most monitors' DV_Fs decrease with increasing array size, though Eagle Mountain Lake C75 (EMTL) increases slightly.

Ozone Monitoring Sites in DFW Area

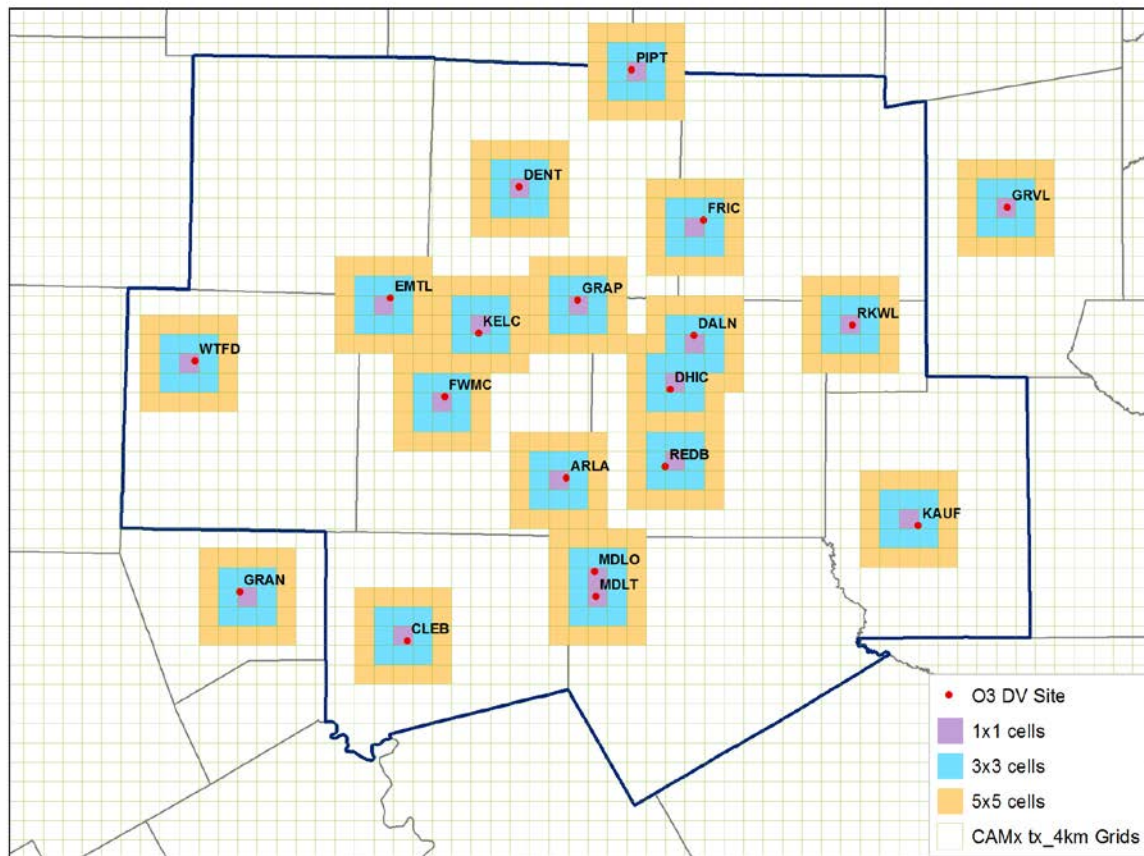


Figure 6-3: Grid Cell Array Size Around DFW Monitors

Table 6-10: RRFs and DV_Fs using 3x3, 5x5, and 7x7 Grid Cell Arrays

Site	RRF (3x3)	DV _F * (3x3)	RRF (5x5)	DV _F * (5x5)	RRF (7x7)	DV _F * (7x7)
DENT	0.821	76.67	0.820	76.50	0.820	76.54
EMTL	0.813	75.90	0.814	75.93	0.814	76.00
KELC	0.824	74.96	0.826	75.21	0.827	75.28
GRAP	0.836	75.78	0.835	75.75	0.833	75.54
FWMC	0.823	73.48	0.824	73.57	0.822	73.43
FRIC	0.834	73.10	0.832	72.94	0.831	72.85
WTFD	0.812	71.18	0.810	71.05	0.808	70.88
CLEB	0.827	70.26	0.840	71.38	0.838	71.20
DALN	0.842	71.54	0.834	70.89	0.831	70.67
REDB	0.833	70.84	0.822	69.84	0.823	69.98
ARLA	0.833	69.39	0.833	69.45	0.832	69.35
GRAN [#]	0.817	67.84	0.816	67.74	0.816	67.69
DHIC	0.839	68.54	0.835	68.20	0.833	68.07
PIPT [†]	0.822	66.60	0.821	66.51	0.821	66.50
MDLT [†]	0.838	67.45	0.842	67.76	0.841	67.70
RKWL	0.845	65.64	0.847	65.79	0.844	65.57
GRVL [#]	0.833	62.46	0.841	63.07	0.840	62.98
MDLO [†]	0.840	62.99	0.830	62.26	0.828	62.13
KAUF	0.833	62.18	0.833	62.19	0.834	62.25

* DV_F values 76 ppb or greater are shown in red.

† PIPT, MDLT, and MDLO did not measure enough data from 2004 through 2008 to calculate a complete DV_B. A DV_B was calculated using all available data for the RRFs and DV_Fs shown.

Granbury C73 and Greenville C1006 are outside the 2008 eight-hour ozone NAAQS DFW nonattainment area

6.2.2. Unmonitored Area Analysis

The EPA guidance (EPA, 2007) recommends that areas not near monitoring locations (unmonitored areas) be subjected to an unmonitored area (UMA) analysis to demonstrate that these areas are expected to reach attainment by the area's attainment year. The standard attainment test is applied only at monitor locations, and the UMA analysis is intended to identify any areas not near a monitoring location that are at risk of not meeting the attainment date. Recently, the EPA provided software that can be used to conduct UMA analyses, but has not specifically recommended using its software (called the Modeled Attainment Test Software (MATS)) in EPA guidance, instead stating that "States will be able to use the EPA-provided software or are free to develop alternative techniques that may be appropriate for their areas or situations."

Delays in the release of MATS prompted the TCEQ to develop its own technique for performing unmonitored area analyses, called the Texas Attainment Test for Unmonitored areas (TATU). While both procedures incorporate modeled predictions into a spatial interpolation procedure, TATU is integrated into the TCEQ's model Linux-based post-processing stream, while MATS

requires that modeled concentrations be exported to a Windows-based platform. Additionally, MATS requires input in latitude and longitude for monitor coordinates, while the TCEQ's procedures work directly with the Lambert Conformal Projection (LCP) monitoring coordinates used in the photochemical modeling applications. Finally, MATS uses the Voronoi Neighbor Averaging (VNA) technique for spatial interpolation, while TATU relies on the more familiar kriging geospatial interpolation technique. For these reasons, TCEQ chose to use TATU for the UMA analysis. More information about TATU is provided in Appendix C: Photochemical Modeling for the HGB Attainment Demonstration SIP Revision for the 1997 Eight-Hour Ozone Standard, Attachment 2.

Figure 6-4: Spatially Interpolated 2006 Baseline (top) and 2018 Future Case (bottom) Design Values for the DFW Area shows two color contour maps of ozone concentrations produced by TATU, one for the 2006 baseline (top) and one for the 2018 future case (bottom). The figure shows the extent and magnitude of the expected improvements in ozone design values, with few grid cells at or above 76 ppb in the future case plot (orange through red colors). The maximum design value in the domain is predicted at 76.8 ppb.

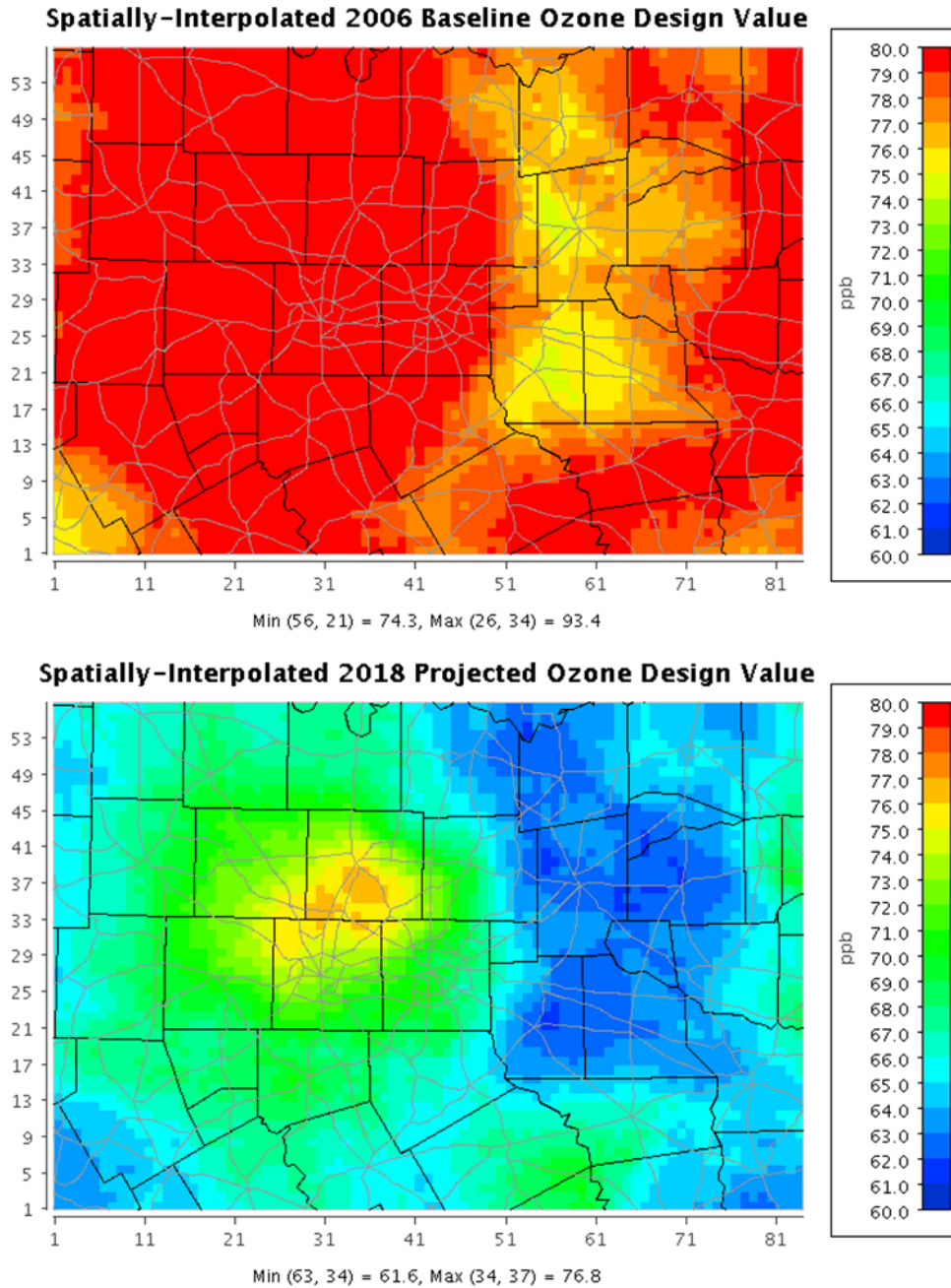


Figure 6-4: Spatially Interpolated 2006 Baseline (top) and 2018 Future Case (bottom) Design Values for the DFW Area

6.2.3. Ozone Metrics

Table 6-11: *Changes in the Area and Population Affected by an Eight-Hour Ozone Design Value Greater than or Equal to 76 ppb in Response to Growth and Controls* shows how the area affected by high ozone is expected to shrink in response to the emission changes projected to occur between 2006 and 2018. Peak ozone drops by 18% and the area with an estimated ozone design value greater than the 75 ppb standard shrinks by 98%. The estimated 2018 population

living in the DFW ten-county area with a 2008 eight-hour ozone design value greater than 75 ppb is also expected to decrease by 98%. The population data is from the 2010 Census and has not been grown to reflect changes in population in those areas in 2006 or 2018. Also, the population numbers reflect areas where people reside, i.e., their home addresses, not necessarily where they might be during the hours of highest ozone during the ozone season. However, the reduction in the area with high ozone suggests that ozone decreases are likely to benefit many residents of the DFW area.

Table 6-11: Changes in the Area and Population Affected by an Eight-Hour Ozone Design Value Greater than or Equal to 76 ppb in Response to Growth and Controls

Run name	Peak Ozone (ppb)	Area with design value >75 ppb, km ²	2010 population in area with design value >75 ppb
2006 baseline (reg2h)	93	5348	6306680
2018 future year (cs00e)	76	120	152690
Percentage decrease from 2006 to 2018	18%	98%	98%

7. MODELING ARCHIVE AND REFERENCES

7.1. Modeling Archive

The TCEQ has archived all modeling documentation and modeling input/output files generated as part of the DFW SIP modeling analysis. Interested parties can contact the TCEQ for information regarding data access or project documentation. Most modeling files and performance evaluation products may be found on [TCEQ's modeling ftp site](ftp://amdaftp.tceq.texas.gov/pub/TX/camx/), at <ftp://amdaftp.tceq.texas.gov/pub/TX/camx/>.

7.2. Modeling References

Environ, 2013. Foreign Contributions to Texas' Ozone, Final Report to the Texas Commission on Environmental Quality, Contract No. 582-11-10365-FY13-14, Environ International Corporation, Novato, CA.

Environ, 2014. User's Guide Emissions Processor, Version 3.21, Environ International Corporation, Novato, CA.

EPA, 2007. Guidance on the Use of Models and Other Analyses for Demonstrating Attainment of Air Quality Goals for Ozone, PM2.5, and Regional Haze, <http://www.epa.gov/scram001/guidance/guide/final-03-pm-rh-guidance.pdf>.

EPA, 2011. Spreadsheet of CSAPR Ozone and PM2.5 Design Values, http://www.epa.gov/airtransport/pdfs/CSAPR_Ozone%20and%20PM2.5_Design%20Values.xls.

MacDonald, Nicole and Hakami, A, 2010. Temporal Source Apportionment of Policy-Relevant Air Quality Metrics, Presented at the 9th CMAS Conference Oct. 11-13, 2010, Chapel, Hill, N.C.

Popescu, Sorin C., Jared Stuke, Mark Karnach, Jeremiah Bowling, Xuesong Zhang, William Booth, and Nian-Wei Ku, 2008. The New Central Texas Land Use Land Cover Classification Project, Final Report to the Texas Commission on Environmental Quality (TCEQ), Contract No. 582-5-64593-FY08-23, Texas A & M University, College Station, Texas.

Smith, Jim and Estes, M, 2010. Dynamic Model Performance Evaluation Using Weekday-Weekend and Retrospective Analysis, Presented at the 9th CMAS Conference Oct. 11-13, 2010, Chapel, Hill, N.C.

TCEQ, 2011. Revisions to the State Implementation Plan (SIP) for the Control of Ozone Air Pollution, Dallas-Fort Worth Eight-Hour Ozone Nonattainment Area Attainment Demonstration, Texas Commission on Environmental Quality (TCEQ), Austin, Texas.

Zhang et al., 2003. A revised parameterization for gaseous dry deposition in air-quality models, *Atmos. Chem. Phys.*, 3, 2067–2082, 2003